Environmental and Instrumental Effects on High Precision Gravimetry - A Case Study in Britain

Hugh Hopewell

A thesis submitted in fulfilment of the requirements
for the degree of Doctor of Philosophy
to the
University of Edinburgh
1999

Abstract

This thesis investigates the removal of environmental and instrumental effects from high precision gravity records and applies the findings to measurements made in Britain.

Ocean loading calculations have been developed by manipulating ocean tide model grids to be of variable size. This has improved the fit to irregular coastlines and the approximation of grid cell masses to point mass loads. Ocean loading is calculated for 12 components at the 69 sites of the British Precise Gravity Network (BPGN). The new ocean loading correction amplitude for Newlyn has increased from 16 to 23 μgal; the set standard deviation of a 24 hour FG5 absolute gravity data set reduces from 4.3 to 1.8 μgal. Adjustment of the BPGN with the new correction reduces the mean site standard error from 3.32 $\pm$ 0.60 μgal to 2.96 $\pm$ 0.46 μgal.

FG5-103 Bidston measurements show a seasonal change of 8 μgal. Water table data after correction for air pressure show a correlation with gravity, having a lag of 3 months. Using 6 months of continuous LaCoste & Romberg (LCR) Earth-tide gravimeter data, the air pressure admittance at Bidston varies seasonally from 0.35 to 0.50 μgal mbar^{-1}. Frequency dependent admittances correcting for instrumental humidity effects and environmental air pressure and rainfall effects removed structure in the data. Admittances derived from LCR Earth-tide data for air pressure and rainfall do not improve the absolute data.

Using synthetic data, the frequencies of damped sinusoids found from FG5 residuals are different to those originally present. Noise found at 9.5 Hz causes gravity changes of < 1 μgal when fitted to the equation of motion with real data. However, gravity changes by 6.3 μgal upon removal of its cause. Fitting frequencies from 4 - 13 Hz to this data creates changes in the order of 10 μgal. Existing noise correction algorithms may miss errors of this size.

FG5-103 produces results consistent with two other FG5s to within 1.5 μgal. Values from FG5-103 have been updated at 3 sites and found for 4 new sites in Britain. The BPGN has been extended with 7 new relative sites and connected to 4 new absolute sites. A significantly different scaling factor is found for LCR G275 of 1.000 656 $\pm$ 0.000 011 compared to 1.000 737 $\pm$ 0.000 018 from BPGN93. The relative gravity values disagree with absolute values by up to 50 μgal; the cause remains uncertain. Individual results of G275 and D145 may exhibit periodic errors with a period expected for these instruments: 603 dial turns, amplitude 30 μgal, and 900 coarse dial turns, amplitude 60 μgal, respectively. Non-linear vertical transfers and improving the connection of the network in the north need to be investigated.

Acknowledgements

This research project was supported financially by a contract between the Ministry for Agriculture, Fisheries and Food and Proudman Oceanographic Laboratory (POL). The absolute gravity fieldwork was funded from this contract by POL. The Ph.D. grant and relative gravity fieldwork was funded through a sub-contract between POL and Edinburgh University.

Many thanks should be given to my supervisor, Roger Hipkin, whose help and guidance have been invaluable, both with the research and reading through drafts of this thesis. He also organised the relative gravity fieldwork.

Trevor Baker of POL should be thanked for being in effect my 'adopted supervisor'. His comments and ideas have been most welcome. Some of the work in this thesis has been made in collaboration with Machiel Bos, based at POL. It has been a pleasure to work with him. Other staff at POL should be thanked for their help and cooperation, namely Bob Edge, Christine Taylor and Donna Hosker. In particular, special thanks should be given to Graham Jeffries with whom all the absolute gravity fieldwork was performed. Not only have his skills been an asset to the team, but he also saved me from dying of boredom during the many hours we spent in a noisy van travelling the motorway network of Europe.

Colleagues and staff at the Department of Geology and Geophysics, Edinburgh University are to be thanked. Especially those responsible for computer support and services. Members of the postgraduate community should be thanked for their distractions from Ph.D. work which helped keep me sane. Further appreciation is given to all my friends elsewhere in the world. In particular I would like to thank Maylis for her help during the thesis writing stage.

Finally, special thanks go to my parents and sister for their love and support.

Contents

Abstract i

Acknowledgements iii

1 Introduction 1

1.1 Isostasy . . . 2
1.2 Relative Sea Level Change . . . 2
1.3 Methods of Measuring Vertical Crustal Movement . . . 8
1.4 Gravity as a Method to Measure Vertical Crustal Movement . . . 8
1.5 Absolute Gravimetry . . . 9
1.6 The FG5 Absolute Gravimeter . . . 10
1.7 Relative Gravimetry . . . 13
1.8 The LaCoste & Romberg Relative Gravimeter . . . 13
1.9 Gravity Measurements in Britain . . . 15
1.10 Problems with Gravity Measurements . . . 16
1.10.1 Environmental . . . 16
1.10.2 Instrumental . . . 17
1.11 Additional Gravity Measurements in Britain . . . 18

2 Ocean Loading 19

2.1 Earth Tides, Ocean Tides and Ocean Loading . . . 19
2.1.1 Tidal Potential . . . 19
2.1.2 Harmonic Tidal Constituents . . . 22
2.1.3 The Response of the Earth . . . 23
2.1.4 The Earth Tide Effect on Gravity . . . 23
2.1.5 Ocean Tides . . . 24
2.1.6 Ocean Loading and Effects on Gravity . . . 25
2.2 Methods of Ocean Loading Calculations . . . 25
2.2.1 The Spherical Harmonic Expansion Method . . . 25
2.2.2 The Convolution Method . . . 26
2.3 Ocean Tide Models . . . 27

2.4 Problems With and Improving Ocean Loading Calculations 30
2.4.1 The Potential Effect Of Grid Misfitting 30
2.4.2 Model Used For Ocean Loading Calculations 33
2.4.3 Previous Tidal Gravity Loading Results Using CONMODA 35
2.4.4 The Interpolation Routine 35
2.4.5 Shortcomings of the Routine 39

3 Air Pressure and Groundwater **40**
3.1 Air Pressure Effects on Gravity 40
3.2 Correcting Gravity for Air Pressure 41
3.3 Groundwater Effects on Gravity 43
3.4 Correcting Gravity for Groundwater Effects 44
3.5 Computing a Frequency Dependent Admittance 45
3.6 The ETERNA Tide Data Processing Software 46
3.7 Earth-Tide Gravity Data 47
3.7.1 Earth-Tide Gravity and Meteorological Data Sets 47
3.7.2 Examination of Earth-Tide Data 50
3.7.3 Constant Admittance Results for Air Pressure 51
3.7.4 Frequency Dependent Admittance Results for Humidity 52
3.7.5 Frequency Dependent Admittance Results for Air Pressure 53
3.7.6 Frequency Dependent Admittance Results for Rainfall 58
3.8 Absolute Gravity Data 60
3.8.1 Absolute Gravity Measurements at Bidston 60
3.8.2 Borehole Measurements at Bidston 61
3.8.3 Potential Gravitational Attraction Effect From Rainfall at Bidston . . 64
3.8.4 Examination of Bidston Rainfall Data 69
3.8.5 Constant Admittance Results for Air Pressure 71
3.8.6 Frequency Dependent Admittance Results for Rainfall 71
3.9 Conclusions 72

4 FG5 Instrumental Effects **74**
4.1 Laser Lock Shifts 74
4.1.1 Lock Shift Detection Using Voltages 75
4.1.2 Lock Shift Detection Using Gravity Values 76
4.2 Comparator Response 79
4.3 Rubidium Frequency Reference Drift 79
4.4 Residuals 80
4.5 Representing Residuals With Damped Sinusoids 81
4.6 Residual Structure Caused by the Scalar Counter 84
4.7 Variation of Residuals Between Sites 86

4.8 Variation of Residuals Between Instruments 91
4.9 Variation of Residuals With Time 92
4.10 Catch Phase 94
4.11 Intercomparison Between FG5-103 and FG5-101 94
4.12 Intercomparison Between FG5-103 and FG5-202 95
4.13 Conclusions 96

5 Absolute Gravity Results **98**
5.1 FG5 Data Processing 98
5.1.1 Equations of Motion 99
5.1.2 Solving for g 100
5.1.3 Corrections 102
5.1.4 Statistics 103
5.2 History of FG5-103 104
5.3 Vertical Gradients 105
5.4 Results of Ocean Loading Improvements 106
5.5 Aberdeen Results 111
5.6 Bidston Results 111
5.7 Edinburgh Results 115
5.8 Herstmonceux Results 116
5.9 Lerwick Results 116
5.10 Newlyn Results 117
5.11 Taunton Results 117
5.12 Wick Results 119
5.13 Summary of Gravity Values 119

6 British Precise Gravity Network **120**
6.1 Gravity Networks 120
6.2 The Establishment of the BPGN 121
6.3 Data Reduction and Analysis 125
6.4 New Relative Data 126
6.4.1 South West England 126
6.4.2 South East England 127
6.4.3 North Scotland 127
6.5 New Absolute Data 128
6.5.1 Revised Values at Earlier Sites 128
6.5.2 Additional Absolute Sites 128
6.5.3 Ex-Centres 128
6.6 Ocean Loading 129
6.6.1 Ocean Loading Correction 129

6.6.2 Effect of Ocean Loading Improvements 129
6.7 Comparison of Relative and Absolute Values 130
6.7.1 Inconsistency Between Relative and Absolute Values 130
6.7.2 Network Adjustment Without Constraint in the South 132
6.7.3 Network Adjustment With Non-Linear Scale Factors 134
6.7.4 Errors in Absolute Gravity Constraints 138
6.8 Comparison of Network Adjustment Results 138
6.9 Discussion 139

7 Conclusions **142**
7.1 Ocean Loading 142
7.2 Air Pressure and Groundwater 143
7.2.1 Earth-Tide Gravity Data 143
7.2.2 Absolute Gravity Data 143
7.3 Absolute Gravimetry 144
7.4 Relative Gravimetry 145

A Ocean Tide Model Interpolation Routine **147**
A.1 The Coastline Database 147
A.2 Arrangement of Coastline Database Files 149
A.3 Extension Of The Model At The Coast 151
A.4 Subdivision Of Grid Cells 151
A.5 Determination Of Whether A Cell Is 'Dry' Or 'Wet' 151
A.6 Coast Factor and Station Factor 152
A.7 Method of Interpolation 153
A.7.1 Bilinear Interpolation 153
A.7.2 2-D Polynomial Interpolation 154

B Ocean Loading Components **155**

C FG5-103 Results **163**

D BPGN Site Gravity Values **174**

List of Tables

1.1 FG5 uncertainty budget estimate. 12

2.1 Details of ocean tide models. 30
2.2 Effect of changing the Coast Factor. 36
2.3 Effect of changing the Station Factor. 36
2.4 The effect of re-interpolation. 37
2.5 Comparison of bilinear and polynomial interpolation results. 37
2.6 Effect of changing the number of iterations. 37

3.1 Amplitude factor and phase values from ETERNA for ET10 at Bidston. . . . 48
3.2 Constant air pressure admittances for Bidston and Edinburgh. 51
3.3 Monthly rainfall totals for Bidston, 1994 - 1996. 64
3.4 Gravitational attraction of a thin plate. 65
3.5 Gravitational attraction of a thin disc. 66
3.6 Effect of changing the depth and radius of the thin disc. 66
3.7 Gravitational attraction of a cylinder. 67
3.8 Correlation between gravity and rainfall at Bidston. 69

4.1 Iodine laser wavelengths and effect on gravity through lock shift. 75
4.2 Example of 1F voltages. 76
4.3 Rubidium oscillator calibration details for FG5-103. 80
4.4 Scalar counter effect residual frequencies and their gravity change. 86
4.5 Damped sinusoids in the residuals of POL1007A. 89
4.6 Damped sinusoids in the residuals of MAC2107A. 89
4.7 Damped sinusoids in the residuals of FG5-101 and FG5-103. 93
4.8 Damped sinusoids in the residuals of POL0508A. 93
4.9 Results of comparison between FG5-103 and FG5-101. 95
4.10 Results of comparison between FG5-103 and FG5-202. 96

5.1 Summary of servicing and changes made to FG5-103 since 1994. 105
5.2 Linear gradients and vertical transfers for absolute sites. 106
5.3 Gravity changes when fitting 140 or 165 fringes with REPLAY. 114

5.4 Gravity values for the absolute sites of Britain. 119

6.1 List of BPGN sites. 123
6.1 Continued list of BPGN sites. 124
6.2 Ex-centre ties to BPGN absolute gravity sites. 129
6.3 Adjustment of BPGN with old and new ocean loading correction. 130
6.4 Scale factors obtained with no absolute constraint in the south. 132
6.5 Network adjustment with no absolute constraint in the south. 134
6.6 Expected periodic errors of G275 and D145. 135
6.7 Coefficients of polynomials used for non-linear scale factors. 135
6.8 Network adjustment with non-linear scale factors. 137

A.1 Inputs required for the ocean tide model interpolation routine. 147
A.2 Effect of changing the number of points to determine wet/dryness. 153

B.1 Ocean loading for sites Aberdeen - Daresbury, components M_2 - P_1. 156
B.2 Ocean loading for sites Aberdeen - Daresbury, components K_2 - $2N_2$. 157
B.3 Ocean loading for sites Dornie - Malvern, components M_2 - P_1. 158
B.4 Ocean loading for sites Dornie - Malvern, components K_2 - $2N_2$. 159
B.5 Ocean loading for sites Methven - Taunton, components M_2 - P_1. 160
B.6 Ocean loading for sites Methven - Taunton, components K_2 - $2N_2$. 161
B.7 Ocean loading for sites Towcester - Wylam, components M_2 - P_1. 162
B.8 Ocean loading for sites Towcester - Wylam, components K_2 - $2N_2$. 162

C.1 FG5-103 DDT results at Aberdeen. 164
C.2 FG5-103 DDT results at Bidston. 165
C.3 FG5-103 DDT results at Bidston continued. 166
C.4 FG5-103 REPLAY results at Bidston. 167
C.5 FG5-103 REPLAY results at Bidston continued. 168
C.6 FG5-103 REPLAY results at Bidston continued. 169
C.7 FG5-103 REPLAY results at Bidston continued. 170
C.8 FG5-103 DDT results at Edinburgh. 171
C.9 FG5-103 DDT results at Herstmonceux. 171
C.10 FG5-103 DDT results at Lerwick. 172
C.11 FG5-103 DDT results at Newlyn. 172
C.12 FG5-103 DDT results at Taunton. 173
C.13 FG5-103 DDT results at Wick. 173

D.1 BPGN site gravity values, Aberdeen - Chapel Haddlesey. 174
D.2 BPGN site gravity values, Crianlarich - Sproughton. 175
D.3 BPGN site gravity values, St. John Commandery - Wylam. 176

List of Figures

1.1 Planetary deformation processes. 3
1.2 Limit of ice sheet at the last glacial maximum. 4
1.3 Estimated vertical crustal movement in Great Britain. 5
1.4 Trends of UK mean sea level. 7
1.5 Schematic diagram of FG5 absolute gravimeter. 11
1.6 Schematic diagram of LaCoste & Romberg relative gravimeter. 14

2.1 Configuration of point P on the Earth's surface relative to celestial body B. . . 20
2.2 Illustration of declination δ, latitude ϕ and hour angle H. 22
2.3 AG95.1 tide model M_2 harmonic and tide gauge observations. 29
2.4 Illustration of the misfit of ocean tide model grid boxes to irregular coastlines. 31
2.5 Dimensions of half ring of water. 32
2.6 Direct vertical attraction versus height of a half ring of water. 33
2.7 Direct vertical attraction versus outer radius of a half ring of water. 34
2.8 Variable sized grid output for Newlyn. 38

3.1 Illustration of gravitational attraction of the atmosphere. 41
3.2 Raw Earth-tide gravity data. 48
3.3 Bidston Earth-tide gravity and meteorological data sets. 49
3.4 Variation of constant air pressure admittance. 52
3.5 Humidity corrected Earth-tide data. 53
3.6 Air pressure corrected Earth-tide gravity data. 54
3.7 Air pressure frequency transfer functions. 55
3.8 First half of Earth-tide data corrected for air pressure. 56
3.9 Second half of Earth-tide data corrected for air pressure. 57
3.10 Earth-tide data corrected for humidity and air pressure. 58
3.11 Earth-tide data corrected for humidity, air pressure and rainfall. 59
3.12 FG5-103 absolute gravity observations at Bidston. 60
3.13 Corrected FG5-103 absolute gravity observations at Bidston. 61
3.14 Borehole water table measurements at Bidston. 62
3.15 Water table level corrected for air pressure. 63

3.16 Set up of the thin circular disc model. 66
3.17 Set up of the cylinder model. 67
3.18 Rainfall and gravity at Bidston. 70
3.19 Absolute data corrected for varying constant air pressure admittance. 70
3.20 Absolute data corrected for rainfall. 72

4.1 Temperature and laser 1F voltage for POL2801A and WET3009A. 77
4.2 Simulated comparator response gravity changes. 79
4.3 Error in estimate of damped sinusoids in residuals: low frequencies. 83
4.4 Error in estimate of damped sinusoids in residuals: high frequencies. 84
4.5 FG5-103 residuals from POL1402A and POL1605A. 85
4.6 Gravity change when fitting damped sinusoids: low frequencies. 87
4.7 Residuals of POL1007A, MAC2107A and POL0508A. 88
4.8 Gravity change when fitting damped sinusoids: high frequencies. 90
4.9 Cut off tests for POL1007A and MAC2107A. 91
4.10 Residuals of WEZ96325 (FG5-101) and WET2111A (FG5-103). 92

5.1 Frequency of points recorded at each fringe number in POL1402A. 102
5.2 Ocean loading correction changes applied to NEW1010A. 108
5.3 Ocean loading correction changes applied to TAU1710A. 109
5.4 Ocean loading correction changes applied to LER2907A. 110
5.5 FG5-103 DDT results at Aberdeen. 111
5.6 FG5-103 REPLAY and DDT results at Bidston. 112
5.7 Frequency of fringe number at fringe index 145 in POL0301A. 113
5.8 Corrected FG5-103 REPLAY results at Bidston. 114
5.9 FG5-103 DDT results at Edinburgh. 116
5.10 FG5-103 DDT results at Lerwick. 117
5.11 FG5-103 DDT results at Newlyn. 118
5.12 FG5-103 DDT results at Taunton. 118

6.1 Map of BPGN sites. 122
6.2 Comparison of relative and absolute gravity values. 131
6.3 Relative and absolute differences for G275 and D145. 133
6.4 Relative and absolute differences of adjustment with no constraint in the south. 134
6.5 G275 and D145 differences from absolute values versus dial turns. 136
6.6 Relative and absolute differences for adjustment with non-linear scale factors. 137
6.7 Difference in site values between adjustments without constraint in the south and non-linear scale factors. 139
6.8 BPGN site gravity values. 141

A.1 Flow diagram of the ocean tide model interpolation routine. 148

A.2 Hierarchical arrangement of coastline database files. 150
A.3 Extension of grid cells on to the land. 151
A.4 Division of grid cells. 152
A.5 Determining wet/dryness of grid cells. 152

Chapter 1

Introduction

This thesis is concerned with improving high precision measurements of gravity. One of the potential applications of high precision gravimetry is monitoring vertical crustal movements. If sufficient long term accuracy can be achieved, it could remove land movements from tide gauge data and so have an important application in the determination of mean sea level change.

Gravimetry may also be applied in a geological context. The gravity value observed at a particular site is compared to the value predicted using a model of the Earth whose density does not vary laterally. The difference between the two values (the Bouguer anomaly) can provide information on the density of subsurface material. For this application the precision of measurements needed is 30 μgal (Telford *et al.*, 1990) (1 μgal = 10^{-8} m s^{-2}).

The research presented in this thesis concentrates on the use of high precision gravimetry to detect vertical crustal movements and sea level change. This application requires a precision of at least 2 μgal (Baker, 1993).

This introduction gives a review of evidence for vertical crustal movement from effects of isostasy and relative sea level change. Findings from the British Isles presented will emphasise the need to monitor land movements. Different techniques of measuring vertical crustal movement are outlined.

High precision gravity measurements can be made with absolute and relative instruments. I have developed techniques with the aim of improving the precision of gravity measurements by removing instrumental and environmental effects. Details of mechanisms causing these are described. An outline of work done in Britain with the establishment of the British Precise Gravity Network (BPGN) gives the current state progress of in this area. I have extended the BPGN to include more sites and make it better constrained. Methods described in this thesis can be applied to all gravity measurements and are not just specific to Britain.

1.1 Isostasy

Isostatic models predict the effect of a loading on the Earth's crust and its consequent deformation. One cause of this is from loading of ice sheets during periods of glaciation. Figure 1.1 relates various mechanisms causing a deformation of the Earth's crust with their time and length scales. It can be seen that glacial isostatic adjustment or rebound occurs over regions of 100 - 10 000 km and periods of 1 - 10 000 millenia. The principal mechanism causing vertical crustal movement in the British Isles is glacial rebound.

During a glacial cycle, ice accumulates over parts of the Earth's surface. In these areas the Earth's crust flexes under the weight of the ice load and is depressed which causes a flow of viscous material under the crust. This is displaced away from the region of compression to the surrounding area causing an elevation of the crust known as the 'peripheral bulge'. When the loading of the ice disappears the process is reversed - the depressed area rises and the periphery sinks (Peltier, 1990).

Lambeck (1993) summarises the evidence detailing the extent to which Britain was covered by ice during the last glacial cycle and produces an ice-sheet model. This is shown in Figure 1.2 for the maximum extent of ice 22 ka BP. The ice covers almost all of Scotland and extends down into southern Ireland, Wales and northern England. He assumes that the North Sea was largely ice free due to evidence that the British ice sheet terminated at the Wee Bankie Moraine off the east coast of Scotland and Norwegian evidence to the effect that the North Sea was an ice-free corridor. The Shetland Islands are assumed not to have been covered by the British or Scandinavian ice sheets - evidence of glacial action there has been interpreted as the effects of a local ice sheet or previous glacial cycle. The ice sheet is assumed to have disappeared by 10 ka BP.

1.2 Relative Sea Level Change

Historical evidence of sea level can only be made relative to the land. This may be through the flora of peats and the position of inter-tidal and shallow water marine mollusc fossils (Lambeck, 1993). Also geomorphological evidence such as raised beaches and erosional features (*eg* shingle beaches, rock platforms) (*ibid.*), sedimentology and radio carbon dating provide evidence.

Figure 1.3 shows estimates of vertical land movements taken from Shennan (1989). This has been compiled using observations of crustal movements and sea level change for the past 8800 years. One can see the land is rising in Scotland and sinking in the south east of England. This is in line with the glacial rebound expected for an ice sheet centred over Scotland. However

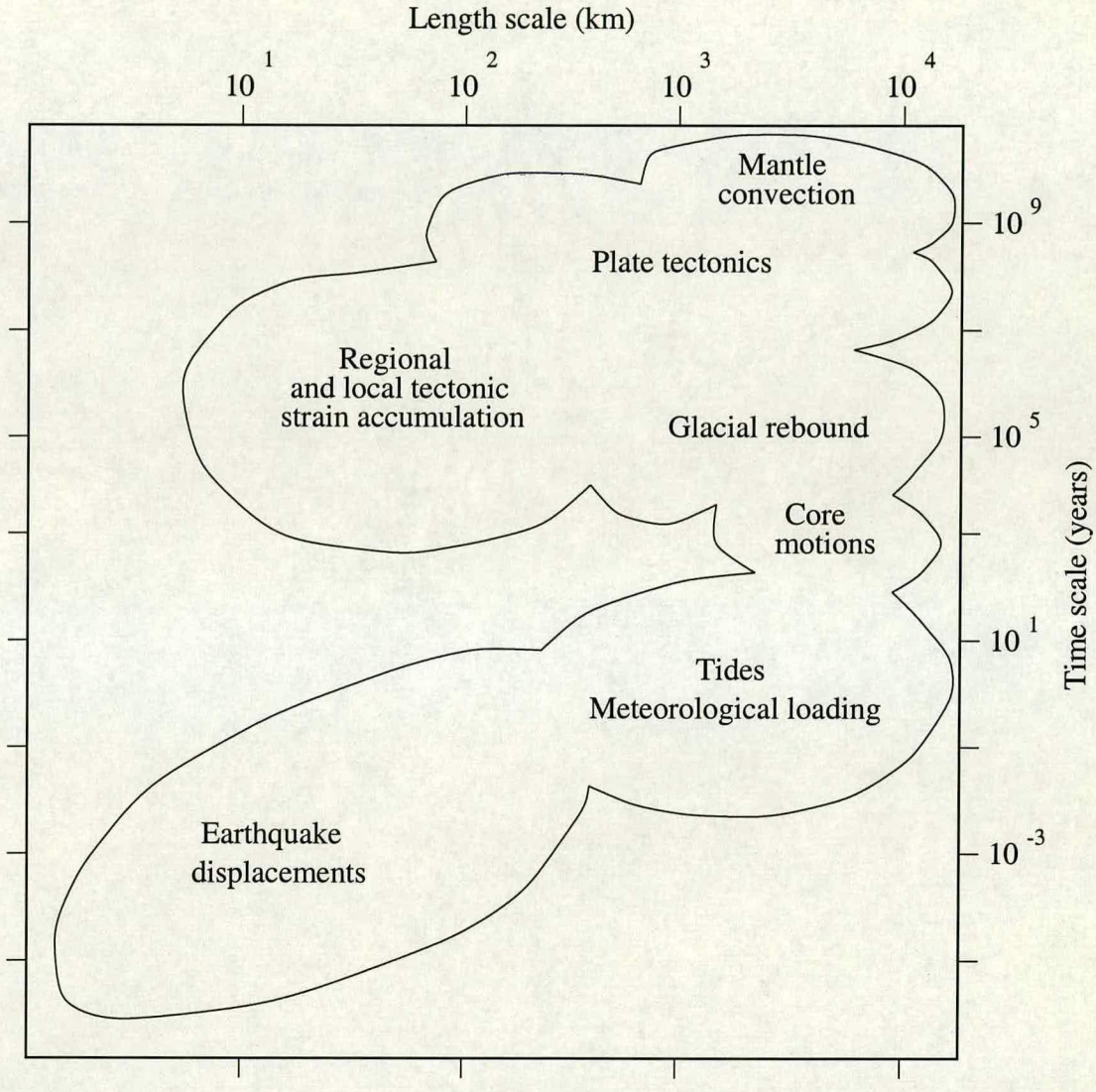

Figure 1.1. Schematic illustration of time and length scales of some planetary deformation processes (Lambeck *et al.*, 1990).

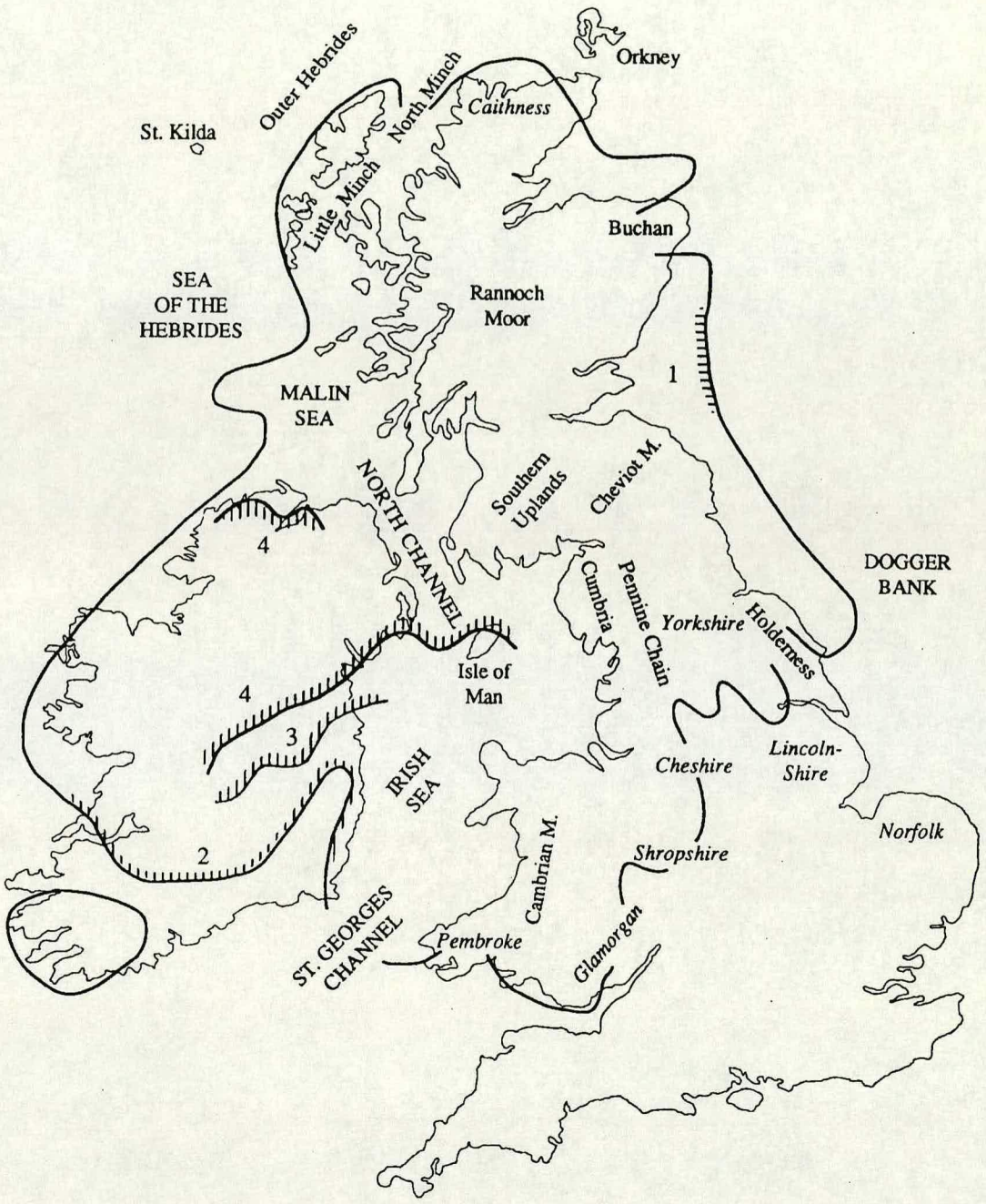

Figure 1.2. Limit of ice sheet at the last glacial maximum. Major terminal moraines are shown as: (1) Wee Bankie Moraine; (2) South of Ireland Moraine; (3) Galtrim Moraine; (4) Drumlin Readvance Moraine and its extension into the Irish Sea (Lambeck, 1993).

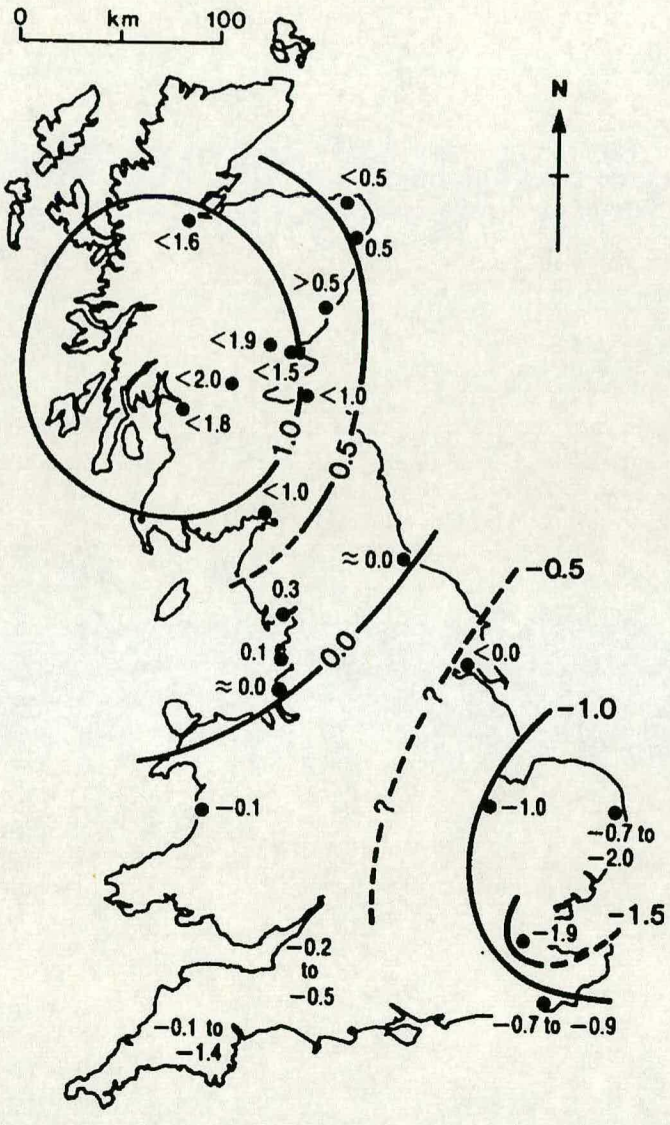

Figure 1.3. Map of estimated current rates (mm yr^{-1}) of crustal movement in Great Britain. Isolines cannot be drawn for much of southern England, point estimates are shown for guidance (Shennan, 1989).

the sinking of land in the south east may be complicated by other mechanisms such as sediment loading (*ibid.*). Because information can only be available near contemporary coastlines, crustal movements over central and south western parts of England are not well known.

More recent evidence of relative sea level change is available from tide gauge records. These vary in their geographical distribution and quality which can be compromised through periods of no measurement. Interannual and decadal variations of sea levels result in annual means having a standard deviation of 30 mm; 30 to 40 years of data are required to determine a trend in the mean sea level with a standard error of 0.5 mm yr^{-1} (Baker *et al.*, 1997).

World wide tide gauge observations have been used to determine global sea level change. Douglas (1991) restricts the tide gauge data he uses to 21 stations considered to have high quality observations resulting in an average record length of 76 years. Using a model to remove post glacial rebound, he finds the period 1880 - 1980 sees a rise in sea level of 1.8 ± 0.1 mm yr^{-1}.

Observations from tide gauges in the British Isles are reported by Woodworth *et al.* (1991). He gives trends in sea level change observed by 12 tide gauges. These were used by Charles (1995) to produce Figure 1.4. It can be seen that there is a general increase of sea level relative to land in the southern part of Britain. Scotland sees virtually no relative change of sea level, suggesting that the land is rising at a rate equivalent to that of sea level rise. Shetland shows a decrease of relative sea level implying a greater rate of elevation of the land. This calls in to question models claiming the Shetlands were not covered by ice during the last glaciation (see Section 1.1).

For the monitoring of absolute sea level, a Woods Hole Oceanographic Institute Report recommends geodetic fixing of tide gauges via a local network of benchmarks (Carter *et al.*, 1989). This should be done using spirit levelling or Global Positioning System (GPS). Further connections should be made to Satellite Laser Ranging (SLR) and Very Long Baseline Interferometry (VLBI) sites using GPS. Absolute gravity measurements should be made at the SLR/VLBI sites. See Section 1.3 for details of these methods.

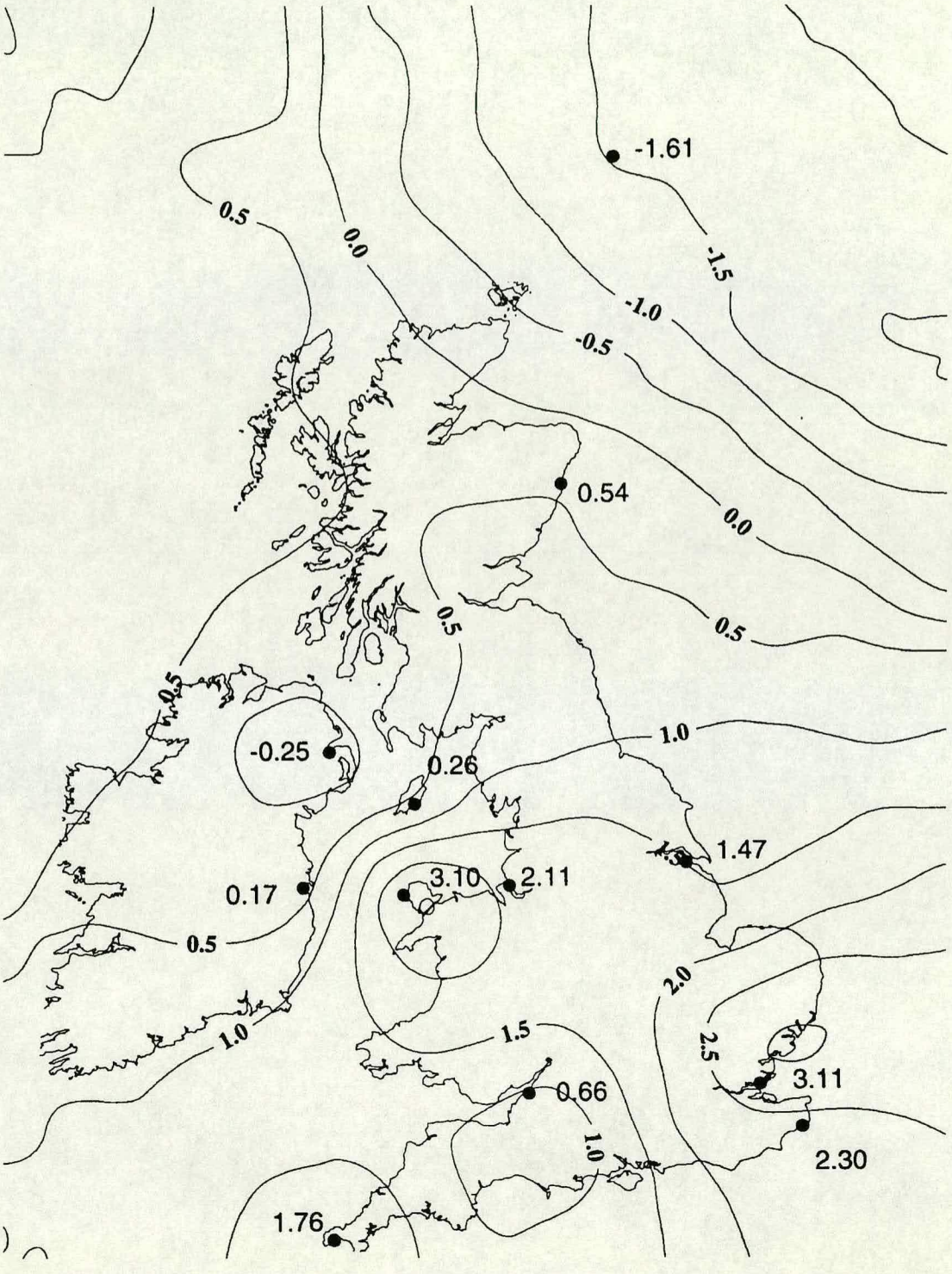

Figure 1.4. Contour map indicative of trends in UK mean sea level. The points are the secular trends in mean sea level (mm yr^{-1}) from Woodworth *et al.* (1991). Reproduced from Charles (1995).

1.3 Methods of Measuring Vertical Crustal Movement

To establish absolute sea level changes with land used as a reference frame, it is necessary to monitor and remove vertical crustal movement. Historically spirit levelling was used with the disadvantage that this can only distinguish vertical movements of points relative to each other. Knowledge of movement of the entire network of measurement points with respect to an external reference cannot be established. The last survey of Britain using this technique took place from 1951 - 59.

Technological advances have resulted in geodetic techniques now being used to measure vertical crustal movements. Space geodetic methods account for the majority of these. Satellite Laser Ranging and Lunar Laser Ranging (LLR) measure the time taken for a laser beam to reach a satellite / the Moon and reflect back. Very Long Baseline Interferometry involves a network of radio telescopes simultaneously monitoring extra-galactic radio sources. The time delays in the radio signals recorded by the telescopes are used to calculate their relative positions. These three techniques are coordinated by the International Earth Rotation Service (IERS). They have a vertical resolution of about 1 cm and have detected vertical motions to within 1 mm yr^{-1} (*pers. comm.* Baker, 16th Nov. 1999).

The Global Positioning System incorporates 21 satellites, their orbits being such that at least 4 are above the horizon at any time. The satellites emit signals at two frequencies. A network simultaneously monitoring the phases of these signals can achieve a relative positioning at the centimetric level over baselines up to 1000 km (Baker, 1993). Results can be affected by meteorological conditions - dry cloudless conditions are the best. GPS can detect vertical movements to an accuracy of 1 mm yr^{-1} after 5 years of measurements (Baker *et al.*, 1997).

The laws of gravity state that the strength of gravitational attraction between two masses is inversely proportional to the square of the distance between them. Thus gravity may be used to monitor vertical crustal motion since changes in the elevation of land perturb the distance from the surface to the centre of the Earth. The following sections outline the concepts and background of using gravity for this purpose.

1.4 Gravity as a Method to Measure Vertical Crustal Movement

The relationship between gravity and vertical displacement was examined by Ekman and Mäkinen (1994). It should take on a value between two theoretical extremes. One case models crustal uplift with the full addition of mass in the upper mantle in the form of an infinite plate. This is known as the 'Bouguer model' and may be written as:

$$\left(\frac{dg}{dh}\right)_B = \frac{2g}{R} + 2\pi G\rho = -1.7\mu\text{gal cm}^{-1} \tag{1.1}$$

where R is the radius of the Earth, G is the gravitational constant and ρ is the density of mantle (3.3 Mg m^{-3}).

The opposite extreme is the 'free air model' where no addition of mass is assumed. This is expressed as:

$$\left(\frac{dg}{dh}\right)_f = \frac{2g}{R} = -3.1\mu\text{gal cm}^{-1} \tag{1.2}$$

In practice the relationship is assumed to be of the order of -2 μgal cm^{-1} (Baker, 1993). It should be noted that the exact value depends on the density of subsurface material.

Gravity measurements are made in two ways - relative and absolute. When monitoring vertical crustal movement, relative gravimeter observations can give only a temporal change in gravity between two sites. Absolute observations measure the actual value of gravity at a given site. Relative gravity measurements involve less time and use more portable equipment. Hence gravity surveys usually involve the establishment of a network of relative observations with links to some absolute sites as a constraint on values.

For the purpose of providing a geodetic fix to tide gauges, it has been recommended that gravity sites should be situated at least 1 km inland (Carter *et al.*, 1989). This should reduce the seismic noise from surf action and the varying gravitational attraction of sea water which impair the accuracy achievable. This thesis examines the accuracy with which ocean tide effects on gravity can be computed, thus enabling gravity sites to be situated closer to tide gauges.

1.5 Absolute Gravimetry

Early absolute gravity measurements were made using a pendulum, a method which is now obsolete. The technique used since is observation of the gravitational acceleration of a mass, either in a rise and fall or drop-only motion. Measurement of distance is typically made using a laser interferometer. A summary of attempts at absolute gravimetry measurements using this method is given by Charles (1995).

The most successful results from rise and fall methods are by Sakuma of the Bureau International des Poids et Mesures (BIPM) (1 - 10 μgal precision), the Instituto di Metrologia 'G.

Colonnetti' instrument (1 μgal precision, < 5 μgal reoccupation accuracy) and the commercial French Jaeger GA60 instrument (standard deviation < 10 μgal).

Considerably better results have been obtained with drop-only instruments. Six instruments produced by the Joint Institute for Laboratory Astrophysics (JILA) were developed in 1980. They have a precision of 1 - 5 μgal and an accuracy of 3 - 10 μgal. An improved design was incorporated into the FG5 gravimeter, which is described in more detail in the following section.

1.6 The FG5 Absolute Gravimeter

The FG5 is a commercial free fall absolute gravimeter. Produced by Micro-g Solutions Inc. (formerly AXIS Instruments) in Boulder, Colorado, it has been available since 1991. Absolute gravity measurements used in this research have been obtained by FG5 gravimeters, most of which were taken by series number 103. This instrument (FG5-103) is owned by the Natural Environment Research Council and based at Proudman Oceanographic Laboratory (POL), Bidston, UK. It was delivered in 1992.

This section aims to provide an overview of how the FG5 works (Niebauer *et al.*, 1995).

Figure 1.5 shows a schematic diagram of the FG5. The device incorporates a 'modified Mach - Zender' interferometer. A laser beam is split in two to give a measuring beam and a reference beam. The measuring beam is reflected off the free falling mass and a second mass acting as an inertial reference. The measuring beam is then recombined with the reference beam. As the mass drops, the path length of the measuring beam changes and so a moving pattern of interference fringes appear in the recombined beam.

Recording the occurrence of fringes against a clock gives the position of the mass as a function of time. For data used in this research, a time is generated every 4000 fringes, corresponding to the mass travelling 2000 wavelengths, about 1.3 mm. Each record is known as a 'scaled fringe'; a time-distance data pair. Up to 200 scaled fringes were recorded per drop, which corresponds to a drop length of about 0.2 m lasting 0.2 s. The data pairs are fitted to a model equation of motion to obtain a value of gravity. Later versions of the instrument record scaled fringes at a greater frequency. FG5-103 was modified in March 1999 (see Table 5.1) to record about 700 scaled fringes per drop. No data produced by FG5-103 since this change has been used in this research. From here onwards a 'scaled fringe' will be referred to as a 'fringe'.

The instrument typically executes one drop every 10 seconds. Normally 200 drops are performed, known as a 'set', after which the instrument then rests before commencing the next set an hour after the previous one started. Usually 24 sets are recorded for each data run. The methods used for data processing are covered in Section 5.1.

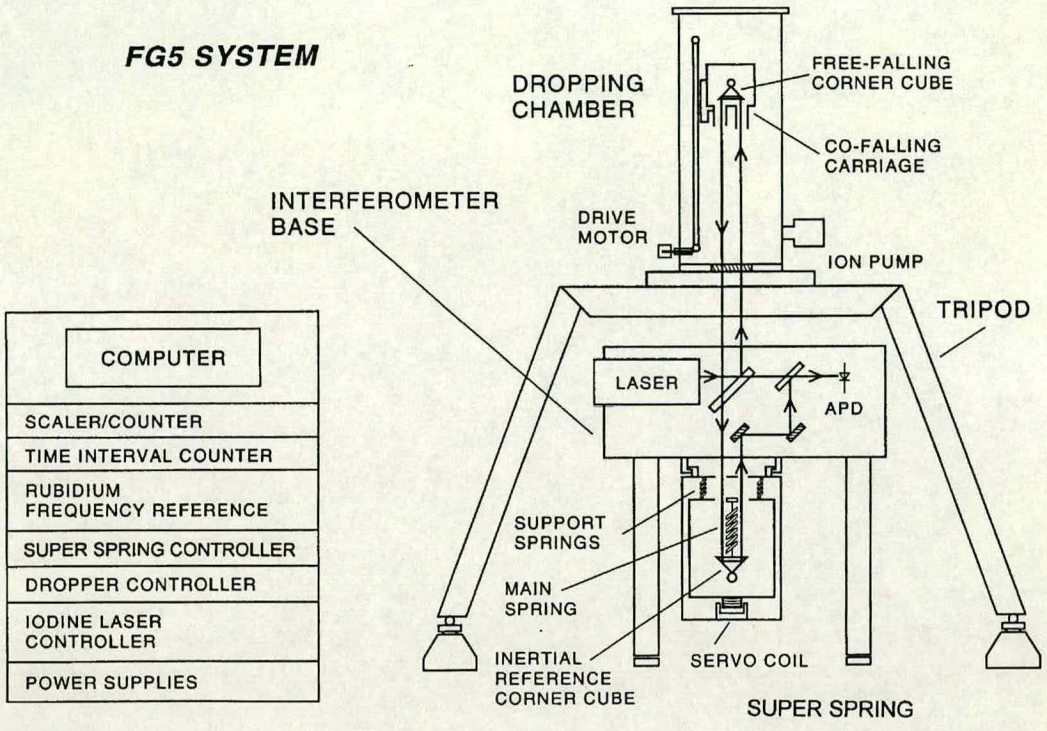

Figure 1.5. Schematic diagram of key systems in the FG5 absolute gravimeter (Niebauer *et al.*, 1995).

The mass is a corner cube reflector located inside a 'carriage' within an evacuated dropping chamber. The carriage falls with the mass by initially accelerating at a rate slightly above g and then maintaining a set distance between itself and the mass. This acts to reduce the effect of drag from residual air molecules on the mass since they will also be in freefall in the carriage. It also shields the mass from external electromagnetic forces since the carriage is conductive, and allows a gentle 'catch' of the mass at the end of the drop (see Section 4.10). Two holes in the bottom of the carriage allow the measuring beam to enter. The dropping chamber itself is held at a pressure typically about 1 μtorr (1.3×10^{-4} Pa) using an ion pump. An optical window at the base of the dropping chamber allows the measuring beam to enter.

The interferometer base is separate and has no physical contact with the dropping chamber. It houses the laser, optical components and avalanche photodiode detector (APD) for monitoring the fringes. This drives a high speed signal comparator which generates digital pulses that are sent to a separate electronics rack.

The laser provides the length standard. Two types of laser have been used on the FG5 system - a polarisation stabilised and an iodine stabilised type. The former type suffers from drift of the wavelength and has been superceded by the latter. The iodine stabilisation works by locking on to one of the highly stable absorption peaks of hyperfine components of $^{127}I_2$. Frequencies

Error source	Uncertainty / μgal	Comments
Residual air pressure	0.1	Pressure dependent
Differential temperature	0.1	Temperature and pressure dependent
Magnetic field gradient	0.1	Difficult to estimate
Electrostatics	0.1	Difficult to estimate
Attraction of apparatus	0.1	Fixed bias in instrument design
Verticality	0.1	Operator dependent, always negative
Air gap modulation	0.6	Set up dependent
Laser wavelength	0.1	Iodine stabilised laser only
Corner cube rotation	0.3	Can degrade with time
Coriolis effect	0.4	Strong latitude and set up dependence
Floor recoil and tilt	0.1	Site dependent
Electronic phase shift	0.6	
Frequency standard	0.2	
Glass wedges	0.3	
Diffraction limit	0.2	Laser system dependent
Total uncertainty	1.1	RSS uncertainty estimate

Table 1.1. FG5 uncertainty budget estimate (Niebauer *et al.*, 1995).

of these modes are known to an absolute accuracy of 2.5 parts in 10^{11}.

Attached to the interferometer base is the super spring which contains the inertial reference mass. This is a corner cube reflector suspended by a spring inside a casing. The casing itself is suspended by three springs. Servo electronics create a force feedback to remove ground acceleration from the casing before it is transmitted to the reference mass. In this way effective periods of over 60 s are achievable.

The electronics rack contains devices to control the dropping chamber, laser, super spring and a personal computer which initiates measurements and performs data processing. The rack also holds the interval counter to measure the time between fringes. A rubidium oscillator provides the time standard. This is subject to drift and needs to be calibrated against a known standard at regular intervals (see Section 4.3). An accuracy of 1 part in 10^{10} can be maintained if this is done frequently.

A breakdown of the uncertainty estimate of the FG5 system is given in Table 1.1, taken from Niebauer *et al.* (1995). The total uncertainty gives rise to an internal accuracy of 1.1 μgal. This is based on calculations of known physical effects that degrade the instrument accuracy. Since this is in cases difficult to estimate and may not include an unrecognised effect, it is subject to future revision.

BIPM hosted the fourth International Comparison of Absolute Gravimeters in 1994 (ICAG94) in which 12 instruments participated including 7 FG5's. Results presented by Marson *et al.*

(1995) showed a standard deviation of 3.3 μgal for all instruments and 2.8 μgal if only FG5 instrument results are selected. This shows that whilst the level of agreement was good, it does not concur with the estimated internal accuracy. Reasons may be due to instrumental problems or operator error. Note that FG5-103 did not participate in ICAG94. Provisional results from the more recent ICAG97 in which the author took part with FG5-103 still give a standard deviation of about 3 μgal over results from about 10 FG5 and JILA instruments (L. Robertsson, paper presented at IAG Workshop, Trieste, 1998).

1.7 Relative Gravimetry

Methods of taking relative gravity measurements are varied. Techniques used include pendulum / inverted pendulum, vibrating string, spring balance and superconducting instruments. The lever spring balance system has found the most widespread use for portable instruments. It can achieve a precision as good as 1 μgal for gravity differences between sites depending on the magnitude of the difference and the time between measurements. Results used in this research are from LaCoste & Romberg instruments, which are of the spring balance type (see Section 1.8 for details).

Superconducting gravimeters are manufactured by GWR Instruments. They use a superconducting sphere levitated by persistent currents in superconducting coils. The vertical position of this coil is dependent on gravity changes which is measured using a capacitance bridge. This set up is located in a vacuum chamber immersed in liquid helium to maintain a low temperature (Carter *et al.*, 1989).

Superconducting gravimeters have the advantage of a low drift rate compared to spring balance systems. As a consequence they are able to detect gravity changes of 0.1 μgal over day or week long periods. The drift rate can differ between instruments; it has been noted to vary from 3 to 21 μgal per year (*ibid.*). This type of instrument is useful for monitoring both tidal and non-tidal gravity changes at a particular site over long periods. In particular, it can detect semi / annual tidal periods and secular gravity changes such as those caused by groundwater.

1.8 The LaCoste & Romberg Relative Gravimeter

Available for use in this research were three LaCoste & Romberg relative gravimeters. These were one Model G (G275) and two Model Ds (D145, D154), owned by the Department of Geology & Geophysics, University of Edinburgh. Also available were data from a LaCoste & Romberg Earth-tide gravimeter. This is essentially of the same design as the relative gravimeters of the same company. This section aims to provide an overview of how the LaCoste & Romberg gravimeter works.

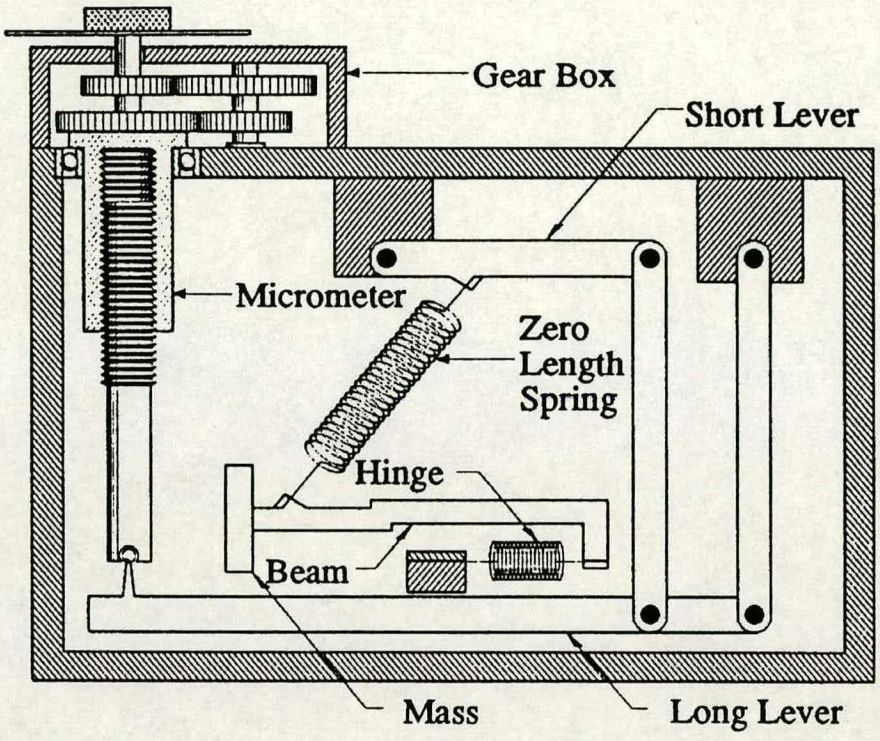

Figure 1.6. Main features of the LaCoste & Romberg relative gravimeter. Reproduced from LaCoste & Romberg Gravity Meters Inc. (1989).

This is a spring balance type of instrument, the design of which was first seen in 1937. Figure 1.6 is a simplified diagram of the main features. The instrument incorporates a 'zero length spring'. This is so called because in the extension range where it is used, a graph of its extension versus force applied extrapolates to pass through the origin, corresponding to an initial or unstretched length of zero. The spring suspends one end of a beam with a mass attached to it. The other end of the beam is fixed via a frictionless hinge. The spring is at an angle of about 45 degrees and the top of the spring may be raised or lowered.

A balance condition will be reached when the torque exerted on the beam from the force of extension of the spring equals the torque in the opposite sense from the weight of the mass. Torque is the product of force and perpendicular distance from the pivot. Under the balance condition, should the mass lower, the extension of the spring will increase with a corresponding rise of the force. At the same time, the perpendicular distance from the spring to the beam pivot will decrease. This is a state of neutral equilibrium that is only achievable for a particular position of the top of the spring.

The raising and lowering of the spring is done via a set of levers. These are moved by rotation of a dial which operates a micrometer screw through a gearbox with a large reduction. Model

G meters have a single dial whilst Model D meters have a coarse and fine dial, the fine dial having a greater gear reduction. There is the potential for periodic errors in measurements due to eccentricities in the gears.

The position of the beam is relayed optically through a view finder. The number of dial turns is recorded when the beam reaches a particular position - the 'reading line' as defined by the manufacturer which corresponds to the balance condition. Model D meters detect the beam position using a capacitance bridge which is output to a galvanometer, a facility which G275 does not have.

Electrostatic nulling of the beam can be made using the capacitance bridge. This involves measuring the voltage required to force the beam to the reading line. Gravity can be calculated as a function of the voltage and number of dial turns. D154 was upgraded during this research to incorporate electrostatic nulling by Zero Length Springs Inc..

The instruments are calibrated in a relative sense by the addition of masses to the end of the beam. This results in a table relating the number of dial turns to a relative value of gravity. The calibration table for each instrument is unique. In addition, a conversion factor to an absolute scale is necessary by measurement on a network of known gravity values.

1.9 Gravity Measurements in Britain

Charles (1995) gives a history of gravity measurements in Britain. The National Gravity Reference Net 1973 (NGRN73) was established along primary geodetic levelling lines. It is composed of Ordnance Survey Fundamental Benchmarks (FBMs) and uses relative measurements made between 1964 - 68 controlled by the 'Airport Net' of 1971 (Masson Smith *et al.*, 1974). Formal errors ranged from 20 to 70 μgal. However, these values are not precise enough to be used in the detection of vertical crustal movements. Also the sites were not formally protected - some have been destroyed and some 'not found' on subsequent visits.

The British Precise Gravity Network 1993 (BPGN93) was established with the aim of providing a reference for future observations of vertical crustal movement in Britain (Charles and Hipkin, 1993; Charles, 1995). A network of 58 sites was established. The sites were chosen subject to the criteria of being stable, having a long ($>$ 30 years) expected lifetime and good accessibility. Measurements were made with three LaCoste & Romberg relative gravimeters.

The network was constrained by FG5 absolute gravimeter observations at three sites. The absolute values used were derived from early data by FG5-103. This instrument has since undergone upgrades and data produced by it since 1995 is considered more consistent and reliable (see Chapter 5).

The three absolute sites enabled linear scale factors to be found in BPGN93 relating the relative to the absolute scale. Three sites are not sufficient to investigate potential non-linear scaling factors which may be caused by periodic errors in the relative gravimeters.

Ocean loading corrections in BPGN93 subtracted only the M_2 term which was derived from an early ocean tide model and did not incorporate site altitude in to the calculations. With the advent of TOPEX/POSEIDON, improved ocean tide models have been made available offering more constituents and higher resolution. Further improvements in the ocean loading effect have been made in this thesis by using site altitude and manipulation of the tide models.

The adjustment of BPGN93 resulted in a mean standard error of gravity sites values as 5 $\pm$ 1.3 μgal in the range of 2 - 8 μgal. It is expected that given evidence from tide gauges, crustal motions should be detectable in less than a decade.

1.10 Problems with Gravity Measurements

Gravity measurements are affected by environmental effects and also potential instrumental effects. These effects may vary temporally over periods ranging from minutes (*eg* attraction of Sun and Moon) to seasons (*eg* groundwater). Alternatively, they may be a fixed offset of gravity, particularly in the case of instrumental errors in absolute gravimeters.

An example of gravity variation has been observed with absolute measurements at Bidston (see Section 5.6). Here the value appears to have a periodic variation of about 8 μgal over 12 months. Understanding and removal of this variation will increase the precision of gravity measurements at this site.

Outlined in this section are some of the recognised factors that influence gravity. Where these have not been previously corrected, I have made an attempt at doing so. In the case of effects that are already corrected for, I have made an attempt at improving the method of correction.

1.10.1 Environmental

Ocean Loading

Ocean loading influences on gravity are due to the varying load of the ocean tides on the Earth's crust. These cause a deformation of the crust with a corresponding perturbation of distance from the Earth's centre and redistribution of mass. The mass of water also creates a gravity signal from its Newtonian attraction.

Ocean loading is corrected for through knowledge of ocean tides which can be obtained from models. Information is held as an array of grid cells. Global ocean tide models typically have a grid size no smaller than $0.5^o \times 0.5^o$. These grids provide a poor fit to irregular coastlines

leading to errors in the calculation of ocean loading effects. Approximation of tidal loading to a series of points also leads to errors in the calculation of their effect on gravity.

I have developed a routine which, by dividing grid cells into smaller parts and interpolating the data to these new points, creates a new grid with a good fit to a high resolution coastline data base and reduces the error in calculating loading effects represented as a series of point mass loads. Details of this are given in Chapter 2.

Air Pressure

As with ocean loading, air pressure creates a loading on the Earth's surface giving rise to similar mechanisms affecting gravity. Normally this is corrected for using barometric readings at the gravity site and assuming a fixed linear relationship or 'admittance' between air pressure and its effect on gravity.

Using some continuous gravity records covering several months, I have investigated seasonal variations of the admittance value. I have also investigated the possibility of a dependency of the admittance value on the frequency of air pressure. In both cases the results have been used to correct gravity measurements and compare with using a simple fixed linear admittance. See Chapter 3 for details.

Groundwater

Gravity measurements are in general not easy to correct for groundwater effects. In practise it is hard to ascertain the exact location, orientation and amount of water held in soil and rocks. The simplest method is to monitor water table level via a borehole.

A possible reason for an annual signal in the gravity record at Bidston is from groundwater. I have investigated ways of modelling this variation by examination of borehole and rainfall data. I compared borehole data with gravity and air pressure data. I also used rainfall data to investigate whether rainfall amounts have the potential to cause the gravity variations observed. I further calculated a frequency dependent admittance between gravity and rainfall and used it to correct the absolute data. See Chapter 3 for findings.

1.10.2 Instrumental

For BPGN93 three absolute sites were used as constraints. This enabled linear scale factors to be found for the relative gravimeters. With the addition of absolute sites to the network bringing the total up to seven sites, I have been able to investigate the need to use non-linear scale factors which may be caused by periodic errors within the relative gravimeters. Results of this can be found in Chapter 6.

I have also stated the known systematic errors of the FG5 absolute gravimeter. Investigations have been made of non-random structure in the residuals, representing the patterns as damped

sinusoids. FG5-103 has been intercompared with two other gravimeters to examine if results between these instruments are consistent. Details can be found in Chapter 4.

1.11 Additional Gravity Measurements in Britain

To provide geodetic fixes to tide gauges, absolute gravity sites have been established at Newlyn, Aberdeen, Wick and Lerwick. In addition, a site has been established at the Herstmonceux SLR base. I have been involved in observations made at these sites with FG5-103 and report on the results. I have also tested the effectiveness of improvements in ocean loading corrections (Chapter 2) to selected gravity observations. Results can be found in Chapter 5.

The BPGN93 extends to most parts of mainland Britain. However, there are a few areas with poor coverage. In particular, East Anglia has no sites. I have been involved in work which has resulted in the addition of sites in East Anglia and to provide nearby geodetic links to tide gauges at Lowestoft, Sheerness and Newlyn. Further work was also made to increase the strength of links to the south west of the network. These have been incorporated in to the adjustment of the network along with the updated absolute constraints. Results of the network adjustment can be found in Chapter 6.

Chapter 2

Ocean Loading

After a review of tides and ocean loading, this chapter describes a method of manipulating data from ocean tide models to improve ocean loading calculations near coastlines. Values obtained from ocean tide models on a coarse grid are interpolated to a finer grid of variable size near the coast.

This method was developed in collaboration with Machiel Bos, a Ph. D. student at Liverpool John Moore's University under the supervision of Prof. T. Baker at Proudman Oceanographic Laboratory.

2.1 Earth Tides, Ocean Tides and Ocean Loading

The orbital movements of the Moon with respect to the Earth and the Earth with respect to the Sun give rise to a varying gravitational attraction felt on the Earth. This causes deformation of the Earth's crust, known as the body tide, and movement of oceanic water giving ocean tides. A secondary effect of this rise and fall of water is differential loading on the crust causing further deformation, known as ocean loading. This section aims to provide an understanding of these mechanisms and their effects on gravity at the surface of the Earth.

2.1.1 Tidal Potential

Gravitational potential is defined as the amount of work required to move an element of unit mass to a point an infinite distance away from the body causing the gravity field. Consider Figure 2.1 where B represents a celestial body of mass M. The gravitational potential V caused by B at a point P on the Earth's surface is defined to be:

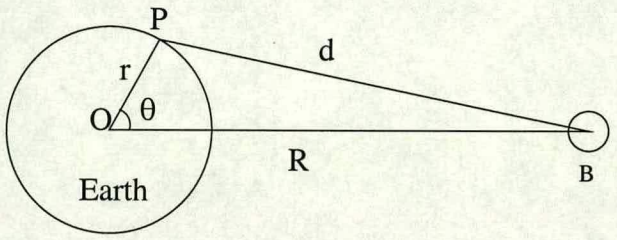

Figure 2.1. Configuration of point P on the Earth's surface relative to celestial body B.

$$V = \frac{GM}{d} \tag{2.1}$$

where G is the gravitational constant.

The cosine rule for triangle OPB states that:

$$d^2 = r^2 + R^2 - 2rR\cos\theta \tag{2.2}$$

Hence

$$V = \frac{GM}{R}\left(1 - \frac{2r}{R}\cos\theta + \frac{r^2}{R^2}\right)^{-\frac{1}{2}}. \tag{2.3}$$

Since $r/R \ll 1$, the Binomial Theorem may be employed giving the result

$$V = \frac{GM}{R}\left(1 + \frac{r}{R}\cos\theta + \frac{r^2}{2R^2}(3\cos^2\theta - 1) + \ldots\right) \tag{2.4}$$

$$= \frac{GM}{R} + W_1 + W_2 + \ldots \tag{2.5}$$

where

$$W_1 = \frac{GMr}{R^2}\cos\theta \tag{2.6}$$

$$W_2 = \frac{GMr^2}{2R^3}(3\cos^2\theta - 1). \tag{2.7}$$

The force created by the potential V is defined to be ∇V. The first term of the potential, GM/R, is constant and hence produces no forces. With the x direction defined to be the line from the centre of the Earth to the centre of the body B, W_1 produces a force

$$\nabla W_1 = \frac{\partial}{\partial x}\frac{GM}{R^2}x = \frac{GM}{R^2} \tag{2.8}$$

The magnitude of this force is independent of location and hence produces no varying forces.

The remaining terms give the tide varying potential caused by body B, W_B, which can be written as:

$$W_B = \sum_{n=2}^{\infty} W_n \tag{2.9}$$

The ratio r/R is 1/60 for the Moon and 1/23 000 for the Sun. So successive terms in (2.9) have a rapidly decreasing effect on the overall tide potential. W_2 accounts for at least 98% of the tide varying potential, and it is only necessary to consider this for the accuracy required.

Figure 2.2 shows the Earth-body system in more detail with the declination δ, latitude ϕ and hour H angles introduced. Spherical trigonometry gives the relation that

$$\cos\theta = \sin\phi\sin\delta + \cos\phi\cos\delta\cos H. \tag{2.10}$$

Substituting (2.10) into (2.7) gives

$$W_2 = \frac{3GMr^2}{4R^3}\left[\cos^2\phi\cos^2\delta\cos 2H + \sin 2\phi\sin 2\delta\cos H + 3(\sin^2\phi - \tfrac{1}{3})(\sin^2\delta - \tfrac{1}{3})\right]. \tag{2.11}$$

Each of the three terms in the brackets has a different dependence on the hour angle H giving rise to three different classes of tides. The first term contains $\cos 2H$. This has a period which is near half a lunar or solar day, assuming the body B is the Moon or the Sun respectively. The tides caused by this are known as semi-diurnal. The second term is dependent on $\cos H$, giving rise to diurnal tides.

The final term has no dependence on H. Tides caused by this are long period, related to the

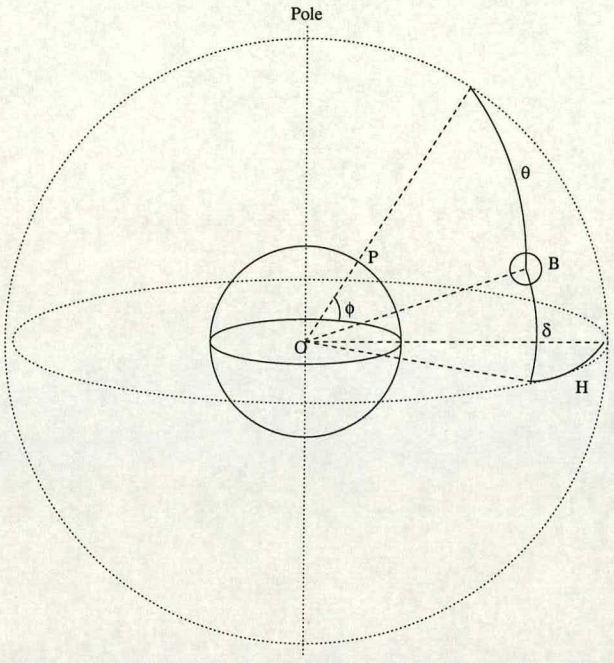

Figure 2.2. Illustration of declination δ, latitude ϕ and hour angle H.

declination of the Sun and the Moon. The periods are 1/2 year and 14 days respectively. Both the semi-diurnal and diurnal tides are modulated by these long term periods.

2.1.2 Harmonic Tidal Constituents

The positions of the Sun and Moon relative to the Earth can be determined with knowledge of the mean lunar and solar time and using a harmonic series containing five fundamental astronomical variables which change at a uniform rate; mean longitudes of the Moon and the Sun, lunar perigee (point of closest approach), ascending lunar node (point where the Moon's orbit crosses the plane of the Earth's orbit from south to north) and solar perihelion (point of closest approach to the Earth).

Hence also the tidal potential can be expressed as a harmonic series. The largest terms, or constituents, have been given names. Those caused by the Moon are in general assigned a letter near 'M' in the alphabet, those for the Sun have letters near 'S'. Subscripts are appended to these letters, using '2' for near semi-diurnal harmonics, '1' for diurnal harmonics and a letter for longer periods (*eg.* 'f' for fortnightly tides). For example, the largest semi-diurnal constituent generated by the Moon is M_2.

2.1.3 The Response of the Earth

At the tidal frequencies produced by the potential W_2, the Earth responds in a linearly elastic manner. Thus the deformation and the potential created by this deformation are directly proportional to W_2. Constants of proportionality h_2 and k_2 are defined such that

$$\delta r = \frac{h_2 W_2}{g} \tag{2.12}$$

$$V_{def} = k_2 W_2 \tag{2.13}$$

where δr is the vertical displacement caused by the potential and V_{def} is the potential of the deformation. h_2 and k_2 are known as Love numbers and are both dependent on the elasticity and density of the Earth's crust. Calculations of Love numbers are made based on Earth models where properties of the crust are derived from seismic and free oscillation data.

2.1.4 The Earth Tide Effect on Gravity

The presence of a celestial body has three effects on gravity at the surface of the Earth. Firstly there is the direct gravitational attraction of the body. This is defined as the gradient of the potential from that body. From (2.7) this gives:

$$g_{attr} = \frac{\partial W_2}{\partial r} = \frac{2W_2}{r}. \tag{2.14}$$

Secondly the deformation of the Earth's crust causes a vertical movement through the free air gravity gradient resulting in a change in gravity. The Earth's gravitational field is

$$g = \frac{-GM_E}{r^2}, \tag{2.15}$$

where M_E is the mass of the Earth, and the gravity gradient is defined as

$$\frac{\partial g}{\partial r} = \frac{2g}{r}, \tag{2.16}$$

then for a vertical displacement of δr and using (2.12), we have

$$g_{fa} = \frac{\partial g}{\partial r}\delta r = h_2 \frac{2W_2}{r}. \tag{2.17}$$

Thirdly, this deformation redistributes the Earth's mass and changes the gravity field. Using the fact that this potential is from within the Earth, and that W_2 is of degree 2, the deformation potential will have the form:

$$W_{def}(r) = k_2 W_2(r_E) \left(\frac{r_E}{r}\right)^3 \tag{2.18}$$

where r_E is the radius of the Earth. So at the Earth's surface,

$$g_{def} = \frac{\partial}{\partial r} k_2 W_2(r_E) \left(\frac{r_E}{r}\right)^3 \Bigg|_{r=r_E} = -3k_2 \frac{W_2}{r_E}. \tag{2.19}$$

The total variation in gravity is as follows:

$$g = g_{attr} + g_{fa} + g_{def} = \frac{2W_2}{r}\left(1 + h_2 - \frac{3}{2}k_2\right) \tag{2.20}$$

The term in the brackets is known as the gravimetric factor, δ_2. It has a value of about 1.16 with an uncertainty of $\pm 0.5\%$, which can be assumed to be known to a sufficient accuracy for most applications (Baker, 1984).

2.1.5 Ocean Tides

There is no direct resemblance between the Earth's body tides and its ocean tides. Several factors combine to create a complex pattern. Firstly the oceans are not of a sufficient depth to allow a wave of water to move around the globe at the rate at which it rotates. Secondly, the oceans are separated by land masses. Each ocean basin has its own particular natural frequencies, some of which may coincide with tidal forcing frequencies. Here resonances arise resulting in larger tidal amplitudes. Thirdly, the rotation of the Earth causes movement of water to take on a curved path. This is caused by the Coriolis force.

Shallow shelf sea areas create additional effects such as friction, reflection, refraction and changes in wave height and speed.

2.1.6 Ocean Loading and Effects on Gravity

Ocean loading is caused by the rise and fall of water in the ocean tides and results in a deformation of the Earth's crust. The effects on gravity consist of three mechanisms. The deformation causes a vertical movement through the gravity gradient. This deformation redistributes the mass of the Earth and changes the gravity field. Finally the mass of water has a direct gravitational attraction.

The Earth's crust can be assumed to respond elastically to ocean loading. Loading Love numbers ($h_n^{'}$, $k_n^{'}$ and $l_n^{'}$ for a degree n load) are calculated based, as before, on a given Earth model. As with body tide Love numbers, various combinations of loading Love numbers give values of the tidal load surface displacement, potential change, gravity, tilt and strain.

2.2 Methods of Ocean Loading Calculations

To perform ocean loading calculations, details of the ocean tides need to be known. Information on ocean tides consists of two pieces of data - amplitude and phase. Convention adopted here is to express the phase lag with respect to the Greenwich Meridian (zero longitude). Displayed graphically, tides can be represented by co-tidal maps with contours connecting places where high tide occurs at the same time, and a separate set of contours or shading to indicate amplitude distribution.

Numerically it is convenient to use complex numbers to represent tides. If η represents a tide, then the real and imaginary parts are defined as follows:

$$\text{real}(\eta) = \text{amplitude} \times \cos(\text{phase}) \tag{2.21}$$

$$\text{imag}(\eta) = \text{amplitude} \times \sin(\text{phase}) \tag{2.22}$$

Baker (1985) gave a review of the various methods of computing tidal loading. These can essentially be divided into two main areas as follows.

2.2.1 The Spherical Harmonic Expansion Method

The spherical harmonic expansion method uses surface spherical harmonics to describe the distribution of each particular tidal harmonic. The form is as follows:

$$\zeta(\theta,\lambda) = \sum_{n=0}^{\infty} \zeta_n(\theta,\lambda) \tag{2.23}$$

where

$$\zeta_n(\theta,\lambda) = \sum_{m=0}^{n} (a_{nm}\cos m\lambda + b_{nm}\sin m\lambda) P_n^m(\cos\theta) \tag{2.24}$$

$\zeta(\theta,\lambda)$ is the tide at colatitude θ and east longitude λ. a_{nm} and b_{nm} are complex coefficients. P_n^m are spherical harmonics of order m and degree n.

The nth degree spherical surface harmonic then gives a gravitational potential which is given by:

$$W_n'(r,\theta,\lambda) = \begin{cases} \dfrac{4\pi G\rho_w a}{(2n+1)} \left(\dfrac{a}{r}\right)^{n+1} \zeta_n(\theta,\lambda) & r \geq a, \\ \dfrac{4\pi G\rho_w a}{(2n+1)} \left(\dfrac{r}{a}\right)^{n} \zeta_n(\theta,\lambda) & r < a, \end{cases} \tag{2.25}$$

where G is the gravitational constant, ρ_w is the density of sea water, a is the radius of the earth and r is the distance from the centre of the earth.

Farrell (1972) solved the equations of motion on a spherical, self gravitating, elastic Earth loaded by a degree n surface mass layer. He calculated the loading Love numbers h_n', k_n' and l_n' up to degree n = 10 000 from which gravity effects can be calculated using W_n' and its derivatives.

This method requires calculation up to high degrees to remove local anomolous tide effects for stations at or near the coast. For example, Pertsev (1970) showed expansion up to n = 32 was sufficient for sites greater than 1500 km from the coast, but expansion up to a much higher degree was necessary for closer sites.

2.2.2 The Convolution Method

Suppose the Green's function giving the response to a point mass load on the Earth's surface at various distances can be found. Then convolving this with the ocean tides will give the ocean tide loading response at any point. If the loading Green's function is given by $G(\underline{r})$, then the loading response function $L(\underline{r})$ is given by:

$$L(\underline{r}) = \rho_w \iint_{oceans} G(|\underline{r} - \underline{r}'|)\zeta(\underline{r}')dA' \tag{2.26}$$

where $\zeta(\underline{r}')$ gives the height of the ocean tide over the surface area dA' at position $\underline{r}'$.

Green's functions are constructed from weighted sums of Love numbers. For example, the total gravitational effect due to a point mass load at angular distance θ is (Farrell, 1972; Longman, 1963):

$$g(\theta) = \frac{g}{M_E} \sum_{n=0}^{\infty} [n + 2h_n' - (n+1)k_n'] P_n(\cos\theta) \tag{2.27}$$

where g is the acceleration of gravity on the Earth's surface, $g(\theta)$ is the difference between g and the acceleration on the deformed surface, P_n is the Legendre polynomial of degree n and M_E is the mass of the Earth.

For every constituent, tidal data is held as a grid of cells. Ocean loading effects are calculated by convolving these data with the appropriate Green's function. The cells are usually assumed to be in the form of discs, yet the Green's function represents loading effects for point loads. Farrell (1973) showed that at distances greater than 10 times the radius of a spherical disc, the loading response is within 1% of an equivalent point mass load acting at the centre of the disc.

Farrell (1973) calculated the response of the Earth to disc loads of various radii and at various distances to construct tables of disc factors. Disc factors are the ratio of the gravity perturbation due to a disc load against the gravity perturbation due to the equivalent point mass load. These can be used to improve loading contributions from cells near the site in question.

2.3 Ocean Tide Models

Ocean tide models are derived using either one or a combination of two main techniques.

The hydrodynamic numerical approach is to model the tides using mathematical equations based on the physics of the oceans. These can incorporate effects such as Earth tides, dissipation, ocean tide loading and attraction. A recent development has been to use finite element methods. This has the advantage of being able to use increased grid resolution over shelf areas where there can be great spatial variation of the ocean tides.

The alternative approach is empirical. It uses measurements of the tides and interpolates to areas where there are no measurements. Initially only *in-situ* tide gauge observations were

available, which do not have an equal global distribution. Huge advances have been made in recent years with the advent of satellite altimetry. Radar ranging gives an instantaneous distance from the satellite to the sea surface with an instrument precision of a few centimetres (Curtis, 1996). Satellite orbits give a near global coverage of the Earth's oceans.

Combining the two techniques by assimilating theoretical models with observations often leads to improvements. The result is that mathematical models are constrained and deficiencies in the observations can be overcome.

The form of an ocean tide model is typically an array of grid cells with fixed latitude / longitude spacing. For each tidal constituent and each grid cell, values are given for the amplitude and phase lag of the tide at the centre of the cell. A special value of say 999.9 is assigned if the cell is not at sea. Figure 2.3 gives an example of the model AG95.1 coverage and resolution for the M_2 constituent around the British Isles.

Various factors need to be considered when selecting an ocean tide model for use in ocean loading calculations. Ocean loading effects are felt not only from local tides, but also from remote tides and hence the area of coverage of a tidal model is important. Satellite orbits for example may not cover certain areas of the globe. Or a hydrodynamical model may omit some sea areas.

Spatial resolution can be a particularly important factor when doing ocean loading calculations for coastal sites. Beyond a certain level all models will not be able to distinguish small scale geographical features. This leads to uncovered areas of sea and covered areas of land. Clearly the higher the spatial resolution the smaller this error is. One solution can be to supplement a global model with a local one of higher resolution. For example, Baker (1980) and Baker *et al.* (1991) used this method by supplementing a coarse global model with a more detailed European shelf model for ocean loading computations in Europe.

Local inaccuracies may also arise from small scale geographic features. Problems can occur with satellite altimetry when the radar beam hits an area which is part sea, part land. This can lead to erroneous results, as seen in Figure 2.3 where tide gauge amplitude observations are plotted alongside the AG95.1 tide model for the Bristol Channel. The observations show the M_2 amplitude to be increasing eastwards, but the tide model shows otherwise.

The number of tidal constituents varies between tide models. The constituents M_2, S_2, K_1 and O_1 account for 95% of the variance in the equilibrium tide (Ray, 1993). Thus 5% of the equilibrium tide may be accounted for by the remaining constituents. Theoretically the more constituents used the greater the proportion of the tide removed and hence the better the loading calculations.

Various tide models were available for use in this research. They were prepared and put in to Network Common Data Format (netCDF) by Bos. Those which have global coverage and the

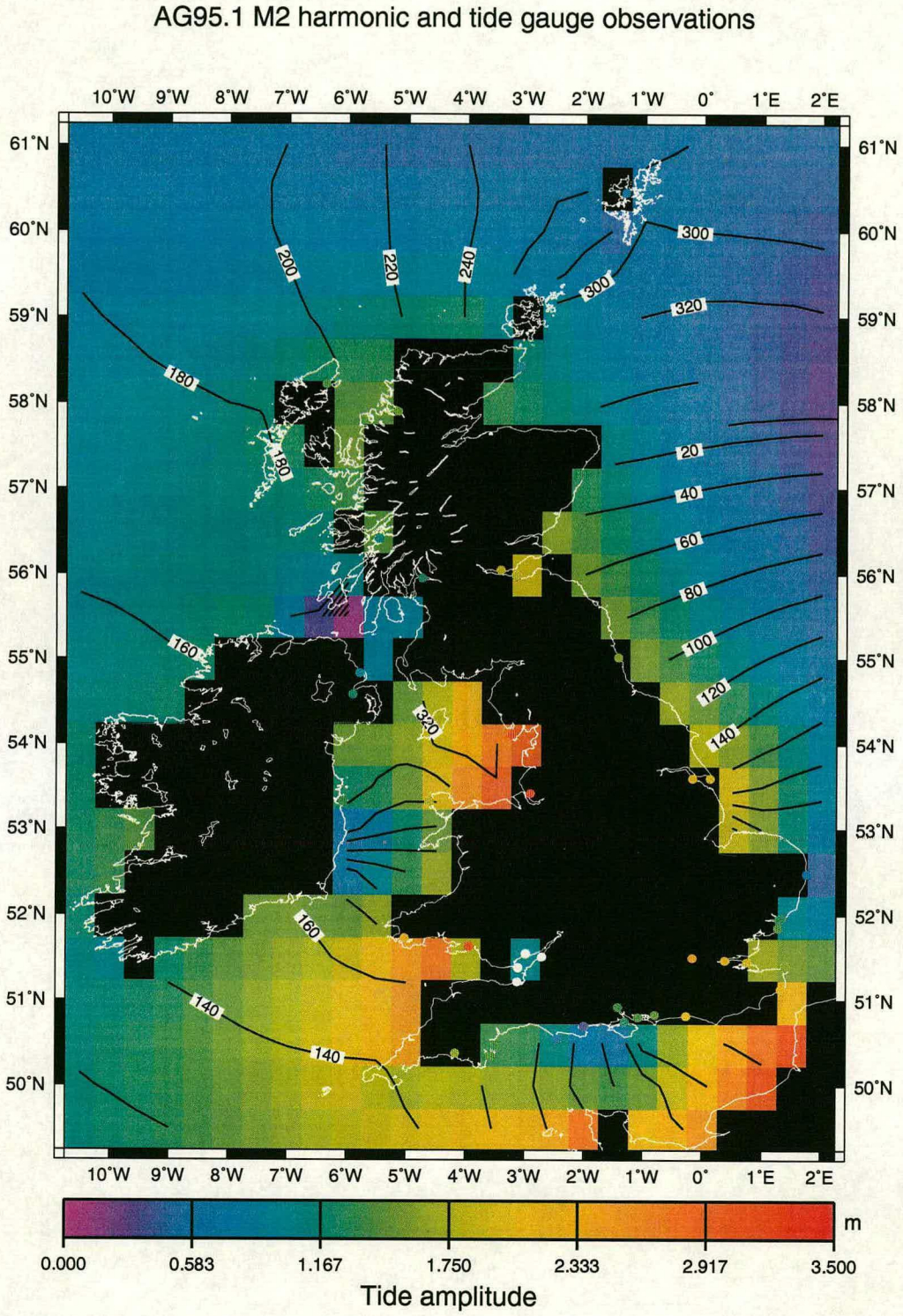

Figure 2.3. AG95.1 M_2 tide model amplitude and phase lag data for the British Isles. The circles represent the location of tide gauges whose observation of the M_2 amplitude is given by the colour. Note that white represents an amplitude off the top end of the colour scale.

Model	Constituents	Method	Remarks
AG95.1	M_2, S_2, K_1, O_1, N_2, K_2, Q_1, P_1, $2N_2$, L_2, μ_2, ν_2	Hydrodynamic with T/P integration	Long wavelength adjustment of FES94.1 M_2 and S_2
CSR3.0	M_2, S_2, K_1, O_1, N_2, K_2, Q_1, P_1,	T/P with hydrodynamic integration	Long wavelength adjustment of FES94.1
FES94.1	M_2, S_2, K_1, O_1, N_2, K_2, Q_1, P_1,	Hydrodynamic	Finite Element Solutions
FES95.2	M_2, S_2, K_1, O_1, N_2, K_2, Q_1, $2N_2$,	Hydrodynamic with T/P integration	Assimilation of FES94.1 with T/P CSR2.0 model

Table 2.1. Details of ocean tide models AG95.1 (Anderson *et al.*, 1995; Anderson, 1995), CSR3.0 (University of Texas), FES94.1 (LeProvost *et al.*, 1994) and FES95.2 (Egbert *et al.*, 1994) available for this research. [T/P = TOPEX/POSEIDON].

finest resolution of $0.5^o \times 0.5^o$ are listed in Table 2.1.

2.4 Problems With and Improving Ocean Loading Calculations

Ocean tide model data are arranged in a latitude-longitude grid with a spacing of usually 0.5^o by 0.5^o. This corresponds to a latitudinal distance of about 50 km. Clearly with an irregular coastline there will be areas where land is covered by a grid box and sea is left uncovered, as seen in Figure 2.4. The errors caused by this misfitting will be at their greatest for sites located near coastlines.

Grid misfitting will always cause an error, but if the grid size is chosen carefully, the errors can be brought down to a level that is lower than the instrumental precision and hence insignificant.

As discussed earlier, the approximation to a point mass load deteriorates with decreasing distance to the load. The strength of the approximation depends on the ratio of this distance to the radius of the spherical disc - the greater the ratio the better. With the appropriate choice of a grid of variable size, this ratio can be kept at a level which maintains a good approximation to the point mass load.

2.4.1 The Potential Effect Of Grid Misfitting

Here the theoretical potential effect of misfitting the ocean tide model grid to the coastline on ocean loading calculations will be examined. The possible extent to which this may occur is unlikely to be greater than 0.25^o of latitude or longitude, since this is half the grid size of the

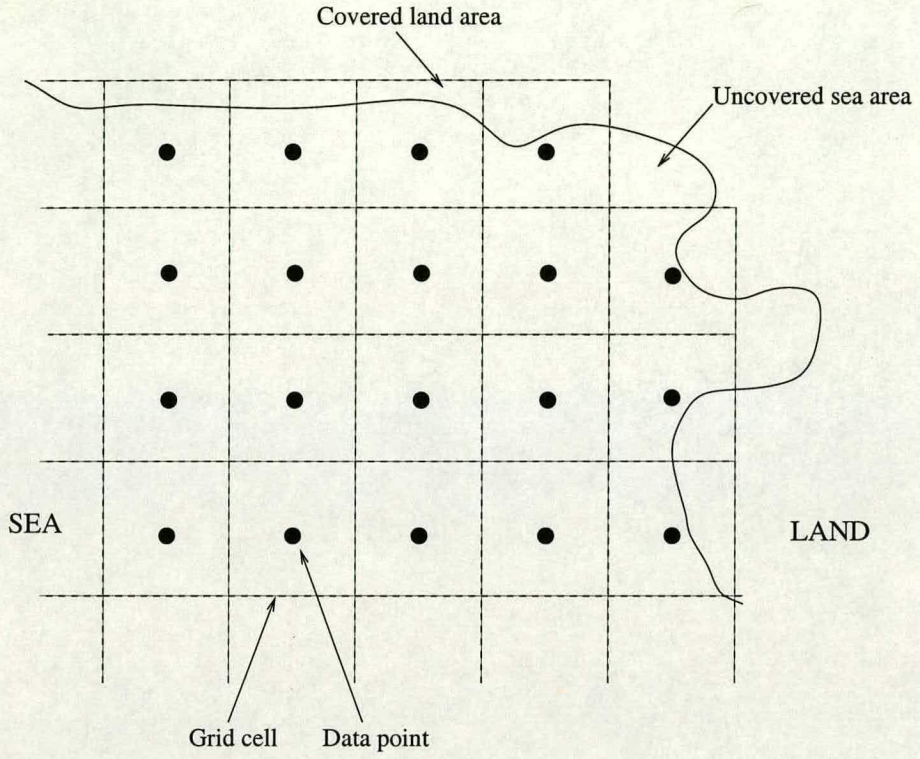

Figure 2.4. Illustration of the misfit of ocean tide model grid boxes to irregular coastlines.

best tide models with global coverage. This corresponds to a latitudinal distance of about 28 km.

Since this distance is not large relative to the Earth, and because only an idea of the magnitude is needed, assumptions have been made to simplify the calculations. The Earth will be assumed to be a flat half-space and have homogeneous elastic properties.

The maximum potential error from grid misfitting will occur for a gravity site located close to the coast at a high altitude where the Newtonian attraction from the tide is at its greatest. The gravity site is assumed to be not less than 1 km from the coast (Carter *et al.*, 1989). Calculations initially performed by Bos for a half ring of water 1 m thick and variable outer radius will be verified. With an inner radius of 1 km this should simulate the error of grid misfitting by leaving sea areas uncovered. With zero inner radius, the error of grid misfitting on to land by greater than 1 km should be simulated.

From Farrell (1972), the vertical displacement due to a point load of 1 N on the surface is:

$$u(r) = -\frac{\sigma}{4\pi\mu\eta r} \tag{2.28}$$

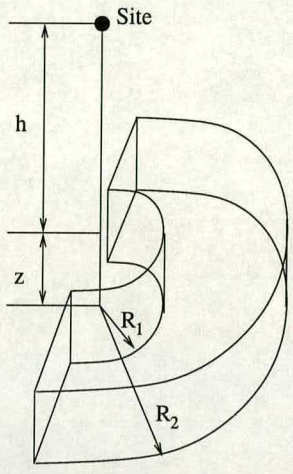

Figure 2.5. Dimensions of half ring of water.

Here r is the distance from the point mass load. $\sigma = \lambda + 2\mu$ and $\eta = \lambda + \mu$ where λ and μ are the Lamé constants. From the Preliminary Reference Earth Model (Dziewonski and Anderson, 1981), $\lambda = 3.4 \times 10^{10}$ Pa and $\mu = 2.6 \times 10^{10}$ Pa. Using these values and assuming $g = 9.81$ ms^{-2}, then for a half ring of water with density 1000 kgm^{-3}, unit depth, inner radius R_1 and outer radius R_2 (see Figure 2.5),

$$u(r) = -1.352 \times 10^{-7}(R_1 - R_2). \tag{2.29}$$

With $R_2 = 28$ km, $R_1 = 0$ km and 1 km gives $u = 3.58$ mm and 3.71 mm respectively. The free air vertical gradient of gravity is $dg/dh = 2g/r_E = -308$ μgalm^{-1} where $r_E = 6371$ km, the radius of the Earth. Thus this amount of vertical movement will correspond to a change in gravity of 1.1 μgal in both cases to one decimal place. The true effect on gravity will be less than this due to elastic deformation of the Earth and redistribution of mass which reduces the gravity gradient.

The Newtonian attraction effect also needs to be considered. At a height h above the circular centre of a half ring of depth z, inner radius R_1 and outer radius R_2 with material density ρ, the direct vertical gravitational attraction exerted is:

$$g = \pi G\rho \left(\sqrt{R_1^2 + (h+z)^2} - \sqrt{R_2^2 + (h+z)^2} - \sqrt{R_1^2 + h^2} + \sqrt{R_2^2 + h^2} \right) \tag{2.30}$$

Figure 2.6 shows the results if the height h of the station is varied, with R_1 = 1 km and R_2 =

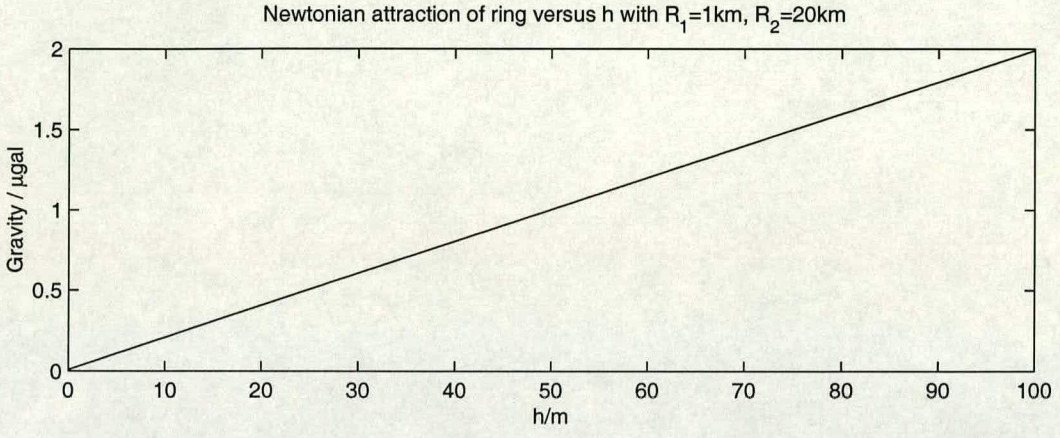

Figure 2.6. Graph showing the direct vertical attraction versus height h of a half ring with inner radius 1 km and outer radius 20 km.

20 km. It shows a linear increase in the effect on gravity with height, up to 2 μgal at 100 m. Sites located at sea level should feel negligible variations since the attraction is almost entirely horizontal.

To examine the maximum potential effect, h is now fixed at 100 m. Figure 2.7 shows the results if R_2 is varied up to 20 km with R_1 = 0 km and 1 km, z = 1 m. As can be seen, the effect on gravity quickly becomes significant ($>$ 1 μgal) if the site is thought to be directly above water, as in the case of R_1 = 0 km. However, the effect is much smaller with R_1 = 1 km but still becomes significant at the 1 μgal level for a misfit greater than 2 km.

2.4.2 Model Used For Ocean Loading Calculations

The computer program used for the computation of the tidal loading constants in this research was developed by Baker at POL. It was written in FORTRAN77 and is known as CONMODA. As well as tidal gravity loading effects, it also has the option of calculating displacement, tilt and strain. The method used is to convolve tabulated Green's functions with point mass loads for grid cells at a distance greater than 10 times the radius of the equivalent disc of equal area. For grid cells located within this distance from the site of interest, tabulated disc factors are used.

The routine has the option of mass conservation, whereby the real and imaginary components of the tide expressed as a complex number in each grid cell are scaled by the cell area and summed globally. The amplitude of the resulting complex number is subtracted from the tide in each grid cell (again scaled by cell area). Throughout this research, mass conservation was used.

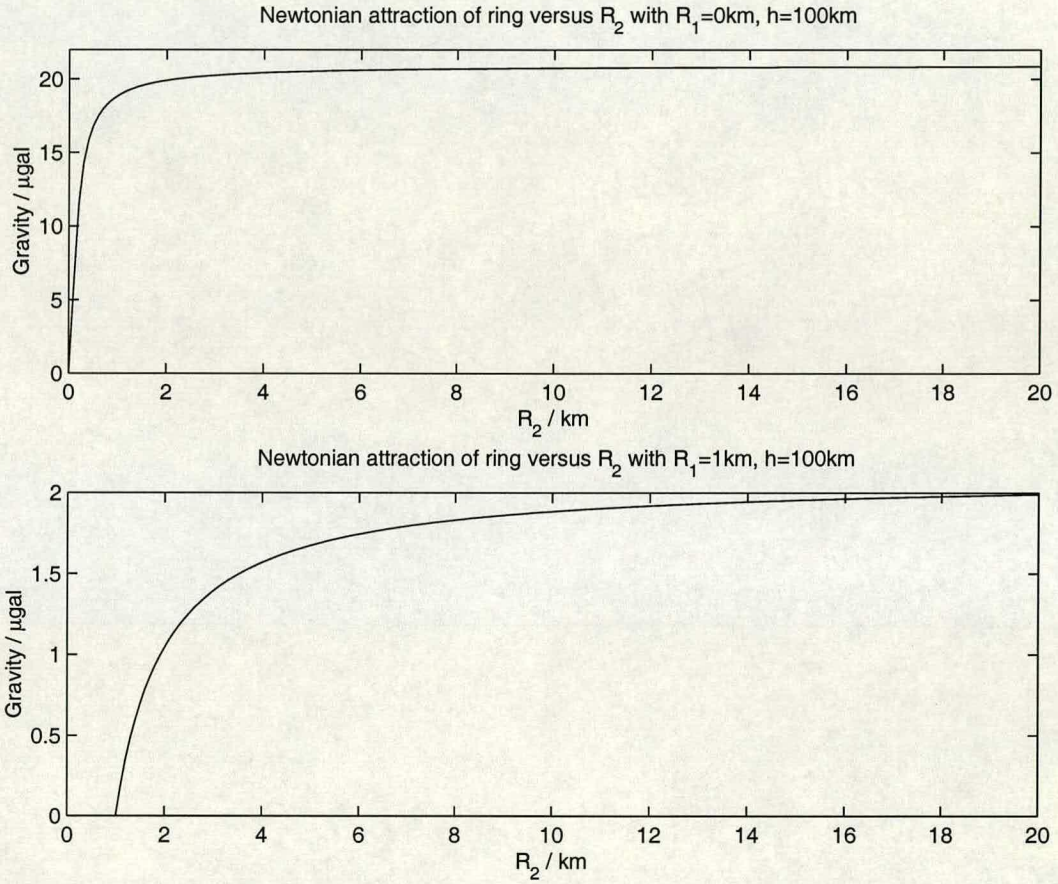

Figure 2.7. Graphs showing the direct vertical gravitational attraction versus outer radius R_2 with h = 100 m and inner radii of 0 km and 1 km.

The disc factors input to the model for this research were those calculated by Baker for gravity loading effects. However these should not have been accessed by the model when using data from the interpolation routine developed. The Green's function input under the suggestion of Baker (*pers. comm.* 1998) was that developed from the Blundell and Parkes (1969) Earth model for the Irish Sea.

The grid cell ocean tide data input in to CONMODA must be in the form of an 'ocean information array'. For each cell, this contains information on the sine/cosine of the cell centre co-latitude/longitude, the radius of the circular disc with area equal to the cell and details of the tide in the form of its real and imaginary components when expressed as a complex number. The software used to calculate the ocean information array was developed by Bos, based on software written by Baker.

2.4.3 Previous Tidal Gravity Loading Results Using CONMODA

Baker (1980) showed that M_2 observations made at 6 sites in Britain agreed to within 0.6 μgal of the theoretical calculations using CONMODA. Baker *et al.* (1991) showed that M_2 and O_1 observations in central Europe were in agreement at the 0.1 μgal level with the theoretical values.

More recently, Curtis (1996) has investigated the effect of changing some of the input parameters to CONMODA. She finds that using different Green's functions based on different Earth models gives a mean difference in the tidal gravity loading of 0.05 μgal. Using mass conservation or not gives a difference ranging from 0.26 μgal for the old Schwiderski 1980 tidal model to 0.01 μgal for the recent CSR3.0 University of Texas tidal model.

2.4.4 The Interpolation Routine

A routine, written in FORTRAN77, has been developed in collaboration with Bos which creates a grid of variable size with the aim of improving the fit at coastlines and obviating the need for disc factors. The coastline database used for this is the World Vector Shoreline with an expected precision of 50 - 500 m. Tidal values from the original ocean tide model are interpolated on to the new grid. This section highlights the principles used, details of which can be found in Appendix A.

Given coordinates of the gravity site for which ocean loading calculations are to be performed, cells are subdivided if they satisfy at least one of two criteria. Both depend on the ratio of the radius of the grid cell in its equivalent disc form of equal area to its distance from the station.

Firstly, if this ratio exceeds the 'Coast Factor' and the cell is situated on the coast, the cell is subdivided. This ensures a better fit of the grid to the coastline.

Secondly, if this ratio exceeds the 'Station Factor' then the cell is subdivided irrespective of being located on the coast or not. This creates a grid of decreasing cell size towards the station.

Table 2.2 shows the results using different Coast Factors. A value of 0.01 was chosen.

Coast Factor	Newlyn		Lerwick	
0.005	16.37	-59.0^o	3.59	93.9^o
0.01	16.42	-58.9^o	3.60	93.4^o
0.05	16.69	-58.4^o	3.71	93.9^o
0.1	17.01	-58.4^o	3.73	94.3^o
0.5	18.57	-58.4^o	4.22	96.3^o

Table 2.2. The effect of changing the Coast Factor on Newlyn and Lerwick M_2 calculations using tide model FES95.2 (amplitude (μgal) and phase lag).

Table 2.3 shows the results using different Station Factors. A value of 0.1 was chosen.

Station Factor	Newlyn		Lerwick	
0.05	16.46	-58.9^o	4.04	95.5^o
0.1	16.42	-58.9^o	3.60	93.4^o
0.2	16.36	-58.9^o	3.99	95.3^o
0.5	16.05	-59.0^o	3.87	94.6^o

Table 2.3. The effect of changing the Station Factor on Newlyn and Lerwick M_2 calculations using tide model FES95.2 (amplitude (μgal) and phase lag).

When a cell is subdivided, it is split into 4 smaller cells. Tidal values are calculated for each of these using interpolation from surrounding values. The routine has the option of bilinear or 2-D polynomial interpolation. Anderson *et al.* (1995) reports that bilinear interpolation is sufficient for tidal data.

To examine the potential effects of using different interpolation methods on tidal data, a test was devised whereby data are interpolated to their midpoints. These results are then used to interpolate back to the original points. The difference between those values and the original values are calculated. The amplitude of the RMS of these differences of the complex components was calculated. Results are given in Table 2.4 for the areas of Northern Europe and the World.

The results show that in both cases, polynomial interpolation is the more accurate method to interpolate tide data with. However, Table 2.5 shows the results of using the 2 methods for 4 sites in Britain. It shows that polynomial and bilinear interpolation gives insignificant differences in resulting ocean loading components. It was decided to use bilinear interpolation.

Amplitude of RMS of differences (m)	Bilinear	Polynomial
Northern Europe	0.1584	0.1410
World	0.0505	0.0400

Table 2.4. The effect of re-interpolation using tide model FES95.2 M_2 on the areas of Northern Europe and the World.

Amplitude (μgal) and Phaselag	Bilinear		Polynomial	
Lerwick	3.76	94.3^o	3.77	94.9^o
Edinburgh	3.14	-78.4^o	3.16	-78.7^o
Bidston	0.87	-108.7^o	0.70	-111.3^o
Newlyn	16.57	-58.9^o	16.60	-59.1^o

Table 2.5. Ocean loading calculated with different interpolation methods for sites around Britain using FES95.2 M_2.

To avoid subdivision of grid cells to unnecessarily small sizes, cells are iteratively subject to subdivision a sufficient number of times to give the accuracy required. Table 2.6 shows the effect of changing the number of iterations. It was decided to use 10 iterations to achieve an accuracy of 1 μgal.

Number of Iterations	Newlyn		Lerwick	
1	14.05	-58.6^o	2.30	81.0^o
3	14.83	-59.1^o	2.53	84.4^o
5	21.87	-57.9^o	3.37	91.9^o
8	17.10	-58.8^o	4.18	96.1^o
10	16.42	-58.9^o	3.60	93.4^o
12	16.35	-59.0^o	3.86	94.7^o
15	16.35	-59.0^o	3.85	94.7^o

Table 2.6. The effect of changing the number of iterations on Newlyn and Lerwick M_2 calculations using tide model FES95.2 (amplitude (μgal) and phase lag).

An example of the resulting grid can be seen in Figure 2.8 for the site of Newlyn in south west Britain.

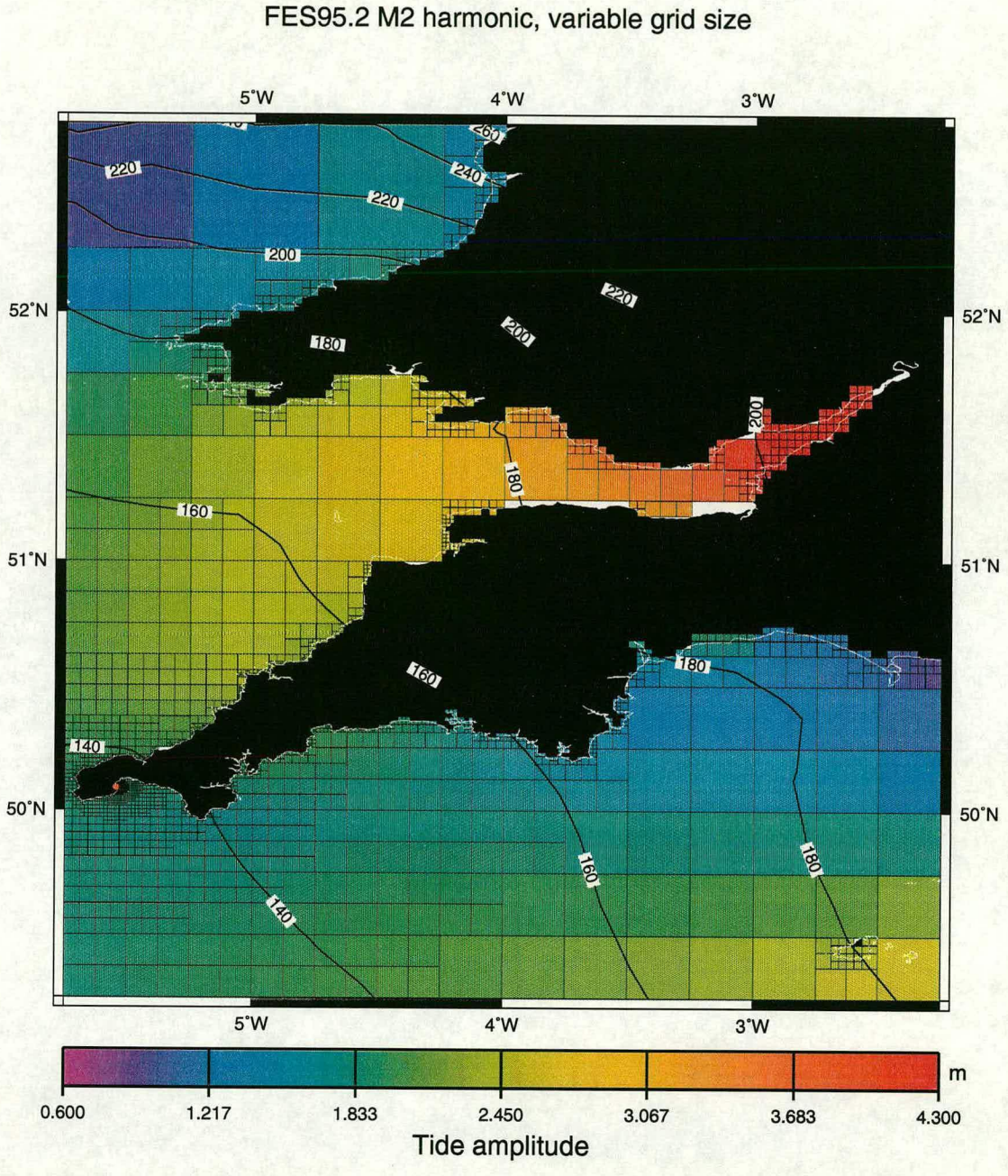

Figure 2.8. Grid output of interpolation routine for gravity station Newlyn, SW Britain using tide model FES95.2 M_2.

2.4.5 Shortcomings of the Routine

Whilst this interpolation routine theoretically increases the accuracy of ocean loading calculations, there are areas in which it could be improved.

As seen in Section 2.3, ocean tide models can disagree with observed amplitude and phase values from local tide gauges. Since this will lead to inaccurate ocean loading calculations, an option in the interpolation routine to override tide model values has been given. The amplitude and phase for any grid point in the tide model can be set to a value of the user's choice.

However, this is a simple manual system and does not allow the user to input the values and coordinates for a specific tide gauge. Some separate kind of hands-on interpolation may be necessary to ensure that the user defined tidal values for a certain area are realistic and smooth.

The interpolation used for subdividing cells assumes the points to be in a simple linear Cartesian system and does not take into account the curvature of the Earth. This may become important at high latitudes. Also mass is not conserved on subdivision of cells.

It should be noted that whenever using surrounding grid cells to calculate intermediate point values, errors may arise with certain land patterns. For example, in the case of a narrow peninsula, tidal values from one side of the peninsula may be used to calculate values at a point on the other side of the peninsula. If the tidal characteristics are different on either side, the results will not be a true representation of reality.

Chapter 3

Air Pressure and Groundwater

Details of the influence on gravity from air pressure and groundwater are described. Using continuous data from a LaCoste & Romberg Earth-tide gravimeter, calculations of the constant air pressure admittance for Bidston and Edinburgh are presented. Frequency dependent admittances are also found between the Bidston data and humidity, air pressure and rainfall.

Results of FG5-103 absolute gravimeter measurements made at Bidston from 1994 - 1998 show a seasonal variation in gravity of the order of 8 μgals. The cause of this variation is investigated by examination of the water table level given by borehole readings, estimation of the potential gravitational effect from rainfall and correlation with actual rainfall amounts. Admittances obtained from the Earth-tide data for air pressure and rainfall are applied to the Bidston absolute data.

3.1 Air Pressure Effects on Gravity

The pattern of air pressure on the Earth's surface varies both spatially and temporally in a complex manner.

These air pressure changes effect gravity in two ways. The dominant one is the direct attraction of the atmosphere. This is of opposite sign to the secondary cause from elastic deformation of the Earth's crust. As with ocean loading (see Chapter 2), the latter effect includes both the gravity changes caused by movement through the vertical gravity gradient and the change in the gravity field caused by redistribution of the Earth's mass.

Consider Figure 3.1 where a simple model view of the Earth and atmosphere is shown. For a given gravity site, it is clear that due to the curvature of the Earth, the direct attraction of some of the atmosphere will have no contribution to vertical gravity since its centre of mass is on the horizon. The gravity effect caused by elastic deformation is smaller and of opposite

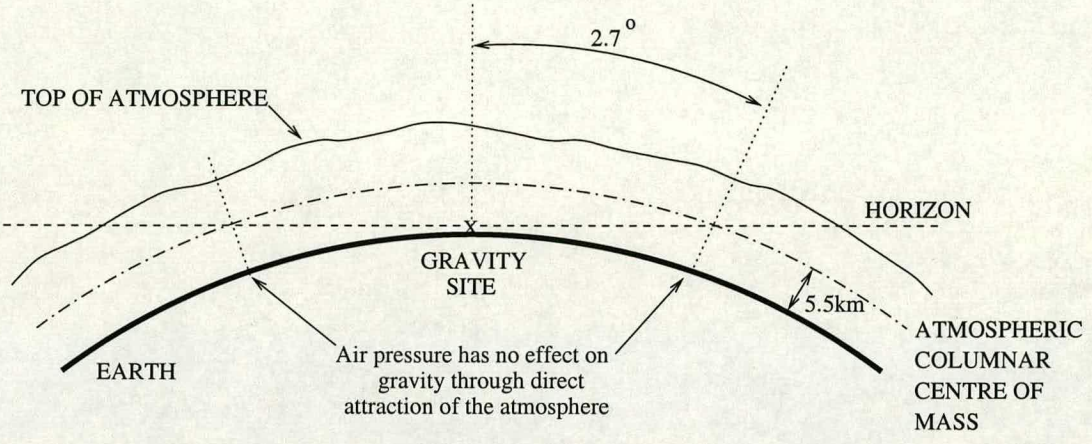

Figure 3.1. Schematic diagram of Earth with enveloping atmosphere, of variable height to represent spatially varying air pressure (not to scale). The centre of mass of a column of air is at a height of about 5.5 km, which at a distance of 2.7^o from the gravity site, is on the horizon (Merriam, 1992). There is no contribution to gravity through direct attraction of the atmosphere at these points.

sign. Hence combining these two factors, there exists a region (where the centre of mass of the atmosphere is close to the horizon) where these two effects cancel each other, producing no net effect on gravity. Thus it is not necessary to have knowledge of air pressure here to apply a correction.

Beyond this region, one would not expect air pressure variations to have a large effect on the local gravity for a given load, in part due to the inverse square law and the fact that elastic deformation effects decrease with increasing distance.

Merriam (1992) showed that for a weather system 1000 km in diameter, 90% of the gravity signal comes from an area within 50 km of the gravity site. Between 50 km and 250 km almost no signal arises. The remaining 10% comes from the zone 250 km to 500 km away.

3.2 Correcting Gravity for Air Pressure

The total effect of air pressure on gravity could be calculated if the global distribution of air mass is known. Since air pressure is a mass loading of the Earth's crust, the principles of Farrell (1973) as seen in Chapter 2 can be used. For example Merriam (1992) calculated Green's functions which can compute gravity effects when convolved with air pressure data. It was found that the functions are relatively insensitive to the model details of the atmosphere. He claims an accuracy of a few tens of ngal in the diurnal band, and to about 100 ngal in the days to seasonal band, but not during extreme weather conditions.

This method is not always convenient. Global knowledge of air pressure is more difficult to obtain, and usually only available at a later date. It is also not always necessary. As already mentioned, most of the gravity effects from air pressure come from the local distribution of air mass. Using only a local knowledge of air pressure may be sufficient for the accuracy required. Methods of this type involve using an admittance function, *ie* the relationship between local air pressure and its effect on gravity.

Methods using only local air pressure data can range from a constant, real admittance to a complex frequency dependent one. The latter uses the fact that the size of a weather system is correlated with its effect on gravity. It also assumes weather systems travel at a uniform rate and do not change spatially. The effect from air pressure can then appear non-causal, since weather systems upstream as well as downstream affect gravity, and hence details of future air pressure values give information on the current perturbation. A phase lead can also be caused by lateral inhomogeneities such as surface topographic effects or a laterally varying inelastic response of the Earth (Crossley *et al.*, 1995).

Empirically the admittance can be calculated using continuous gravity records such as those from Earth-tide or superconducting gravimeters. After the gravity record has had tides and ocean loading subtracted, it is linearly regressed with the local barometric record to find the admittance value. Splitting the data records into subsections, a seasonal variation of the constant admittance has been observed in some instances (Elstner *et al.*, 1997).

The most straightforward technique using only local air pressure data is the constant admittance method whereby a linear relationship between gravity and air pressure is assumed. For a uniform pressure on a flat, unyielding Earth, the admittance is $\frac{2\pi G}{g} \approx 0.43$ μgal mbar^{-1}. Typically a value of 0.3 μgal mbar^{-1} is used. Since meteorological events such as fronts create pressure gradients, the local pressure may differ from the regional pressure, and admittance values can range from 0.27 to 0.43 μgal mbar^{-1} (Merriam, 1992). The admittance value is also site dependent (caused by factors such as local topography) and can vary with the season due to a dependence on temperature (Merriam, 1992; Niebauer, 1988).

Superconducting gravimeter data has been used to develop frequency dependent admittance functions. Crossley *et al.* (1995) found an admittance of 0.2 μgal mbar^{-1} for frequencies less than 0.1 cycles per day (cpd), rising to 0.35 μgal mbar^{-1} at frequencies greater than 3 cpd. This agrees with theoretical calculations that admittance values decrease for larger weather systems (Merriam, 1993; Sun *et al.*, 1993). In common with all findings are that the admittance at harmonics of a day are difficult to interpret because of contamination from tidal and temperature effects (so called S-waves) (Merriam, 1993).

Vauterin (1997) reports a 10 - 20% reduction in residuals using a complex frequency dependent admittance function on superconducting gravimeter data compared with using a constant admittance value. The frequency dependent admittance approach is not very effective at tidal

frequencies such as 2 cpd (Kroner and Jentzsch, 1997).

Each method has its own particular merits and disadvantages. Corrections using only local air pressure can be carried out without too much expenditure of data or time. However, they can only remove 70 - 90% of the effects (Elstner *et al.*, 1997). Using global air pressure and Green's functions removes most measurable effects on gravity, but requires more extensive computation and the data are not immediately available. Kroner and Jentzsch (1997) report on a comparison of the different methods. They find that whilst regression methods compare well with using Green's functions for the short period tidal bands, for long periods better results are obtained using Green's functions.

3.3 Groundwater Effects on Gravity

Groundwater is defined to be water situated below the Earth's surface. This can be within either soil or rock. The amount of water a material is able to hold depends on the characteristics of that material; an indicator often used is the porosity. This is defined as the ratio of the volume of void space in a given sample to the total volume of that sample. It is usually expressed as a percentage.

However, other factors also affect the potential water capacity of a material. These include the size of the free air pockets (too fine a size and water molecules may not be able to infiltrate) and whether they are interconnected (isolated pockets of space will be externally inaccessible to water). Hence a more accurate parameter to use when determining the amount of water a material is able to hold is the effective porosity, defined as follows:

$$\text{effective porosity} = \frac{\text{volume of void space through which water is able to circulate}}{\text{total volume of material}}$$

There are various ways of measuring and monitoring groundwater including moisture detection with a neutron probe and electrical resistivity. The simplest method, and that which has been used in this research, is measurement of the depth of the water table level via a borehole.

The water table is the point at which the rock/soil is saturated with water. When measured through a well or borehole, the level of water is the point where hydrostatic pressure equals atmospheric pressure. Due to capillary action, the true level of saturation may be higher than this.

Assuming the groundwater takes the form of an infinite plate, the gravitational attraction felt by a change δh in the water table level is given by:

$$\delta g = 2\pi G P \rho_w \delta h \tag{3.1}$$

where P is the porosity of the rock/soil, ρ_w is the density of the water and G is the gravitational constant. Water alone (*ie* with $P = 1$) gives a signal of 0.42 μgal cm^{-1}.

The differential loading caused by water table variations may also induce elevation and thus gravity changes. Mäkinen and Tattari (1989) state that this can happen through soil compaction or expansion; only on a large scale is lithospheric deformation likely.

3.4 Correcting Gravity for Groundwater Effects

Correcting for groundwater effects invariably involves developing some model relating measurements made to an assumption of the layout of the groundwater. The simplest form may just use water table level measurements and assume an infinite plane of water for the saturated portion of the rock. Other factors should be considered such as the distance to water table and depth of soil as a source of moisture, and whether the hydrogeology varies locally.

It is possible that knowledge of rainfall can be used to find a relationship with gravity effects. Intuitively one would expect a possible delay between rainfall and gravity effect due to infiltration of water into the ground. There may also be a relationship between intensity and duration of rainfall and gravity effect due to runoff, giving rise to a frequency dependence. This will be explored later.

There have been several studies in to the gravity effects from groundwater changes at specific sites. Mäkinen and Tattari (1989) monitored water table and soil moisture and considered the attraction of snow at 2 sites in Finland. They found observations agreed well with predicted values to 2.0 μgal rms for a 13 μgal peak to peak variation of gravity.

Delcourt-Honorez (1991) considered the three layered aquifer system at the Royal Observatory of Belgium, Brussels. Using borehole measurements, she predicted the gravitational effects of the loading and attraction of subsurface water. She took into account capillary action within the rock by modelling three states of water concentration - saturation, funicular (water is interconnected in one phase but the rock is not saturated) and pendular (water is in the form of disconnected rings around contact points of adjacent particles). With water table changes of up to 0.3 m, she predicted gravity attraction effects up to 2.3 μgal and loading effects up to 50 ngal.

Peter *et al.* (1995) considered a site in Richmond, Florida. Linear regression between gravity data and water table change gave an effective porosity of 43%. They found that a seasonal

change of 0.5 m in the water table gives an attraction of 9 μgal and a loading effect of 0.8 μgal. Rainstorms were found to give a signature as high as 20 μgal.

3.5 Computing a Frequency Dependent Admittance

As already mentioned, the relationship between gravity and air pressure is related to the frequency of the air pressure. There is also a possible mechanism relating gravity to rainfall frequency through effects such as runoff. A method has been utilised to empirically develop a frequency dependent transfer function between gravity measurements and meteorological parameters.

Given a time series of gravity measurements $g(t)$ and a meteorological parameter $p(t)$, we assume a relationship as follows:

$$g(t) = \int q(t_o)p(t - t_o)dt_o + n(t) \tag{3.2}$$

where $q(t)$ is the transfer function between gravity and the parameter, and $n(t)$ is the remaining noise.

The integral is a convolution, so representing Fourier Transforms by upper case letters, (3.2) is equivalent to:

$$G = QP + N \tag{3.3}$$

Just as the convolution of two functions $a(t)$ and $b(t)$ becomes AB in the wavenumber domain, so their cross-correlation becomes AB^* (denoting complex conjugation by *). Cross-correlating gravity and pressure involves multiplying (3.3) through by P^* and gives

$$GP^* = QPP^* + NP^* \tag{3.4}$$

Since the remaining noise, N, is independent of P then the cross-correlation NP^* averaged over some interval will be zero. Denoting averaging by $< . >$, (3.4) can be re-written as:

$$< Q >= \frac{< GP^* >}{< PP^* >} \tag{3.5}$$

A routine was developed to calculate the frequency dependent admittance. Before Fourier Transforming, the data were first detrended so the spectra were less contaminated by long period noise. This was achieved by using the residuals from a least squares straight line fit. Next a Fast Fourier Transform was performed on the data. Finally the transfer function Q was calculated using equation (3.5).

Averaging spectra was accomplished by a moving window centred at the point of the required average. Crossley *et al.* (1995) found little change in using windows varying from 0.01 - 1.0 cpd in size. For his results he used a 0.1 cpd window. Neumeyer (1995) found that with a window size of 0.05 - 0.1 cpd, S-wave peaks occur in the complex admittance, but they disappear for window sizes of 0.5 - 1.5 cpd. For the purposes of this research a window averaging size of 0.1 cpd was used.

3.6 The ETERNA Tide Data Processing Software

The ETERNA software package processes Earth-tide gravity data and produces observed tidal constituent amplitude factors and phases. Amplitude factors are the ratio of the observed amplitude to the amplitude for a rigid Earth. It can also calculate linear relationships between gravity and meteorological parameters. For the purposes of this research, it has been used to find constant air pressure admittance values. A copy of version 2.0 was available, which was registered at Proudman Oceanographic Laboratory (POL). It is written by H. Wenzel of the Geodätisches Institut, Universität Karlsruhe, Germany. An overview of the software is given, for more details refer to Wenzel (1993, 1994, 1997).

The software performs a least squares adjustment of tidal parameters. *A priori* amplitude factors are used from the Wahr-Dehant-Zschau model based on an elliptical, uniformly rotating, oceanless Earth with liquid outer core and viscous mantle (Dehant, 1987). The Nearly Diurnal Free Wobble resonance in the diurnal band is accounted for from Wahr's 1981 model.

Several high pass filters can be applied to the data within the software. These range from having lengths of 37 hours to 239 hours. If no filtering is chosen, the drift can be removed by fitting Chebyshev polynomials up to a degree which is optional. For this research a filter of 51 hours in length was used. This produced results with the smallest standard deviations for amplitude factors and phases.

When a high pass filter is used, the data are split into two parts, consisting of frequencies below 0.7 cpd and above 0.7 cpd. Least squares are used to fit to the tidal constituents and linear regression is performed on the meteorological parameters. The frequency transfer function of the high pass filter is taken into account when this is performed.

3.7 Earth-Tide Gravity Data

Gravity data used to find frequency dependent admittances or varying constant admittances needs to be given at regular time intervals. Since absolute gravity measurements are made at irregular intervals, continuous Earth-tide gravity data has been used to find these admittances. This section describes the data and results obtained.

Note that when correcting for more than one meteorological parameter with the frequency dependent admittance method, the corrections were performed sequentially. After subtraction of the predicted gravity effects of the first meteorological parameter, the results were again detrended before the process is repeated since another Fourier transformation is performed.

3.7.1 Earth-Tide Gravity and Meteorological Data Sets

The gravity data sets used were recorded by a LaCoste & Romberg Earth-tide gravimeter (number ET10). The design is essentially the same as that of a LaCoste & Romberg relative gravimeter (see Chapter 1). As described by Baker (1984), it involves the extension of a zero length spring suspending a mass. A complex system of levers give a high mechanical amplification of the movement of the mass. This is detected electronically using a capacitance transducer. Feedback, either mechanical via electric motor adjustment of a measuring screw, or electrostatic via a capacitance transducer, keeps the mass in a fixed position. Due to creep, presumably in the spring and lever system, the raw gravity data has a drift which is usually about 4 μgal per day.

The Earth-tide gravimeter was installed in a cellar of Bidston Observatory at POL. Hourly values were logged for the six month period from 25th May to 24th November 1984. The data used was corrected for jumps. A plot of the data is shown in Figure 3.2, where the tidal frequencies can clearly be seen, and an overall drift is apparent.

The gravity data had body tide and ocean loading effects removed using amplitude factors and phases from ETERNA output. These are detailed in Table 3.1. For those constituents not found by ETERNA, amplitude factors of 1.159 and 1.042 for second and third degree tides respectively were used. The drift of the instrument was assumed to be linear and subtracted by doing a least squares linear regression. This detrending also has the advantage of removing long period noise from the Fourier Transforms. Figure 3.3(a) shows the gravity data after these operations have been performed, note the change in the scale of the vertical axis compared with Figure 3.2.

Meteorological data used were recorded in a Stevenson screen in the grounds of Bidston Observatory. They consist of 3 hourly measurements for air pressure, rainfall and dry and wet bulb temperatures. The recordings were linearly interpolated to give hourly values.

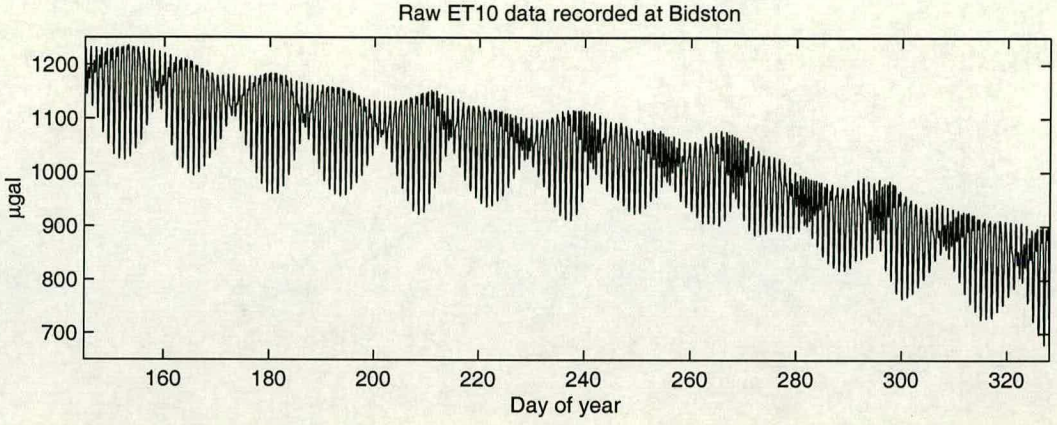

Figure 3.2. Raw ET10 data recorded at Bidston from 25th May to 24th November 1984.

Constituent	Amplitude Factor	St. dev.	Phase lag (^{o})	St. dev.
Q_1	1.13341	0.00616	-1.361	0.311
O_1	1.13530	0.00118	+0.004	0.060
M_1	1.15201	0.01499	+1.040	0.746
$P_1S_1K_1$	1.14266	0.00084	-0.005	0.042
J_1	1.14343	0.01500	+0.089	0.752
OO_1	1.13857	0.02738	-0.777	1.378
$2N_2$	1.18442	0.03075	+6.068	1.488
N_2	1.14374	0.00491	+0.188	0.246
M_2	1.14842	0.00094	+0.257	0.047
L_2	1.07188	0.03326	-2.452	1.778
S_2K_2	1.16293	0.00202	-0.028	0.100
M_3	1.01340	0.04326	-3.953	2.446

Table 3.1. Amplitude factor and phase values from ETERNA for ET10 at Bidston.

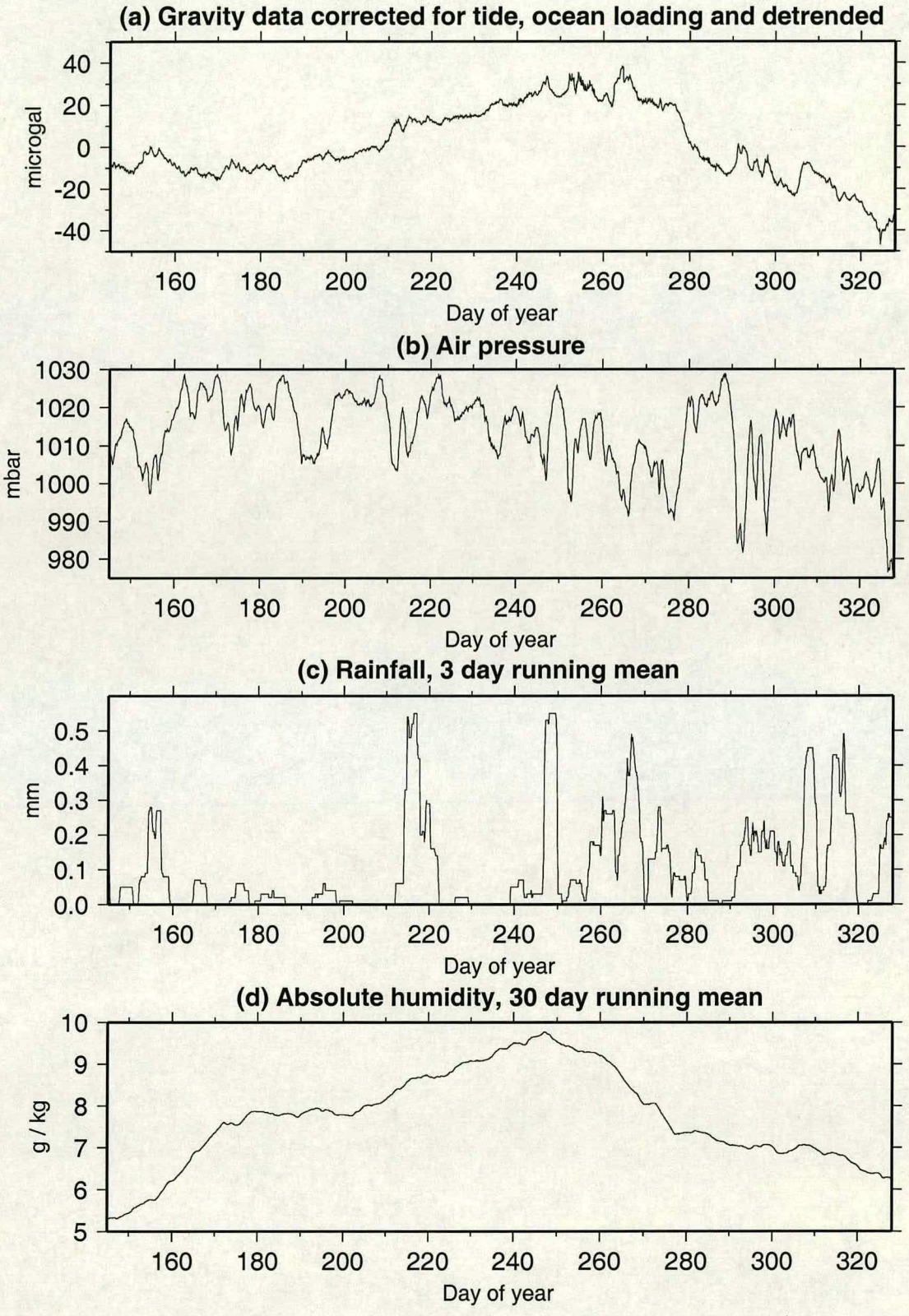

Figure 3.3. Bidston Earth-tide gravity and meteorological data sets.

Absolute humidity is the ratio of the mass of water vapour to mass of air. This was found from the dry and wet bulb temperature and air pressure data (T_D, T_W and p respectively). If absolute humidity is q, then

$$q = \frac{0.622e}{p - e} \tag{3.6}$$

where e is the vapour pressure which, for instruments in a Stevenson screen, is given by:

$$e = 6.11 \times 10^{\frac{7.5T_D}{T_D+237.3}} - 0.8(T_D - T_W) \tag{3.7}$$

Air pressure data can be seen in Figure 3.3(b). Running mean calculations were performed on the rainfall and absolute humidity meteorological data. The running mean value for a particular time was found by averaging all values over a fixed interval previous and up to that time. This has the advantage of removing the high frequency nature of the measurements, resulting in a smoother signal. It was found that results with the least scatter were obtained using a 3 day average for rainfall and a 30 day average for absolute humidity. These data sets can be seen in Figures 3.3(c) and (d). Detrending of the meteorological data sets was performed in a similar way to the gravity data.

Two shorter data sets were also available from when the gravimeter was installed in Edinburgh at the British Geological Survey, Murchison House. Hourly values were recorded in 1986. The first data set covers 35 days from 27th February to 2nd April. The second covers 60 days from 10th May to 8th July. Air pressure data used was recorded at the Meteorological Department, University of Edinburgh situated within 500 m. The data were in the form of barographs; hourly values were extracted using a digitising table.

Due to the greater length of data set and the observed seasonal variation of gravity at Bidston from absolute measurements, only data from this site was used for the frequency dependent admittance method.

3.7.2 Examination of Earth-Tide Data

The Bidston gravity (Figure 3.3(a)) data exhibit a long term rise and fall, varying by about 70 μgal. The maximum is at about day 250 of the year, which corresponds to mid-September. This variation is unlikely to be environmental and does not concur with absolute observations made at Bidston which vary seasonally by about 8 μgal and peak at the end of the year. Further examination indicates a correlation with absolute humidity. The correlation coefficient

between these two data sets is 79.7%.

Humidity effects on long term gravity recordings with LaCoste & Romberg instruments have been observed before (Dittfeld, 1989; Jentzsch and Melzer, 1989). Bastien and Goodacre (1990) conducted a controlled experiment. Annual changes in the gravity record disappeared when the gravimeter was placed in a humidity controlled container. The drift was found to be positively correlated with the amount of humidity. The reason is not known, spraying the electronics with a silicone resin did not cure the problem. It is suspected that the rubber seals between the interior and exterior of the meter cause the effects.

In addition to the long period variation of gravity, there are short period features. These may be either local environmental changes in gravity or instrumental effects. The latter may be due to factors such as re-adjustment of the instrument, earthquakes and other unknown instrumental effects.

However, it is possible to see that some of the features are environmental. For example, the decrease in gravity at day 185 corresponds to an increase in air pressure. It is also possible to see a correlation between rainfall and gravity, such as at day 308 where a period of rain coincides with an increase in gravity. Care should be taken on making such claims though since rainfall is itself related to air pressure, with low pressure weather systems in general bringing higher quantities of rain. This gives the same expected effect of an increase in gravity. It will be seen how an attempt was made to overcome this interdependence of the meteorological parameters.

3.7.3 Constant Admittance Results for Air Pressure

The Earth-tide gravity data recorded at Bidston and Edinburgh were processed by ETERNA to find the constant air pressure admittance value. The two Edinburgh data sets were combined to find the overall value for all the data available at that site. The results can be seen in Table 3.2.

The admittance values are considerably higher than the 0.3 μgal mbar^{-1} normally assumed. In particular, the Bidston value is higher than the 0.43 μgal mbar^{-1} stated by Merriam (1992) as being the upper limit. It could be that the close proximity of the sea to the Bidston site is

Site	μgal mbar^{-1}	Standard Deviation
Bidston	0.4443	0.0071
Edinburgh	0.3985	0.0036

Table 3.2. Constant admittance pressure values for ET10 data at Bidston and Edinburgh.

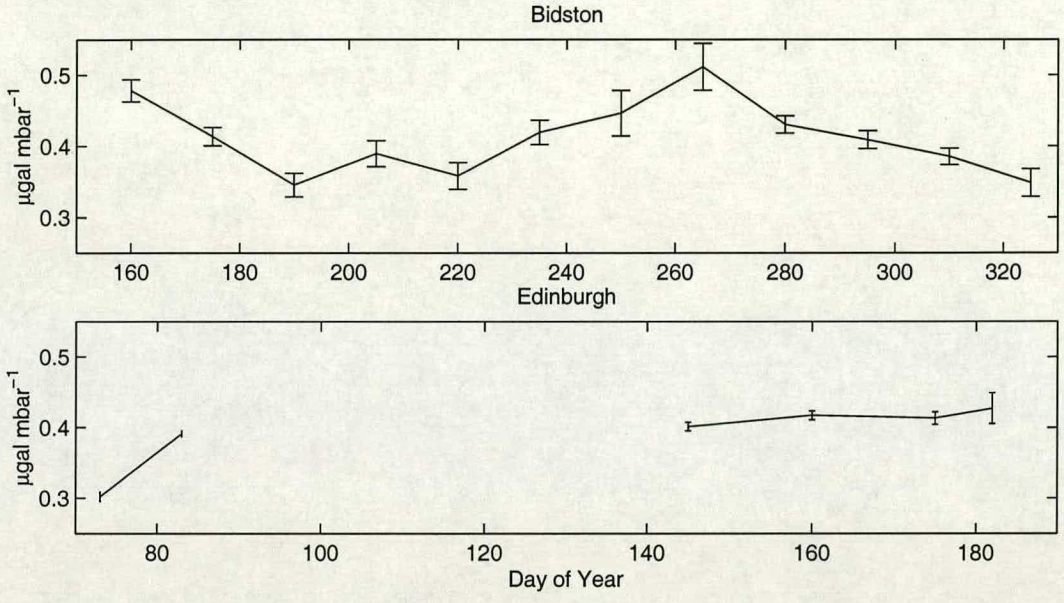

Figure 3.4. Variation of constant barometric admittance using 30 day length data blocks with 15 day overlap for Bidston and Edinburgh. Error bars are standard deviation.

creating an additional effect on gravity through air pressure influences on sea level.

The data were also split into subgroups of equal length to investigate how the admittance value changes over time. Figure 3.4 shows the results if the data are split into 30 day segments, each one overlapping by 15 days.

Clearly there is a significant variation of the admittance beyond the standard errors at Bidston from about 0.35 to 0.5 μgal mbar^{-1}. It is harder to draw any conclusions from the Edinburgh data. Ideally more data are needed.

3.7.4 Frequency Dependent Admittance Results for Humidity

Since it has been observed that humidity affects the gravity record, it is valid to remove its effects from the data. As there is a high correlation, it would be sufficient to simply subtract the effects by doing a linear regression. In practise, the differences in the results between doing this and using the frequency transfer method are small. Figure 3.5 shows the original and humidity corrected gravity data using the frequency transfer method.

The graph shows that the method has successfully removed most of the long term variation in gravity. The exception is from the start up to about day 175, presumably the reason being that absolute humidity is not correlated with gravity during this period. The small scale features still exist with gravity variations of up to 30 μgal.

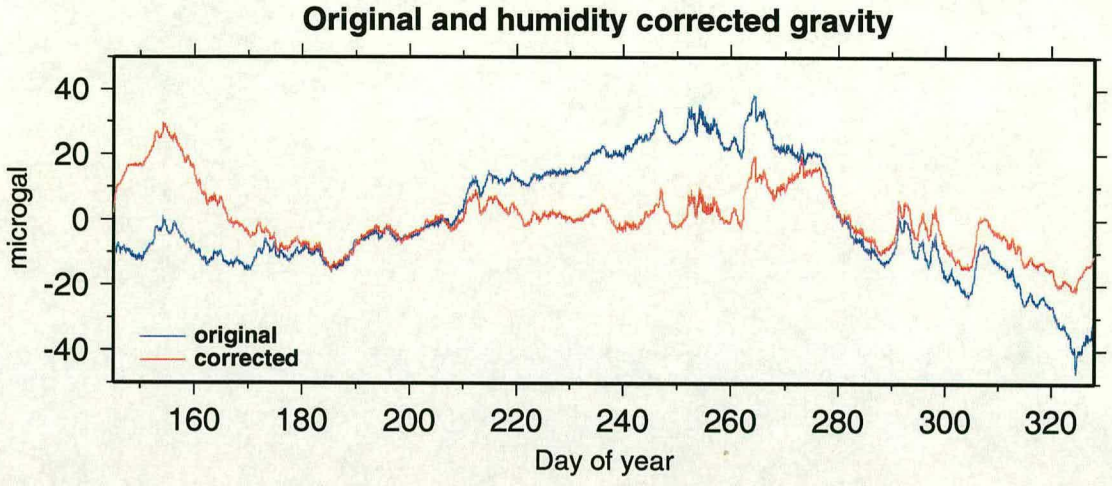

Figure 3.5. Original and humidity corrected gravity using the frequency dependent admittance method.

3.7.5 Frequency Dependent Admittance Results for Air Pressure

Two ways of utilising the frequency dependent transfer function method have been used on the air pressure data. One has been to simply use the entire data set. The second has been to split the data set into two and use the transfer function from one half to correct gravity from the other half. This has the advantage that the correction is completely independent of the data it is being applied to. The results are compared with using a constant admittance value.

Using the entire data set, Figure 3.6(a) shows the results using the frequency dependent admittance method plotted alongside the original gravity data. Figure 3.6(b) shows the results of using the constant admittance value from Section 3.7.3 applied to the gravity data, again plotted with the original data.

It is evident that while the frequency dependent method has been successful in removing features from the gravity data, it is not as successful as the constant admittance method. Consider the period from the start up to day 160, or from day 310 to the end, the results of the latter method are smoother with most of the features removed. However, there are still features, such as around day 250 where the former method appears to work more effectively.

With the data split into two parts of 3 months, the first encompassed 25th May to 25th August, the second 26th August to 24th November, corresponding approximately to the seasons of summer and autumn. The frequency transfer functions for each half can be seen in Figure 3.7.

The amplitude plots both display similar characteristics of an admittance value around 0.25 μgal mbar^{-1} for long periods, rising in a linear manner for higher frequencies. This is in agreement with theory stating that admittance values decrease for larger weather systems (Section

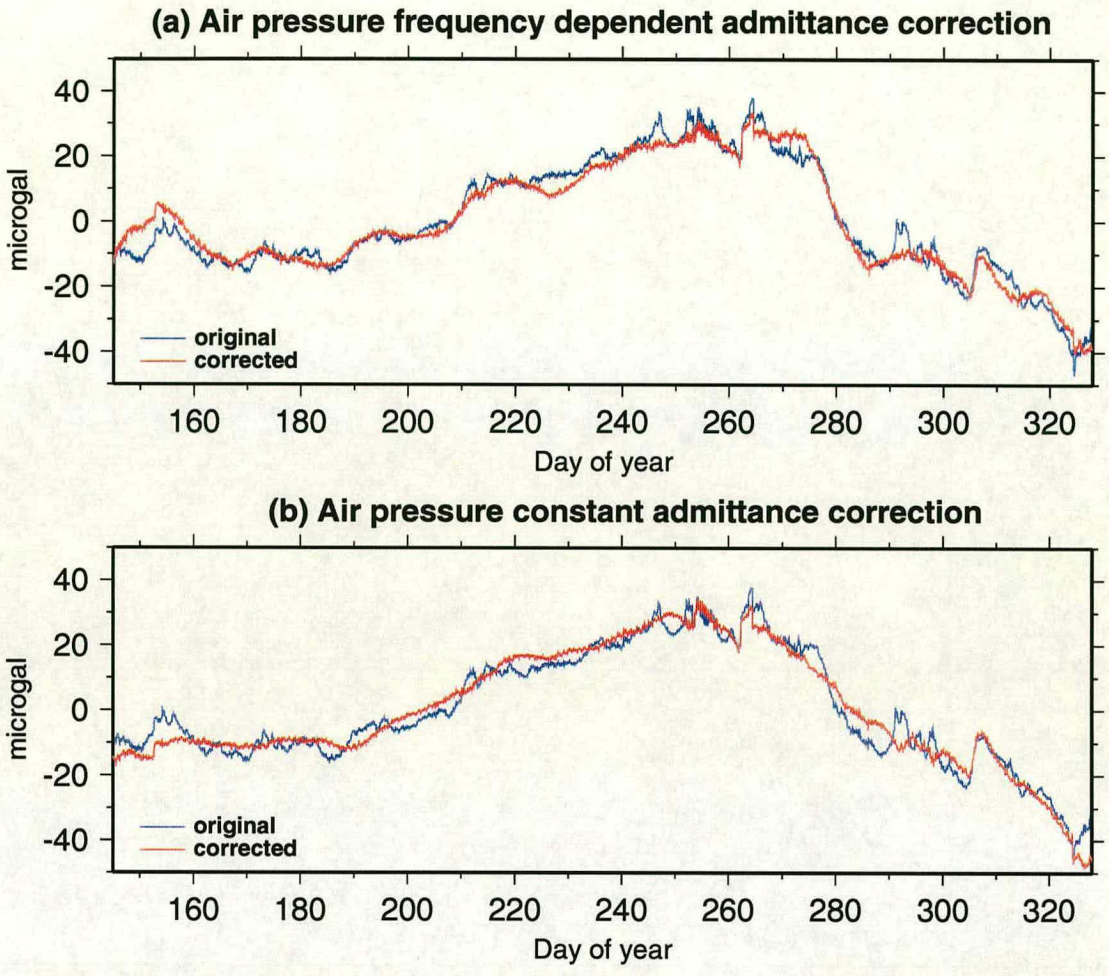

Figure 3.6. Original gravity data plotted alongside gravity corrected for air pressure with (a) frequency dependent admittance and (b) constant admittance value.

3.2). However, the admittance rises to an unexpectedly large 1.5 μgal mbar^{-1} for higher frequencies which cannot be explained. It is unlikely that these will affect the results much since there is not expected to be much power in the gravity spectrum here. It is also evident that the admittance is contaminated at S-wave frequencies, in particular for results from the first half of the data at 4, 6 and 10 cpd.

The phase plots indicate an average value of approximately zero, or no phase lag. The transfer function for the second half appears to have more noise, this could be due to the greater variation of air pressure that occurs in the autumn season.

Figure 3.8(a) shows the results of applying the transfer function found using the second half of the data applied to the first half to correct for air pressure compared with (b) using a constant admittance value. Figure 3.9 shows the corresponding results for the second half of the data set.

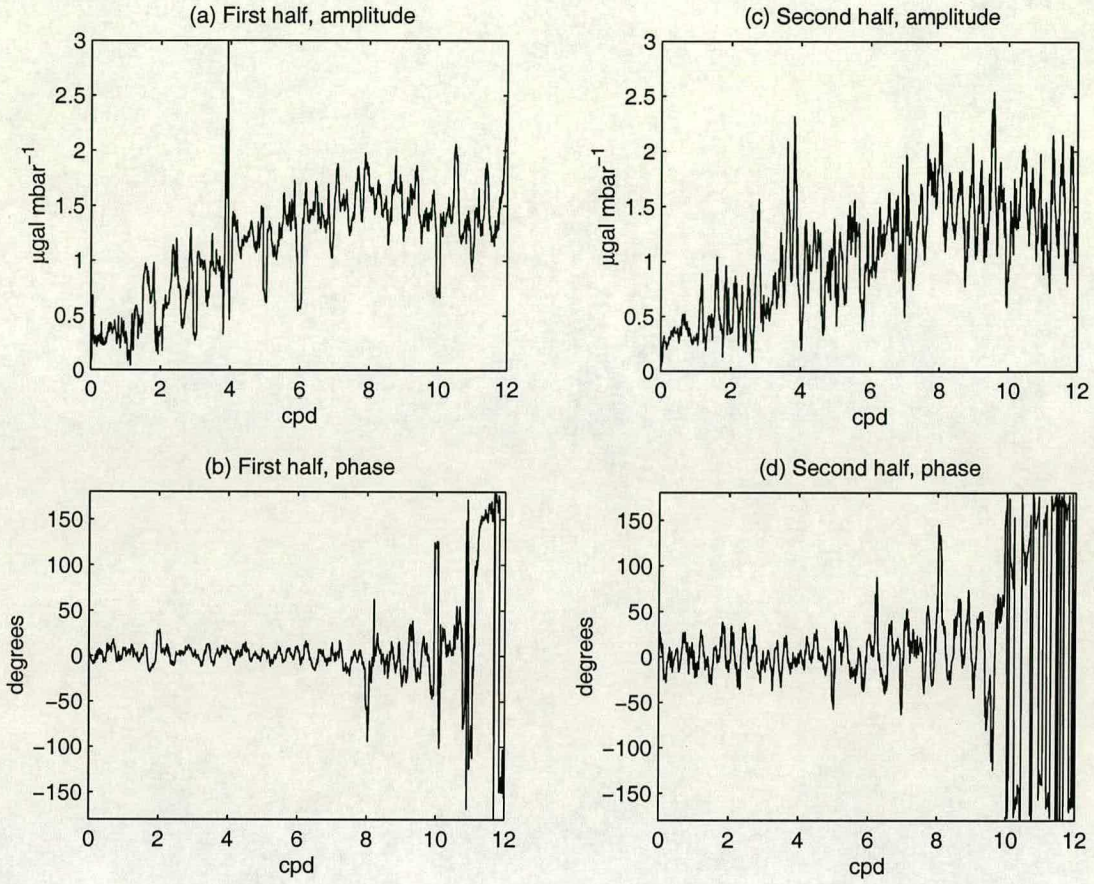

Figure 3.7. Frequency transfer functions between gravity and air pressure shown as amplitude and phase plots for the first and second halves of the data sets.

The graphs suggest that the frequency dependent method is successful in removing some of the features in the gravity data caused by air pressure. The corrections applied in both cases are independent of the data they were performed on and yet still have an element of success. The method is not as effective when using the transfer function for the first half applied to the second half. This could be due to the different air pressure characteristics related to the seasons the data sets are split up into. However, the constant admittance correction proves to be more successful for both first and second halves of the data sets.

Figures 3.10(a) and (b) show the results of applying air pressure corrections to gravity data already corrected for humidity (as in Section 3.7.4). Here the differences between the two methods do not seem so evident. Indeed, examining the period from days 290 to 300 indicates that the frequency dependent method is possibly more successful.

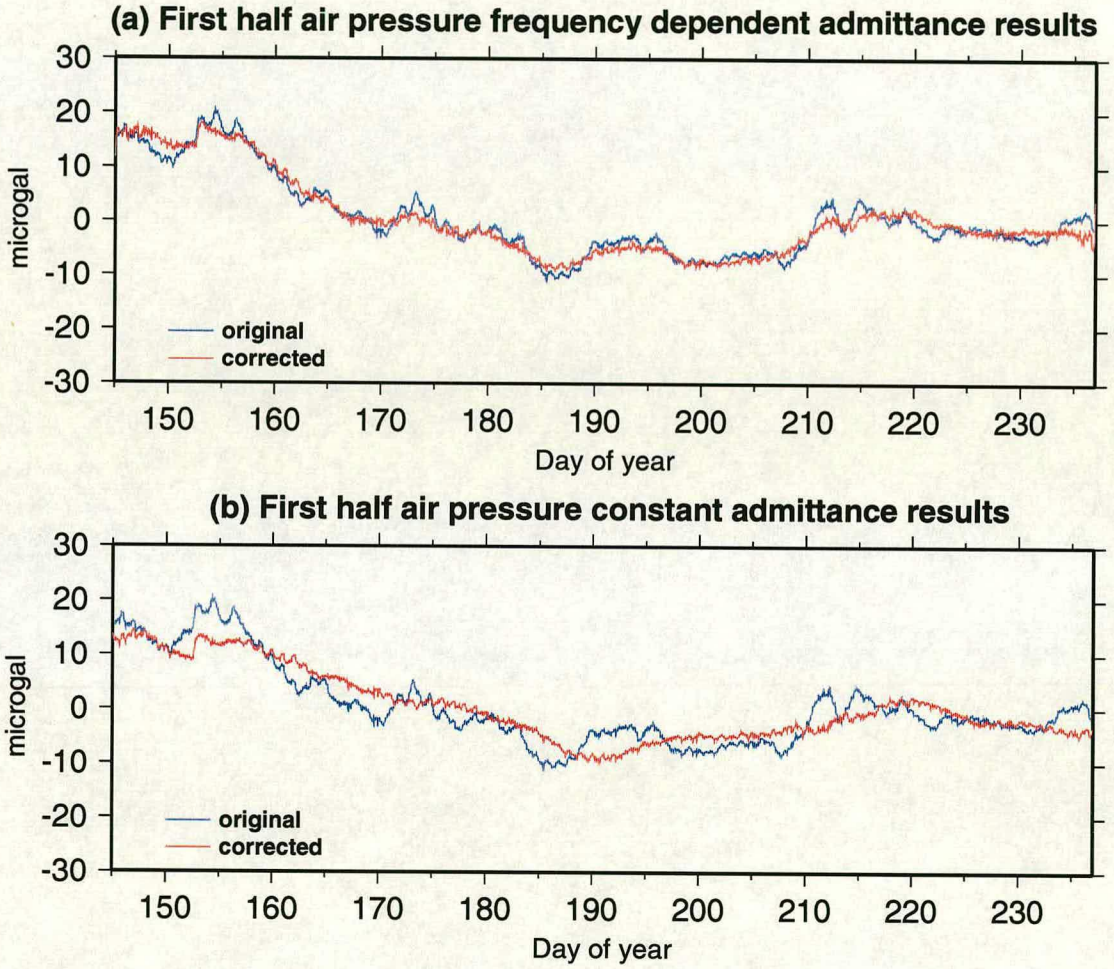

Figure 3.8. First half of gravity plotted alongside gravity corrected for air pressure with (a) frequency dependent admittance calculated from the second half and (b) constant admittance value.

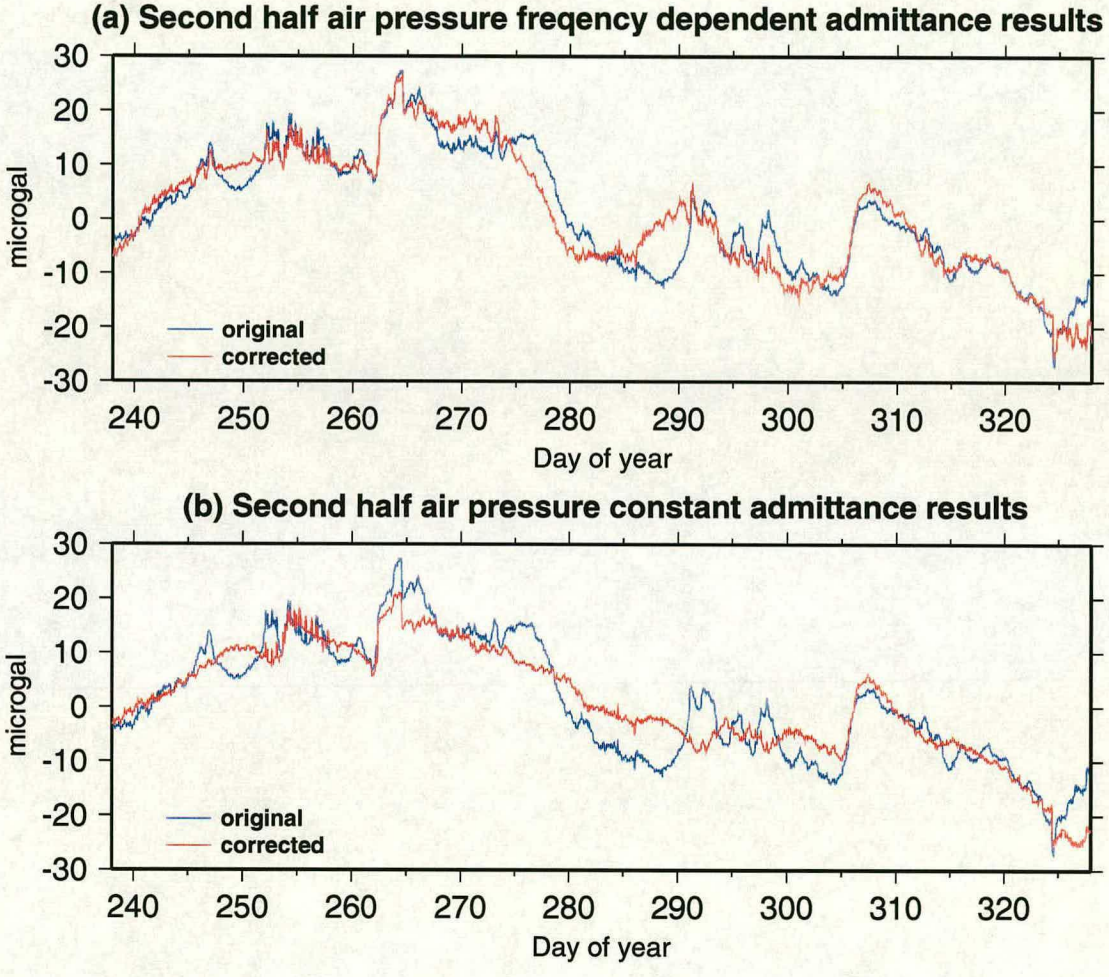

Figure 3.9. Second half of gravity plotted alongside gravity corrected for air pressure with (a) frequency dependent admittance calculated from the first half and (b) constant admittance value.

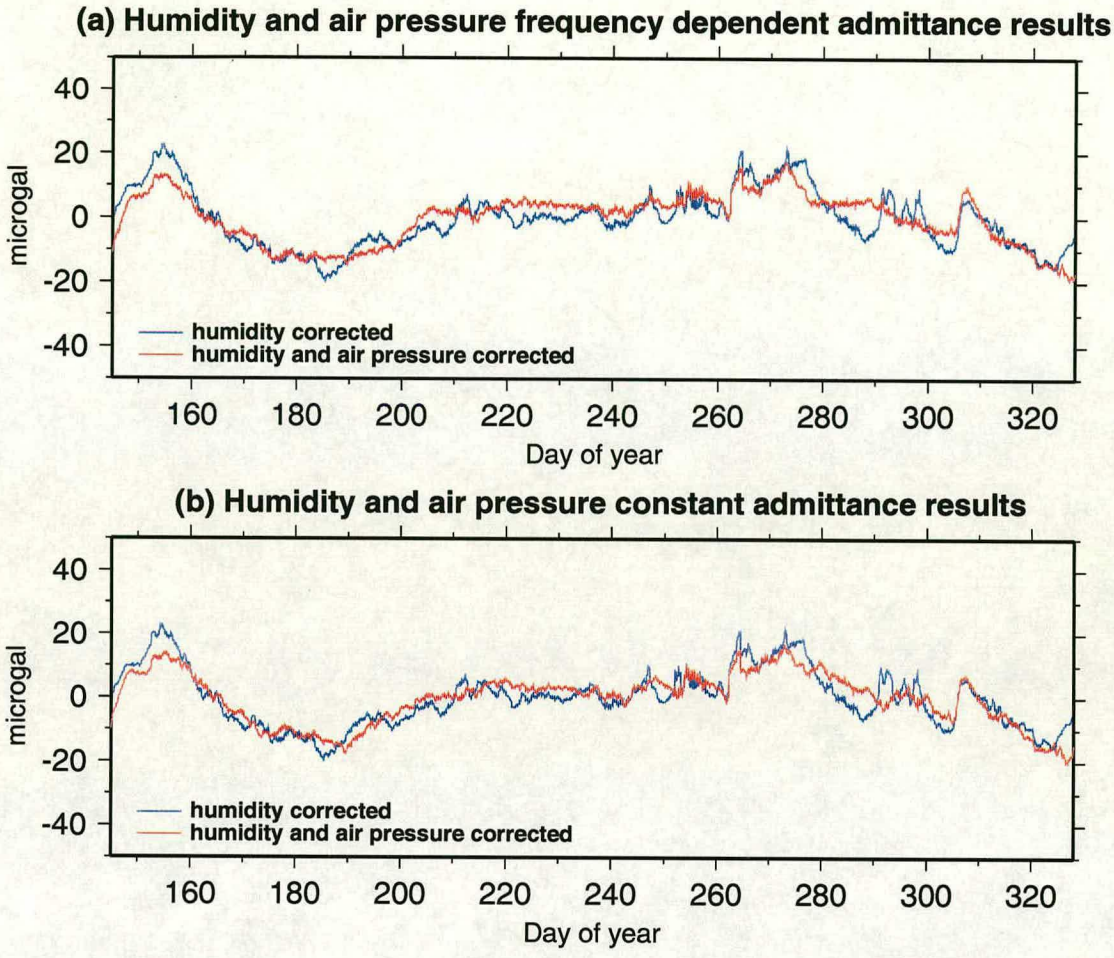

Figure 3.10. Humidity corrected gravity data shown alongside humidity *and* air pressure corrected gravity data using (a) frequency dependent admittance method and (b) constant admittance method.

3.7.6 Frequency Dependent Admittance Results for Rainfall

Features still exist in the gravity data after correction for humidity and air pressure. The frequency transfer method was applied to these data using rainfall data. It was decided to use gravity data corrected for air pressure with a constant admittance value. The results using this method are very similar to using the frequency dependent admittance, and in most cases appear better.

As discussed earlier, rainfall is related to air pressure. Correcting for the part of the rainfall signal which is independent of air pressure was investigated. This was found by using the frequency transfer function method to subtract the interdependent part from the rainfall, and use the remaining values.

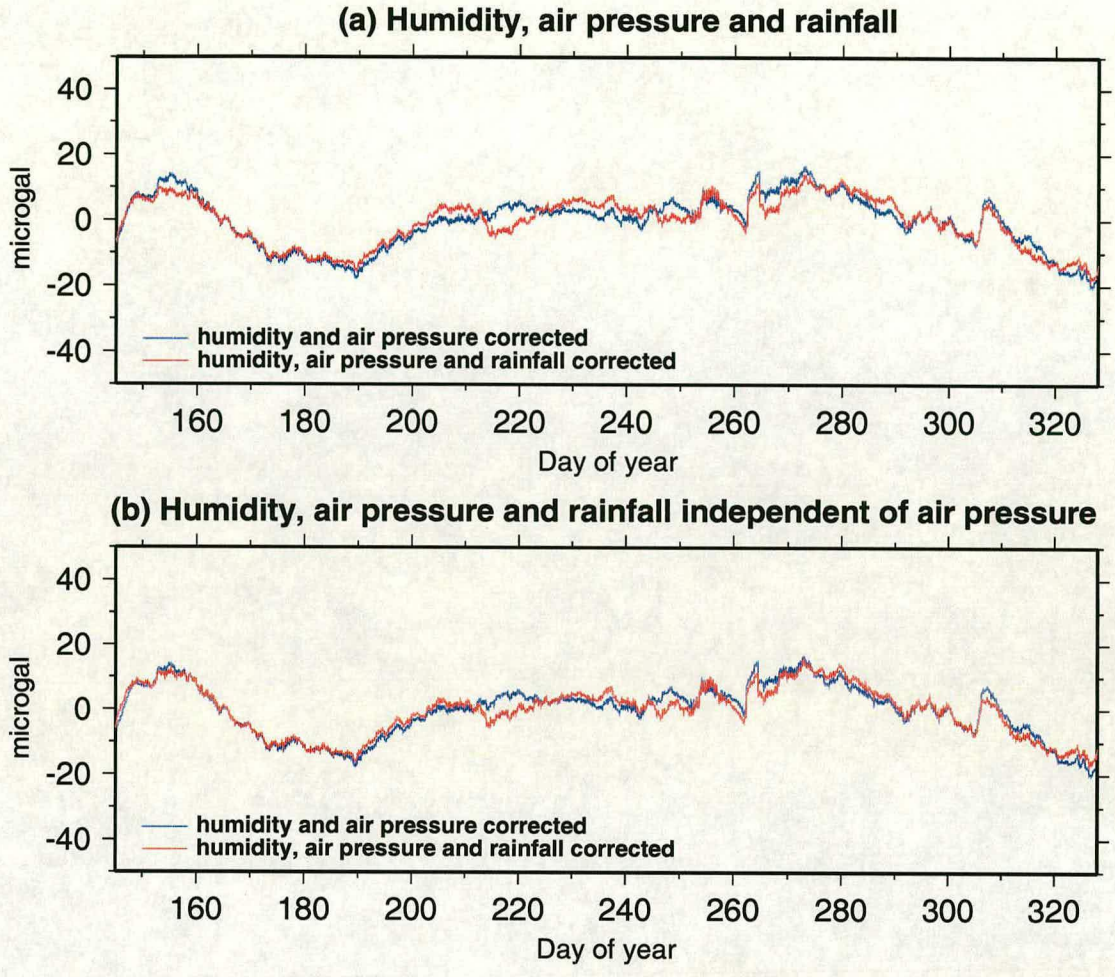

Figure 3.11. Gravity corrected for humidity (frequency dependent method), air pressure (constant admittance method) then (a) rainfall and (b) non-air pressure dependent part of rainfall.

Figure 3.11 shows the results of correcting for rainfall (a), and the part of rainfall not dependent on air pressure (b), from humidity and air pressure corrected gravity data. The plots are in most cases very similar to each other. In the cases where correcting for rainfall appears to have removed features (such as days 155, 248 and 312), results are better using rainfall data not corrected for air pressure effects.

3.8 Absolute Gravity Data

This section presents the problem of seasonally varying absolute gravity measurements at Bidston. Investigations are presented as to whether this is caused by water table changes and if the rainfall at Bidston has the potential to cause the gravity changes. A relationship between gravity and rainfall is investigated and results obtained from the Earth-tide gravity data are applied to see if the seasonal variation can be corrected for.

3.8.1 Absolute Gravity Measurements at Bidston

The FG5-103 absolute gravimeter is based at POL, Bidston and has been making measurements regularly since its purchase in 1992. Due to instrumental problems, early data are not considered reliable and are generally ignored. Data from 1994 onwards have been compiled to give a long term record of gravity observations at Bidston.

Figure 3.12 shows the results of gravity observations from 1994 to 1998. The data were processed by staff at POL on Micro-g Solutions REPLAY software Version 2.2 with all corrections applied. Data sets which failed to meet the criteria of having at least 18 sets, a set standard deviation of less than 5 μgal and a mean standard deviation of less than 55 μgal are not shown. Periods where there is no data are most likely to be due to the instrument being away on fieldwork or needing repairs.

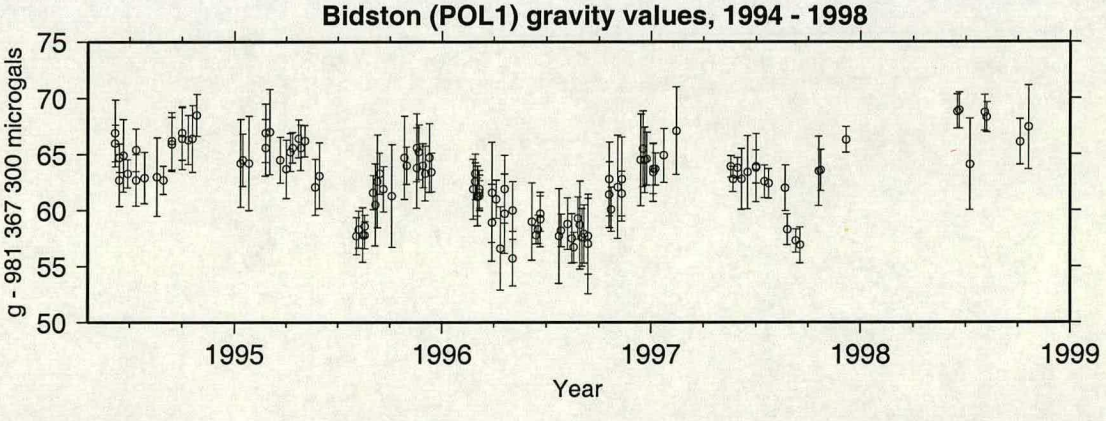

Figure 3.12. FG5-103 absolute gravimeter observations made at site POL1, Bidston from 1994 to 1998. Error bars are set standard deviation.

Subsequent investigation has found some of these values to be in error. These errors have been corrected for, which in the case of data from 1995 to early 1997, is an approximate correction. Figure 3.13 shows the results of these corrections. See Section 5.6 for full details.

It is evident from Figure 3.13 that there is a seasonal variation of gravity. For example, consider

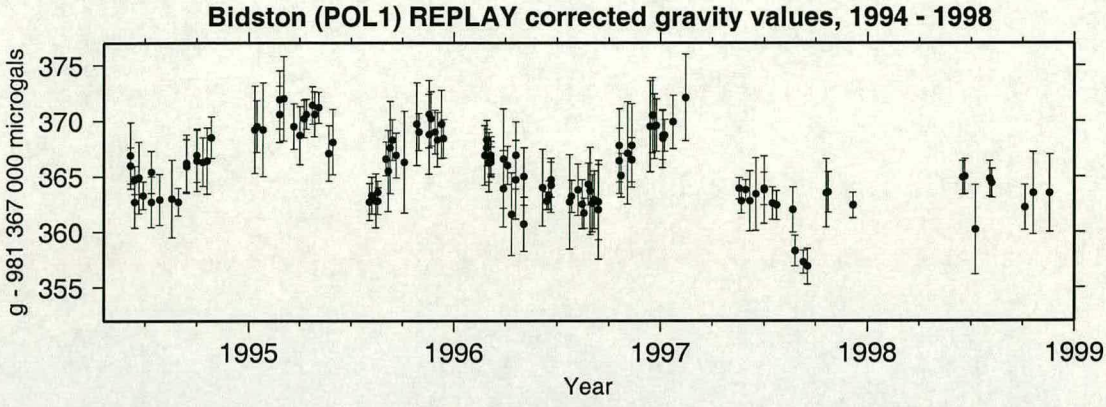

Figure 3.13. Corrected FG5-103 gravity values for POL1, Bidston. Error bars are set standard deviation.

the period 1996 - 1997. Here gravity appears to reduce from the beginning to two-thirds of the way into 1996 by about 5 μgals. There is then an increase of about 8 μgals through to early 1997. This pattern appears to be repeated up to mid-1997, hereafter it is not apparent.

It is thought that the cause of this is most likely to be environmental. An obvious hypothesis would be that seasonal rainfall / groundwater variations are causing the changes. Gravity rises during the onset of autumn which coincides with an increase of rainfall. If this leads to an increase in the amount of groundwater, this could cause gravity to increase. Similarly, gravity falls through the seasons of spring and summer, possibly because decreasing rainfall levels lead to an overall reduction of groundwater in the local environment.

Various investigations have been made in to establishing if groundwater is influencing gravity at Bidston, and whether measurements can be corrected for this effect. Due to the late stage at which the REPLAY gravity data were found to have errors, all investigations in this chapter have been using the uncorrected data of Figure 3.12.

3.8.2 Borehole Measurements at Bidston

A borehole was drilled at POL with the aim of monitoring the water table level to establish if variations in this were causing seasonal changes in gravity. The hole was drilled outdoors to a depth of 60 metres and within 10 metres of the gravity site.

As described in Section 3.3, the level of water in a borehole is the point where hydrostatic pressure equals air pressure. Thus the level will be a combination of influences from the water table level and atmospheric pressure.

Measurements of the borehole water level were taken using a tape measure. This was performed once a day, however there are gaps in the data due to an absence of measurements

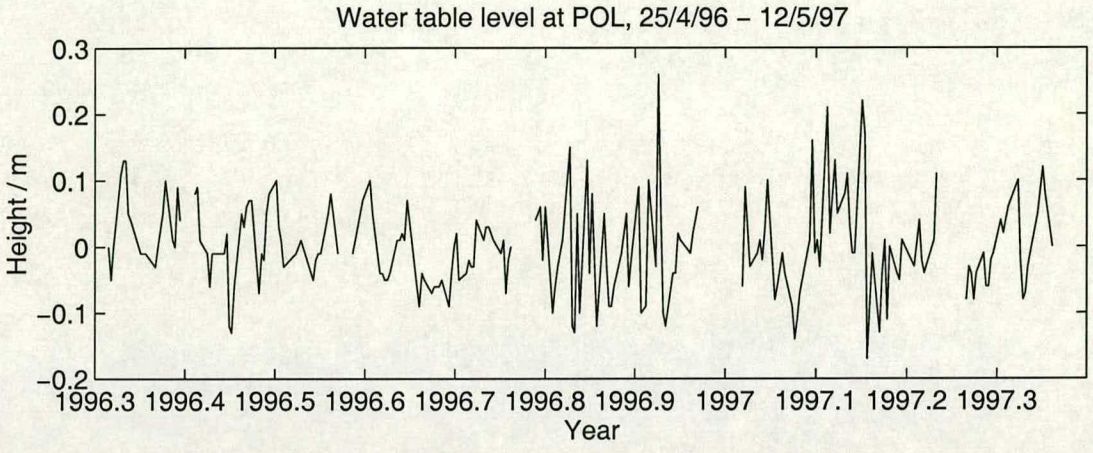

Figure 3.14. Borehole water level measurements at Bidston relative to the mean value.

being made at weekends or during holidays. The period of measurement was from 25/4/96 to 12/5/97.

Figure 3.14 shows the results expressed as height of borehole water level with respect to their mean value. Periods when measurements were not made for over 5 days are shown as gaps in the plot. The mean value was found to be 53.09 metres below the surface. The height of the land is approximately 60 metres above sea level and hence the water level is about 7 metres above sea level.

As can be seen, the level of water varies by up to 0.4 metres peak to peak with no seasonal pattern visible. Under the assumption that the water table level is behaving exactly as the borehole water level, the effect on gravity can be calculated. For this, a knowledge of the rock porosity is needed. Bidston is based on rock of the Sherwood Sandstone group. Porosity of this has been found to range from 1.5% to 26.3% with a median of 15.6% (UK Nirex Ltd., 1993).

Even with a high rock porosity of 25%, variations in the water table of 0.4 metres correspond to a gravity change of only 1.05 μgal assuming the groundwater takes the form of an infinite plate.

Analysis of the measurements showed that the borehole water level is strongly related to air pressure. The correlation factor between the two variables indicated that the borehole water level acts as an inverted barometer with 73.3% efficiency. Simple linear regression revealed an admittance value of 0.46 ± 0.03 cm mbar^{-1}. Assuming that the borehole water level is a combination of water table level and air pressure effects, removing the inverted barometer signal from these data should result in information on the water table level.

Figure 3.15(a) shows the results of using the above admittance to correct the borehole water

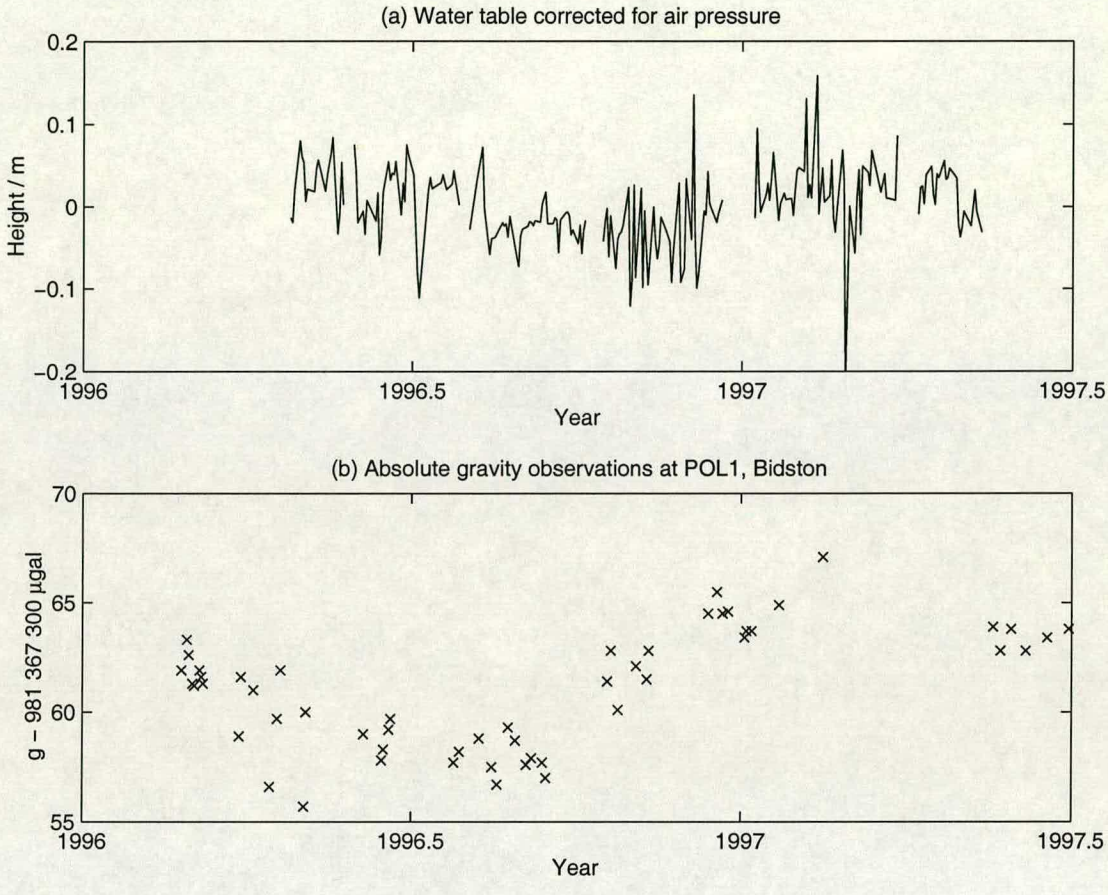

Figure 3.15. (a) Water table level after correcting for air pressure using an admittance value of 0.46 cm mbar^{-1}, relative to the mean value. (b) Corresponding absolute gravity observations for the same period

level for air pressure effects. Now a seasonal variation is visible corresponding to that expected, *ie* a low water table level at the end of summer followed by a rise peaking in late winter. Ignoring noise the peak to peak variation is no greater than 0.1 m corresponding to a gravity effect of 0.27 μgal using the same model as before.

Figure 3.15(b) is a plot of the corresponding absolute gravity observations for the same period. It is evident that there is some correlation with a phase lag since changes in gravity appear to occur about 3 months before a change in the water table level.

A possible mechanism to explain this could be that rain water takes about 3 months to percolate down through the ground before affecting the water table. Indeed, there is no evidence of a simple relationship between water table level and rainfall. The correlation coefficient between the borehole water level corrected for air pressure and rainfall is only 0.015.

In theory it may be possible to correct gravity measurements by using the air pressure adjusted

borehole water level and taking in to account a phase lag. Borehole measurements were made for just over a year and then ceased since no changes in the level had been observed to account for the gravity variations observed. Results presented here indicate that there may be a relationship between the borehole water level corrected for air pressure and gravity. More measurements are needed, and it is suggested that an automated system be installed to monitor the borehole water level continuously giving more frequent and regular data to use.

3.8.3 Potential Gravitational Attraction Effect From Rainfall at Bidston

To assess whether rainfall has the potential to change gravity by the amounts observed at Bidston, calculations have been performed based on simple models using actual amounts of rainfall recorded at Bidston. These are based only on the direct gravitational attraction exerted by water in the ground. The gravity effects caused by deformation of the ground are expected to be less than the instrumental precision and hence insignificant (see Section 3.4).

Table 3.3 gives the monthly rainfall totals for Bidston in the years 1994 - 1996. Note that there is in general an increase in precipitation from September onwards, coinciding with the onset of autumn. The cumulative effect of rainfall occurring in the autumn months will be examined by summing the monthly rainfall amounts from September to December. This will find the maximum potential change in gravity assuming there is no surface run-off or drainage of ground water out of the local environment.

mm	Jan	Feb	Mar	Apr	May	June
1994	50.0	34.6	60.6	82.9	39.0	33.2
1995	99.8	71.2	55.2	32.2	56.0	20.0
1996	13.4	35.2	26.8	59.6	36.4	31.6
mm	July	Aug	Sept	Oct	Nov	Dec
1994	6.8	46.6	78.6	96.2	71.6	103.0
1995	42.2	13.4	128.4	15.6	47.0	40.2
1996	18.6	92.6	24.0	88.8	116.4	48.4

Table 3.3. Monthly rainfall totals for Bidston, 1994 - 1996.

The gravity effect will be calculated by supposing the ground water is arranged in various simple configurations.

Thin Plate

This, the simplest model, is an infinite plane plate of uniform surface density. It is not a realistic model since the site is on top of a hill and hence an infinite plane will not be true for ground water contained within the hill. It is also unlikely that the ground water is held in the bedrock as a thin layer.

The formula used to calculate the gravity effect is:

$$\Delta g = 2\pi G\sigma \tag{3.8}$$

where G = gravitational constant and σ = surface density.

The results using this formula are given in Table 3.4.

Year	Sept	Sept+Oct	Sept+Oct+Nov	Sept+Oct+Nov+Dec
1994	3.3	7.3	10.3	14.7
1995	5.4	6.0	8.0	9.7
1996	1.0	4.7	9.6	11.7

Table 3.4. Gravitational attraction of a thin infinite plate with uniform density. Values are in μgal.

Thin Disc

Here a circular disc replaces the infinite plate creating a more realistic scenario for a site based on top of a hill. Once again it is assumed that the water is held as a thin layer, and also that the hill is of a circular shape, whereas in reality it is elongated. The formula used is:

$$\Delta g = 2\pi G\sigma(1 - \cos\alpha) \tag{3.9}$$

where the angle α is defined as shown in Figure 3.16.

Assuming Bidston Hill is roughly 1500 m $\times$ 800 m, an approximate disc radius of 500 m has been used. The disc is assumed to be 50 m below the surface which is approximately the depth of the water table level. Results are given in Table 3.5.

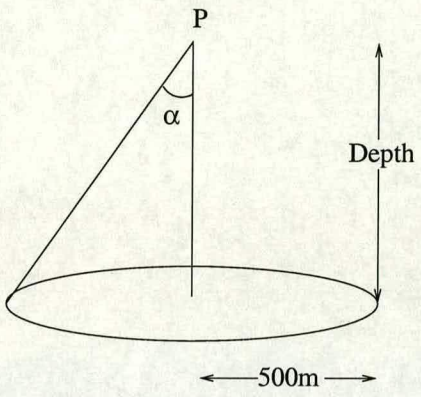

Figure 3.16. Set up of the thin circular disc model.

Year	Sept	Sept+Oct	Sept+Oct+Nov	Sept+Oct+Nov+Dec
1994	3.0	6.6	9.3	13.2
1995	4.9	5.4	7.2	8.7
1996	0.9	4.3	8.6	10.5

Table 3.5. Gravitational attraction of a thin disc of uniform density and radius 500 m at a distance of 50 m. Values are in μgal.

The effect of changing the depth of the disc below the surface for the 1994 Sept+Oct values can be seen in Table 3.6. It is clear that the variations are less than 1 μgal and can be considered insignificant.

Table 3.6 also shows the effects of varying the radius of the disc for the 1994 Sept+Oct values. Changes are below 1 μgal if the radius is not allowed to fall below 200 m, approximately the dimensions of Bidston Hill.

Depth (m)	5	10	20	30	40	50
μgal	7.2	7.2	7.0	6.9	6.7	6.6
Radius (m)	100	200	300	500	750	1000
μgal	3.7	5.5	6.1	6.6	6.8	7.0

Table 3.6. The effect of changing the depth and radius of the thin disc on Sept+Oct 1994 values.

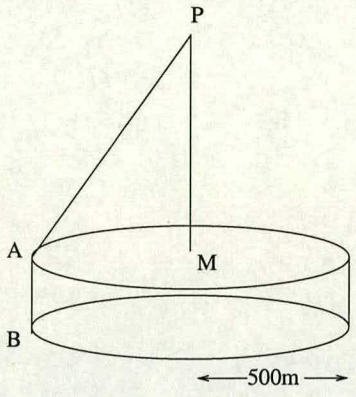

Figure 3.17. Set up of the cylinder model.

Cylinder

The thin disc model is developed here by assuming the ground water is configured in the shape of a cylinder. The cylinder has density ρ which is equivalent to the porosity of the rock, hence the height of the cylinder varies according to the rainfall. The formula is:

$$\Delta g = 2\pi G\rho(AB + PA - PB) \tag{3.10}$$

Refer to Figure 3.17 for details of what the distances refer to. The radius is once again chosen to be 500 m, and the depth of the bottom of the cylinder 50 m below the ground which is approximately the depth of the water table level. This means that the height AB will vary according to how much water is contained within. Porosity of the rock is assumed to be 15%. Table 3.7 gives the results using these dimensions.

Year	Sept	Sept+Oct	Sept+Oct+Nov	Sept+Oct+Nov+Dec
1994	3.0	6.6	9.3	13.2
1995	4.9	5.4	7.3	8.7
1996	0.9	4.3	8.7	10.5

Table 3.7. Gravitational attraction of a cylinder with a 500 m radius and variable height according to rainfall amount, the furthest face being at a distance of 50 m. Values are in μgal.

Entire hill saturation

To examine the maximum potential effect of ground water on gravity at Bidston Hill, a calculation has been made under the assumption that all the bed rock is saturated with water. The cylinder model is once again used, but in the case that the site is at the centre and on the upper surface of the cylinder (*ie* P coincides with M in Figure 3.17). The following formula is used:

$$\Delta g = 2\pi G\rho \left(AB + AM - \sqrt{AM^2 + AB^2} \right) \tag{3.11}$$

With a porosity of 15% and cylinder height AB = 50 m (almost to the water table), the result is Δg = 300 μgal.

This would correspond to the water table being at the surface of the hill top, which is physically unrealistic.

Summarising

The results clearly show that the rainfall amounts are sufficient to cause gravity changes of the order of 8 μgal. The results of the various models are very similar, with the maximum potential effect from rainfall on gravity for the four months examined ranging from about 9 μgal for 1995 to about 15 μgal for 1994.

This is with the assumption that there is no outlet of groundwater from the environment. Taking different time intervals or using different proportions of the monthly rainfall totals may give more realistic results. It may also be worthwhile looking at the extra rainfall in autumn above that which falls during summer since it is the increase in rain that appears to cause the change in gravity.

The calculation of the potential maximum effect has shown that the gravity changes observed are much less than this. This implies that the hill is holding only a small fraction of water compared with its maximum capacity. It is not known whether the moisture is held throughout the entire depth of the hill, as layers that may percolate down through the hill, or some other process.

Running mean length (days)	Correlation coefficient
10	0.1204
20	0.0839
30	0.0834
45	0.1886
60	0.3070
75	0.4364
90	0.4698
120	0.5807

Table 3.8. Correlation coefficients between absolute gravity measurements at Bidston and running mean of rainfall for different window sizes.

3.8.4 Examination of Bidston Rainfall Data

It has been established that rainfall has the potential to cause the seasonal gravity variations observed at Bidston. Daily measurements of rainfall were available for the period of observations. These were smoothed through use of a running mean window. Values from this were then selected for the days on which gravity measurements were made to find the correlation coefficient.

Table 3.8 shows the correlation coefficient between gravity and running mean rainfall values for different sizes of window. The correlation coefficient increases up to about 50% for running mean window sizes of around 100 days in length.

Figure 3.18 is a plot of the 90 day rainfall running mean alongside Bidston gravity values. It is evident where some of the correlation occurs, for example in late 1995 and late 1996 where larger rainfall amounts coincide with higher gravity values.

It is possible that more complex models of rainfall / groundwater interaction may give higher correlations with gravity changes. For example, a model incorporating a lag between rainfall and its effect on gravity. Or alternatively a model giving a low weighting to high intensity rainfall to account for run off. Time restraints did not permit this to be investigated further. It should also be noted that the gravity data presented in Figure 3.18 had not been corrected for errors found at a subsequent date (see Section 5.6). The corrected data (Figure 3.13) show a pattern that may produce a higher correlation with rainfall.

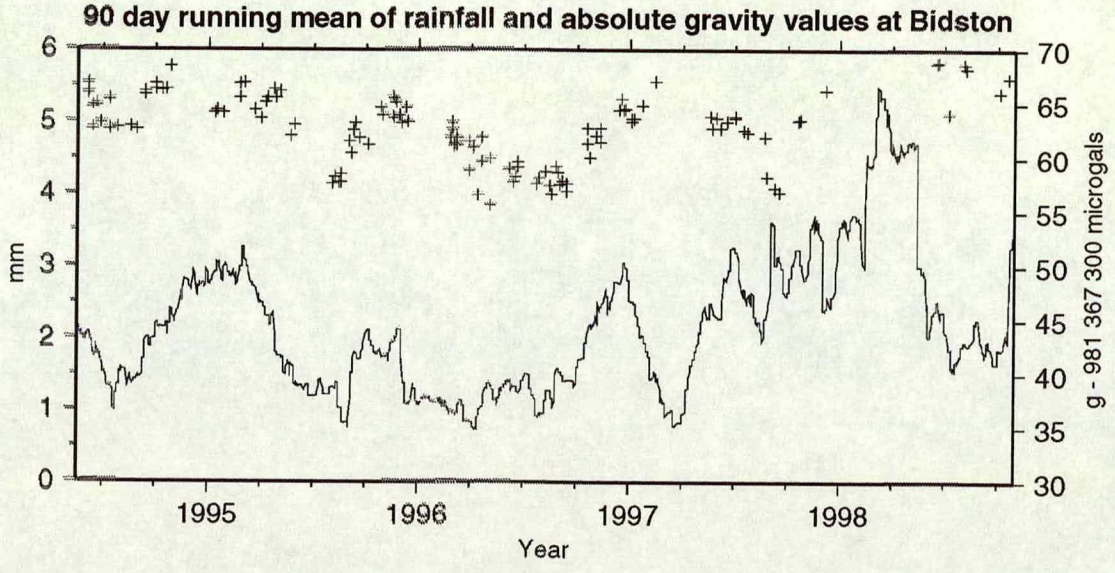

Figure 3.18. 90 day running mean of rainfall plotted together with gravity values for Bidston.

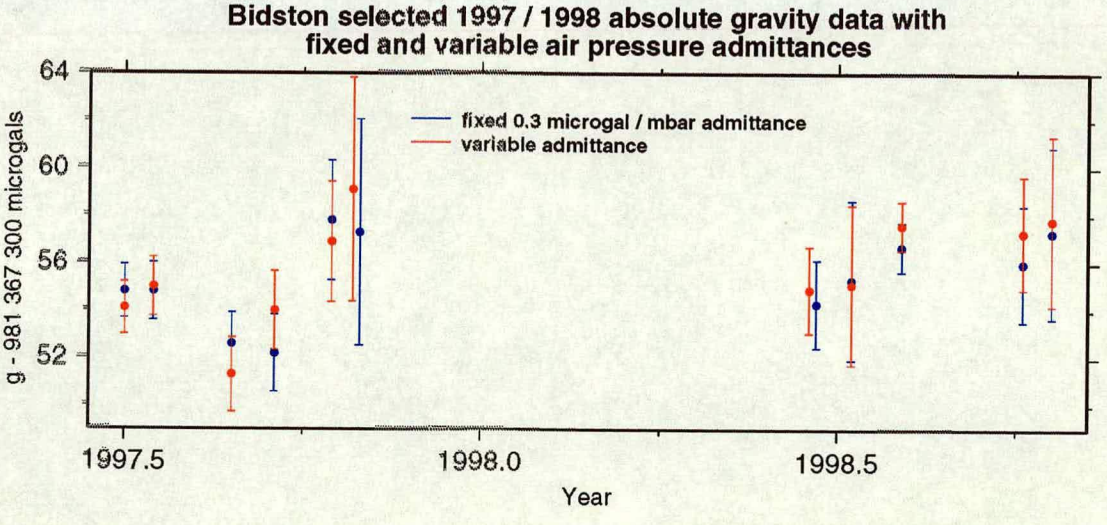

Figure 3.19. Comparison of Bidston observations July - November 1997 and 1998 with fixed (0.3 μgal mbar^{-1}) admittance and variable admittance using ET10 data results. Error bars are set standard deviation.

3.8.5 Constant Admittance Results for Air Pressure

Figure 3.19 shows the results of applying the varying admittance at Bidston from Section 3.7.3 to selected absolute observations during periods of 1997 and 1998 which coincide with the period of Earth-tide measurements. The admittance value was found by linearly interpolating from the results to the appropriate day for which the data set was taken. The data were processed using Edinburgh DDT software, and values obtained using the standard 0.3 μgal mbar^{-1} admittance are plotted alongside.

For the 1997 data, there is a possible reduction in the scatter using the variable admittance. In particular, the third to sixth data points now show a steady linear rise in gravity. The 1998 data exhibit a less obvious change in the character of the measurements. It is possible that the admittance results of the ET10 gravimeter in 1984 were specific to that epoch due to the particular air pressure characteristics of that year. It may not be appropriate to apply them in general. More observations would be needed to test this theory, and to also find the admittance variation for the entire year.

3.8.6 Frequency Dependent Admittance Results for Rainfall

Figure 3.20 shows the Bidston absolute gravity data corrected for rainfall using the frequency dependent transfer function found from the Earth-tide gravimeter data already corrected for humidity and air pressure, as in Section 3.7.6. A 3 day running mean of the daily values of rainfall was used.

Contrary to the aim of removing the seasonal signal in the gravity data, correcting for rainfall has resulted in scattering the data and removed some of the structure that was evident before correction. Taking as an example the data from 1995, during the first half a few data points are now about 8 μgal below the general cluster of points for this period. During the last quarter of 1995, data that were before correction self consistent are now more scattered, having been corrected in both a positive and negative direction.

Correcting the absolute gravity values recorded at Bidston using a frequency transfer function developed empirically from 6 months of Earth-tide gravity data from a different epoch has not removed a seasonal signal in the data.

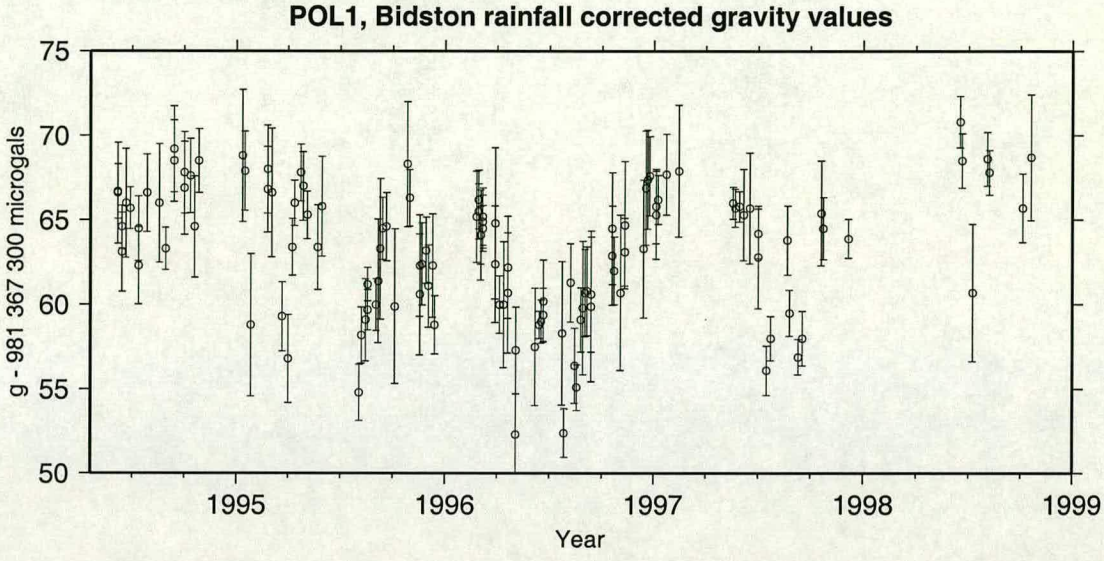

Figure 3.20. FG5-103 absolute gravity measurements at POL1, Bidston for 1994 to 1998 corrected for rainfall using the frequency dependent transfer function from Section 3.7.6. Error bars are set standard deviation.

3.9 Conclusions

Using Earth-tide gravimeter data, constant air pressure admittance values have been found for Bidston and Edinburgh. They are considerably higher than the 0.3 μgal mbar^{-1} value normally assumed. This suggests that gravity data should be processed with these values for improved accuracy.

Examination of how the constant air pressure admittance varied with time revealed a variation from 0.35 to 0.5 μgal mbar^{-1} at Bidston. Of the data available at Edinburgh, there appeared to be little variation of the constant admittance.

The frequency dependent admittance method was successful in removing a long period 70 μgal signal in Bidston Earth-tide gravity data using humidity. This concurs with previous reports that humidity has an affect on LaCoste & Romberg Earth-tide gravimeter data. The use of air pressure data are on the whole less effective at removing features from the gravity data using a frequency dependent admittance method than using a constant admittance value. However, the former method showed some success in removing features when rainfall data were used.

Throughout the use of the Earth-tide data, it was assumed that the drift of the instrument was linear. This may not be true since drift characteristics can change, for example after a large earthquake.

A possible relationship has been found between absolute gravity observations and borehole water table level. Theoretical calculations showed that rainfall amounts have the potential to

cause the seasonal changes of gravity observed. A weak correlation was found between gravity and running mean rainfall values. This could be improved by using more sophisticated models.

Results from the Earth-tide gravimeter were used to correct FG5 absolute gravity observations at Bidston. Using the Bidston constant admittance variation applied to absolute data, there did not appear to be any reduction in the scatter of gravity values. This suggests that the scatter of absolute data is not solely due to air pressure effects. Consideration should also be given to the fact that the admittance variation presented may be unique to that particular period of time. The frequency transfer function found using rainfall data applied to absolute observations increased the scatter.

It is possible that further work could bring more success in correcting for the seasonal variation of absolute gravity values at Bidston. In particular, results here have been obtained using absolute gravity data found at a subsequent date to have errors. Making corrections for these appears to increase the correlation between rainfall and gravity. Using data re-processed to avoid these errors may improve results.

However, more continuous and extensive measurements may be necessary. Continuous monitoring of the water table level is recommended since further data are needed to examine the potential relationship presented in this chapter. Installing a superconducting gravimeter would bring the advantage of higher precision and a much lower drift rate than a spring balance gravimeter. Other methods may also be considered such as electrical resistivity.

Chapter 4

FG5 Instrumental Effects

The aim of this chapter is to present known effects in FG5 absolute gravimeters that cause changes in the values produced by them. The FG5 gravimeter is a collection of electronic and mechanical components, and so the source of these effects is usually either electronic or mechanical.

Effects presented include those from laser lock shifts, the comparator response and the scalar counter. Some mechanical effects are shown as manifestations in the residuals. The magnitude of these effects on gravity are estimated using both real and artificial data.

It should be noted that these are known effects, and there may be unknown factors not yet accounted for. As the accuracy and precision of gravimetry increases with improving technology, the trend tends to be that more effects are discovered or become significant.

The results presented are, when not stated otherwise, from absolute gravimeter FG5-103. This is owned by the Natural Environment Research Council and based at Proudman Oceanographic Laboratory (POL), Bidston. The majority of absolute gravity data used in this research was produced by this instrument.

Also presented are intercomparisons of FG5-103 values with FG5-101 and FG5-202. This was important to ensure that the values returned are in agreement with other instruments and so increase the validity of results produced by this instrument.

4.1 Laser Lock Shifts

The iodine stabilised laser works by using the absorption peaks of $^{127}I_2$ to emit light at one of a selection of fixed wavelengths. The wavelength of the light is 'dithered' at a certain frequency to allow detection of and lock on to these peaks. To maintain a fix on these peaks, the length of the light cavity within the laser needs to be kept at a certain value. This is done using electronic

Peak	Wavelength (nm)	Gravity change from shift to higher lock (μgal)
D	632.991 177 539	0.00
E	632.991 194 728	-26.65
F	632.991 212 588	-27.69
G	632.991 230 227	-27.35
H	632.991 368 898	-215.02
I	632.991 398 220	-45.47
J	632.991 427 042	-44.69

Table 4.1. Iodine laser wavelengths. Also shown are the corresponding changes in gravity due to lock shifts, calculated assuming a gravity value of 9.815 ms^{-2}.

heating to generate thermal expansion. The voltage supplied to this heating is output in the '1F' channel.

Occasionally the laser lock 'shifts' on to a different peak. The cause may be due to internal reflections in the laser head (*pers. comm.* T. Niebauer, 8th August 1997). This results in fringe data being processed using a different distance spacing to what is actually being measured. As a result the gravity value is changed, the relationship being linear with respect to the change in wavelength of the light. Since the difference in wavelength between the iodine peaks is known, correcting gravity for these shifts is in principle straight forward.

The peaks are represented by letters, with the FG5 iodine laser able to emit light on those of *D, E, F, ... J*. Typically peaks *E* or *F* are selected. Table 4.1 shows the light wavelength for each of the peaks and the change in gravity that would be observed should the peak shift to an adjacent one.

In practice, it is necessary to know at which point the laser shifts lock. If the peak shifts, the 1F voltage will change. Recording this while measuring (usually on 'Channel 4' of the environmental sensor inputs) can be used to detect peak shifts. However, not all data sets, in particular early ones, have this information. The only method of correcting without the 1F voltage is to look for distinct changes in the gravity values. These two methods are explored.

4.1.1 Lock Shift Detection Using Voltages

To enable detection of laser lock shifts via monitoring the 1F voltage, before commencing a data run it is necessary to record the voltage for each peak lock manually. Table 4.2 gives an example of typical values.

Note that the voltages fall for increasing peak lock until peak *H* beyond which they rise. Peak shifts between *G* and *H* should not be possible (*pers. comm.* T. Niebauer, 8th August 1997).

Peak	*D*	*E*	*F*	*G*	*H*	*I*	*J*
Volts	+0.203	-0.109	-0.371	-0.653	-1.005	-0.799	-0.589

Table 4.2. Typical 1F voltages for laser lock peaks (taken from data set MED2711A, Medicina 1996).

The Edinburgh DDT FG5 gravity data processing software (see Section 5.1) was programmed to look for lock shifts between *D* - *G* and *H* - *J* by examining where the 1F voltage falls with respect to the half way mid-point voltages of the peak locks.

Examination of the Micro-g Solutions Inc. REPLAY software Version 2.2 showed that a similar method was utilised except that it assumes *increasing* voltages for peaks *D* - *G*. Technically this is incorrect, possibly resulting in the wrong laser lock being used in some instances.

Figure 4.1(a) shows the 1F voltage for data set POL2801A taken at Bidston in 1997. Here a good example of two lock shifts can be seen, the first occurring during set 4 and the second in the opposite direction at the end of set 11 lasting 5 sets. Note that the temperature throughout this data run was stable (Figure 4.1(b)).

It is possible that the 1F voltages for each peak can drift during operation. This may happen soon after the laser is turned on whilst still warming up, and also if the ambient temperature is varying. Figure 4.1(c) shows how the 1F voltage varied during the data set WET3009A taken at Wettzell in 1997, where there were no apparent laser lock shifts.

One can see initial rapid fluctuations while the laser was warming through. The voltage settles down to an equilibrium level by hour 9. It undergoes further variation from hour 20 which corresponds to a change in the temperature (see Figure 4.1(d)). These variations are up to 0.2V, which is greater than half the separation gap between different peak voltages (for example, in Table 4.2).

Note that in this case, it takes at least 9 hours for the laser 1F voltage to settle (this may in part be due to coincident ambient temperature fluctuations), and that temperature variations of less than 1^{o}C are sufficient to cause a voltage change greater than half the separating gap between the peaks.

If the 1F peak voltages are varying by more than half the separation gaps, then the voltage peak detection will be unreliable and should not be used.

4.1.2 Lock Shift Detection Using Gravity Values

Using only gravity values recorded to detect laser lock shifts presents a greater challenge. For a set of 200 drops and a typical gravity change of 28 μgal, the lock shift should be known to

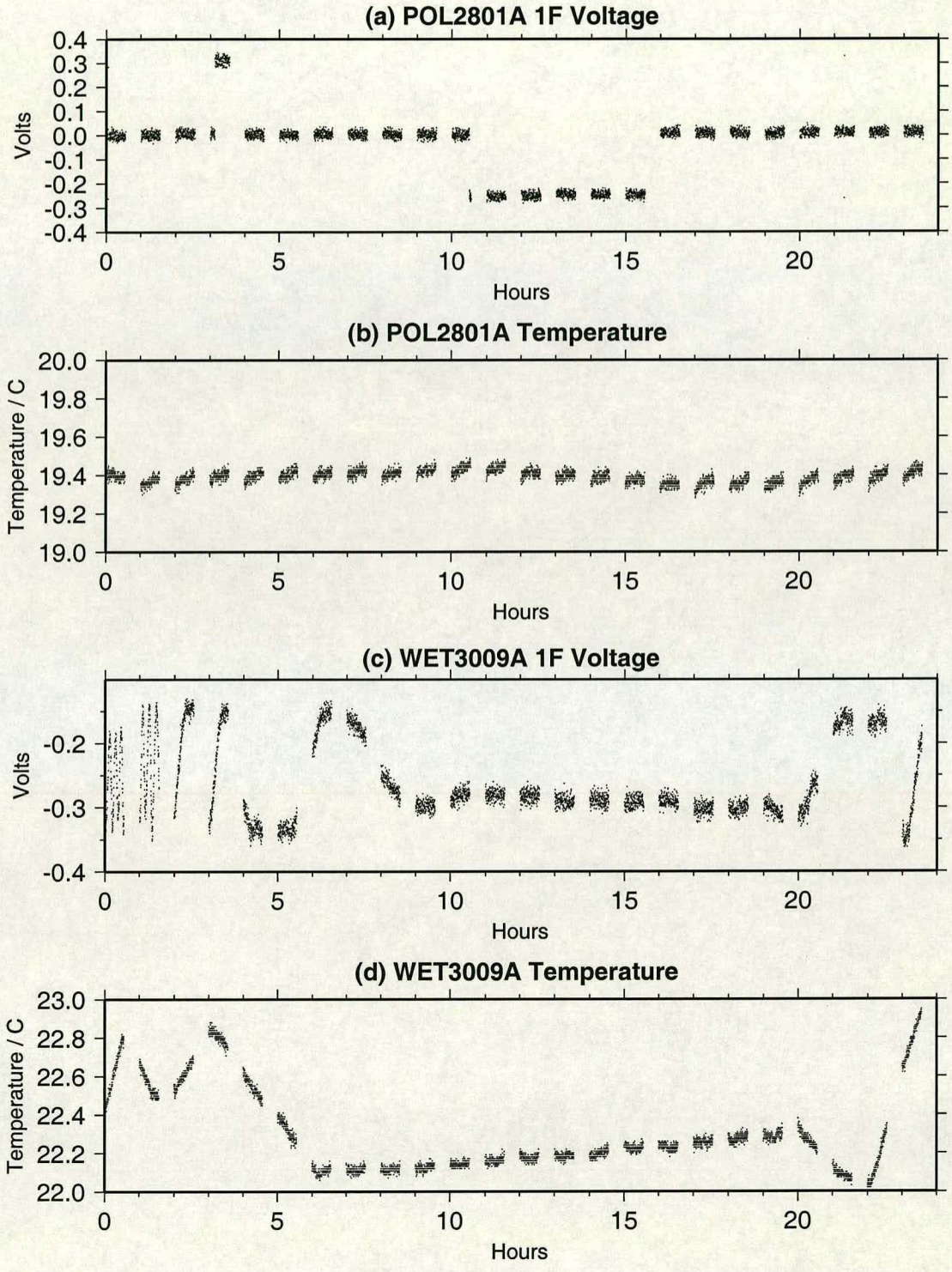

Figure 4.1. Laser 1F voltage and temperature for data sets POL2801A(1997) (a)&(b) and WET3009A(1997) (c)&(d).

within 7 drops for an accuracy of 1 μgal.

It is quite common that set average values are distinctly different from each other, implying that the laser shifted lock either while the gravimeter was resting in between two set runs, or perhaps more likely that the lock was perturbed when the gravimeter started operation for the next set. In these cases it should be sufficient to assume the entire set was affected by the lock shift.

However, it is not so easy to pin-point lock shifts occurring part way though a set. With a drop to drop scatter typically as high as 50 μgal, changes of 28 μgal are not very distinct. A routine, RUNNINGMEAN, was written to calculate the running mean of the gravity values and look for changes in this as an indicator.

The routine was found to give the best results when using a running mean size of 10 drops. The gravity data were first filtered using a 50 μgal boxcar filter centred on each set mean. Using the remaining values, distinct changes in gravity were reported from the point where the running mean changed by an amount greater than 20 μgal and lasted for more than 20 drops. The method was executed by examining the data set from beginning to end and then repeating the process by examining the data from end to beginning.

This routine was applied to various data sets where the 1F voltage was recorded to see if the predicted results from the program agreed with observations from the 1F output. POL0608A taken at Bidston in 1998 could be regarded as a 'quiet' data set with a drop to drop standard deviation of 10.8 μgal. It has a laser lock shift in set 1 from drops 1 to 132. RUNNINGMEAN results say that drops 1 to 149 are affected.

Data set MAC0811A was taken at Aberdeen in 1995. It has a drop to drop standard deviation of 25.5 μgal. The data are affected by laser lock shifts from set 10 drop 70 to set 14 drop 200 and also the whole of set 22 only. RUNNINGMEAN claims there are lock shifts from set 9 drop 66 to set 13 drop 189 and also set 21 drop 26 to the end of set 22.

Clearly the results of RUNNINGMEAN are in poor agreement with the true occurrences of laser lock shifts. In general, it is more reliable to check for possible laser lock shifts by examining the set averages by eye. Where a shift occurs part way through a set, it would be advisable to simply discard the data from that set.

Given that laser lock shifts disrupt little gravity data, that the 1F channel is not recorded only on early data sets, and that other complications such as ocean loading effects within the gravity data could confuse the routine further, use of RUNNINGMEAN was not pursued.

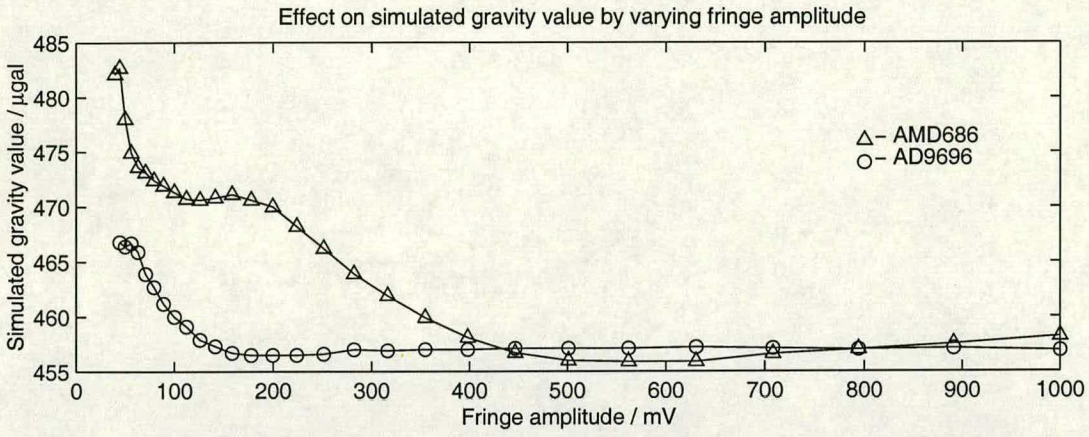

Figure 4.2. The effect on simulated gravity by varying fringe amplitude for comparator types AMD686 (old) and AD9696 (new) (Niebauer *et al.*, 1995).

4.2 Comparator Response

The fringe signal output from the laser interferometer is detected by a high speed avalanche photodiode. This is passed through an AC-coupled high speed comparator which produces digital pulses at zero fringe signal crossings. A delay between the zero fringe signal being detected and the digital pulse being produced may result in an effect on the gravity value. If the delay time is constant, there will be no gravity effect. However, a delay time that is frequency or amplitude dependent will appear as a gravity signal and perturb results.

Two types of comparator have been used in FG5 gravimeters. Originally type AMD686 was used. This was superceded by a faster comparator, type AD9696. Niebauer *et al.* (1995) found that low fringe amplitude, or light levels cause changes in the gravity value. This was tested systematically using apparatus consisting of a function generator, attenuator, detector boards and the standard FG5 electronics and gravity data processing software.

Figure 4.2 shows the effect on the simulated gravity value caused by varying the fringe amplitude using the attenuator. Type AMD686 produces a greater change for low light levels, whilst both comparators agree at high light levels. Based on these findings, gravity values are always corrected to the 457 μgal level depending on the fringe voltage at time of measurement.

4.3 Rubidium Frequency Reference Drift

The FG5 absolute gravimeter uses a rubidium oscillator for its time standard. The frequency output from this is set to be 10 MHz, but has a tendency to drift with time. Calibration against

Date	Frequency (MHz)	Effect on gravity (μgal)
26/04/97	10.000 000 002 9	0.57
13/11/97	10.000 000 002 0	0.39

Table 4.3. Details of the calibration of the rubidium oscillator in FG5-103. The gravity effect is the difference in gravity that would be found by processing data assuming the frequency was at 10 MHz.

a known fixed standard, such as a caesium beam, allows this to be corrected for. Niebauer *et al.* (1995) claim operating experience indicates that the rubidium frequency can be maintained at 1 part in 10^{10} with frequent calibration, and puts the FG5 instrumental error budget from this effect to be 0.2 μgal (see Section 1.6).

Details of two calibrations made to the rubidium oscillator in FG5-103 were available to the author. These are presented in Table 4.3 along with dates and the corresponding effect on gravity. They show that the effect on gravity is below 0.6 μgal, and the drift over approximately 6 months is under 0.2 μgal. The effect of this is insignificant at the 1 μgal level, and ideally details of further calibrations would need to be available before considering whether to apply a correction for this effect to all data sets.

4.4 Residuals

Residuals are the difference between the model equation of motion fit and the actual observed time-distance pairs of numbers. It is common for there to be systematic structure within them, often caused by mechanisms relating to the operation of the gravimeter. Most are caused by mechanical oscillation of the gravimeter but some may be the result of electronic defects.

Depending on the characteristics of these structures, their effect can be to appear as a gravity signal. There are two factors to consider, firstly the fact that the signal may perturb the gravity results. Secondly that this perturbation may vary according to the number of time-distance pairs used in the fit to the equation of motion. Thus it is desirable to identify and remove these patterns, or establish the effect on gravity they cause.

One of the main known reasons for structure in the residuals is due to the 'system response' of the gravimeter. As the mass is released, an impulse is imparted between the gravimeter and the floor. This impulse can induce movement in the gravimeter through flexing of the instrument or deformation of the floor. The dropping chamber is disconnected from the rest of the instrument and hence may move relative to it. The result is that the optical path length of the laser light affected by refraction through air varies since the dropping chamber is at a near

vacuum whilst the rest of the instrument is at atmospheric pressure. This changing optical path length will manifest itself as a signal in the residuals.

When the drag free chamber prepares to catch the falling mass, structure may also appear in the residuals, known as the 'catch phase'. These may similarly be caused by mechanical flexing and also other effects such as electrostatic forces due to the changing distance between the mass and drag free chamber, effectively putting the mass out of free fall.

This theory suggests that residual structures are site and instrument dependent, which was found by Charles (1995). The structure of the residuals may also be time variant due to degradation of components or the effects from transport of the instrument between sites.

The instrument has many components, both mechanical and electrical and so there are other possible sources of mechanisms that could cause structures in the residuals. For example, it has been observed that the super spring creates a 30 Hz frequency whilst stabilising after a recent unclamping.

The following sections show how the structure in residuals may be described and give an example of how one particular pattern is caused by an electronic peculiarity of the scalar counter along with its effect on gravity. Further evidence is given to back up the findings by Charles (1995) that residuals are site and instrument dependent. Also it will be shown that they can vary with time. 'Cut off' tests will be given illustrating that changing the number of fringes fitted can affect the gravity value and demonstrating the problems of using the catch phase as part of the fit.

4.5 Representing Residuals With Damped Sinusoids

Patterns in the residuals often appear in one of two forms. Some residual structures appear as 'spikes', such as those created during the catch phase. However, evidence has shown that many of the structures can be represented by damped sinusoids (Charles, 1995). Whilst this may not be a true representation, it is a useful way of describing them.

The effect of damped sinusoids in residuals on gravity measurements has been investigated using two methods. The Edinburgh DDT software has the option of including damped sinusoids in the equation of motion. With this operating for a specific frequency and decay constant, it is possible to see the change in gravity compared to fitting no sinusoids.

The second method has been to create an artificial set of time-distance numbers for specific gravity, initial velocity and displacement values using software written by Hipkin. With a damped sinusoid added and the data processed in the normal manner (*ie* as real data would be with DDT) using fringes 10 to 160, the effect on gravity can be seen for simulated noisy data.

Previously the damped sinusoid model has been used by Klopping *et al.* (1991). Their technique was to split the residuals into two halves. Fourier Transforms of these are taken to find frequencies. Their amplitude change between the two halves is used to find the decay constant.

For this research, the routine PERIOD, written by Hipkin, was used to search for damped sinusoids. It cycles through frequency and decay constant values with a progressively finer search for those whose removal causes the largest reduction in variance. Once the best solution is found, it has the option to remove this damped sinusoid from the data and perform a search for another.

There are limitations to the damped sinusoid model through the fitting of a quadratic to the time-distance number pairs. If there is noise in the data of a sinusoidal form, this may be changed when fitting since sinusoids have a close approximation to quadratics. In particular, one would expect this to have the largest effect if half a cycle of the frequency (which closely follows a parabola) occurs over exactly the duration of the drop. This reasoning implies that the frequency and decay constant found from the residuals is not necessarily an accurate representation of the true sinusoidal noise in the original data.

The time elapsed between fringes 10 and 160 is approximately 0.15 s, which corresponds to half a frequency cycle at 3.3 Hz. Hence whilst it is expected that all frequencies will have *some* effect, low frequencies of this order will produce the largest disturbance in the estimate of gravity.

Artificially produced data with a sinusoidal noise term was processed in the normal manner and then the resulting residuals were analysed. (Parameters used to create the artificial data were of a typical Bidston data set: g_o = 981 367 360 μgal, v_o = 485 600 500 nm s^{-1}, z_o = 11 393 841.100 nm, g'=-215.3 μgal m^{-1}). Figure 4.3 shows that neither the decay constant nor the frequency are estimated correctly. Figures 4.3(a) & (b) show the effect of noise described by a sine term and Figures 4.3(c) & (d) a cosine term, both with a decay constant of -10. Parts (a) & (c) show the amount by which the estimated frequency exceeded the true frequency when the frequency ranged from 7 to 13 Hz. Parts (b) & (d) show the estimated decay constant when the true frequency was varied over the same range but the true decay constant kept fixed.

It is clear that for both sine and cosine terms, the frequency in the residuals is as much as 3 Hz different from the true frequency in the original data. The decay constant also exhibits large variations from the true value.

In contrast, consider Figure 4.4 which shows the same information for a sine term with a decay constant of 0 over the frequency range 15 - 120 Hz. This indicates that modification of sinusoidal noise through processing at higher frequencies is much less and can be considered insignificant. Results for the corresponding cosine term are similar.

Whilst fitting the output of PERIOD to either synthetic or real data will remove that sinusoid

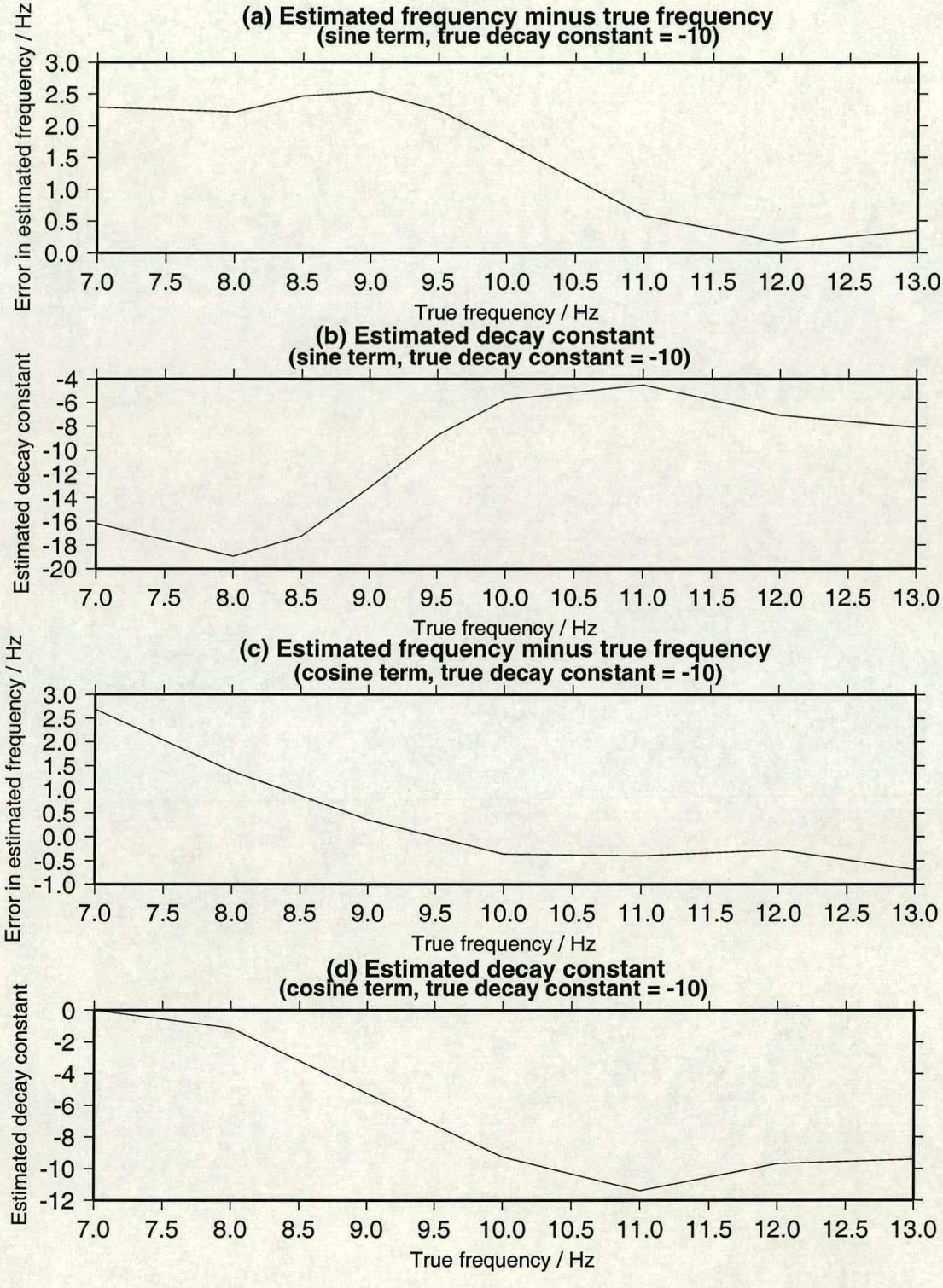

Figure 4.3. Error in estimating frequency and decay constant from residuals: low frequency case.

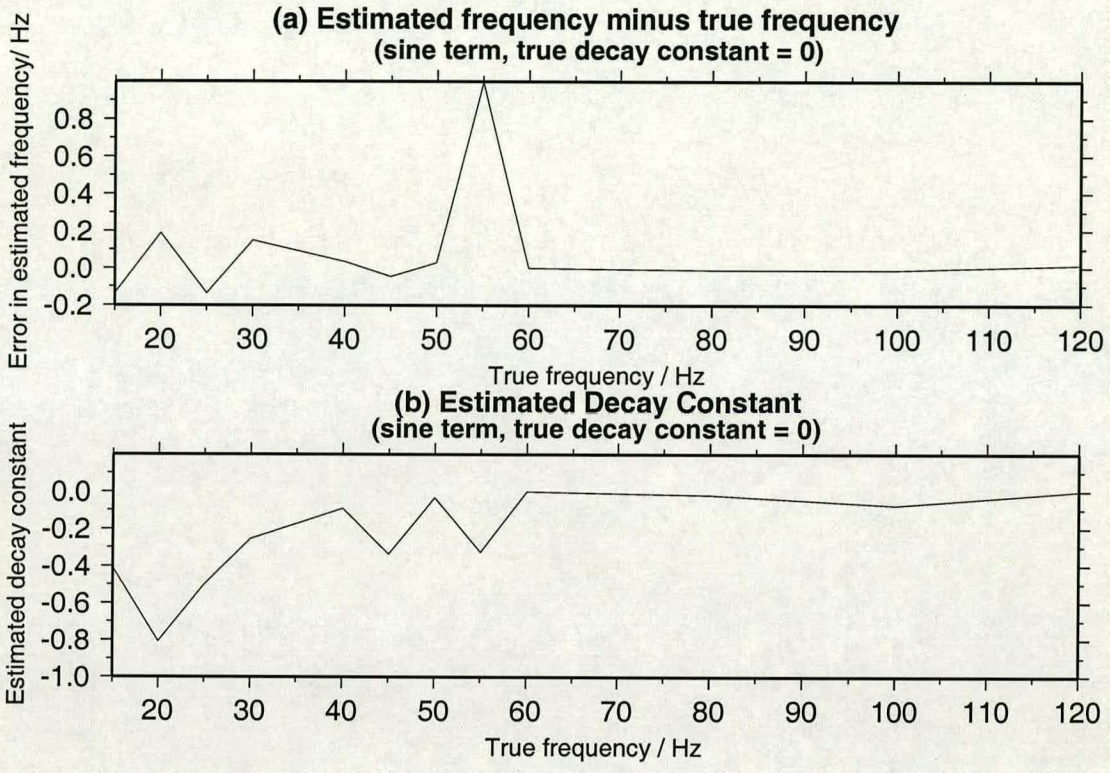

Figure 4.4. Error in estimating frequency and decay constant from residuals: high frequency case.

from the residuals, it does not mean that the noise in the pre-processed gravity data has the same characteristics. Hence the gravity change through removing these sinusoids is not necessarily the correct amount. An example of this can be found in the next section (4.6) on the Scalar Counter Effect.

4.6 Residual Structure Caused by the Scalar Counter

The scalar counter measures the time interval between detection of scaled fringes. The source of a low period frequency within the gravity residuals was found to be from an electronics board within this component. On replacement of this with a newer version, the frequency disappeared. Figure 4.5 shows the average residuals for data sets before (POL1402A) and after (POL1605A) changing the board, taken at Bidston in 1997. It is clear that a low frequency component is no longer present.

Using PERIOD, selected data sets of FG5-103 exhibiting this effect were examined to find details of this frequency. Results are given in Table 4.4. They show that the frequency is typically around 9.5 Hz with a decay constant ranging between -13 and -9.

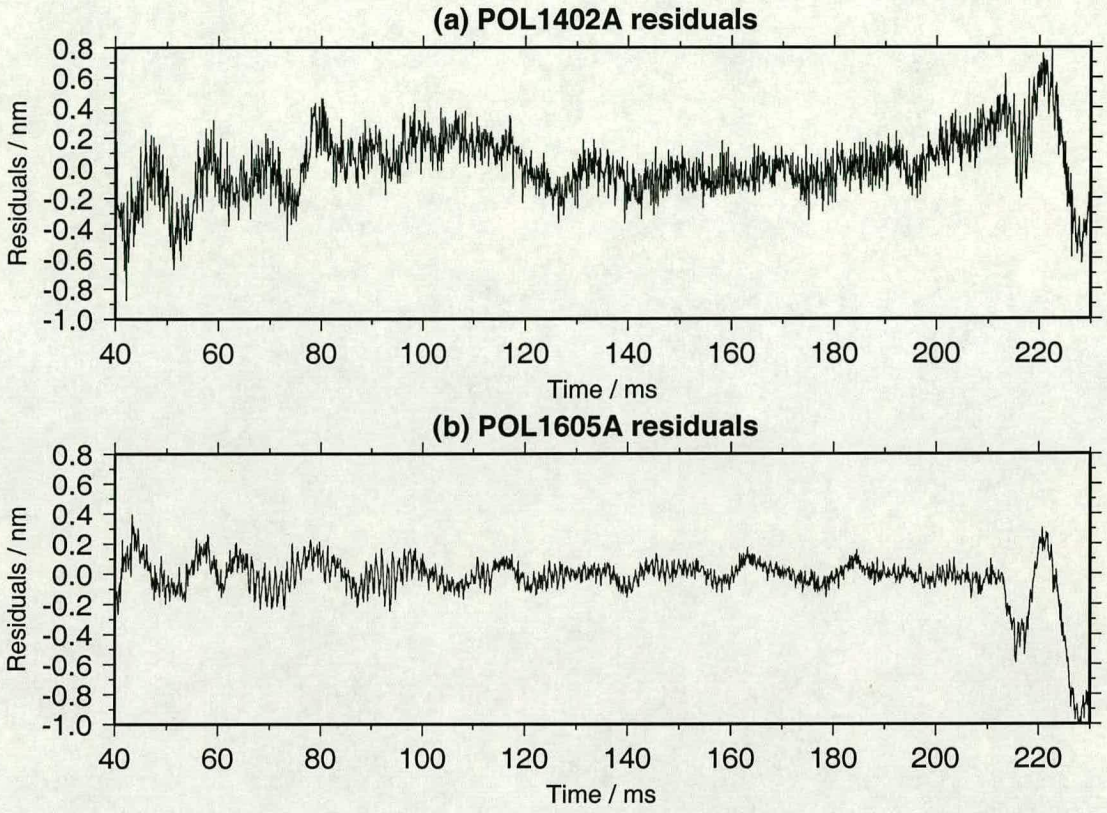

Figure 4.5. Example of FG5-103 average residuals before (POL1402A) and after (POL1605A) scalar counter electronics board was changed, taken at Bidston in 1997.

The details of these damped sinusoids were used to manufacture artificial data consisting of a noiseless gravity signal with the sinusoids added. The damped sinusoids were also used as part of the equation of motion fit to the real data using Edinburgh DDT software. In both cases the change in gravity caused by the sinusoids was noted. The fringes fitted started at 10 and ended at 160. Table 4.4 gives results of these two methods.

The results of using artificial and real data to fit the damped sinusoid are not notably different, and all below 1 μgal. They suggest that this effect does not cause a significant gravity perturbation. Hosker (1996) obtained a similar outcome using Klopping's routine.

These results do not concur with reality. Micro-g Solutions Inc. observed an increase of 6.3 μgal for FG5-103 when replacing the old board with new. This value is based on data processed using REPLAY software, starting at fringe 5 and fitting 165 (*pers. comm.* T. F. Baker, November 1998).

To investigate whether a frequency of the order of 9.5 Hz could produce a gravity change of 6.3 μgal when removed from the data, damped sinusoids of varying frequency and decay constant were removed from data set POL0603A (1996). This was selected since it has relatively quiet

Data set	Damped sinusoid				Gravity change	
	Hz	decay	sin term	cos term	Artificial data	Real data
POL0603A(1996)	9.41	-12.30	0.13	-0.34	-0.07	0.68
POL1806A(1996)	9.69	-13.22	0.13	-0.33	0.17	0.27
POL2210A(1996)	9.50	-11.11	0.08	-0.25	0.17	0.45
POL0301A(1997)	9.55	-12.97	0.09	-0.24	0.03	0.47
POL1402A(1997)	9.40	-9.33	0.06	-0.24	0.08	0.40

Table 4.4. Details of frequencies and decay constants found by PERIOD caused by the scalar counter effect and the change in gravity when fitted to the data. Sin & cos terms are in nm, gravity changes are in μgal.

data, only the first 6 sets were used to reduce computation time.

Figure 4.6 shows the change in gravity against frequency and decay constant of the damped sinusoid used to fit to the data compared to that if no sinusoid is fitted. There are clearly a distinct set of frequencies and decay constants that would produce a gravity change of 6.3 μgal.

This example illustrates that existing methods used to find the system response function for low frequency noise do not work. Whilst the different algorithms (Klopping and PERIOD/DDT) give similar results, neither estimates the true frequency and decay constant correctly and so do not give the correct magnitude of the gravity correction.

4.7 Variation of Residuals Between Sites

To illustrate how residual characteristics can vary between sites, two data sets taken by FG5-103 have been selected from 1998. The first was recorded at Bidston and the second was the next to be taken by the instrument, at Aberdeen. Figures 4.7(a) & (b) show average residuals for all drops obtained from these two data sets using Edinburgh DDT software, stacked by time.

It is clear that the Aberdeen data set has a frequency in the residuals during the middle part of the drop with a period of about 30 ms that is not evident in the Bidston data. There are also spikes towards the beginning of the drop in the Aberdeen residuals absent from those of Bidston. On the whole, the Bidston residuals are much quieter and less structured.

Tables 4.5 and 4.6 give results of the first five frequencies and decay constants found by PERIOD along with their sin/cos terms. There are clearly frequencies of about 33 Hz and 85 Hz with large amplitude in the Aberdeen data that are absent from Bidston data.

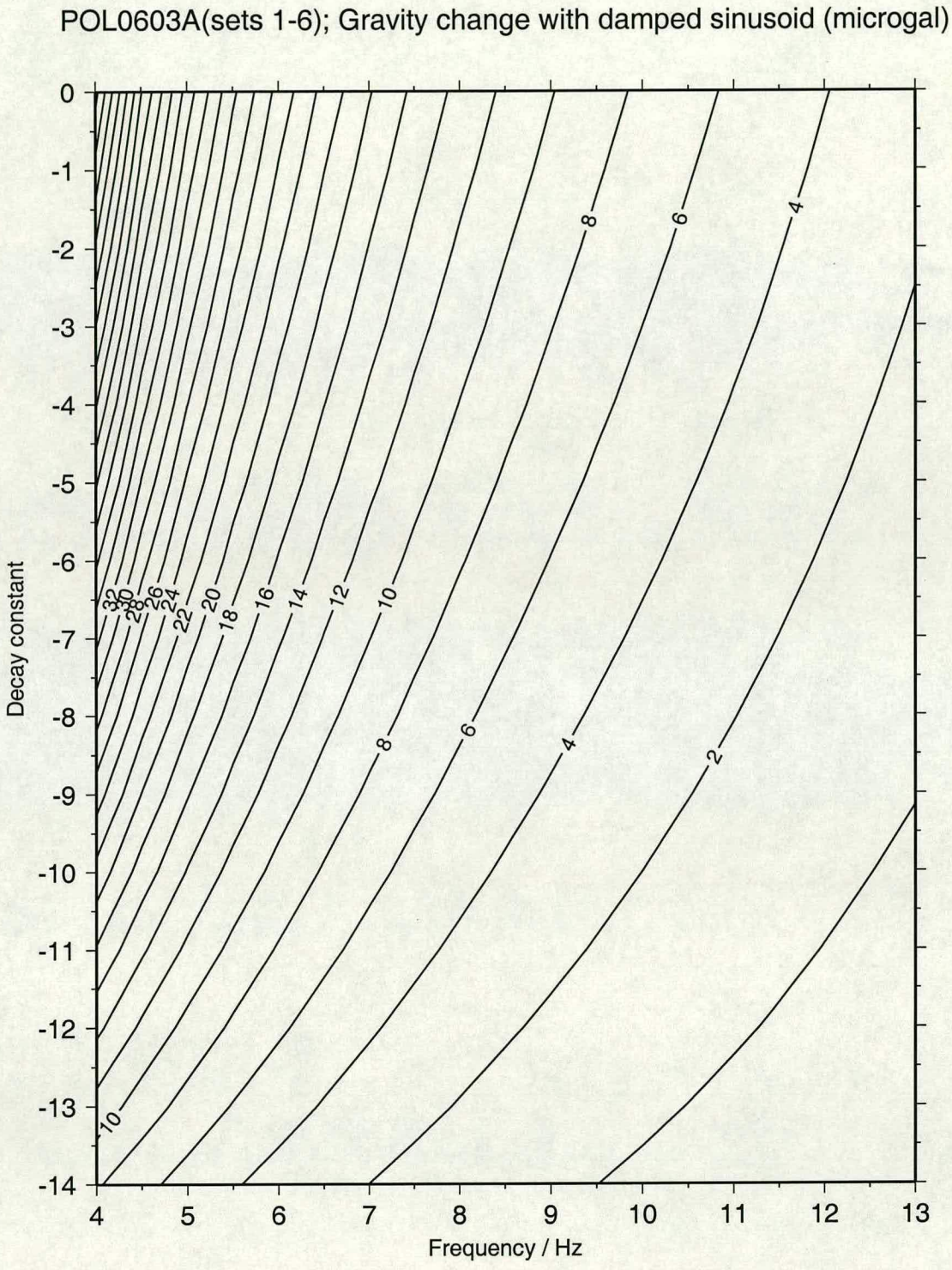

Figure 4.6. Change in gravity through including a damped sinusoid of various frequencies and decay constants in the equation of motion. For data set POL0603A(1996) sets 1-6 only.

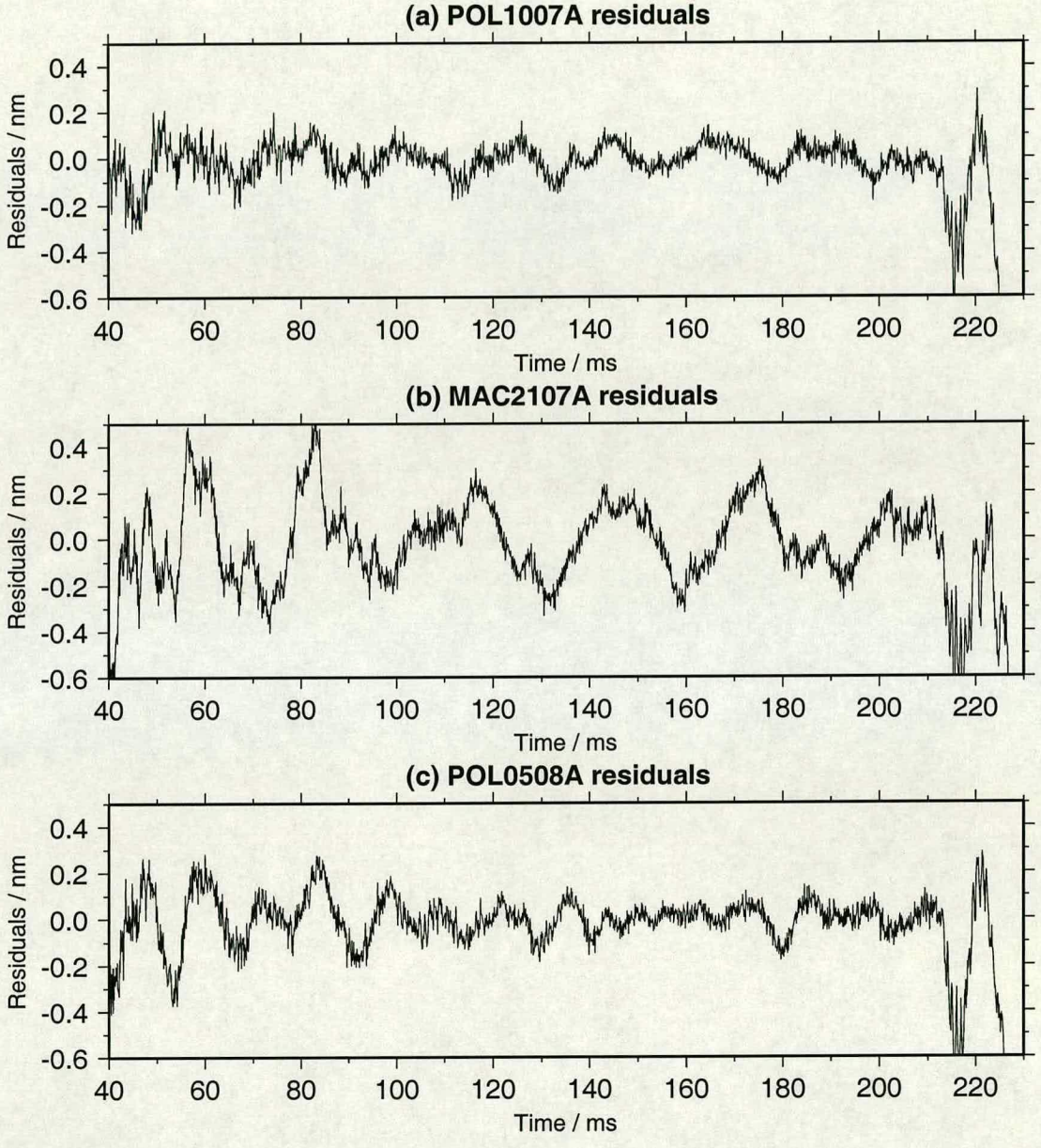

Figure 4.7. Average residuals stacked by time for (a) Bidston data set POL1007A, (b) Aberdeen data set MAC2107A) and (c) Bidston data set POL0508A, all taken in 1998.

POL1007A(1998) frequencies				Gravity change (μgal)	
Hz	decay	sin term	cos term	Artificial	Real
45.79	0.00	0.05	-0.02	0.31	-0.28
107.30	0.00	0.02	0.00	0.03	0.07
10.89	0.00	0.01	0.00	-0.40	0.20
54.19	-15.69	0.00	0.03	0.10	0.02
90.76	-5.31	-0.01	0.02	-0.01	0.01

Table 4.5. Bidston data set POL1007A(1998): details of the first five damped sinusoids found by PERIOD and the change in gravity when removed from artificial and the real data. Sin & cos terms are in nm.

MAC2107A(1998) frequencies				Gravity change (μgal)	
Hz	decay	sin term	cos term	Artificial	Real
33.69	0.00	0.20	0.04	2.49	1.02
85.30	-14.22	-0.13	-0.13	-0.35	-0.42
46.65	-14.74	0.01	-0.15	-0.38	-0.36
56.32	0.00	-0.03	0.02	0.24	0.83
29.52	-14.30	-0.06	-0.02	-0.17	-0.24

Table 4.6. Aberdeen data set MAC2107A(1998): details of the first five damped sinusoids found by PERIOD and the change in gravity when removed from artificial and the real data. Sin & cos terms are in nm.

Also in these tables are details of how gravity is affected if these sinusoids are removed using the two methods described in Section 4.4. In most cases, the change in gravity is less than 1.0 μgal apart from the 33 Hz frequency of the Aberdeen data. The artificial data predicts the gravity change to be 2.5 μgal whilst when this frequency is removed from the data using DDT, the change is 1.0 μgal.

As discussed in Section 4.5, it is not expected that high frequencies have a great effect on gravity. This was tested on data set POL1007A(1998) by subtracting frequencies ranging from 20 - 100 Hz and decay constants between -10 and 0 using DDT. Results of the change in gravity can be seen in Figure 4.8. Note that they do not concur with those of Table 4.5 because only sets 1 - 6 were used.

The Figure shows that for all frequencies in the range 20 - 100 Hz and decay constants between -10 and 0, the change in gravity is insignificant, being no greater than 0.9 μgal.

To examine further the effect of these structures, cut off tests were performed whereby the start fringe number to be used in the fit was fixed at 10 and the end fringe fitted was varied. Results can be seen in Figure 4.9. Plotted alongside are the average stacked residuals with respect to

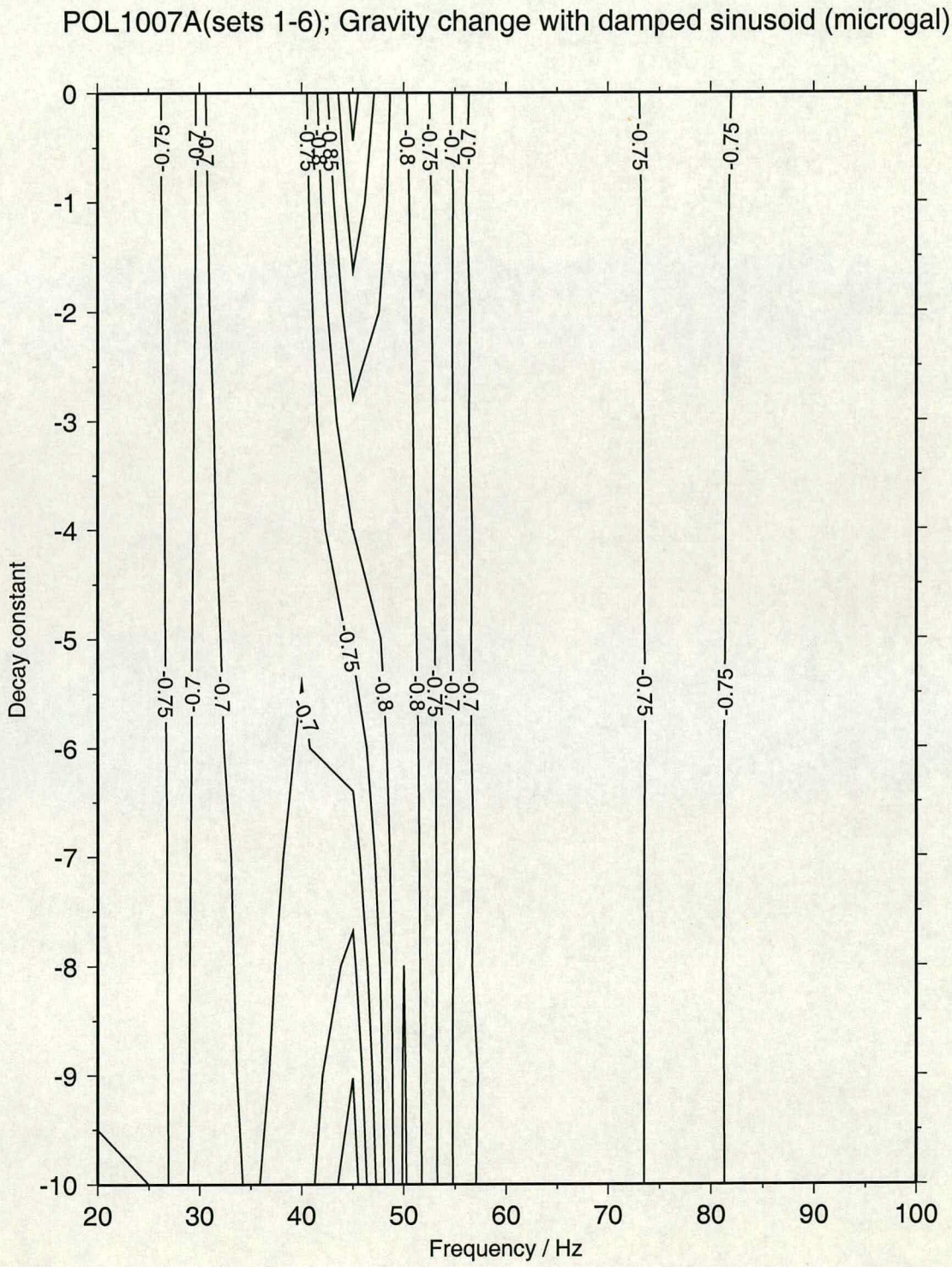

Figure 4.8. Change in gravity through including a damped sinusoid of various frequencies and decay constants in the equation of motion. For data set POL1007A(1998) sets 1-6 only.

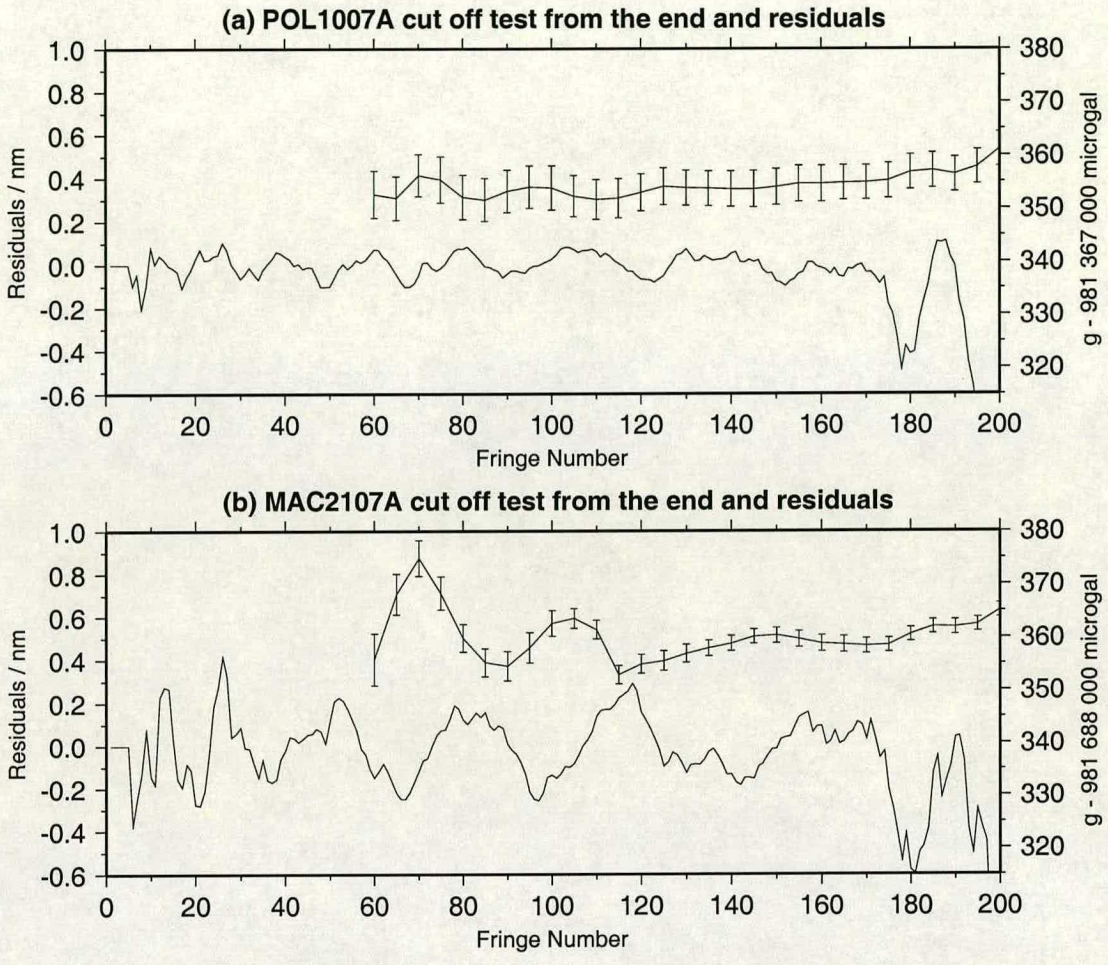

Figure 4.9. Residuals with respect to fringe number and cut off tests (starting at fringe 10, varying the end fringe fitted) for (a) POL1007A(1998), Bidston and (b) MAC2107A(1998), Aberdeen. Error bars are Set Standard Deviation.

fringe number.

It is evident that when varying the fit of the drop through these structures there are variations in gravity of up to 20 μgal. In comparison the Bidston data varies by little more than 5 μgals. However, in both cases there is no significant change in gravity beyond the error bars when ending the fit at 160 $\pm$ 10 fringes - typically the length of drop used for processing the data.

4.8 Variation of Residuals Between Instruments

Figure 4.10 shows the residuals for gravimeters FG5-101 and FG5-103 from the Wettzell intercomparison of November 1996 (see Section 4.11). Both the data sets shown were taken at the North site of Wettzell.

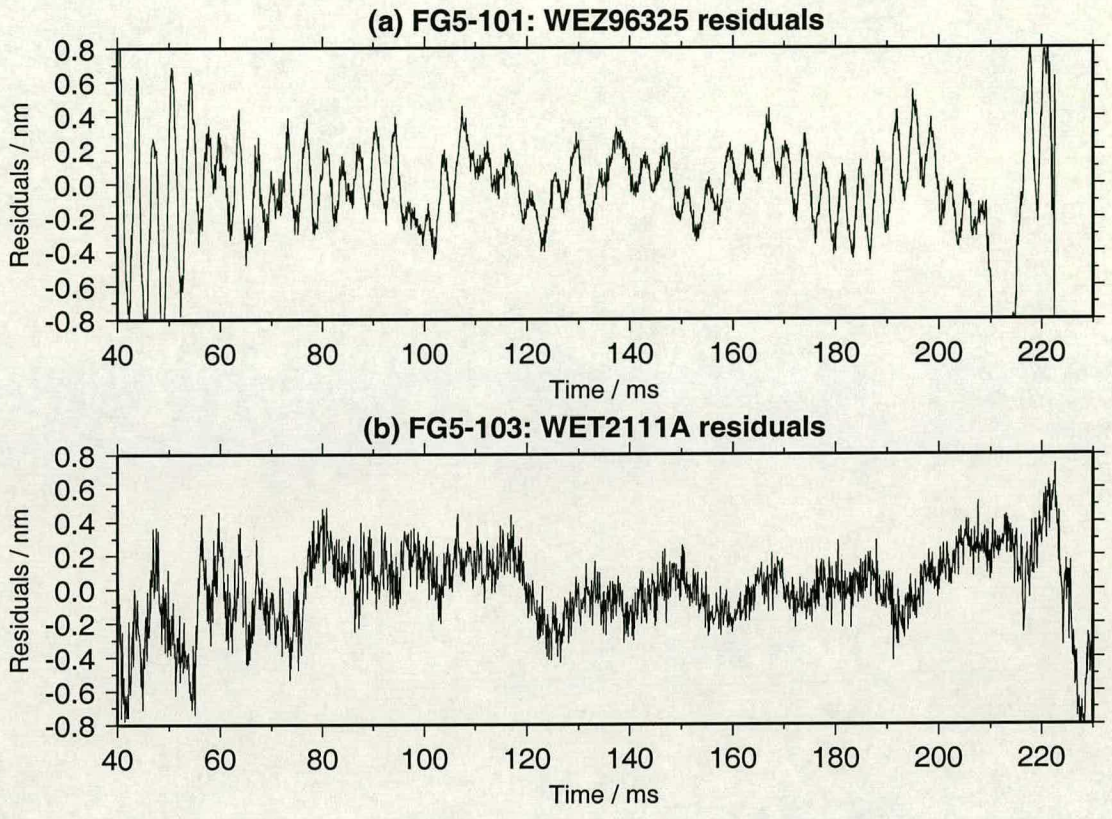

Figure 4.10. Stacked average residuals for data sets taken at Wettzell in November 1996 by (a) FG5-101 and (b) FG5-103.

There are clearly different characteristics for these two sets of residuals. FG5-101 residuals have a high frequency signature absent from FG5-103 residuals. The two instruments also have different catch phase signals, occurring earlier for FG5-101 and of a different pattern.

Table 4.7 gives the first five frequencies found by PERIOD for these two data sets. One can see that FG5-101 has a strong frequency of 37 Hz, and also another of 91 Hz, both of which are absent from FG5-103 results. The strongest frequency of FG5-103 (9.6 Hz) is due to the scalar counter effect (see Section 4.6). These results illustrate that different characteristics are possible between FG5 instruments.

4.9 Variation of Residuals With Time

Consider Figure 4.7(c) which are the average stacked residuals for data set POL0508A taken at Bidston on 5th August 1998. This is the next data set to be taken at Bidston after POL1007A of Figure 4.7(a), recorded on 10th July 1998, with an intervening field trip to Aberdeen and Lerwick.

FG5-101 (WEZ96325)				FG5-103 (WET2111A)			
Hz	decay	sin term	cos term	Hz	decay	sin term	cos term
36.70	0.00	0.14	0.06	9.64	-12.50	0.08	-0.25
58.02	0.00	0.04	-0.05	57.34	0.00	-0.08	-0.05
48.53	-8.10	-0.05	0.07	33.55	-3.45	0.06	0.06
101.49	-0.59	-0.04	0.01	100.88	-12.32	-0.11	0.03
90.99	-10.19	-0.03	0.09	21.07	-7.23	0.05	0.04

Table 4.7. First five frequencies found by PERIOD for data sets from FG5-101 and FG5-103. Sin & cos terms are in nm.

There has been a change in the characteristics of the residuals during the interim period. It should be noted that the patterns are not unique to these data sets - all residuals preceding the field trip are similar to those of POL1007A and residuals after the field trip are similar to those of POL0508A.

Table 4.8 shows the first five frequencies found by PERIOD for POL0508A. Comparing these with those of POL1007A in Table 4.5, one can see that a frequency of 79 Hz has appeared, the 54 Hz frequency is much stronger and the 107 Hz frequency no longer exists in POL0508A residuals.

POL0508A frequencies				Gravity change (μgal)	
Hz	decay	sin term	cos term	Artificial	Real
79.36	-13.46	-0.16	-0.06	-0.40	-0.29
54.76	-10.69	-0.08	-0.03	-0.27	-0.34
45.97	-5.81	0.03	-0.03	0.08	-0.11
36.25	-4.47	0.01	0.02	0.15	0.10
10.75	-13.65	0.04	-0.01	-0.05	-0.12

Table 4.8. Bidston data set POL0508A(1998): details of the first five damped sinusoids found by PERIOD and the change in gravity when removed from artificial and the real data. Sin & cos terms are in nm.

It is possible that knocks incurred during transit may have contributed to this change. Whilst the effects observed here are unlikely to have a significant impact on measurements beyond the data errors, this illustrates how the instrument may be susceptible to producing different gravity values over time and the importance of returning to measure at a stable gravity site for calibration.

4.10 Catch Phase

In all the plots of residuals presented, the 'catch phase' is evident as a perturbation towards the end of the drop. As the mass falls inside the drag-free chamber, a fixed distance is maintained between the two. The chamber catches the mass at the end of the drop, this needs to be done smoothly to reduce wear on the components. Hence shortly before the end of the drop, the separation distance is reduced to lower their relative velocities on impact. This 'preparation to catch' phase imparts an impulse on the gravimeter and floor and may also create electrostatic forces, manifesting themselves as a signal in the residuals.

In Figure 4.7 the catch phase is evident from 210 ms onwards. The cut off tests of Figure 4.9 show the effects of including the catch phase in the fit to the equation of motion. Whilst there is not a significant change of gravity through fitment of the catch phase, it should be noted that in these cases the amplitude of the effect is small. For example, the residuals of FG5-101 in Figure 4.10(a) show the amplitude of the catch phase signal to be at least twice as great. The effect of fitting in to the catch phase has been noted to vary between data sets for the same instrument (see Section 5.6). It is for this reason that fringes from the catch phase should not be used in the fit. All data processed in this research using Edinburgh DDT software has the last fringe fitted set at 160 to ensure the catch phase is not encountered.

4.11 Intercomparison Between FG5-103 and FG5-101

An intercomparison was made between absolute gravimeters FG5-103 of POL and FG5-101 of the Institut für Angewandte Geodäsie (IfAG), Germany. The measurements took place at Wettzell in the south east of Germany during November 1996. The site consisted of a large rectangular granite block inset into the floor. The two gravimeters were situated at either end of the block, known as sites 'North' and 'South' due to its orientation.

Three data runs were taken with the two instruments present. Only data recorded simultaneously within these runs were used. This consisted of a 20 hour data set followed by a 24 hour data set. After the first two runs the instruments swapped positions and recorded one further 15 hour data set simultaneously.

Previous findings from processing this data using REPLAY software reported a discrepancy of 14 μgal between the instruments (H. Wilmes, paper presented at Chapman Conference on Microgal Gravimetry, St. Augustine, Florida, 1997). However it was discovered that this used a fit which included part of the catch phase.

For this research the data were processed using Edinburgh DDT software. Fringes 10 to 160 were used for both instruments to ensure the catch phase was not encountered with a wide margin of error. All corrections were applied with the exception of the Comparator Response

Site	FG5-101		FG5-103	
	Gravity / μgal	Data sets	Gravity / μgal	Data sets
North	268.5 $\pm$ 2.0	WEZ96324 WEZ96325	266.9 $\pm$ 1.1	WET2111A
South	258.9 $\pm$ 1.0	WET96326	260.2 $\pm$ 2.0	WET1911A WET2011A

Table 4.9. Results of FG5-101 & FG5-103 1996 Wettzell intercomparison. Values are g - 980 835 000 μgal. Errors are Set Standard Deviation.

for FG5-101 since fringe voltage information was not available to the author. The effect of this is not expected to be greater than 1 μgal. Since there was no environmental information available from the FG5-101 data, barometric values from FG5-103 data were used to make the air pressure correction to FG5-101 data. Ocean loading corrections were made with 12 components calculated from the method described in Chapter 2.

Table 4.9 gives the results of the instruments at the North and South ends. Data sets were combined for ends where more than one were recorded. A relative gravity tie made at the time of the intercomparison between the two ends of the block with an IfAG Scintrex gravimeter at a height of 130 cm found that gravity at the North end was greater by 5.5 $\pm$ 1.0 μgal.

For each of the block ends, the two instruments are in good agreement within the errors stated. This contradicts the findings of Wilmes since the catch phase is now avoided. The discrepancy of 14 μgal can be explained since examination of Figure 4.10 shows that the amplitude of the catch phase signal in FG5-101 is much greater than that for FG5-103.

4.12 Intercomparison Between FG5-103 and FG5-202

Absolute gravimeter FG5-202 is owned by the Royal Observatoire de Belgique. It is based at Membach in eastern Belgium. A comparison was made between the values produced by this instrument and FG5-103. Measurements were made at Membach by FG5-103 and at POL, Bidston by FG5-202. Note that there were no simultaneous measurements and hence this intercomparison is subject to real environmental changes in gravity between the measurements.

Measurements at Membach by FG5-103 were taken in November 1997. Two runs consisting of 24 hours and 19 hours were made. Results from these were compared with those of an 81 hour data set available to the author taken by FG5-202 in April 1996.

FG5-202 measurements at POL consist of one 24 hour data set taken in May 1997. This was compared with results of an FG5-103 measurement made 2 days later. In this manner, the problem of seasonally varying gravity at Bidston should be eliminated.

Site	FG5-103		FG5-202	
	Gravity / μgal	Data set	Gravity / μgal	Data set
Membach	419.2 ± 1.1	MEM1811A	426.0 ± 0.9	ME96101
	426.1 ± 1.0	MEM2011A		
Bidston	360.3 ± 5.0	POL1605A	360.1 ± 1.6	PO97134A

Table 4.10. Results of FG5-103 & FG5-202 observations at Membach and Bidston. For Membach values are g - 981 046 000 μgal. For Bidston values are g - 981 367 000 μgal. Errors are Set Standard Deviation.

The data were processed in the same way as the Wettzell intercomparison (Section 4.11). Once again the Comparator Response correction was not performed on FG5-202 data, but this is not expected to be greater than 1 μgal.

Results can be seen in Table 4.10. For Membach, values obtained by the two data sets from FG5-103 differ significantly beyond the standard deviations stated by 7 μgal. The reason for this is unclear. It is possible that the instrument was 'settling in' during the first data run - a phenomenon that is often observed when installing at a site. Assuming this to be the case and ignoring MEM1811A, values from the two instruments are in good agreement.

Similarly, results from Bidston also show a good agreement between the two instruments.

One can conclude that comparisons of FG5-103 and FG5-202 measurements at the same sites show that these instruments are producing the same gravity values within statistical limits.

4.13 Conclusions

Two methods of searching for laser lock shifts have been presented. For data runs without a record of the 1F voltage from the laser, it is advised that sets with a suspected shift occurring part way through are discarded. With the 1F voltage information, automatic peak detection is only reliable if the voltages are not varying by greater than half the separation gaps between peaks. If this is not the case, manual correction for peak shifts must be done by eye. However it is theoretically possible that an automated system could be developed by using a running mean of the 1F output that will allow for drift of voltages.

Effects on gravity from the Comparator Response and Rubidium Clock Drift are well known. The former can be corrected for by recording the fringe voltage at the start of measurement and using values giving the gravity effect found empirically. The latter needs frequent calibration of the rubidium oscillator. For FG5-103, at time of writing details of 2 such calibrations are known, and the corresponding effect on gravity is approximately 0.5 μgal. No correction to

data used in this research was made for rubidium drift influences - the effects are small and more calibrations would be needed.

Structures in residuals may be represented by damped sinusoids. However, and in particular for residual frequencies below 15 Hz, these are not an accurate representation of the true frequency in the data since they resemble a quadratic which is removed from the time-distance number pairs through processing. Higher frequencies in the residuals are in general a good representation of the true noise signal, but produce an insignificant gravity effect at the 1μgal level.

One particular structure of the residuals is present in earlier data and caused by the Scalar Counter. Represented by a damped sinusoid it has a frequency of 9.5 Hz and a decay constant of about -10. The change in gravity from fitting this using synthetic and real data is less than 1 μgal. However, the manufacturer states that changing a component to eradicate the sinusoid gives a gravity change of 6.3 μgal. Fitting frequencies from 4 - 13 Hz to data with this characteristic show a gravity change of up to 50 μgal. Existing methods of correcting for systematic structure in the residuals do not work and errors up to 6 μgal can be missed.

Evidence has been presented showing that the characteristics of residuals vary between sites, instruments and with time. In some cases residual structure can cause a gravity shift beyond 1 μgal depending on which fringes are used in the equation of motion fit. In particular, the catch phase should be avoided when determining which fringes to use.

Intercomparing data produced by FG5-103 and FG5-101 taken at Wettzell in 1996 shows an agreeement to 1.5 μgal. Measurements taken by FG5-103 and FG5-202 at both Bidston and Membach in 1997 agree to within 0.2 μgal.

Chapter 5

Absolute Gravity Results

Chapter 1 gave an outline of how the FG5 gravimeter works. For one drop an observed value of gravity is obtained from a set of time-distance number pairs. Here the methods used to obtain this gravity value are given. Also the statistics used to achieve the overall average gravity value are presented.

The FG5-103 gravimeter was one of three instruments constructed in 1992 as the initial production run. Many hardware modifications were made by the manufacturers in the following years. A history is given of these changes for this gravimeter.

Most results in this research have been obtained by this instrument. Results of occupations made at 8 absolute gravity sites in Britain are presented. Some sites have been occupied once, some have had repeat measurements. In the case of the latter, intercomparison of the values obtained has been made. In particular, Proudman Oceanographic Laboratory (POL), Bidston is where the instrument is based and has had regular gravity measurements made here since its purchase in 1992.

Average values of gravity for these absolute sites of Britain are given, to be used in the adjustment of the British Precise Gravity Network (Chapter 6).

5.1 FG5 Data Processing

Each drop of the mass in an FG5 instrument produces a set of time-distance number pairs (Chapter 1). From these the value of gravity can be calculated, along with other parameters such as initial velocity, initial displacement and the residuals. Necessary corrections are applied to the gravity values obtained to remove environmental and instrumental effects.

The FG5-103 gravimeter typically performs 200 drops every 10 seconds, known as a 'set'. It then rests until starting a new set one hour after the previous one commenced. A whole data

run usually consists of 24 sets. Environmental and instrumental corrections are applied to each gravity value and statistics are performed on these values to obtain an overall average.

Two packages were available to the author for FG5 data processing. The OLIVIA/REPLAY package is provided by the manufacturer Micro-g Solutions Inc.. The OLIVIA program is for real time acquisition of data from the instrument. REPLAY allows for reprocessing of this data with adjusted parameters using the same methods as in OLIVIA. Charles (1995) reports on results from using Version 1.2. This has been superceded by Version 2.2 from which results were available for this research. At time of writing, the latest upgrade (Version 3.2) has been made available (*pers. com.* G. Jeffries, 8th April 1999).

The DDT/MEAN package is written by R. G. Hipkin. The DDT routine calculates the results from each drop. The MEAN routine performs statistics on these results. Together they do a similar job to REPLAY with subtle differences and allow greater flexibility for examination of the data.

In this research, all results have been obtained using DDT/MEAN. The following subsections give an overview of the methods employed to process data from FG5 gravimeters. Emphasis will be given to the DDT/MEAN package.

5.1.1 Equations of Motion

The equation of motion which the time-distance number pairs are fitted to is a model of how the mass should fall under the assumption of a particular gravity field. This depends on whether gravity is constant or varies over the length of the drop.

Assuming there is no gradient (*ie* constant gravity) means the solution will define an average value of gravity which will be equal to gravity at some point part way down the drop. This is known as the 'Effective Measurement Height'. The position of this is not known exactly; Niebauer (1989) deduces that it is approximately 5 / 14 down the drop for data equally spaced in distance, with a more exact formula depending on the initial position and velocity. With conventional software like REPLAY, these quantities are not available.

Both software packages give the option of fitting to a linear gradient. DDT also has the option of fitting to a quadratic gradient. However findings by Charles (1995) showed this to have an insignificant effect on gravity results. Throughout this research a linear gradient was assumed.

Fitting to a linear gradient, the solution is given at the top of the drop. There are two definitions of where this is; zero distance and zero time. The former is well defined from the dimensions of the instrument. The latter is where the first fringe is fitted. If this is fringe 5, for example, it is about 5 mm below the top of the drop.

The 'zero distance' definition is adopted by DDT software. The equations presented here are from Charles (1995). The assumption of a linear gradient γ means the mass undergoes an acceleration of:

$$\ddot{z} = g_{z_o} + \gamma z \tag{5.1}$$

which, when neglecting second order terms, gives the equation of motion as:

$$z(t) = z(0)\left[1 + \frac{1}{2}\gamma t^2\right] + v(0)t\left[1 + \frac{1}{6}\gamma t^2\right] + \frac{1}{2}g_{z_o}t^2\left[1 + \frac{1}{12}\gamma t^2\right] \tag{5.2}$$

The 'zero time' definition is adopted by REPLAY software. Now the acceleration is represented by:

$$\ddot{z} = g_{t_o} + \gamma[z - z(0)] \tag{5.3}$$

A similar derivation leads to the result that:

$$z(t) = z(0) + v(0)t\left[1 + \frac{1}{6}\gamma t^2\right] + \frac{1}{2}g_{t_o}t^2\left[1 + \frac{1}{12}\gamma t^2\right] \tag{5.4}$$

The difference between these two derivations is the $\frac{1}{2}\gamma t^2 z(0)$ term. It alters the gravity value by about 1.5 μgal for a fit starting at fringe 5 (Charles, 1995). The difference increases if the fitting interval begins at a later fringe.

In both cases, an additional sinusoidal term is included in the equation of motion if data is recorded using an Iodine laser. This accounts for the fact that the operation of the laser causes the wavelength of the light to 'dither' around the iodine absorption line at a known frequency f (see Section 4.1). For FG5-103, f = 1171.874 Hz.

5.1.2 Solving for g

The equation of motion presents 3 unknowns (5 in the case of an Iodine laser). Suppose there are n time-distance pairs of numbers (t_i, z_i) to be used in the fit, then the matrix equation $\mathbf{Ax} = \mathbf{B}$ is established as follows:

$$\begin{bmatrix} \frac{1}{2}t_1^2+\frac{1}{24}\gamma t_1^4 & t_1+\frac{1}{6}\gamma t_1^3 & 1+\frac{1}{2}\gamma t_1^2 & \cos(ft_1) & \sin(ft_1) \\ \frac{1}{2}t_2^2+\frac{1}{24}\gamma t_2^4 & t_2+\frac{1}{6}\gamma t_2^3 & 1+\frac{1}{2}\gamma t_2^2 & \cos(ft_2) & \sin(ft_2) \\ \frac{1}{2}t_3^2+\frac{1}{24}\gamma t_3^4 & t_3+\frac{1}{6}\gamma t_3^3 & 1+\frac{1}{2}\gamma t_3^2 & \cos(ft_3) & \sin(ft_3) \\ \vdots & \vdots & \vdots & \vdots & \vdots \\ \frac{1}{2}t_n^2+\frac{1}{24}\gamma t_n^4 & t_n+\frac{1}{6}\gamma t_n^3 & 1+\frac{1}{2}\gamma t_n^2 & \cos(ft_n) & \sin(ft_n) \end{bmatrix} \begin{bmatrix} g \\ v_o \\ z_o \\ a \\ b \end{bmatrix} = \begin{bmatrix} z_1+\epsilon_1 \\ z_2+\epsilon_2 \\ z_3+\epsilon_3 \\ \vdots \\ z_n+\epsilon_n \end{bmatrix} \tag{5.5}$$

where the ϵ_i are the residuals, a and b are constants to be found from use of the Iodine laser. Typically n is at least 150 and so the problem is over - determined. Both DDT and REPLAY software obtain the solution using least squares through converting $\mathbf{A}$ into upper triangular form with Householder rotations.

Hipkin (1993) and Charles (1995) claim there are errors in the subroutine SOLVDROP of REPLAY Version 1.2 where these calculations take place. They report on an unnecessary double displacement of an index and improper sign convention for the gradient. These were corrected in later versions of the manufacturer's software.

DDT and REPLAY do essentially the same job in the calculation of g and produce consistent results (Charles, 1995). The main difference arises in their selection of data to be used in the equation of motion.

The operator has the choice of which time-distance number pairs, or fringes, are to be used in the fit. Here an important difference between DDT and REPLAY arises. REPLAY uses the *fringe index* (related to the number of fringes recorded) to determine which fringes to use, whilst DDT uses the *fringe number* (related to the position of the fringe down the drop).

As the velocity of the mass accelerates during a drop, fringes are detected at increasing frequency. Beyond a certain point, they occur too quickly for them all to be detected by the hardware. Hence some fringes are missed leading to a discrepancy between the fringe index and fringe number.

Figure 5.1 shows the number of data points at each fringe number for data set POL1402A(1997). One can see that fringes are missed, with increasing frequency, beyond fringe number 105.

The consequence of this is that the fringes chosen by a REPLAY operator will in general extend the fit to an unknown point beyond that expected. This may include the catch phase (Section 4.10). The DDT operator has the advantage of knowing exactly at which point down the drop his/her fit will end, even though the number of points fitted is variable and unknown (depending on how many fringes are missed).

For the purposes of this research, fringe numbers 10 to 160 have been used.

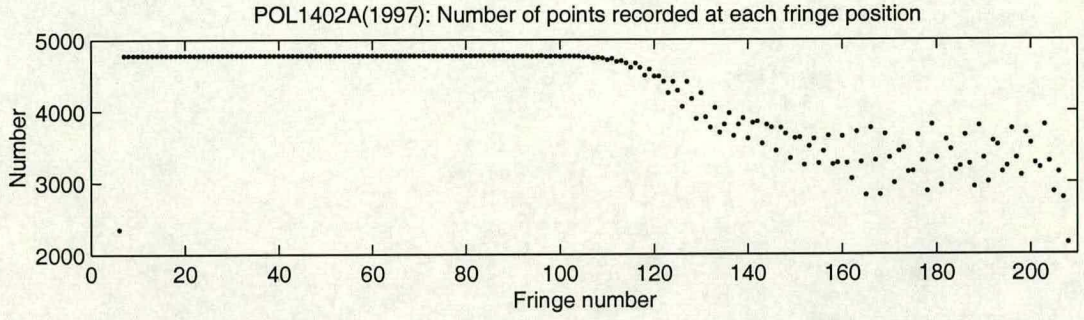

Figure 5.1. Number of points recorded at each fringe point for data set POL1402A(1997).

5.1.3 Corrections

Speed of Light

The laser light takes less time to traverse around the gravimeter as the mass falls since its path length reduces. To account for this, time values are retarded according to how far the mass has fallen. If the mass has fallen a distance z and the speed of light is c, then the time is reduced by $2z/c$; the factor of 2 is present since the light has to travel up *and* down the drop.

Tidal Correction

The TIDAL subroutine of DDT removes the gravity effect due to the presence of the Sun and Moon along with the associated elastic response of the Earth. This is done using the Cartwright - Taylor - Edden (CTE) harmonic expansion involving 484 terms. Gravimetric factors used are 1.160 and 1.043 for second and third degree tides respectively. This includes the static tide which has been multiplied by a gravimetric factor of 1.16, *ie* the Honkasalo correction has not been made.

Ocean Loading

Also using the CTE expansion within DDT, ocean loading has been removed from the observations. Twelve components were subtracted (M_2, S_2, K_1, O_1, N_2, P_1, K_2, Q_1, L_2, μ_2, ν_2, $2N_2$) based on calculations made using the method described in Chapter 2.

Air Pressure

The effects of air pressure on gravity include the direct attraction of the air mass and the corresponding loading of the Earth's surface (see Chapter 3). Gravity has been corrected to a nominal air pressure value depending on the altitude at which observations were made. This is given by the formula:

$$p_{nominal} = 1013.2(1 - 2.2557 \times 10^{-5}h)^{5.2613} \text{ mbar} \tag{5.6}$$

where h is the height in metres. The standard admittance of 0.3 μgal mbar^{-1} has been assumed (see Section 3.2).

Polar Motion

Shifts in the rotation axis of the Earth cause changes in the geometric latitude of a gravity site. This corresponds to changes in the gravity value. The formula used to correct for this effect is:

$$g_{pomo} = -0.039 \sin(2\phi')(x \cos\zeta - y \sin\zeta) \text{ ms}^{-2} \tag{5.7}$$

where ϕ' is the colatitude, ζ the east longitude and x and y the coordinates of the pole in radians.

Peak Detection

As discussed in Section 4.1, the option is given in the software to monitor the '1F' output voltage from the laser to detect shifts of the peak locked on to. Data sets have in general been processed without this, instead manual manipulation of the data has been made where necessary.

5.1.4 Statistics

A data run with 24 sets of 200 drops produces 4800 values of gravity. These are processed to give an overall mean gravity value along with standard deviations of the set averages and drop to drop values. MEAN calculates the statistics of the output from DDT, REPLAY incorporates statistical calculations within itself.

The option of setting a tolerance limit on the residuals is given by the DDT/MEAN package. For each drop, should the magnitude of one of the residuals ϵ_i of equation (5.5) for a fringe used in the fit exceed a value set by the operator, this drop is discarded and not processed as part of the statistics. In this research a tolerance limit of 5 nm has been used.

Both REPLAY and MEAN filter the observations to discard outliers. REPLAY applies a boxcar filter centred around the median followed by an $n\sigma$ filter based on the mean of each set. Sizes of these are typically set to 100 μgal and n=3 respectively. Two passes over the data are performed. The weighted average of the set average values is given as the overall mean. Also the Set Standard Deviation and Mean Standard Deviation are output. The latter is the average of the standard deviations for each set.

MEAN iteratively adjusts the weighting of gravity values for each set. Parameters ONE and ZERO are given whereby values greater than ZERO standard deviations from the weighted mean are given zero weight, and less than ONE standard deviations away are given unit weight. Between these, a cosine taper is assigned such that the weight w_i is:

$$w_i = \frac{1}{2}\left\{1 + \cos\left[\frac{\pi}{\text{ZERO} - \text{ONE}}\left(\frac{g_i - \bar{g}}{\sigma} - \text{ONE}\right)\right]\right\} \tag{5.8}$$

for a value g_i and weighted average $\bar{g}$. Iterations are made until there is no change. Results of this research use values of 1.5 for ONE and 6.0 for ZERO.

In MEAN the data may be processed as sets, giving a weighted mean of the set weighted means and associated standard deviation. Or it may be processed as a whole whereby the weighted mean of all the values is given and their standard deviation. Results have shown that these two means differ by no more than 0.5 μgal.

The author added to MEAN the option of processing data affected by earthquakes and laser lock shifts. The operator is prompted for the start and end drop / set during which these events have happened. In the case of earthquakes, these drops are ignored. For laser lock shifts, a value specified by the operator is added to gravity.

5.2 History of FG5-103

Delivery of FG5-103 was made at POL in August 1992. Charles (1995) reports on data recorded at POL up to early 1994. There were various changes made to the instrument relating to different 'phases' of measurements. The laser was changed on three occasions, alternating between a He-Ne polarisation stabilised and an Iodine absorption stabilised type. On one of these occasions, subsequent re-aligning of the optics was needed. Also an upgrade was performed which included a new version of software, addition of environmental sensors and change from collecting 90 fringes to 170 fringes per drop.

The changes in gravity between these phases are as high as 60 μgal. Reasons for these discrepancies can be explained by the various hardware changes such as using different numbers of fringes in the equation of motion fit and poorly aligned optics. There were many instrumental problems with reliability and repeatability of the data being poor compared to post-1994 data. As a consequence, FG5-103 results used in this research have only used data recorded from 1994 onwards.

Table 5.1 summarises the servicing and changes made to FG5-103 since 1994. A change in gravity occurred through fitment of the new comparator board type APD9696. The value of the

Month	Year	Details
August	1994	New ion pump, snubbers tightened
September	1994	Laser cleaned
October	1994	Service & change from 170 to 180 fringes collected per drop
May	1995	New laser tube
March	1996	Beamsplitter installed, polariser removed
April	1996	Software upgrade to Version 2.2
June	1996	New laser tube
July	1996	APD9696 comparator board installed
February	1997	Service & new scalar counter electronics board installed
November	1997	Laser cleaned
June	1998	New laser tube
March	1999	Service including new ion pump controller, scalar fringe counter and software upgrade to Version 3.2
December	1999	New ion pump

Table 5.1. Summary of servicing and changes made to FG5-103 since 1994.

effect is known and can be corrected for (see Section 4.2). Also a new scalar counter resulted in a gravity change. The effect of this is discussed in Section 4.6 and corrected for.

5.3 Vertical Gradients

The vertical gradients used for processing absolute data were measured with LaCoste & Romberg relative gravimeters (G275 and D145). Ties were made between a dish placed on the floor and another mounted on a tripod so that the sensor of the gravimeter is close to the top of the drop for the FG5 instrument (about 130 cm). Three or four occupations at each dish were made by each instrument.

Investigations into the non-linearity of the gradient have been made by taking further measurements at different heights (Charles, 1995). This is particularly likely at sites with uneven surrounding mass distribution, such as those in basements of buildings. Her findings show that there is a significant change beyond the errors when using a quadratic as opposed to linear vertical gradient for the vertical transfer of gravity values. The effect of using a quadratic gradient in the equation of motion fit is less than 1 μgal.

Table 5.2 gives the linear vertical gradients for all absolute sites in the British Precise Gravity Network (BPGN) (see Chapter 6). Also the vertical transfers from 130 cm (approximately the top of the drop) to 12 cm used to apply FG5 data to the BPGN are given. Those for sites Bidston, Edinburgh and Taunton are reproduced from Charles (1995), the remaining were found as part of this research.

Site	Vertical gradient (μgal cm^{-1})	Vertical transfer 130 cm - 12 cm (μgal)	Dates Measured
Aberdeen	-3.032 $\pm$ 0.011	357.8 $\pm$ 1.3	10/11/95
Bidston POL1	-2.153 $\pm$ 0.031	277.5 $\pm$ 3.4	02/92 & 02/94
Edinburgh	-3.023 $\pm$ 0.035	349.6 $\pm$ 0.3	12/92 & 12/93
Herstmonceux	-2.522 $\pm$ 0.017	297.6 $\pm$ 2.0	03/09/96
Newlyn	-2.912 $\pm$ 0.011	343.6 $\pm$ 1.3	13/10/95
Taunton	-2.982 $\pm$ 0.015	352.3 $\pm$ 0.9	09/93 & 08/94
Wick	-2.435 $\pm$ 0.016	287.3 $\pm$ 1.9	11/10/96

Table 5.2. Linear vertical gradients and transfers for absolute sites of the BPGN. Bidston, Edinburgh and Taunton results are from Charles (1995) and quote a linear vertical gradient measured over the drop length of the FG5 along with a non-linear vertical transfer.

Consideration should be given to the fact that the vertical gradient may vary with time. This could arise due to changes in the local mass distribution. A change in the vertical gradient of 1% would cause the vertical transfer from 130 - 12 cm to change by about 3 μgal. For this reason the dates when the gradients were measured are also given in Table 5.2.

5.4 Results of Ocean Loading Improvements

The routine described in Chapter 2 to increase the accuracy of ocean loading calculation has been applied to absolute data. To determine the improvement this has made to the results, data has been processed using components calculated with and without use of the routine.

In many cases depending on location, ocean loading effects are small. Some areas of Britain have very low loading component amplitudes. For example the M_2 component has a loading effect on gravity with amplitude less than 1 μgal in the Moray Firth and south east England, whereas this same effect reaches over 12 μgal in the south western extremes of Cornwall (Baker, 1980).

The benefits of the ocean loading calculation improvements may only be significant at the 1 μgal level for sites located close to the coast. For example, whilst Taunton experiences significant ocean loading variations in gravity (M_2 amplitude over 5 μgal, *ibid.*), it is located over 25 km inland where the problems of being near the coast are small.

Ocean loading for twelve components have been calculated using the AG95.1 model (Anderson *et al.*, 1995; Anderson, 1995) with a 0.5^o x 0.5^o grid. Comparisons of results have been made between FG5-103 data before and after ocean loading correction, with and without use of the routine of Chapter 2.

A site of particular importance is Newlyn which is the worst case for being affected by ocean loading out of all gravity sites in Britain. The magnitudes of the some of the constituents in SW England are great and the problem is exacerbated by the fact that the Newlyn site is located close to the coast (within 1 km) and at high altitude (90 m).

Figure 5.2 shows the results applied to data set NEW1010A, recorded at Newlyn in 1995. One can see a very large semi-diurnal signal having an amplitude of over 20 μgal in the data with no correction. The results using an ocean loading correction based on the original model still show a strong semi-diurnal signal with an amplitude of about 6 μgal. Results using the refined ocean tide model clearly show a reduction of this signal, and a drop of the Set Std Dev from 4.3 to 1.8 μgal. Comparison of the two corrections indicates a difference in amplitude of about 5 μgal with no apparent phase shift.

The site of Taunton, as already discussed, is in an area where ocean loading is high. Yet the site is inland so the benefits of using the more sophisticated method to correct for ocean loading are likely to be less. Figure 5.3 shows the results of data set TAU1710A taken at Taunton in 1995 with varying levels of ocean loading correction. Note the different vertical scale used than in Figure 5.2.

It can be seen that whilst the ocean loading signal is visible in the raw data, it is not evident in either sets of the corrected data and there is very little difference between the two correction values. There is no significant change in the Set Std Dev.

Ocean loading effects on a small island are expected to be large since areas of sea are in close proximity in all directions. This poses a particular problem when using ocean tide models to calculate loading effects, especially with a coarse grid since it is difficult to get a good fit to the coastline and take local oceanographic effects in to account. Such a site is that of Lerwick, Shetland which consists of a cluster of many small islands, no point of land being greater than 5 km from the sea.

Figure 5.4 gives the results of data set LER2907A taken at Lerwick in 1998. One can see an ocean loading signal in the gravity both without correction and with using the raw ocean tide model. In the case of using the refined model, there is still structure evident and a small improvement in the Set Std Dev from 1.7 to 1.5 μgal. Comparison of the correction values indicates that the amplitude using the refined model is about 2 μgal greater than that of the original model.

Due to the topography of the land, if the remaining structure is caused by ocean loading effects, it is unlikely to be accounted for using a coarse ocean tide model. Local oceanographic factors need to be considered such as the pattern of water currents through the cluster of islands and their associated tidal effects which will not be present in a coarse grid.

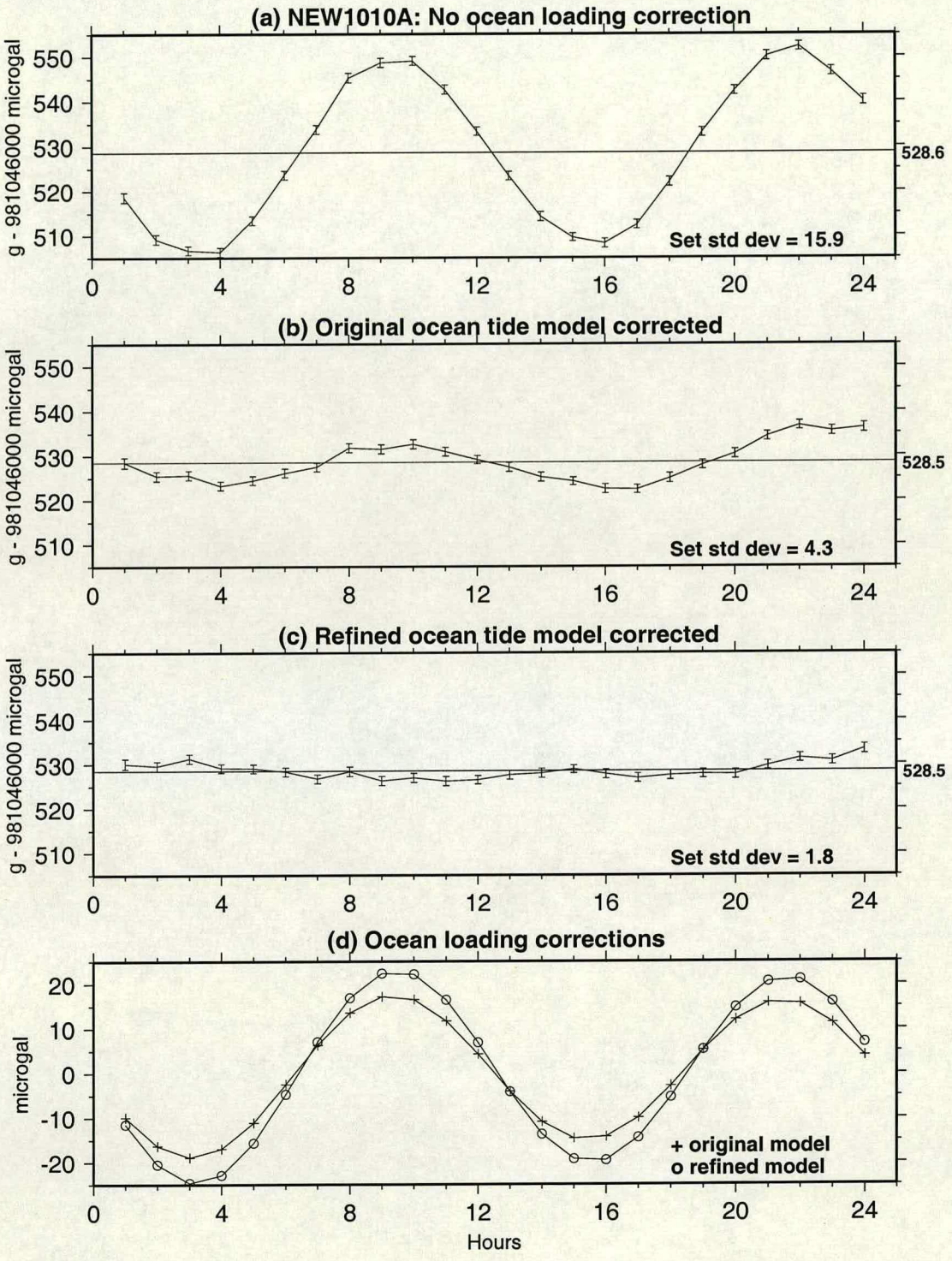

Figure 5.2. Results of data set NEW1010A(1995) (a) without ocean loading correction, (b) with ocean loading correction derived using the raw ocean tide model and (c) using the ocean tide model in a refined form. (d) shows the correction applied in each case.

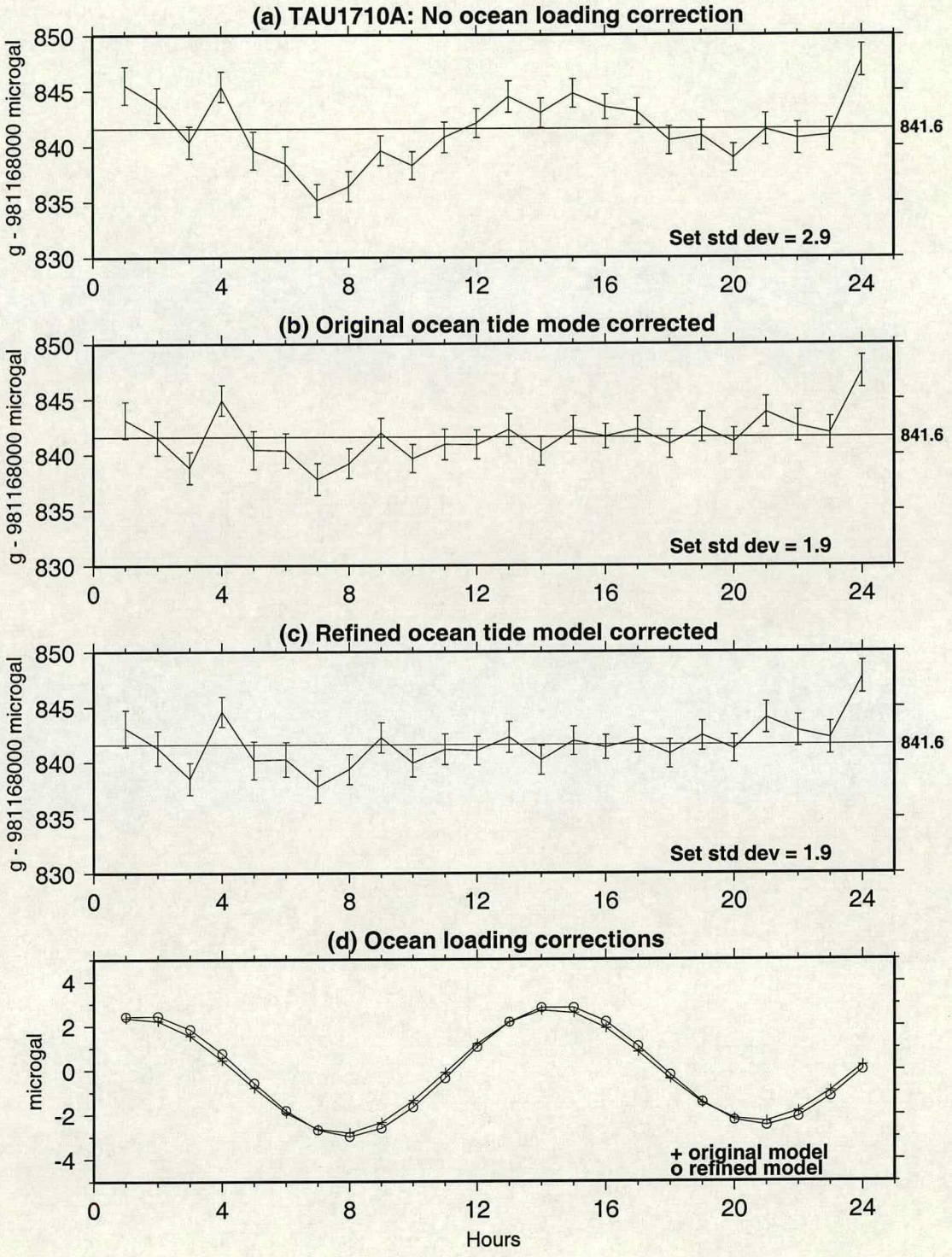

Figure 5.3. Results of data set TAU1710A(1995) (a) without ocean loading correction, (b) with ocean loading correction derived using the raw ocean tide model and (c) using the ocean tide model in a refined form. (d) shows the correction applied in each case.

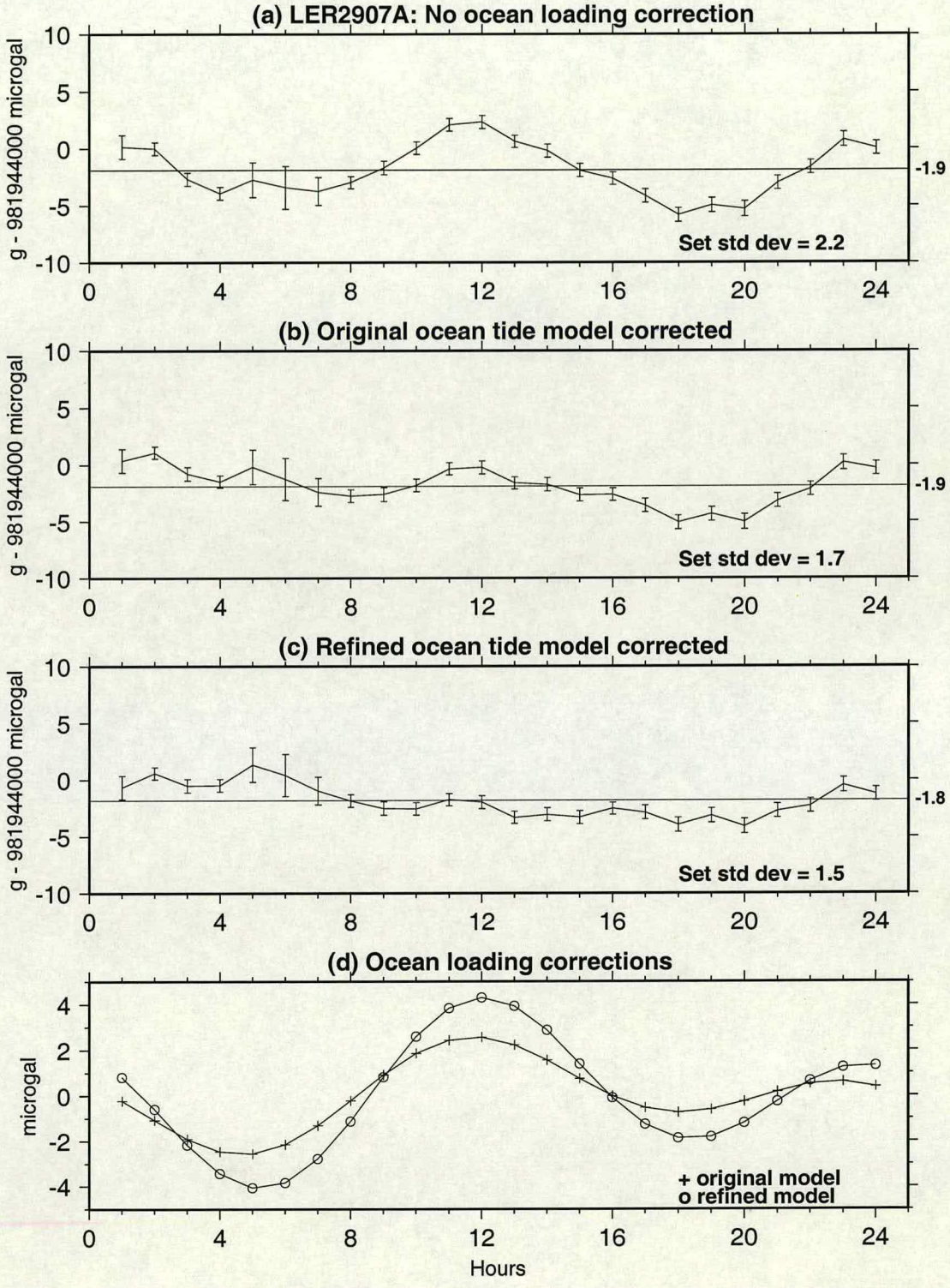

Figure 5.4. Results of data set LER2907A(1998) (a) without ocean loading correction, (b) with ocean loading correction derived using the raw ocean tide model and (c) using the ocean tide model in a refined form. (d) shows the correction applied in each case.

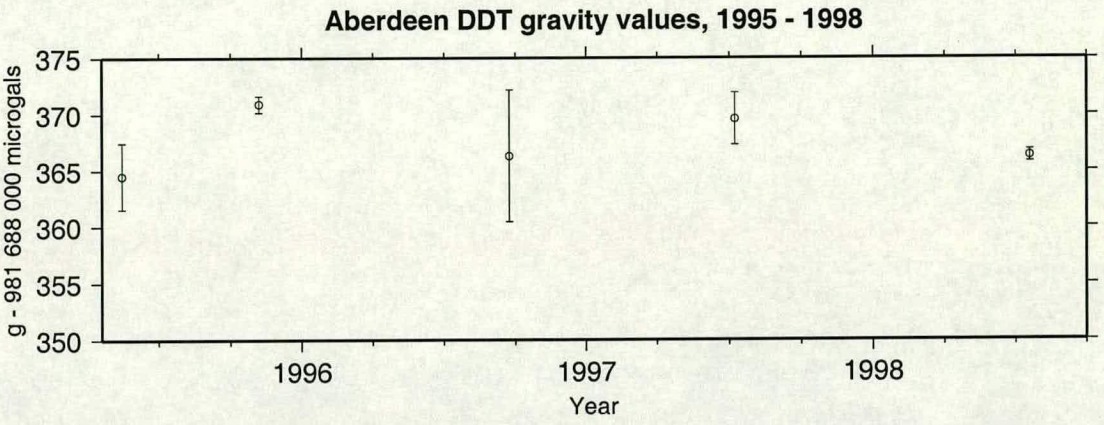

Figure 5.5. DDT results of FG5-103 measurements at St. Machar's Cathedral, Aberdeen, 1995 - 1998.

5.5 Aberdeen Results

The absolute gravity site at Aberdeen is located in St. Machar's Cathedral on a large slab of granite. The underlying bedrock is granite, hence due to its impermeability there are not expected to be any measurable groundwater influences on gravity.

FG5-103 has made five occupations of this site. Two were made during 1995 in May and November. A return visit was made in this year due to the low laser power during the first occupation. Here the fringe voltage was at 52 mV leading to a large comparator response correction of 20 μgal. Further visits were made in September 1996, July 1997 and July 1998.

Figure 5.5 shows the results from these occupations and their associated one standard error range. It can be seen that for these standard errors, all observations are in agreement.

Taking a weighted average of these values, gravity derived for this site is 981 688 367.5 $\pm$ 4.0 μgal.

5.6 Bidston Results

Many data sets have been recorded at this location over a long period of time. There are two sites - POL1 and POL2, both of which are in a basement. Most observations have been made at POL1.

The author has had a selection of post-1994 data sets to use for data processing. POL also supplied results from all data sets which they processed using REPLAY subject to the criteria that cases where the Set Std Dev is greater than 5 μgal or the Mean Std Dev is greater than 55

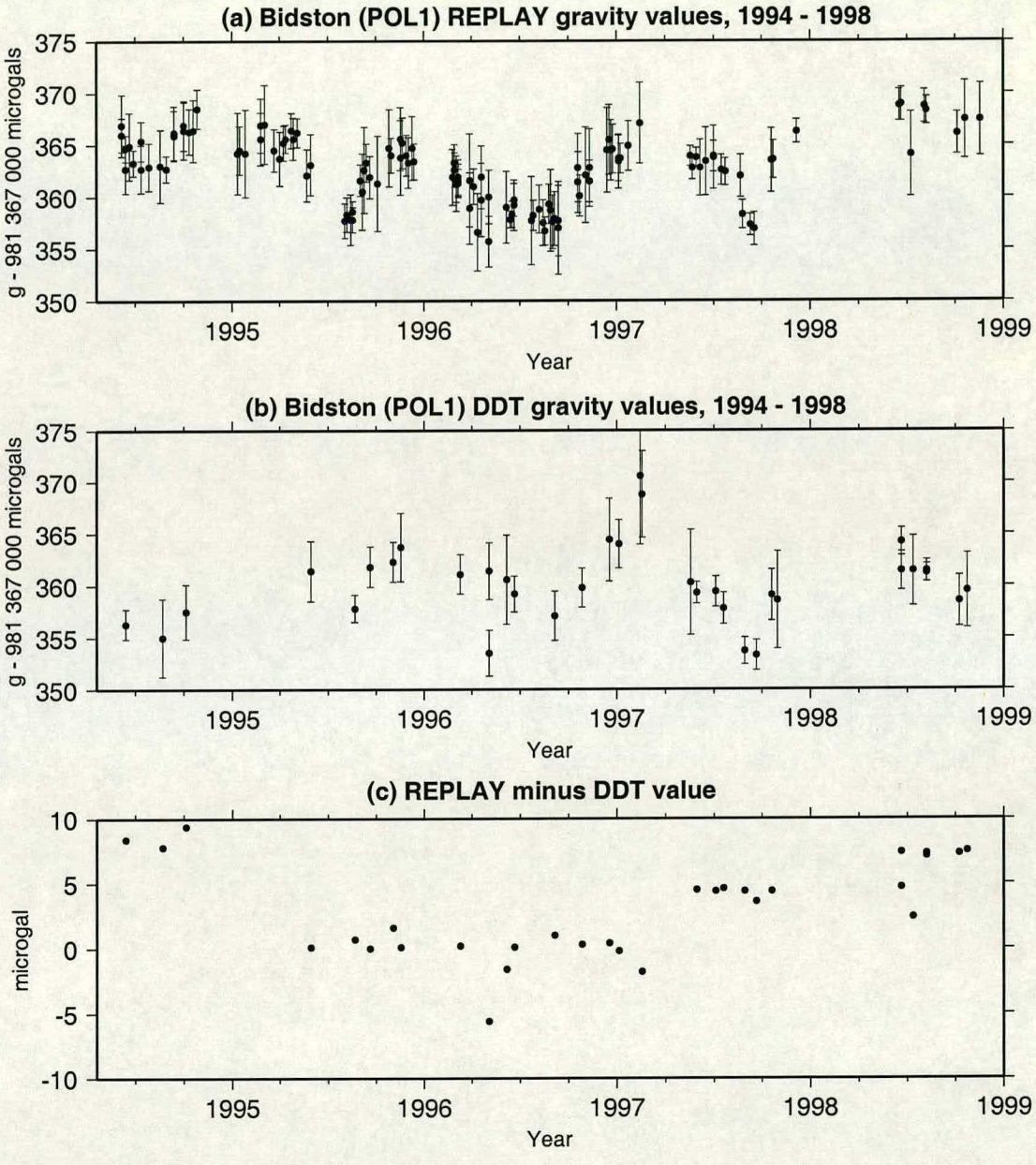

Figure 5.6. Results of FG5-103 measurements at POL1, Bidston for 1994 - 1998 using (a) REPLAY and (b) DDT. (c) shows the differences between these values.

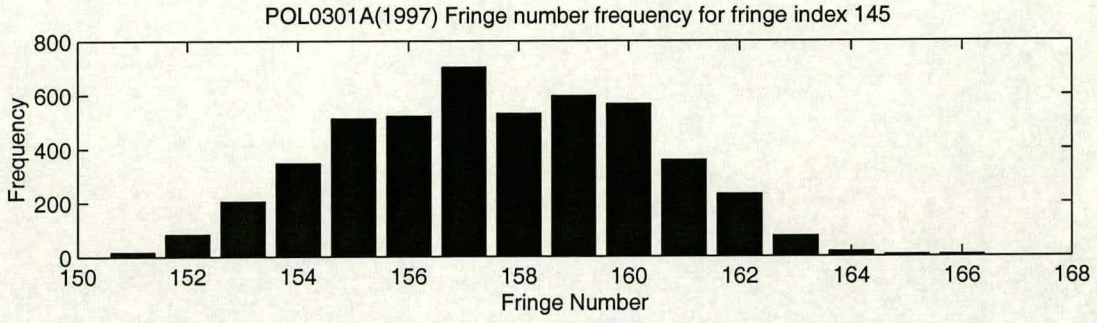

Figure 5.7. Frequency of fringe number occurring as fringe index 145 for the data set POL0301A(1997).

μgal have been ignored. These have been processed using a fit starting at fringe 5 and fitting 165 for data before the scalar counter was changed (February 1997) and fitting 140 thereafter, with all known corrections applied (*pers. comm.* T. F. Baker, 25th November 1998).

Figure 5.6 shows gravity values obtained at POL1, Bidston for (a) all data sets using REPLAY and (b) for those whose data files were in possession by the author using the DDT/MEAN processing package. Part (c) gives the difference in values produced by the two software packages.

It can be seen that REPLAY values are about 8 μgal higher than DDT in 1994, 4 μgal high for the period of mid-1997 and 7 μgal high in 1998. Reasons for these discrepancies can be explained as follows.

For the period 1995 to early 1997, REPLAY results use a fit starting at fringe 5 and fitting 165. Due to missed fringes the fit ends well in to the catch phase, thus perturbing gravity. To enable a comparison of REPLAY with DDT values using fringe numbers 10 to 160, it is necessary to find which fringe index corresponds approximately to fringe number 160.

Figure 5.7 shows the frequency of fringe numbers occurring as the 145^{th} fringe index for data set POL0301A from 1997. It can be seen that most occur between numbers 155 and 160, thereafter tailing off. Thus the best approximation using REPLAY to end the fit at fringe number 160 with a start at fringe 5 is to fit 140 fringes. Note that this will vary between data sets.

Table 5.3 compares results using the two different fits for 3 datasets from the period 1995 to early 1997 with REPLAY Version 2.2. The gravity value is higher when fitting 140 as opposed to 165 fringes, ranging from 2.9 to 7.3 μgal. The average of the differences presented is 4.9 μgal which will thus bring the difference between REPLAY and DDT results for this period up to about 5 μgal.

Data set	Year	Fitting 140	Fitting 165	Difference
POL1808A	1995	70.5	63.2	7.3
POL0603A	1996	65.1	62.2	2.9
POL0301A	1997	55.9	51.4	4.5

Table 5.3. Gravity results obtained by REPLAY Version 2.2 using a fit starting at fringe 5 and fitting 140 or 165. Mean values are g - 981 367 300 μgal, difference is in μgal.

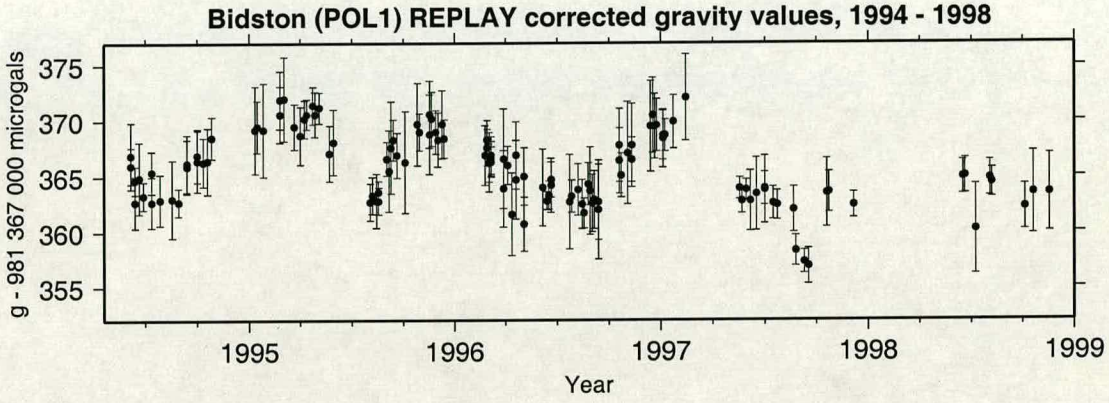

Figure 5.8. Corrected POL REPLAY values for site POL1, Bidston.

It has been found that data for the period from December 1997 onwards has been processed by REPLAY with an incorrect input to one of the parameter files. A calibration of the clock rubidium frequency in November 1997 was input as 10.000 000 02 MHz. It should have been 10.000 000 002 MHz (see Section 4.3). The effect on gravity is to make values 3.5 μgal too high. Thus the discrepancy between REPLAY and DDT values for this period will reduce to about 5 μgal.

The result is that all post-1995 REPLAY values are about 5 μgal higher than DDT which can be accounted for by the different ways that the static tide is removed. REPLAY results use a gravimetric factor of 1.00 whilst DDT results are processed with a factor of 1.16. The static tide at Bidston is -34.5 μgal and hence the larger gravimetric factor used by DDT reduces values by a further 5.5 μgal.

Values of 1994 still have a remaining discrepancy of about 3 μgal which cannot be explained. The instrument underwent a change from collecting 170 fringes per drop to 180 in between these periods (see Section 5.2). Results taken at Edinburgh and Taunton (Sections 5.7 and 5.11) also suggest that pre-1995 data is inconsistent with subsequent data and hence these have not been used.

Figure 5.8 shows the REPLAY results of POL corrected for the known discrepancies as described. For data from December 1997 onwards, 3.9 μgal has been removed to ensure no correction is made for the rubidium frequency drift. For data from 1995 to early 1997, 4.9 μgal has been added. Note that this latter value is an average based on three data sets where individual changes have been found to vary from 3 to 7 μgal, and so is only a rough correction.

The corrected REPLAY results appear to show a seasonal variation in gravity of up to 8 μgal which peaks in the first quarter of the year and troughs about 6 months later for the period from 1994 to the middle of 1997. Thereafter this pattern is not apparent. DDT results of Figure 5.6(b) in general show the same pattern. A possible reason for the seasonal variation are from the effects of groundwater. This was investigated in Chapter 3.

The resulting weighted average value of gravity at Bidston from DDT results is 981 367 360.7 $\pm$ 4.4 μgal. For REPLAY results the value is 981 367 365.7 $\pm$ 3.2 μgal. The 5 μgal difference between the DDT and REPLAY means is due to the different gravimetric factors used for the static tide.

5.7 Edinburgh Results

Absolute gravity measurements at Edinburgh have been performed at two sites. At the British Geological Survey (BGS), instrument JILA4 took measurements in 1989. Results from these are only available as a quote of the gravity value and hence subject to uncertainties in the data processing method leading to the decision to not use these results (Charles, 1995). An occupation by FG5-103 has also been made at BGS in 1992.

A new absolute gravity site was established in the Grant Institute (GI) of King's Buildings, Edinburgh University with the intention of this being the main site of the university. Measurements have been made here by FG5-103 in December 1992, July 1994 and May & November 1995. The occupations of 1995 both consist of installation on the way to and on return from an excursion to Aberdeen.

Charles (1995) reports on results of all occupations before 1995. She claims that FG5 values from 1992 and 1994 differ by up to 13 μgal. For the same reasons as given in Section 5.2, 1992 values have been discarded. The figures she quotes for Edinburgh gravity values differ from those obtained in this research due to different versions of data processing software and additional corrections such as the Comparator Response and Scalar Counter.

Figure 5.9 gives the results for the FG5 occupations made in 1994 and 1995. It is evident that whilst those of 1995 are in good agreement, results from 1994 are about 16 μgal lower. Due to results elsewhere suggesting that 1994 values are less reliable and not consistent with ensuing observations (*eg* Section 5.6), it was decided not to use these.

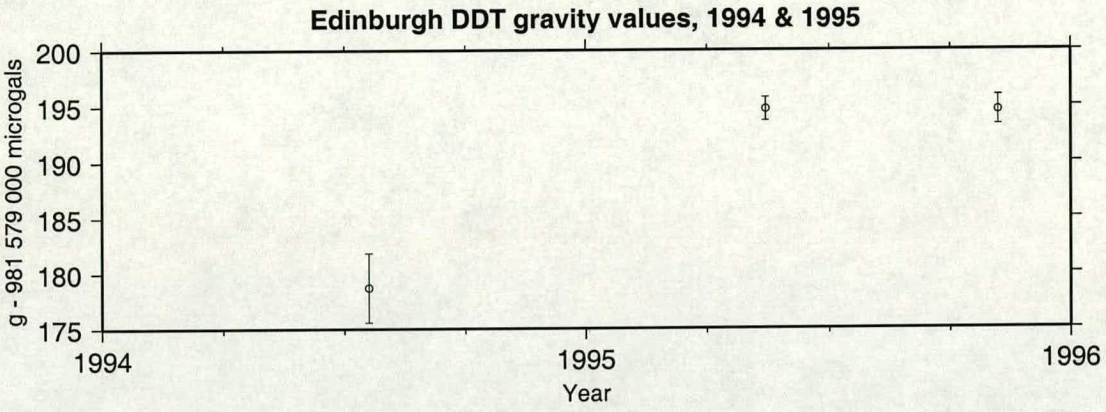

Figure 5.9. DDT results of FG5-103 measurements at the Grant Institute, Edinburgh in 1994 and 1995.

The weighted average value for gravity at the GI site, Edinburgh is 981 579 194.7 $\pm$ 1.2 μgal.

5.8 Herstmonceux Results

A new site was established in the basement of the Satellite Laser Ranging installation at Herstmonceux. One occupation has been made by FG5-103 when four data sets were taken in May 1996. The first two had to be discarded due to laser problems manifesting themselves as a signal in the gravity residuals.

The resulting average gravity value at Herstmonceux is 981 123 987.5 $\pm$ 2.7 μgal.

5.9 Lerwick Results

The absolute gravity site at Lerwick was established in the basement of the High School on a large paving stone. Whilst measuring, it was noticed that the area is subject to water seeping into the room during damp conditions. This lies as a shallow puddle near the place of occupation. It was also noticed that the paving stone moves - a person standing on one end of the slab causes a drift in the levelling bubbles on the gravimeter. This does not appear to have affected gravity measurements but suggests the potential for an effect from groundwater and questions the stability of the site.

It should be noted that the vertical gradient has not been measured at this site. The standard value of -3.086 μgal cm^{-1} has been assumed. The true value may differ, as is often the case with sites located underground.

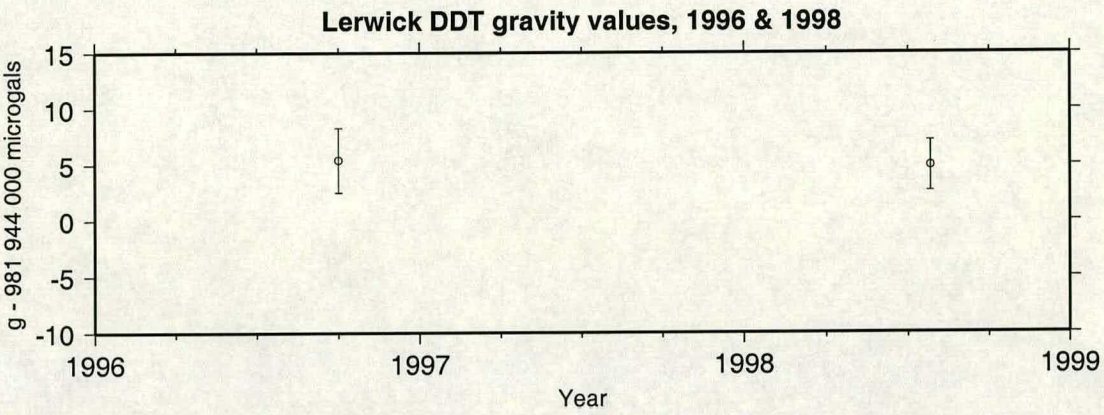

Figure 5.10. DDT results of FG5-103 measurements at Lerwick in 1996 and 1998.

This site has been measured at by FG5-103 in October 1996 and July 1998. Figure 5.10 gives the results of these two occupations. One can see that the two values are in very good agreement with each other.

The weighted average for gravity at Lerwick from these data sets is 981 944 004.9 $\pm$ 2.3 μgal.

5.10 Newlyn Results

The absolute site established for Newlyn is located on a large granite slab in St. Pol de Leon church of the nearby village of Paul. This site has the advantage of being on impermeable granite bedrock. It has the disadvantage of being at high altitude (90 metres above sea level) and close to the coast (within 1 km) making ocean loading effects potentially large (see Section 5.4).

Measurements have been made by FG5-103 in October 1995, June 1997 and June 1998. Figure 5.11 gives results of these occupations. It can be seen that the first two values are in good agreement, whilst the third is about 5 μgal lower.

The weighted average value of gravity for Newlyn is 981 046 524.2 $\pm$ 2.7 μgal.

5.11 Taunton Results

The absolute gravity site in Taunton is located at the Hydrological Office. FG5-103 has made measurements in July 1994 and October 1995. The second set of measurements consisted of two installations on the way to and from an occupation at Newlyn. Measurements have also been made here by FG5-107 in September 1993.

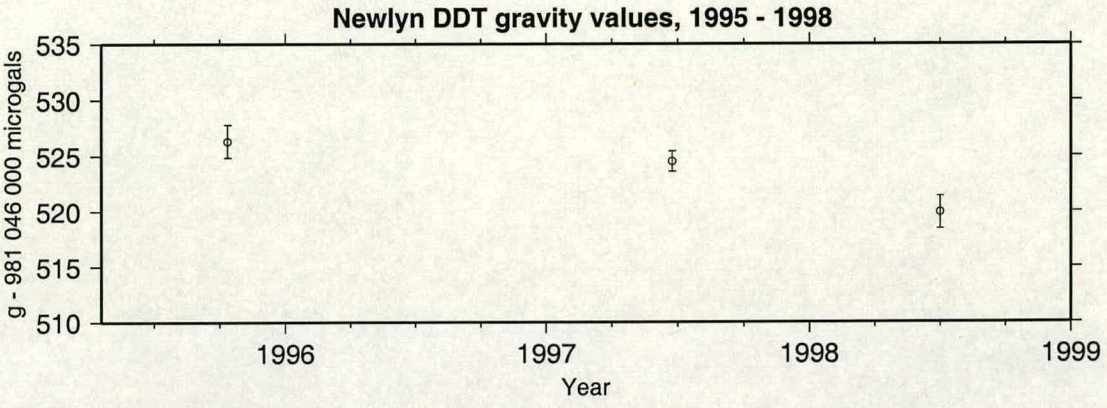

Figure 5.11. DDT results of FG5-103 measurements at Newlyn, 1995 - 1998.

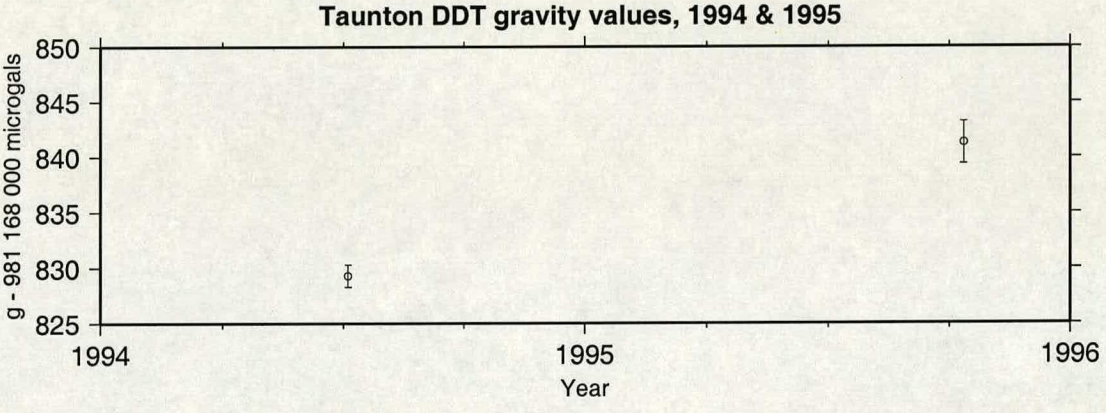

Figure 5.12. DDT results of FG5-103 measurements at Taunton in 1994 and 1995.

Charles (1995) reports on the results she found from the FG5-103 1994 and FG5-107 data. There is a discrepancy of 15 μgal which could be explained due to an incorrect instrument height term for the latter instrument. Because of this uncertainty, results of FG5-107 have not been used.

Figure 5.12 gives the results for the two FG5-103 occupations at Taunton. There is a gravity shift of 12 μgal between the two values. For the same reasons as with the Edinburgh results (Section 5.7), 1994 values have not been used due to the dubious reliability of these data.

The weighted average value of gravity for Taunton is 981 168 841.2 $\pm$ 2.0 μgal.

Site	Gravity at 130 cm	Gravity at 12 cm	Gravity at 12 cm (Charles, 1995)
Aberdeen	981 688 367.5 ± 4.0	981 688 725.3 ± 4.2	
Bidston	981 367 360.7 ± 4.4	981 367 638.2 ± 5.7	981 367 644.3 ± 4.3
Edinburgh	981 579 194.7 ± 1.2	981 579 544.3 ± 4.3	981 579 544.8 ± 2.3
Herstmonceux	981 123 987.5 ± 2.7	981 124 285.1 ± 3.7	
Lerwick	981 944 004.9 ± 2.3	981 944 369.0 ± 2.3	
Newlyn	981 046 524.2 ± 2.7	981 046 869.4 ± 3.0	
Taunton	981 168 841.2 ± 2.0	981 169 193.5 ± 2.7	981 169 188.4 ± 3.2
Wick	981 807 407.1 ± 3.2	981 807 694.3 ± 3.7	

Table 5.4. Mean gravity values for absolute sites in Britain (μgal). Values produced by Charles (1995) are also included for Bidston, Edinburgh and Taunton.

5.12 Wick Results

The new absolute gravity site established at Wick is located in the basement of the High School. One installation has been made by FG5-103 when three data sets were taken in October 1996.

The resulting average gravity value for this site is 981 807 407.1 ± 3.2 μgal.

5.13 Summary of Gravity Values

Table 5.4 summarises the mean gravity values using DDT results for all British absolute gravity sites. Values are given at heights of 130 cm and 12 cm for use in the British Precise Gravity Network (Chapter 6). Results of the individual data sets to obtain these means can be found in Appendix C.

A comparison is possible with values used by Charles (1995) for the sites of Bidston, Edinburgh and Taunton. Her values are 6.1 μgal high and 5.1 μgal low for Bidston and Taunton respectively. The Edinburgh result differs by 0.5 μgal. Within the errors stated, the results are consistent.

Chapter 6

British Precise Gravity Network

The British Precise Gravity Network (BPGN) was established in 1993 (Charles and Hipkin, 1993; Charles, 1995). It was observed with relative gravimeters but constrained by absolute gravity values derived from FG5-103 data at 3 sites. Since then FG5-103 has undergone various instrument upgrades and results are now considered more reliable than the pre-1995 data used for BPGN93. Further data have been recorded at the 3 BPGN93 absolute sites and at 4 extra sites (see Chapter 5).

An overview is given of the background of the network, how it was measured and how the data were processed. Following this, details of improvements to the BPGN93 are given, which include the addition of 7 new relative gravity sites and better subtraction of ocean loading from the gravity data. Adjustment of the network as a set of relative gravity values is compared with absolute gravity values at 7 sites. Unlike the 1993 adjustment, this now allows the hypothesis that the relative gravity meters need only a linear scale correction to be tested.

6.1 Gravity Networks

A gravity network consists of a series of sites, each one connected to one other or more by a relative gravity tie. The size of a network can vary from international (*eg* the International Gravity Standard Network 1971 (IGSN71), Morelli *et al.* (1974)) to a local 'micro-network' (*eg* the interconnection of absolute gravity sites at the Bureau International des Poids et Mesures, Sèvres, Becker *et al.* (1995)).

Relative measurements only give the change in gravity between sites. Therefore, one absolute value must be imposed to fix the datum level. Also the scale of a relative network may not be well enough determined by the manufacturer's calibration functions, so may be left unconstrained and free to adjust to the measurements obtained and their associated errors. To

constrain a linear correction to the instrumental calibration functions, at least two absolute values should be added.

6.2 The Establishment of the BPGN

The purpose of the BPGN is to monitor vertical crustal movements within Britain. It supercedes the National Gravity Reference Network (NGRN) of 1973 which had a formal standard error on gravity site values of 20 - 70 μgal. The BPGN93 has an average gravity site value error of 5 μgal (Charles, 1995).

The network consists of 58 sites connected by relative gravity observations. The fieldwork for this took place mostly during three campaigns in 1992 and 1993. It was constrained by three absolute gravity sites. Figure 6.1 shows a map giving the location of these sites and the links measured between them. Table 6.1 contains the site code, coordinates and height for each site.

The sites were selected under the requirement that they are still likely to be in existence in a few decades time. Also accessibility, suitability for making gravity measurements with some protection from the elements and close proximity to major roads for reduced transport times between sites was needed.

Most sites are doorsteps of old churches which have the advantage that they should be well settled and unlikely to suffer from structural subsidence. It was not always possible to find a suitable building, particularly in remote parts of Britain such as Scotland. In some cases, Ordnance Survey Fundamental Benchmarks were used which was not ideal since they are no longer maintained.

Gravimeters used for relative gravity measurements between sites were all of LaCoste & Romberg design. They consisted of one G-meter (G275) and two D-meters (D145 & D154). Absolute measurements use data from FG5-103.

The sequence of measurements between sites used a 'double forward looping' technique. For example, if measuring at sites A, B and C, the order of measurement would be A-B-A-B-C-B-C.

A connection was made between each absolute site and an out-of-doors 'ex-centre'. This usually involved four occupations by relative gravimeters at each of the two sites. Hence greater ease of access for connection to the network and improved security of the absolute site is provided.

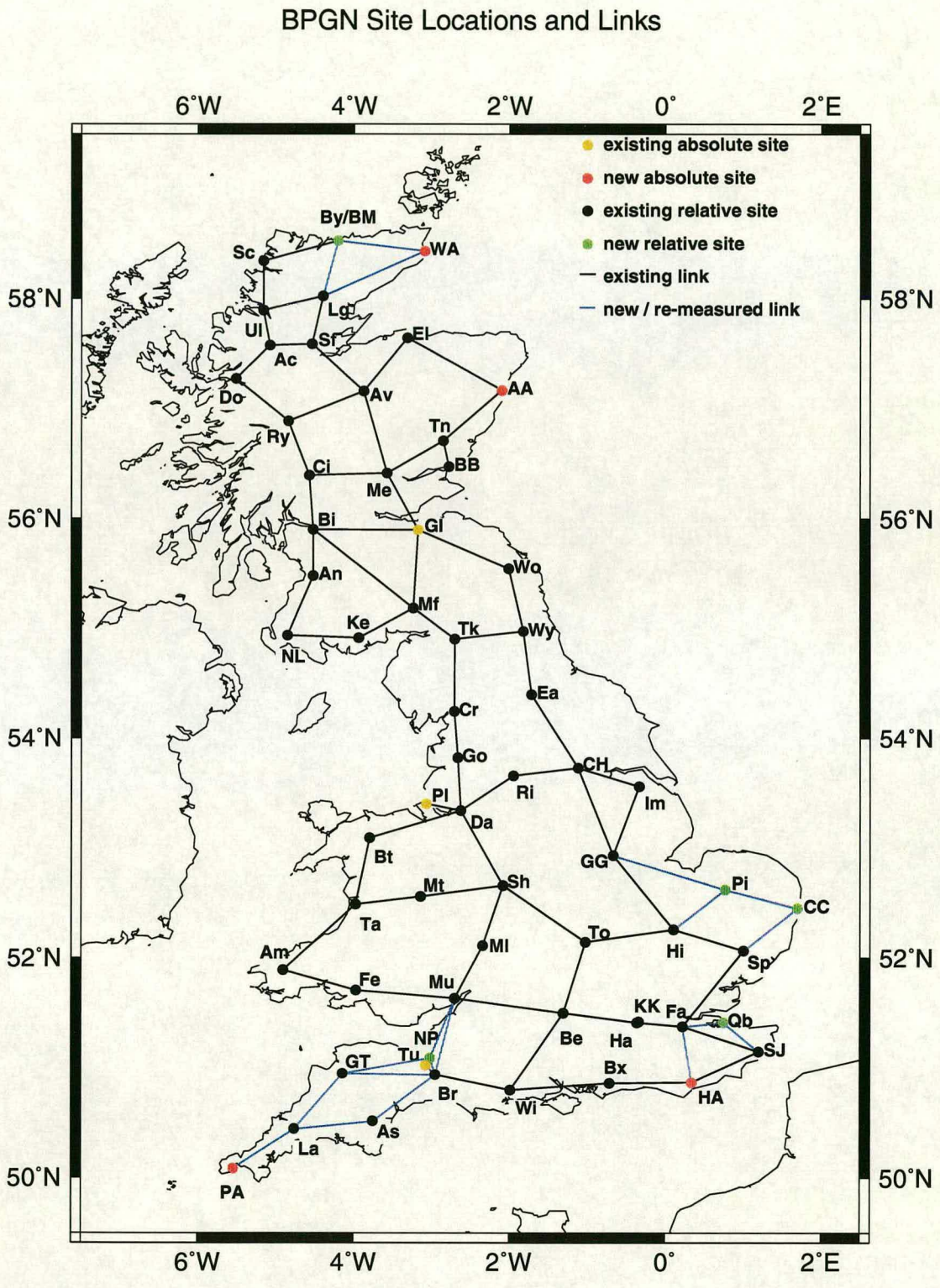

Figure 6.1. Map of existing and new BPGN sites and the links measured between them.

Site name	Code	Latitude (^{o})	Longitude (^{o})	Height (m)
Existing Sites				
Bidston POL1 Absolute	Pl	53.40333	-3.07166	46.00
Edinburgh GI Absolute	GI	55.90000	-3.17700	75.00
Taunton Absolute	Tu	51.02506	-3.07866	15.00
Aberdeen St. Machar's	Ab	57.17000	-2.10100	19.00
Achnasheen FBM	Ac	57.57900	-5.08000	156.00
Alvie	Av	57.16100	-3.87800	216.00
Ambleston	Am	51.89400	-4.90600	134.00
Ashburton	As	50.51400	-3.75600	75.00
Barry Buddon VLBI	BB	56.47800	-2.78100	7.00
Beedon	Be	51.49900	-1.30500	170.00
Bettyhill FBM	By	58.48600	-4.21400	61.00
Betws	Bt	53.09100	-3.80200	18.00
Bishopton	Bi	55.90460	-4.51979	31.00
Boxgrove	Bx	50.86000	-0.71000	29.00
Broadway	Br	50.93900	-2.95400	46.00
Chapel Haddlesey	CH	53.72700	-1.11700	6.00
Crianlarich FBM	Ci	56.39700	-4.57100	166.00
Crooklands	Cr	54.24500	-2.71100	91.00
Daresbury	Da	53.34000	-2.63000	60.00
Dornie	Do	57.27800	-5.51000	12.00
Easby	Ea	54.39800	-1.71400	92.00
Elgin South	El	57.64600	-3.31400	18.00
Farningham	Fa	51.37900	0.22300	28.00
Felindre	Fe	51.70600	-3.97100	85.00
Goosnargh	Go	53.82333	-2.66666	61.00
Great Gonerby	GG	52.93200	-0.66400	94.00
Gt Torrington	GT	50.95200	-4.14300	94.00
Hampton Church	Ha	51.41300	-0.36000	19.00
Herstmonceux	Hx	50.86700	0.33400	24.00
Histon	Hi	52.25500	0.10400	12.00
Immingham	Im	53.56000	-0.33200	20.00
Kelton	Ke	54.92100	-3.93700	67.00
Teddington KK Bld1	KK	51.41970	-0.33774	10.00
Lairg	Lg	58.02500	-4.39900	110.00
Lanivet	La	50.44400	-4.76200	78.00
Malvern	Ml	52.11200	-2.34600	244.00
Methven	Me	56.41600	-3.57900	70.00

Table 6.1. List of all BPGN sites with coordinates and altitudes.

Site name	Code	Latitude (^{o})	Longitude (^{o})	Height (m)
Existing Sites continued				
Moffat TH	Mf	55.19000	-3.24000	120.00
Montgomery	Mt	52.56000	-3.14600	160.00
Mounton	Mu	51.63300	-2.70400	23.00
New Luce	NL	54.94200	-4.85000	55.00
Rishworth	Ri	53.65800	-1.95200	190.00
Roybridge	Ry	56.89200	-4.83900	97.00
Scourie	Sc	58.34800	-5.15900	6.00
Shareshill	Sh	52.65700	-2.08300	136.00
Sproughton	Sp	52.06300	1.00000	13.00
St John Commandery	SJ	51.15100	1.19200	149.00
Strathpeffer	Sf	57.58900	-4.53800	76.00
Talkin	Tk	54.90800	-2.70300	165.00
Talybont	Ta	52.48900	-3.97900	64.00
Tannadice	Tn	56.71100	-2.85770	65.00
Towcester	To	52.14300	-1.02200	119.00
Ullapool Mus	Ul	57.89600	-5.16100	12.00
Wick church of S	Wk	58.44400	-3.09400	3.00
Wimborne	Wi	50.79855	-1.98723	29.00
Wooler	Wo	55.54600	-2.01100	67.00
Wylam	Wy	54.97700	-1.82200	34.00
New sites				
Aberdeen Absolute	AA	57.17000	-2.10100	19.00
Herstmonceux Absolute	HA	50.86700	0.33700	17.00
Wick Absolute	WA	58.43800	-3.09600	18.00
Newlyn (Paul) Absolute	PA	50.08932	-5.54475	91.00
Bettyhill Museum	BM	58.53000	-4.20800	8.00
Carlton Colville	CC	52.45100	1.69500	8.00
North Petherton	NP	51.09383	-3.02127	46.00
North Pickenham	Pi	52.62000	0.76700	61.00
Paul	Pa	50.08932	-5.54475	91.00
Queenborough	Qb	51.41700	0.74500	3.00
Wick High School	WS	58.44400	-3.09400	18.00

Table 6.1. Continued list of all BPGN sites with coordinates and altitudes.

6.3 Data Reduction and Analysis

Measurements from the relative gravimeters are recorded as numbers of dial turns. These are converted in to gravity values using the Edinburgh program REDUCE. For each instrument, this uses a ninth degree polynomial to represent the manufacturer's calibration function. Gravity values obtained have Earth body tide, ocean loading and air pressure effects subtracted.

For relative gravity observations, the network adjustment is based on the following equation for observation i using meter f on traverse k at site m,

$$(1 + C_f)g_i = G_m + (a_k + b_k t) + \epsilon_i \tag{6.1}$$

where g_i is the observed gravity, G_m the adjusted gravity, C_f the scale correction factor for meter f, ϵ_i the residual and a_k and b_k give details of the drift for this traverse.

Various drift characteristics have been tested by Charles (1995) for the relative instruments such as zero drift or a cubic fit, but best results were obtained by assuming the drift was linear. She found that for the Scotland leg of the BPGN93 fieldwork, the drift was 3.08 ± 0.32 μgal/day for G275, 12.06 ± 0.36 μgal/day for D145 and 19.66 ± 0.48 μgal/day for D154. The average daily drift rate for each traverse with all BPGN data used in this research was 22.7 ± 76.3 μgal/day for G275, 36.2 ± 120.5 μgal/day for D145 and 44.0 ± 147.9 μgal/day for D154.

The meter scale correction factors may be fixed, or free to be included as part of the adjustment. With no constraint of the scale from absolute meters, the whole network is adjusted to the scale of one relative gravity meter. G275 was chosen as the primary instrument amongst the relative gravimeters since it in general produces the least scattered observations.

Each observation is assigned a weight w_i which is a combination of a meter weight w_f and a blunder weight w_{bi} such that $w_i = w_f w_{bi}$. The meter weight w_f is defined to be the reciprocal of the standard deviation for that particular instrument, σ_f, scaled by a constant, c, so that $w_f = \frac{c}{\sigma_f}$. The constant c is chosen such that the sum of weights w_f equals the number of observations scaled by blunder weights. The blunder weight is designed to reduce the contribution from observations of dubious quality which sometimes occur due to operator error, instrument problems, poor floor surfaces and so on. It is defined such that:

$$w_{bi} = \begin{cases} \dfrac{1}{1 + 4\left(\frac{\epsilon_i^2}{\sigma_f^2} - 4\right)^2} & \epsilon_i^2 \geq 4\sigma_f^2, \\ 1 & \epsilon_i^2 < 4\sigma_f^2. \end{cases} \tag{6.2}$$

The Edinburgh program NETWORK performs least squares iterative adjustments based on these equations.

The characteristics of the residuals are a combination of a set of random errors with normal distribution and a set of blunder errors with uniform distribution. The variance of these residuals may not be a good estimate of the true variance due to contamination by blunders.

To test the strength of the estimate, the residuals are sectioned off into 16 intervals of equal size within ± 2 times this standard deviation where random errors dominate. The distribution of residuals in each interval is compared with what would be expected if they were distributed normally. The 'Chi-squared method' is used to test the hypothesis that the actual distribution of residuals is normal. A result in the 80% confidence interval was required. Given that there are 14 degrees of freedom (16 classes minus 2 for the mean and standard deviation), this would require acceptable values of χ^2 to be such that $7.79 < \chi^2 < 21.06$.

Convergence of the iterations is defined to be when the rms of the previous iteration (σ_{prev}) has changed a small amount from the new rms (σ_{new}) such that $\left|\left(1 - \frac{\sigma_{prev}}{\sigma_{new}}\right)\right| < 0.001$. The iteration chosen as the solution is that which has converged and has the smallest root mean square (rms) with an acceptable value of χ^2. In the case of equal rms, the iteration with a χ^2 value closest to the number of degrees of freedom is chosen. Up to 20 iterations are performed.

The adjustment constrained by absolute gravity data is carried out in a similar manner. The absolute gravity data has no scale correction factor and is assigned an *a priori* standard error of 3 μgal which is held fixed.

6.4 New Relative Data

The additions made to BPGN93 through relative gravity measurements can be broken down into fieldwork campaigns and their respective regions of Britain. Details of all new measurements are given in the following subsections. For a map giving the location of new sites and new / re-measured links, refer to Figure 6.1. Table 6.1 details the site codes and location coordinates.

6.4.1 South West England

During October 1995, measurements were taken in the south west of England. A new absolute gravity site had been established in the village of Paul, near Newlyn. Connection was made to an ex-centre and the rest of the network via Lanivet. Newlyn is an important site since it is the datum reference point for the Ordnance Survey and has a long tide gauge record. Ideally a relative tie should be made to more than one gravity site so it is not 'out on a limb'. However, due to the geography in that it is situated at the end of a peninsular, this was not practical.

A new site was established at the Ordnance Survey Fundamental Benchmark (FBM) of North Petherton. This is close to the absolute site of Taunton. Measurements were made from Taunton to nearby Broadway and North Petherton to provide more than one link to the absolute site. Also measurements were made between Broadway and North Petherton to Great Torrington and Mounton. This now means that the south west of the network is connected to the rest with a braced polygon, whereas before there was just a single link via Broadway.

The links from Ashburton to Lanivet and Broadway were re-measured. This was to strengthen the previously weak links here due to a battery failure in G275 during the field campaign of September 1992.

6.4.2 South East England

During August / September 1996, a field campaign in the south east of England extended the network in to East Anglia - an area previously with little coverage. Two new sites were established, at North Pickenham FBM and Carlton Colville. The latter was chosen to be in close proximity to the tide gauge in Lowestoft.

A third new site was established at Queenborough on the Isle of Sheppey. This was chosen to provide a link to the tide gauge in Sheerness. Further measurements were made at Herstmonceux, a site where new absolute observations had been made. The BPGN Herstmonceux site was connected to the absolute site and a link to Farningham made to increase the strength of this now more important site.

6.4.3 North Scotland

Absolute gravity measurements were made at Wick in October 1996. The absolute gravity site was located in a cellar at the High School, and an ex-centre was measured to on the school doorstep. Unfortunately, it was discovered that the BPGN93 site at a church in Wick had been destroyed due to renovation. It was then necessary to connect the Wick School site to the adjacent BPGN sites of Lairg and Bettyhill. The Bettyhill site is an Ordnance Survey FBM which we were unable to find. A new BPGN site was established at Bettyhill Museum. Time did not permit a connection from Bettyhill to Scourie, the slowest and most difficult link in the whole of BPGN. As a consequence, this part of the network is entirely new and connected to the rest of the network only via Lairg.

In subsequent correspondence with the Ordnance Survey, it is claimed that the Bettyhill FBM does still exist (*pers. comm.*, 1998). Further measurements need to be taken in this area, either to find the FBM and connect it to the Bettyhill Museum or tie the new Bettyhill site with Scourie.

6.5 New Absolute Data

6.5.1 Revised Values at Earlier Sites

BPGN93 was constrained by three absolute sites at Bidston, Edinburgh and Taunton. Since this adjustment, further measurements have been made at Bidston on a regular basis, as this is where FG5-103 is based. Additional measurements were also made at Edinburgh during November 1995. Also additional corrections for instrumental effects have led to new gravity values being derived for these sites.

6.5.2 Additional Absolute Sites

Extra absolute gravity sites have been established in Britain which have been connected to BPGN so that these data can be used to constrain the network. The site established at Aberdeen was conveniently located in St. Machar's cathedral - where the BPGN site is. FG5-103 took measurements here in May and November 1995, September 1996, July 1997 and July 1998. The site is situated on granite and hence results from these occupations are unlikely to be subject to groundwater effects.

The absolute site established at Newlyn is also located on granite. Observations were taken here in October 1995, June 1997 and June/July 1998.

Two further absolute sites have been established where repeat measurements have not been made. These are the satellite laser ranging site at Herstmonceux (May 1996) and Wick (October 1996).

6.5.3 Ex-Centres

With the addition of four new absolute sites, ties from these to a nearby ex-centre site were made to connect to the relative network. These involved four measurements at each of the absolute and ex-centre locations. They usually were done at the same time as measurement of the vertical gradient and as such included as part of the same traverse in the calculations. Table 6.2 gives the results for the new absolute sites.

Sites		Gravity difference at 120mm above the floor
Aberdeen Absolute	- Doorway (BPGN)	-87.5 ± 1.9
Herstmonceux Absolute	- Church (BPGN)	1937.9 ± 2.8
Newlyn Absolute	- Granite slab (BPGN)	73.2 ± 1.1
Wick Absolute	- Doorway (BPGN)	489.9 ± 1.6

Table 6.2. Ex-centre ties to BPGN absolute gravity sites. Values are μgal.

6.6 Ocean Loading

6.6.1 Ocean Loading Correction

For BPGN93, only M_2 ocean loading was subtracted from the gravity data and assumed an altitude of zero. This means that the direct attraction of the local ocean tide, which may be measurable for stations near the coast at high altitude, was not included. It was calculated from the Schwiderski (1980) tidal model.

Ocean loading for 12 components (M_2, S_2, K_1, O_1, N_2, P_1, K_2, Q_1, L_2, μ_2, ν_2, $2N_2$) have been calculated for all BPGN sites using the method described in Chapter 2. Ocean tide model AG95.1 was used (Anderson *et al.*, 1995; Anderson, 1995). This was done with station altitude taken into account.

6.6.2 Effect of Ocean Loading Improvements

Table 6.3 is a comparison of the results obtained when processing the gravity network corrected for ocean loading in two ways. The 'old' way is using the M_2 components of BPGN93, the 'new' way is using 12 components (see Section 6.6.1 for details). This should illustrate the effect that improving the ocean loading has had on the network.

It can be seen that in either case of absolute constraint or not, results have smaller errors with the new ocean loading correction. The weighted rms drops by 1.2 μgal with FG5 constraint and 0.3 μgal without. In both instances the mean site standard error also reduces.

It should also be noted that the scaling factor for G275 changes significantly beyond the standard errors from 1.000 705 ± 0.000 012 to 1.000 656 ± 0.000 011 with the new ocean loading correction. Whilst this is inconsistent with the scale factor found for BPGN93 using the old ocean loading correction and 3 absolute constraints (1.000 737 ± 0.000 018, Charles and Hipkin (1993)), it is consistent with a scale factor found for G275 using the IGSN71. This was 1.000 622 ± 0.000 027 derived from a measurement between Edinburgh and Rome in 1986 (Hipkin *et al.*, 1988).

	With FG5 constraint		Without FG5 constraint	
Ocean loading	Old	New	Old	New
χ^2	20.729	20.267	20.027	18.323
weighted rms	6.98	5.74	6.23	5.91
G275 rms	5.05	4.10	4.45	4.28
D145 rms	9.35	7.79	8.45	7.60
D154 rms	16.94	16.86	18.08	15.74
C_f G275	1.000 705 $\pm$ 0.000 012	1.000 656 $\pm$ 0.000 011	1.000 705	1.000 656
C_f D145	1.001 031 $\pm$ 0.000 018	1.000 984 $\pm$ 0.000 015	1.001 031	1.000 984
C_f D154	1.001 395 $\pm$ 0.000 032	1.001 352 $\pm$ 0.000 032	1.001 395	1.001 352
mean std error of sites	3.32 $\pm$ 0.60	2.96 $\pm$ 0.46	5.10 $\pm$ 1.72	4.93 $\pm$ 1.59

Table 6.3. Results of BPGN adjustment using the old ocean loading correction of BPGN93 and the new correction with a refined ocean tide model. Adjustments with and without FG5 absolute constraints are given. The scaling factors found with FG5 constraint were used as fixed in the adjustments without FG5 constraint. Errors are in μgal.

6.7 Comparison of Relative and Absolute Values

6.7.1 Inconsistency Between Relative and Absolute Values

For the adjustment of BPGN93, values from 3 absolute gravity sites were available to compare with relative network gravity values. It was found that relative and absolute data were consistent with a linear scale correction factor (Charles, 1995). Since then values at these 3 absolute sites have been updated, and values from a further 4 absolute sites have been made available.

To test the quality of the relative network, a comparison has been made between relative and absolute gravity values at the 7 absolute sites where FG5-103 has measured. The network was first processed using all absolute sites as constraints and free scaling factors. The factors output from this were then used for a second adjustment without absolute data. The resulting relative site values were then multiplied by the appropriate scaling factor and compared with the absolute values.

Figure 6.2(a) shows the relative site value subtracted from the FG5 value, plotted as site code against gravity. It can be seen that the values are discrepant in a range of $\pm$ 25 μgal. This suggests a strong disagreement between relative and absolute values.

To investigate further, the network was processed by constraining at the absolute sites of Wick and Newlyn (essentially the two sites at the extreme north and south ends of the network). The

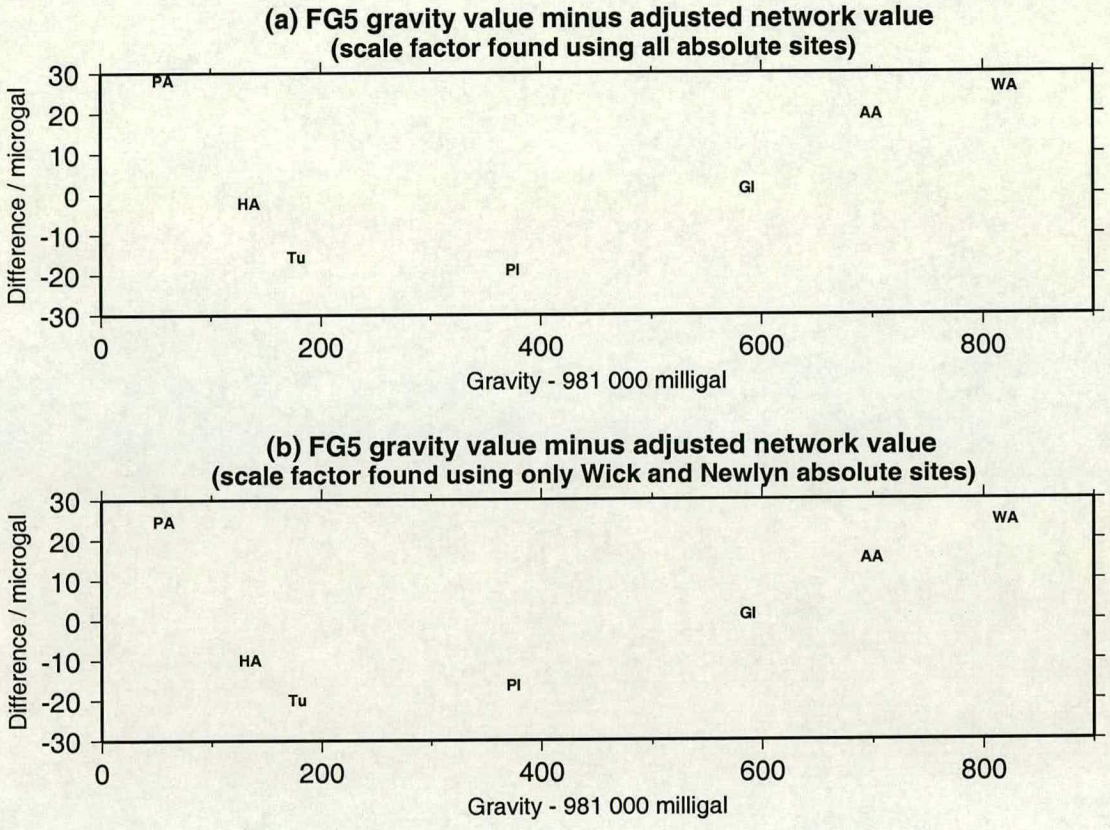

Figure 6.2. Comparison of FG5 absolute gravity values with relative network values.

aim of this was to examine how the network behaves compared to absolute values while being held fixed at each end. Results of this can be seen in Figure 6.2(b).

The two plots of Figure 6.2 show the same pattern, namely that relative gravity values at either north or south end of the network are too low, and in between are too high compared to absolute data. The range of discrepancy is about 50 μgal. Possibilities for these differences are that the relative values are in error, the absolute values are in error, or some combination of both. The first two hypotheses presented here account for the discrepancy by attributing it to error in the relative data.

It is suggested that there is a problem with the network in the south of Britain. Figure 6.2(b) shows the differences decreasing in a linear manner from Wick (code WA) to Taunton (code Tu). South of here (Newlyn (PA) and to a lesser extent Herstmonceux (HA)) this linear pattern is not evident. The scaling factors were assumed to be linear, a pattern not exhibited by the two southernmost absolute sites. Hence this may be explained by some network error occurring only in the south. Section 6.7.2 investigates this possibility.

The second suggestion is that the assumption of linear scale factors is incorrect. The discrepancies of Figure 6.2 are plotted against gravity which roughly coincides with dial turns on the relative gravimeters. Non-linear scale factors would manifest themselves as the pattern seen here. If this is the case, fitting non-linear scale factors would resolve the problem. This possibility is investigated in Section 6.7.3.

The possibility of errors in the absolute data is discussed in Section 6.7.4.

6.7.2 Network Adjustment Without Constraint in the South

The assumption that there exists a problem with the network in the south of Britain means that using absolute constraints from this area will perturb the resulting linear scale factors. Hence it is necessary to adjust the network without absolute constraints in this area to find a set of scale factors and use those in the adjustment of the overall network.

Each instrument was examined individually. Figure 6.3 shows the difference between FG5 values and a network adjusted with constraints at Wick and Newlyn using data from only (a) G275 and (b) D145. Meter D154 was not processed in this manner due to not making enough occupations at absolute sites to enable comparison and in general having a low weight in adjustments meaning it will have a relatively small influence on the outcome.

Figure 6.3(a) for G275 shows that it is possible to include Herstmonceux in the fit to find a linear scale factor. Only the Newlyn FG5 constraint was excluded. Results for D145 in Figure 6.3(b) show that a linear pattern is feasible if sites Newlyn and Herstmonceux are ignored. Processing the instruments separately with the constraints as described, Table 6.4 gives the scaling factors found.

Instrument	Scale factor	FG5 constraints excluded
G275	1.000 623 ± 0.000 013	Newlyn
D145	1.001 173 ± 0.000 022	Newlyn Herstmonceux
D154	1.001 279 ± 0.000 040	None

Table 6.4. Scale factors found for each instrument individually with FG5 constraint except at those sites listed.

Table 6.5 details adjustments of the network using the scale factors of Table 6.4 with and without absolute constraint (in this case using all absolute site values). Figure 6.4 displays

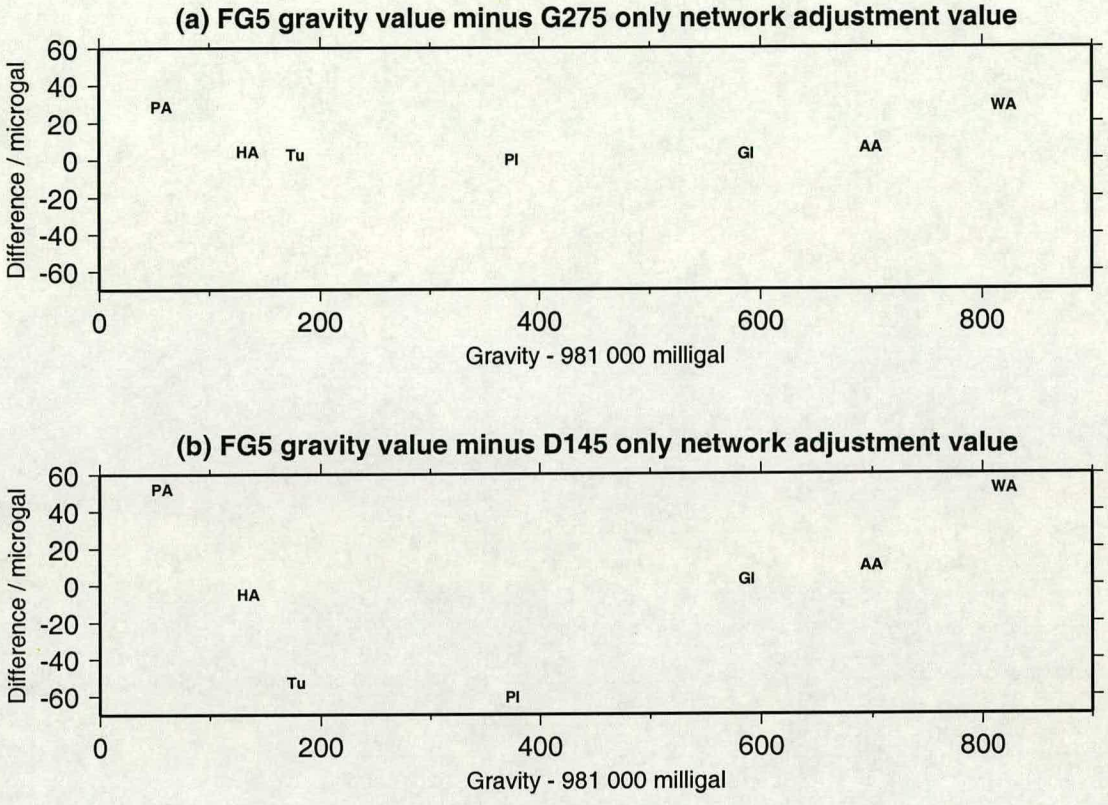

Figure 6.3. Difference between FG5 absolute gravity value and network adjustment for (a) G275 and (b) D145 separately constrained by Newlyn and Wick absolute values.

the differences between absolute gravity values and relative network values when processed without absolute constraint.

It can be seen that whilst Figure 6.4 is an improvement on Figure 6.2(a), discrepancies still exist in sites from Wick to Herstmonceux ranging over 30 μgal. A straight line could be fitted to these, however the pattern is also suggestive that a polynomial such as a quadratic or cubic could be fitted. As expected, the discrepancy at Newlyn (PA) is large (50 μgal) since this was excluded from the constraints for instruments G275 and D145.

Comparing the errors of the adjustments in Table 6.5 with those of the adjustment using all absolute constraints in Table 6.3, it can be seen that errors in the case of the former are higher. For example, the weighted rms is 6.46 μgal as opposed to 5.91 μgal when using scale factors found using all absolute constraints.

	With FG5 constraint	Without FG5 constraint
χ^2	16.473	19.007
weighted rms	6.92	6.46
G275 rms	5.09	4.72
D145 rms	8.61	8.12
D154 rms	16.45	16.50
mean std error of sites	3.22 ± 0.58	5.11 ± 1.56

Table 6.5. Details of network adjustment using scale factors of Table 6.4 with and without absolute constraint. Errors are in μgal.

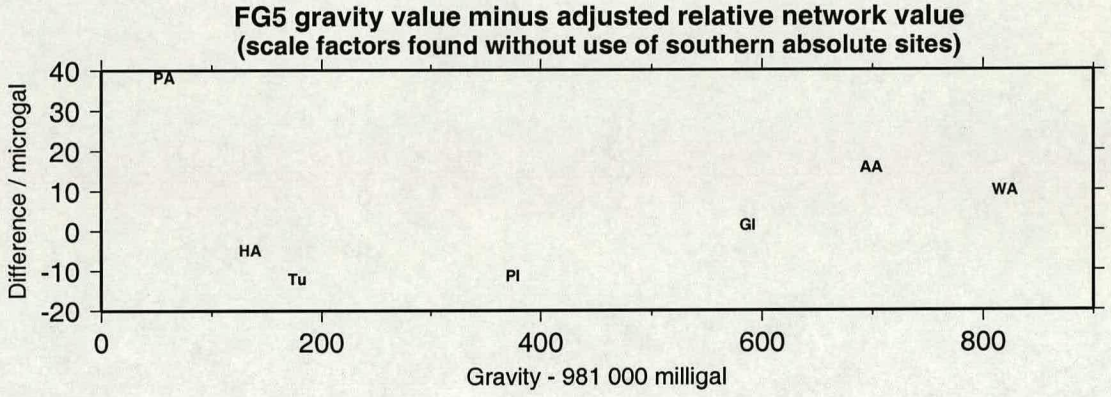

Figure 6.4. Difference between FG5 absolute gravity values and relative network values using scale factors calculated for G275 without constraint at Newlyn and D145 without constraint at Newlyn or Herstmonceux.

6.7.3 Network Adjustment With Non-Linear Scale Factors

This section investigates the proposal that the discrepancies outlined in Figure 6.2(b) are caused by instrumental effects resulting in the assumption of linear scale factors being incorrect.

Non-linear scaling factors may arise due to periodic errors within the relative gravimeters. Periodicities can be caused by eccentricities in the gears. Charles (1995) reports that given the gear ratios of the instruments, periods may be expected at certain numbers of dial turns. These are reproduced in Table 6.6.

A periodicity may not be noticed in a gravity network that covers only part of that period. In this case the effect can be absorbed by linear scale factors. With BPGN now having 7 absolute sites ranging over 800 milligal as opposed to the previous 3 ranging over 400 milligal, it is possible that an undetected periodicity has now become apparent.

Dial turns	G275	D145 coarse dial	D145 fine dial
long period	1206.00 (603.00)	1800 (900)	1500 (750)
primary ratio	70.94 (35.47)	100 (50)	50 (25)
quarter turn		25	12.5
second gear	7.88 (3.94)	10	5
one turn	1.00	1	1

Table 6.6. Expected periods in dial turns for G275 and for the coarse and fine dials on D145. The figures in brackets are equal to half of the calculated periods. From Charles (1995).

To adjust for a non-linear scale factor, the discrepancy between G275 and D145 readings with absolute values was examined with respect to dial turns. A polynomial was then fitted to these points and incorporated in the calibration function which converts dial turns to gravity for each instrument. For D145 this was only done with respect to the coarse dial since this was used to balance the instrument whilst the fine dial was held at a fixed position. Once again D154 data were not used in this method due to having fewer occupations and a lower weight in the adjustments.

Figure 6.5 shows the discrepancies between absolute and relative values for adjustments with only (a) G275 and (b) D145 plotted against dial turns. Both instruments exhibit a pattern that is approximately sinusoidal, having periods that appear to be about 700 dial turns for G275 and 1000 coarse dial turns for D145. These are similar to half the long periods expected of these instruments, being 603 dial turns for G275 and 900 coarse dial turns for D145 (Table 6.6).

For G275 a quadratic was fitted to the points. This is also shown in Figure 6.5(a). A cubic was also tried with very similar results to those presented, hence it was decided to use the simpler function. In the case of D145 a better fit was found with a cubic (as shown in Figure 6.5(b)). The coefficients for these polynomials are given in Table 6.7.

Term	G275	D145
Constant	5.24×10^{3}	2.29×10^{5}
Degree 1	-2.20×10^{0}	-9.87×10^{1}
Degree 2	2.31×10^{-4}	1.41×10^{-2}
Degree 3		-6.72×10^{-7}

Table 6.7. Coefficients of the polynomials displayed in Figure 6.5 relating dial turns to gravity.

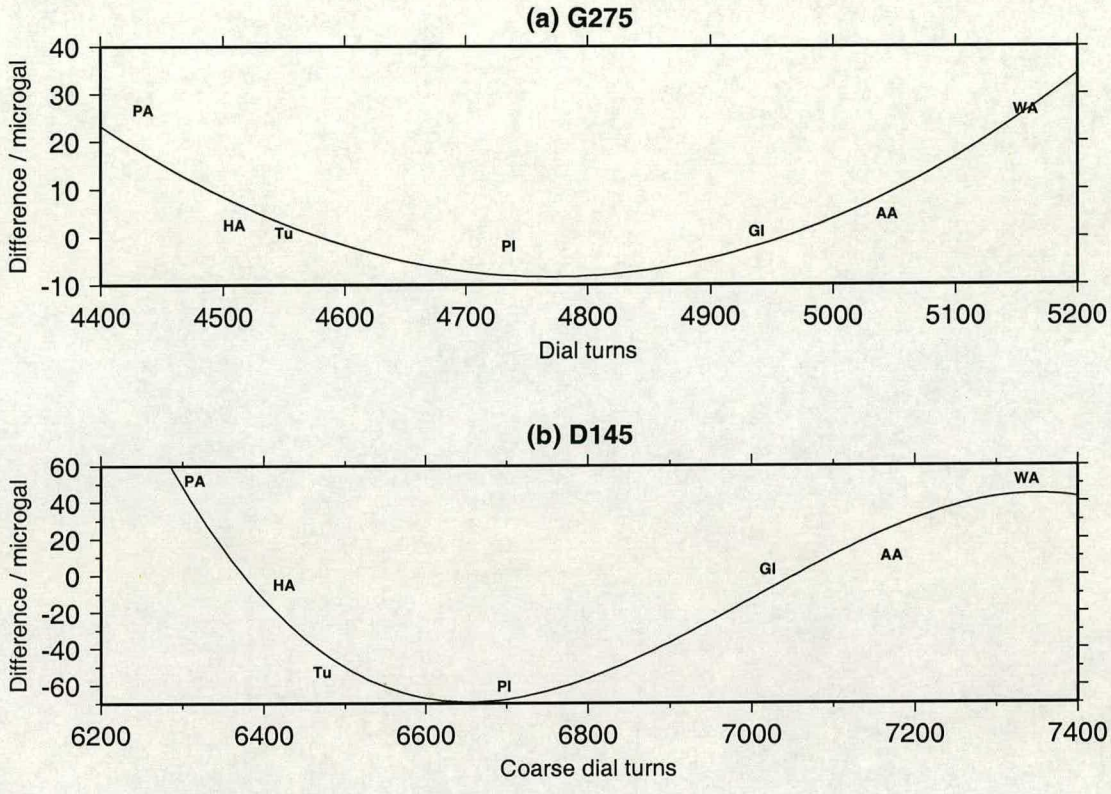

Figure 6.5. FG5 absolute gravity values minus individual instrument network adjustment values for (a) G275 against dial turns and (b) D145 against coarse dial turns. Polynomial fits of degree 2 and 3 respectively to these values are shown.

With these polynomials as corrections in the calibration function for each instrument, the data were re-processed. Details of the adjustment both with and without absolute constraints can be seen in Table 6.8.

Figure 6.6 shows the resulting difference between the relative network and absolute values when using non-linear scale factors. The differences lie within a range of $\pm$ 12 μgal.

It is possible to explain the pattern exhibited by comparing with Figure 6.5 which shows the polynomials used and the values they were fitted to. For example, the polynomials for both G275 and D145 are high compared to the actual discrepancy for Taunton (Tu) resulting in the relative value being high compared to the FG5 value in Figure 6.6. The opposite is the case at the Bidston site (Pl), explaining why the relative value is low compared to the FG5 value in Figure 6.6.

The discrepancy at Wick (WA) in Figure 6.6 cannot be explained by this reasoning. It is possible that this may be due to the relatively weak link to this site or potential errors in the vertical transfer (see Section 6.7.4).

	With FG5 constraint	Without FG5 constraint
χ^2	19.801	20.841
weighted rms	6.04	6.14
G275 rms	4.43	4.52
D145 rms	7.82	7.78
D154 rms	15.76	15.92
C_f G275	1.000 678 ± 0.000 011	1.000 678
C_f D145	1.000 987 ± 0.000 016	1.000 987
C_f D154	1.001 333 ± 0.000 031	1.001 333
mean std error of sites	3.04 ± 0.50	5.16 ± 1.52

Table 6.8. Results of network adjustment using non-linear scaling factors incorporated in to the calibration function with and without absolute constraint. Errors are in μgal.

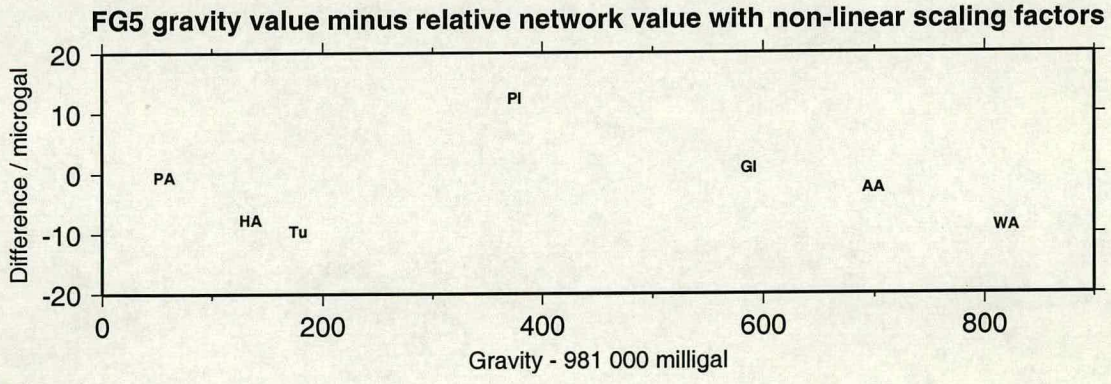

Figure 6.6. Difference between FG5 absolute values and relative network using non-linear scale factors.

Errors of the adjustment using non-linear scale factors are higher than those obtained with linear factors (see Tables 6.8 and 6.3). The change is generally of the order of 0.25 μgal higher. For example, the weighted rms of the adjustment without absolute constraint is 6.14 μgal with non-linear scale factors and 5.91 μgal with linear scale factors.

6.7.4 Errors in Absolute Gravity Constraints

Absolute values output by the FG5 gravimeter are for the top of the drop. This is about 130 cm above the floor. To enable comparison with the relative network, these need to be transferred to 12 cm above the floor - the height of the sensor in the LaCoste & Romberg instruments.

The vertical transfers have in most cases been measured only once and are used under the assumption that they do not change with time. In reality variations in the local mass distribution may occur causing changes in the vertical transfer. These could arise from mechanisms such as the movement of groundwater. The sites of Herstmonceux, Bidston and Wick may in particular be prone to this since they are situated underground.

Instrumental errors in FG5 absolute gravity observations are typically a fixed offset which will not affect a network adjustment. However, it has been noted that structure in the residuals is site dependent (see Section 4.7). Errors in the absolute gravity values caused by these residual structures would then be site dependent and affect a network adjustment. Results presented in Chapter 4 indicate that errors caused by patterns in the residuals of FG5-103 are not greater than 6 μgal.

6.8 Comparison of Network Adjustment Results

The results of Section 6.7.2 which assumes there to be errors in the south of the network, and Section 6.7.3 which fits non-linear scale factors to the instruments are compared here. Figure 6.7 plots the difference in gravity values for each site, represented as their codes.

The plot shows a general trend resembling a quadratic ranging over 90 μgal. This can be explained by the fact that one method uses linear scale factors whilst the other uses non-linear scale factors. Differences at sites in the south are skewed to a greater extent due to there being no absolute constraints used from this area for one of the methods.

The differences at the absolute sites fit in to the overall pattern apart from Wick. The potential error of sites, in particular Wick, was discussed in Section 6.7.4. An error here may have strengthened the use of a linear scale factor without constraint in the south and hence gave rise to the difference between the networks shown at this site.

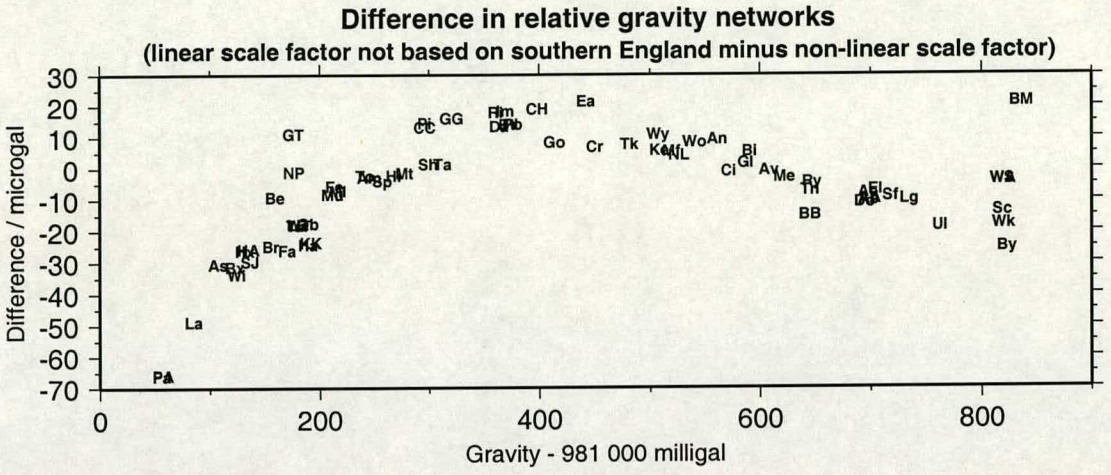

Figure 6.7. Difference between site gravity values between adjustments without absolute constraint for the two relative networks using linear scale factors calculated without southern absolute constraint and non-linear scale factors.

Bettyhill Museum (BM) is about 40 μgal away from that expected given the pattern exhibited. This site is poorly linked to the network with few observations which may account for this fact.

6.9 Discussion

Investigation in to the discrepancies between absolute and relative gravity values has illustrated that the problem may be due to periodic errors in the relative gravimeters. Both G275 and D145 exhibit the pattern of a periodicity which is in line with the long periods expected given the gear ratios of each instrument. The pattern was not evident with the adjustment of BPGN93 which used fewer absolute constraints over a smaller gravity range.

The evidence for periodic errors was also apparent when disregarding southern absolute gravity sites as constraints. The results shown in Figure 6.4 indicate a pattern that could be quadratic, in particular if the Wick absolute value is in error.

It is possible that the pattern of differences between absolute and relative values is the result of aliasing by sampling a shorter period. The fact that it is exhibited by both instruments separately suggests that this is unlikely.

If these patterns are indeed caused by periodicities, the data of Figure 6.5 indicate that their amplitudes are about 30 μgal peak to peak for G275 and 60 μgal peak to peak for D145 with periods of 603 dial turns and 900 coarse dial turns respectively.

The correction of D145 data with non-linear scale factors was done against the coarse dial. This was always used to balance the instrument. The fine dial was usually held at a fixed

value, however for approximately 20% of the observations this was about 400 fine dial turns higher compared to the rest of the data. This will offset the coarse dial by about 40 turns.

The lowest network adjustment errors are found when using all absolute constraints and linear scale factors as opposed to discarding absolute constraint in the south or using non-linear scale factors. A possible explanation for this is that individual instrument results disagree with each other, a consequence of which may be that the results of one instrument effectively pull the results of another away from its desired outcome, thus increasing errors.

It should also be noted that a periodicity of similar magnitude to that of D145 may be present in D154 data of which there were insufficient measurements to enable investigation. If this is present, correcting for periodicities in G275 and D145 whilst not in D154 would lead to a bias of the network adjustment by the latter instrument.

Whilst further work needs to be made to investigate the discrepancies between relative and absolute values, due to the changes and additions made to BPGN since the adjustment of 1993, results of site gravity values are given in this thesis. These are for the adjustment with linear scale factors and all absolute constraints. Figure 6.8 gives the gravity values for each BPGN site and they can also be found listed in Appendix D.

Further investigation in to the absolute - relative value discrepancies may be needed by re-measuring of the vertical transfer at the absolute sites. Particular attention should be paid to those located underground (*ie* Herstmonceux, Bidston and Wick). Connections to the extreme north of the network need strengthening, which includes the Wick absolute site. Relative gravimeter periodicities may be further tested by linking the BPGN to the absolute site at Lerwick. This would increase the gravity range by 100 milligal.

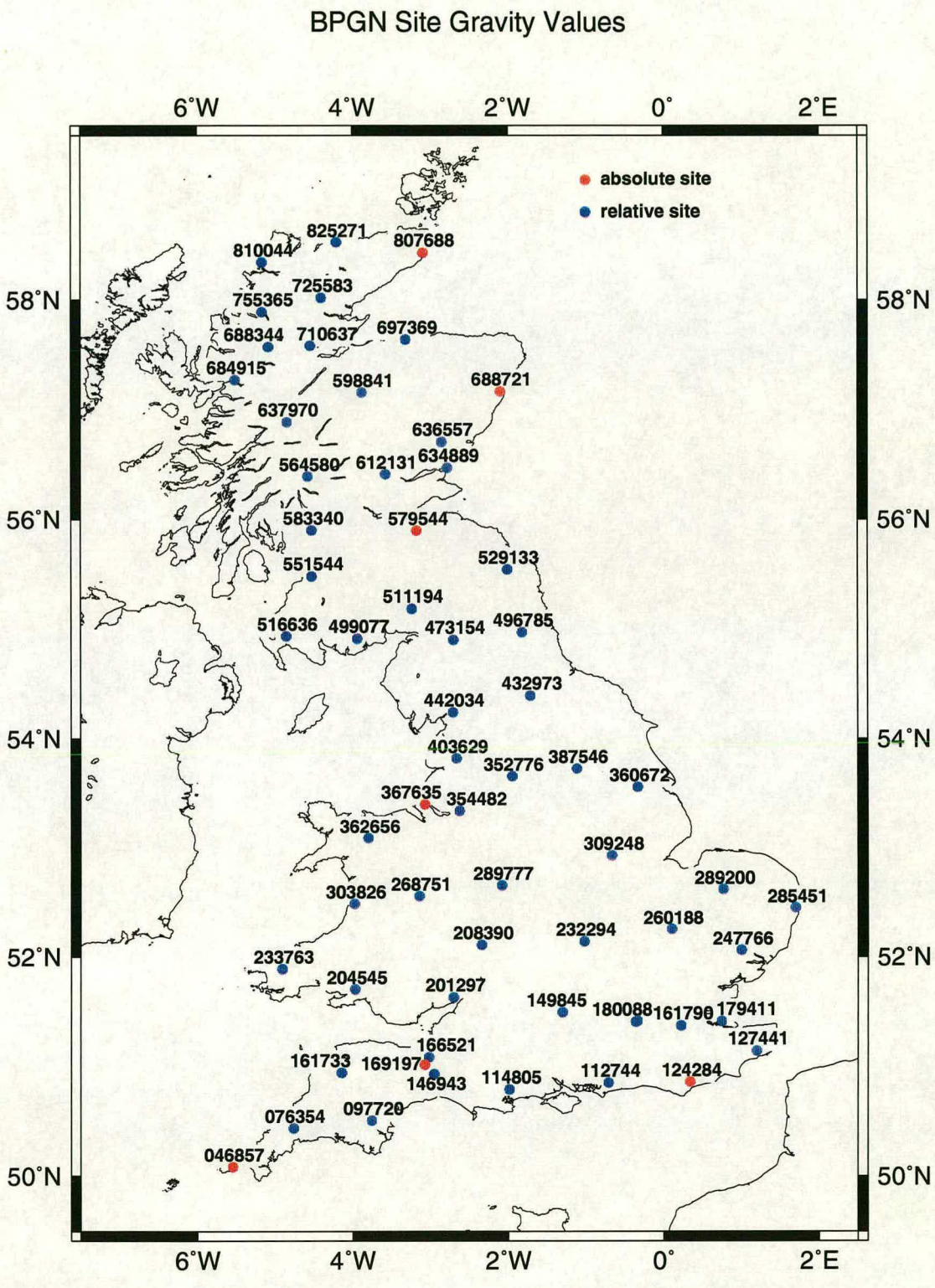

Figure 6.8. Map of BPGN site gravity values for the adjustment with all absolute constraints and linear scale factors. Values are g - 981 000 000 μgal.

Chapter 7

Conclusions

7.1 Ocean Loading

By manipulation of ocean tide models, a routine has been developed to improve the correction for ocean loading gravity effects. The routine subdivides model grid cells to provide a better fit to coastlines and improve the approximation to a point mass load. These are done to a level determined by their proximity to the site at which loading effects are being calculated for.

Applied to absolute data at the site of Newlyn which experiences large ocean loading and is located at high altitude within 1 km of the sea, this method reduces the set standard deviation of a 24 hour data set from 4.3 μgal to 1.8 μgal. No significant change was found for the site of Taunton. This is located 25 km inland where the benefits of using the routine are not expected to be large.

For Lerwick, located on a cluster of small islands, the routine has not shown any significant improvement. Here the method is limited by the ocean tide model. For a global model with $0.5^o \times 0.5^o$ resolution, this cannot take into account local oceanographic details. Calculation of loading effects in cases such as these needs further information about the local tidal characteristics. This could be through incorporation of a local tidal model with higher resolution.

The routine could be developed by changing from Cartesian to polar coordinates and using mass conservation on division of grid cells. Also the way data is handled around peninsulas could be improved by using only tidal data on the same side of the peninsula as the point of interpolation.

7.2 Air Pressure and Groundwater

Absolute gravity measurements made at Bidston from 1995 onwards with FG5-103 show a seasonal variation of 8 μgal. These readings are taken at irregular intervals resulting in a data set with large gaps where potential gravity variation is unknown. This makes correlation with environmental signals difficult. Continuous LaCoste & Romberg Earth-tide gravity data were used in the hope that this would provide more details of variations. Relationships between a 6 month record from 1984 and meteorological data have been examined.

7.2.1 Earth-Tide Gravity Data

Dividing the Earth-tide data into equally spaced intervals 30 days long, a frequency independent air pressure admittance was found to vary from 0.35 to 0.50 μgal mbar^{-1} at Bidston. Applying this variation to absolute results, the scatter of values was not reduced. It is possible that the variation of air pressure admittance observed is specific to the period of Earth-tide data observations.

The Earth-tide gravity record was found to have a strong correlation with humidity. This is an instrumental effect that has previously been observed (Bastien and Goodacre, 1990). It was removed using a frequency dependent admittance.

A frequency dependent admittance was found between Earth-tide gravity data and air pressure. In comparison, using a constant admittance had more success in removing short period features from the data, but some features were removed by the frequency dependent admittance and not the constant admittance.

Using the frequency dependent admittance method to correct Earth-tide data for rainfall removed some of the short period features. This was applied to absolute results with an increase in the scatter of the data.

Unfortunately the Earth-tide data were found to be affected by instrumental effects from drift and humidity to an extent that variations are hard to distinguish. Ideally gravity should be recorded continuously at Bidston with a superconducting gravimeter - an instrument with a very low drift rate.

7.2.2 Absolute Gravity Data

Investigation in to the seasonal variation of Bidston absolute values was made by examination of borehole water table level data. This showed a strong correlation with air pressure. After removing the air pressure signal from the borehole water table level, the remaining values indicate a possible correlation with absolute gravity values, having a lag of about 3 months.

Calculation of the theoretical gravitational attraction that Bidston rainfall would have if absorbed in to the ground in various configurations has shown that the quantity of rainfall at Bidston has the potential to cause the gravity variation observed by the absolute data. When represented as a running mean, the rainfall data show a correlation with gravity.

Further work should be done in to relationships between gravity and rainfall. Whilst this research investigated using rainfall running means, it did not incorporate a time lag. This may achieve a stronger relationship.

The potential relationship between absolute gravity and borehole water table level readings corrected for air pressure also needs further investigation. The main limitation with the borehole readings available was that they were sporadic. With equipment installed to monitor the water table level continuously, a stronger relationship may result.

The analysis of the correlation of absolute gravity measurements with environmental data at Bidston was made before an error in values produced by Proudman Oceanographic Laboratory (POL) was detected. The need to reprocess the absolute gravity data set is noted in the next section.

7.3 Absolute Gravimetry

Instrumental effects of the FG5 gravimeter on resulting gravity values have been investigated. In the case of laser lock shifts, comparator response and rubidium frequency clock drift, these are known and can be monitored and corrected for.

It has been shown that there is systematic structure within residuals when the equation of motion is fitted to time-distance data down the drop. This varies between instruments, sites and with time. However, the form of oscillations in the residuals is not a true representation of noise patterns in the original data. Structure is changed when fitting a quadratic.

It is possible to represent oscillations in the residuals with damped sinusoids. Low frequencies (below 15 Hz) have the greatest effect on gravity: they most closely resemble a parabola over the length of the drop.

While most oscillations are a mechanical effect triggered by the drop, a faulty electronic component produced a frequency of about 9.5 Hz in the residuals. The gravity change found when a sinusoid of this frequency is removed from both real and artificial data is under 1 μgal using Edinburgh software and that of Klopping *et al.* (1991) (Hosker, 1996). Yet empirical observation of the gravity change on replacement of the faulty component was 6.3 μgal.

Experiments with synthetic data showed that neither the frequency nor decay constant is recovered correctly from the residuals. Fitting damped sinusoids of various decay constants and

frequencies from 4 - 13 Hz to real data with a specific decay constant and frequency present identified gravity changes of up to 50 μgal. This shows that existing methods of attempting to correct for low frequency coherent residual noise do not work and errors up to 6 μgal can be missed.

Structure in the residuals can also be found in the catch phase at the end of the drop. If this part is used in the fit to the equation of motion, gravity may be perturbed as a result. Edinburgh processing software avoids this problem by using fringe number to select time-distance data down the drop. The commercial software REPLAY uses fringe index which, due to missed fringes, means the fit can extend unpredictably into the catch phase.

At a late stage in this research project, it was discovered that some of the absolute gravity results for Bidston produced by POL using REPLAY were affected by including part of the catch phase in the fit. It was shown for these data that the effect on gravity through this fitment into the catch phase ranges by at least 3 - 7 μgal. A further error was found through an incorrect input of a rubidium frequency calibration. Making corrections for these appeared to improve the correlation between rainfall and absolute gravity measurements at Bidston. It is recommended that the whole of the Bidston REPLAY data are reprocessed.

Results of FG5-103 from 7 sites in Britain have been presented. They show that the gravimeter is now producing reliable and consistent results compared to pre-1995 data. It has also been shown that FG5-103 produces values consistent with those of FG5-101 and FG5-202.

7.4 Relative Gravimetry

The British Precise Gravity Network has been developed with new observations in the south east and re-measuring and more links to the south west which have added 7 new relative sites. Also 4 new absolute sites have been linked to the network and new gravity values calculated for the existing 3 absolute sites.

The improved ocean loading correction has been applied to BPGN and compared with the previous correction used for BPGN93. The mean site standard error reduces from 3.32 $\pm$ 0.60 μgal to 2.96 $\pm$ 0.46 μgal with the new correction. Also the scale factor for G275 is significantly different using the new ocean loading correction, changing from 1.000 705 $\pm$ 0.000 012 to 1.000 656 $\pm$ 0.000 011. It now in agrees with an earlier result obtained for this instrument based on the IGSN71 (1.000 622 $\pm$ 0.000 027, Hipkin *et al.* (1988)).

Relative gravity values were found to be in disagreement with absolute values by up to 50 μgal. Reasons for the discrepancies were investigated by excluding absolute constraints in the south of the network and fitting non-linear scaling factors. Lower errors were achieved through the second method.

The pattern of differences suggests a periodic error in G275 of 603 dial turns, peak to peak amplitude 30 μgal and in D145 of 900 coarse dial turns, peak to peak amplitude 60 μgal. These long periodicities are expected given the gear ratios of the instruments.

The errors of the network adjustment using non-linear scale factors were 0.25 μgal higher than using linear scale factors. For this reason and since more work needs to be made in to the absolute - relative discrepancies, results have been given for the adjustment using all absolute constraints and linear scale factors.

The possibility of periodic errors should be investigated further by connecting the network to Lerwick on the Shetland Islands which would increase the gravity range by a further 100 milligal. Further work to investigate potential errors of the absolute values could be made by re-examination of the vertical transfers from the top of the FG5 drop to 12 cm above the floor. This in particular may be a problem for sites located underground, such as at Bidston, Herstmonceux and Wick. Also the link from Wick (and nearby Bettyhill) to the rest of the network is weak and needs strengthening due to the importance of this absolute site.

Appendix A

Ocean Tide Model Interpolation Routine

This appendix is intended to give more details on how the ocean tide model interpolation routine works. It is summarised by a flow diagram in Figure A.1. The input parameters and files required by the routine are summarised in Table A.1. The following sections describe in greater depth various aspects of the routine.

Input required	Details
Control file	Tide model file names and station coordinates
User input	Coast / station factor; number of recursions; bilinear / polynomial interpolation; model extension option
Tide model data files	Amplitude and phase data in netCDF format
List of regions file	List of coastline database files

Table A.1. Inputs required for the interpolation routine.

A.1 The Coastline Database

Wessel and Smith (1996) present a high resolution database that can be accessed on the Internet in Network Common Data Format (netCDF). It consists of an amalgamation of 2 publicly available databases. The World Data Bank II (WDB) (also known as CIA Data Bank) contains

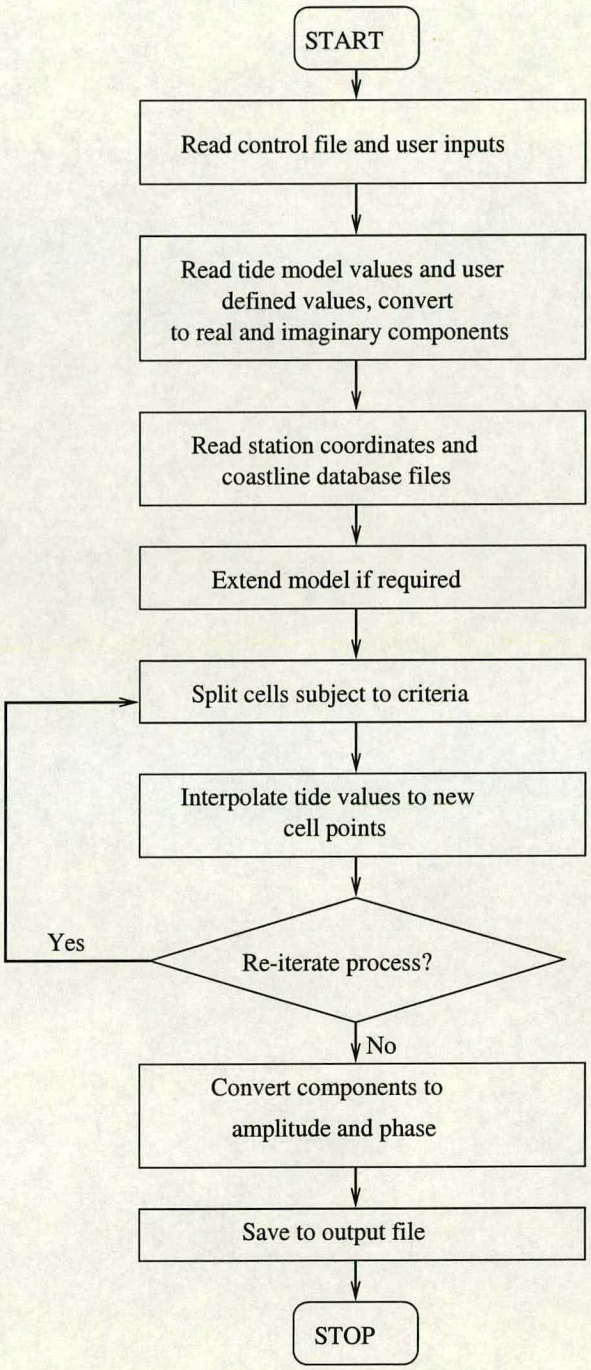

Figure A.1. A flow diagram outlining the processes performed by the interpolation routine.

coastlines, lakes, political boundaries and rivers. They report that it appears to have a precision of 500 - 5000 m. The World Vector Shoreline (WVS) contains only shorelines on the ocean/land interface. It has a precision one order of magnitude better than the WDB database. Since only coastline information is needed to improve the tide model grid fit, only the WVS derived part of this database will be accessed, so a precision of 50 - 500 m can be expected.

This coastline database can be used with Generic Mapping Tools (GMT) (*ibid.*). Offered in the public domain are a collection of algorithms which can be used to manipulate and plot data in both ASCII and netCDF format. For this research, Version 3.0 of GMT was used.

A.2 Arrangement of Coastline Database Files

The GMT coastline database uses about 44 MB of memory in fine resolution form. This is too much to be loaded in to computer memory for use in the interpolation routine. It is also not necessary; only local tides give the greatest source of error due to grid misfitting, so only the local coastline needs to be known to a high resolution. For this reason, a hierarchical arrangement of files was created.

The entire globe is covered by a set of files of sufficient resolution to improve the fit of an ocean model and improve ocean loading calculations for distant tides. For nearby local grid fitting, files containing coastline data of higher resolution but smaller area are created for subregions of the areas covered by the global files. Further data files of even higher resolution can be nested within the subregions. Thus, a hierarchical structure is created whereby files of increasing resolution can be nested within each other to the desired degree of accuracy required, and centred on the site for which ocean loading calculations are to be performed. Figure A.2 illustrates this arrangement.

When the interpolation routine determines whether a point on the globe is at sea or not, it selects the data file which contains this point and has no subregions within the area it covers which also contain the point. The point closest to the one under examination in the data file is then selected.

The data files are created using the GMT routine *grdlandmask*. An example of how such a datafile would be created for the south coast of Britain is:

grdlandmask -Gscoast.grd -R357/360/50.5/51 -I0.0025 -Df -F -V -N0/1/1/1/1

Here, the file created, *scoast.grd*, covers the area from 3^oW to 0^oW and 50.5^oN to 51^oN. It contains a datapoint for every 0.0025^o in latitude and longitude. The '$-N$' option means the value at each point will be a '0' if the point is at sea, a '1' otherwise. Thus for example inland lakes where no tides occur will be regarded as dry by the interpolation routine.

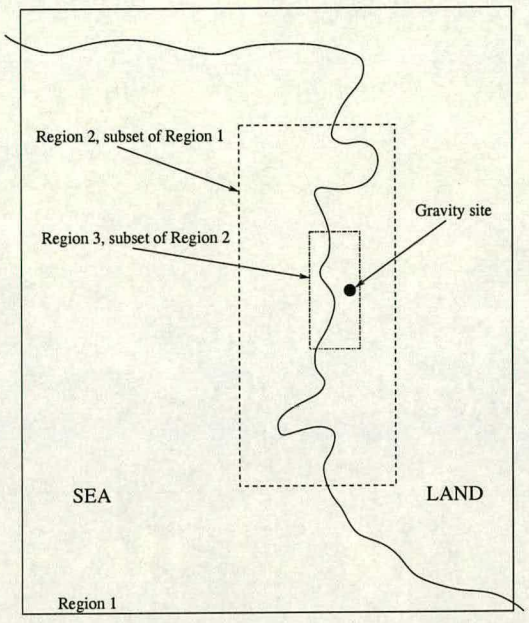

Figure A.2. Illustration of the hierarchy arrangement of coastline datafiles.

The file created is in netCDF format. Standard subroutines for reading these files were incorporated in the interpolation program. Each file was limited by the program array size to containing no more than 300,000 data points.

It should be noted that some bugs were found when using GMT *grdlandmask*. If a file is created containing the Greenwich meridian, then the information contained within can be wrong. This can be seen for example when creating a file covering the area 4^oW to 9^oE and 50^oN to 61^oN with a spacing of 1^o.

The problem was reported to the creators of GMT, with no response as to whether it has been fixed. It was overcome by ensuring that none of the data files straddled the Greenwich meridian.

A second problem encountered was that occasionally a data file created with *grdlandmask* would contain details of a coastline which bore virtually no resemblance to reality. For example this was found in the areas of 5^oW to 3.8^oW, 52^oN to 53^oN and 4.5^oW to 2.2^oW, 51^oN to 52^oN with a resolution of 0.0025^o. In both cases the problem was solved by changing the eastern longitude limit of the region by 0.1^o. No pattern can be seen as to why this occurs, and for this reason it is recommended that results are plotted when using newly created coastline data files with *grdlandmask* to check the grid produced fits the coastline.

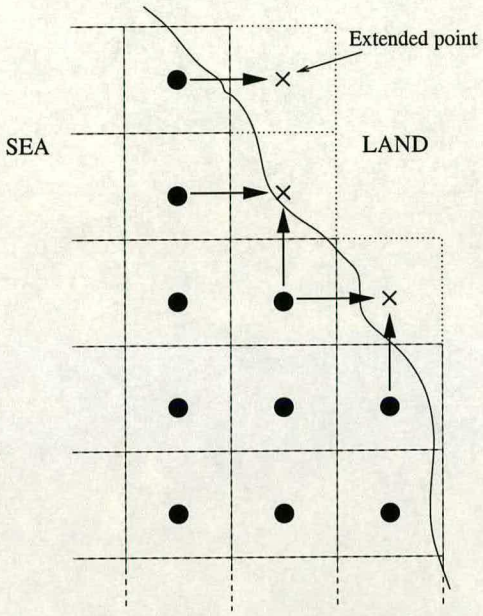

Figure A.3. Illustration of how grid cells are extended at the coast on to land to cover exposed sea areas.

A.3 Extension Of The Model At The Coast

The interpolation routine creates a grid of variable size by subdividing existing cells. Hence areas of sea left uncovered by the tide model will never be covered. The program has the option to extend the model at the coast by one grid cell on to land. Figure A.3 shows the method of extension, grid cells are added to adjacent existing cells at the coast, provided the new cells are not located entirely within land. The tidal values in the extended model are an average of all the surrounding tidal values.

A.4 Subdivision Of Grid Cells

To create a grid of finer size, existing grid cells need to be subdivided in to a set of smaller cells. Under subdivision, the interpolation routine creates 4 new cells as shown in Figure A.4. The tide amplitude and phase values are given for the centre of all grid cells.

A.5 Determination Of Whether A Cell Is 'Dry' Or 'Wet'

To determine whether a grid cell is at sea, on the coast or entirely on land, the interpolation routine selects 36 points in the cell as shown in Figure A.5. Each of these is tested to see

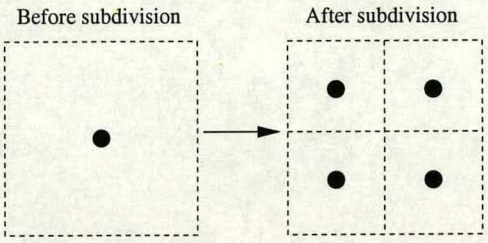

Figure A.4. Illustration of how cells are subdivided into 4 smaller cells.

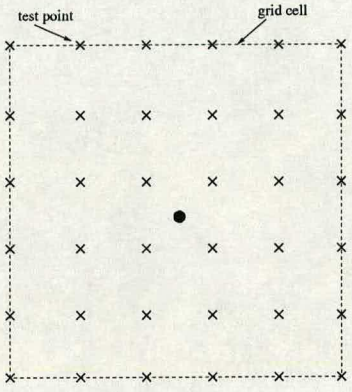

Figure A.5. The points chosen in a grid cell to be used to determine whether the cell is at sea, on the coast or inland.

whether it is at sea or not. If all of the 36 points are at sea, the cell will not need subdividing. If some but not all are at sea, the cell is on the coast and is subject to subdivision. If none of the points are at sea, the cell is entirely on land and is discarded.

It was decided to set the number of points examined in a cell to 36 after experimentation showed it to be the optimum value to get the desired accuracy and save on computing time. Table A.2 shows the results of M_2 computation at Newlyn and that there is insignificant change in the results beyond using 36 points.

A.6 Coast Factor and Station Factor

The Coast and Station Factors are user adjustable parameters and determine the criteria for cell subdivision. In Chapter 2 this was described as being dependent on the ratio of the radius of the grid cell in question, as a circular disc of equal area, to its distance from the station. Here it is described in a different way.

The Coast Factor limits the extent to which the ocean tide model is subdivided to improve the

Number of points tested in grid cell	Amplitude (μgal)	Phaselag
4	16.09	-59.2^o
16	16.35	-59.0^o
36	16.41	-58.9^o
64	16.42	-58.9^o
100	16.44	-58.9^o

Table A.2. The effect of changing the number of points tested in a grid cell for Newlyn, M_2, tide model AG95.1.

fit to the coastline, since the errors for misfitting are only significant for nearby tides. Suppose the coast factor is C, the distance from the site to the centre of the grid cell under consideration is d, and the radius of the disc with area equal to the area of the grid cell under consideration is r, then the criteria for whether the grid cell is to be subdivided is:

IF(cell is on coast .AND. $r > Cd$) THEN subdivide cell

This ensures that cells beyond a certain distance from the site are not subdivided, and that grid cells within that distance are not subdivided beyond a certain point through each iterative passage of the routine.

Now suppose the Station Factor is S, d and r are defined as before, then the criteria for cell subdivision is:

IF($r > Sd$) THEN subdivide cell

This ensures that a grid of decreasing size with decreasing distance to the site is created.

A.7 Method of Interpolation

When a cell is subdivided, tide amplitude and phase need to be known at the centre of the 4 new cells. The surrounding values of the tide model are used to interpolate to the new positions.

The program has the option of bilinear and polynomial interpolation.

A.7.1 Bilinear Interpolation

Suppose (x_1,y_1),(x_2,y_1),(x_2,y_2) and (x_1,y_2) are the coordinates of the 4 points surrounding (x, y), the point to be interpolated to. If the data values at these 4 points are z_1, z_2, z_3 and z_4 respectively, then the formula for 2D bilinear interpolation is:

$$z(x,y) = (1-T)(1-Q)z_1 + T(1-Q)z_2 + TQz_3 + (1-T)Qz_4 \qquad \text{(A.1)}$$

where

$$T = \frac{x - x_1}{x_2 - x_1} \tag{A.2}$$

$$Q = \frac{y - y_1}{y_2 - y_1} \tag{A.3}$$

If some of the 4 points are missing, such as at coastlines, then the formula is adjusted to make the best use of the points that are available. For example, if (x_1,y_1) is missing, the formula used is:

$$z(x, y) = (1 - Q)z_2 + (1 - T)z_3 + (Q + T - 1)z_4 \tag{A.4}$$

A.7.2 2-D Polynomial Interpolation

The algorithm for 2-D polynomial interpolation involves taking a grid of points that contain the desired coordinates to be interpolated to. If $M - 1$ order interpolation is to be done in the x direction, and $N - 1$ order in the y direction, a sub-block of $M \times N$ points is selected. M 1-D interpolations are performed in the y direction and these results are used for interpolation in the x direction to get the result.

The subroutines for this method were taken from Numerical Recipes (Press *et al.*, 1992) and changed to use sub-blocks only of size 4×4, *ie* degree 3 polynomial interpolation. However, in the case of missing data the interpolation is simply to the highest degree possible. The method used for the 1D interpolation is *Neville's* algorithm.

Appendix B

Ocean Loading Components

Tables B.1, B.2, B.3, B.4, B.5, B.6, B.7 and B.8 contain details of the ocean loading components for all BPGN sites, given as amplitude and phase values. They were calculated using the method as described in Chapter 2 with the ocean tide model AG95.1.

Site name	M_2	S_2	K_1	O_1	N_2	P_1
Aberdeen Absolute	2.12	0.85	0.79	0.71	0.46	0.26
	-103.5	-64.2	-24.7	-142.9	-129.1	-37.8
Achnasheen FBM	3.58	1.41	0.89	0.65	0.66	0.29
	-25.3	11.9	-41.1	-160.1	-36.9	-51.0
Alvie	2.31	0.90	0.78	0.61	0.42	0.26
	-45.3	-6.5	-36.7	-153.6	-61.6	-47.3
Ambleston	7.47	2.31	0.72	0.51	1.31	0.24
	-43.6	-1.8	-58.2	-173.2	-66.7	-66.2
Annbank	2.14	0.94	0.77	0.59	0.38	0.25
	-58.0	-14.7	-34.5	-155.1	-62.5	-44.0
Ashburton	8.10	2.56	0.71	0.49	1.50	0.23
	-48.1	-4.0	-67.2	179.9	-67.5	-74.6
Barry Buddon VLBI	3.68	1.41	0.77	0.70	0.74	0.26
	-97.4	-53.4	-23.4	-141.0	-115.8	-36.5
Beedon	3.23	1.00	0.50	0.33	0.65	0.17
	-51.0	-10.9	-58.1	-162.4	-75.5	-64.4
Bettyhill FBM	2.80	1.11	1.00	0.76	0.54	0.33
	4.5	38.8	-38.5	-159.8	-8.7	-49.1
Bettyhill Museum	3.24	1.26	1.08	0.81	0.63	0.35
	14.8	48.2	-38.3	-161.4	1.0	-48.9
Betws	2.46	0.87	0.63	0.48	0.57	0.21
	-45.8	-7.1	-43.8	-159.8	-80.6	-52.3
Bidston POL1 Abs	0.58	0.29	0.61	0.51	0.44	0.20
	-111.2	-54.9	-35.0	-152.7	-110.5	-44.1
Bishopton	2.83	1.12	0.75	0.57	0.51	0.25
	-51.1	-10.8	-37.6	-155.4	-62.5	-47.1
Boxgrove	1.79	0.53	0.57	0.36	0.41	0.19
	-51.4	-15.3	-59.5	-163.9	-75.6	-65.3
Broadway	6.02	1.88	0.64	0.43	1.08	0.21
	-44.1	-0.1	-63.0	-174.0	-67.3	-70.1
Carlton Colville	1.96	0.56	0.16	0.18	0.38	0.06
	-56.5	-14.3	-75.8	-85.0	-75.2	-62.0
Chapel Haddlesey	3.19	1.05	0.41	0.37	0.67	0.15
	-57.1	-14.7	-34.6	-136.7	-79.9	-44.1
Crianlarich FBM	3.12	1.20	0.77	0.58	0.55	0.25
	-43.7	-6.5	-38.7	-156.0	-58.6	-48.3
Crooklands	2.00	0.69	0.57	0.48	0.53	0.19
	-79.6	-31.9	-33.4	-147.8	-96.1	-43.2
Daresbury	2.30	0.80	0.53	0.42	0.57	0.18
	-59.5	-18.8	-41.4	-152.8	-86.1	-50.0

Table B.1. Ocean loading for BPGN sites, components M_2, S_2, K_1, O_1, N_2 and P_1. Upper value is amplitude (μgal), lower value is Greenwich phase lag (^{o}).

Site name	K_2	Q_1	L_2	μ_2	ν_2	$2N_2$
Aberdeen Absolute	0.26	0.22	0.06	0.08	0.09	0.07
	-71.0	154.8	-85.8	-148.8	-128.3	-158.9
Achnasheen FBM	0.38	0.23	0.09	0.10	0.13	0.06
	9.0	141.2	-8.6	-59.2	-39.7	-64.3
Alvie	0.25	0.20	0.06	0.06	0.08	0.04
	-12.7	146.3	-27.8	-88.3	-62.7	-103.0
Ambleston	0.59	0.19	0.19	0.22	0.25	0.16
	-9.8	133.2	-26.7	-104.0	-67.4	-109.5
Annbank	0.28	0.21	0.06	0.05	0.07	0.04
	-21.7	151.0	-41.1	-71.5	-66.4	-100.8
Ashburton	0.68	0.18	0.20	0.23	0.28	0.18
	-10.2	127.4	-30.7	-96.0	-68.1	-97.3
Barry Buddon VLBI	0.41	0.22	0.10	0.12	0.14	0.11
	-58.7	156.5	-76.7	-135.6	-116.0	-142.8
Beedon	0.27	0.12	0.08	0.12	0.12	0.09
	-21.3	142.3	-34.4	-99.1	-73.8	-106.5
Bettyhill FBM	0.30	0.26	0.07	0.08	0.10	0.05
	37.4	141.7	21.9	-30.5	-10.4	-19.4
Bettyhill Museum	0.35	0.28	0.09	0.10	0.12	0.06
	47.6	141.0	32.2	-20.4	-0.7	-7.6
Betws	0.25	0.18	0.07	0.13	0.10	0.11
	-20.1	147.0	-22.6	-108.2	-79.9	-122.7
Bidston POL1 Abs	0.17	0.18	0.02	0.12	0.08	0.11
	-52.7	155.2	-54.2	-110.2	-114.4	-129.8
Bishopton	0.32	0.20	0.08	0.07	0.10	0.05
	-16.8	147.9	-34.2	-84.2	-64.9	-99.0
Boxgrove	0.15	0.13	0.04	0.08	0.07	0.06
	-29.6	144.5	-34.5	-94.6	-73.9	-114.7
Broadway	0.48	0.16	0.14	0.18	0.20	0.13
	-9.7	132.7	-28.5	-95.3	-67.0	-98.9
Carlton Colville	0.16	0.07	0.05	0.06	0.07	0.05
	-26.3	-157.6	-40.0	-93.2	-71.5	-97.3
Chapel Haddlesey	0.31	0.13	0.08	0.12	0.12	0.10
	-22.4	161.7	-36.8	-101.5	-78.0	-105.9
Crianlarich FBM	0.33	0.20	0.08	0.08	0.10	0.06
	-12.0	146.1	-29.3	-82.8	-60.8	-94.8
Crooklands	0.25	0.17	0.05	0.11	0.10	0.10
	-39.5	156.4	-53.4	-106.5	-97.4	-120.5
Daresbury	0.25	0.15	0.06	0.12	0.10	0.10
	-29.4	151.4	-37.2	-105.8	-85.8	-117.3

Table B.2. Ocean loading for BPGN sites, components K_2, Q_1, L_2, μ_2, ν_2 and $2N_2$. Upper value is amplitude (μgal), lower value is Greenwich phase lag (^{o}).

Site name	M_2	S_2	K_1	O_1	N_2	P_1
Dornie	4.76	1.88	0.94	0.68	0.84	0.31
	-24.5	13.3	-41.4	-162.5	-33.3	-50.7
Easby	3.06	1.06	0.49	0.44	0.66	0.17
	-65.3	-22.3	-30.7	-138.8	-86.6	-41.3
Edinburgh GI Abs	2.99	1.14	0.68	0.57	0.60	0.23
	-75.7	-33.0	-30.7	-145.8	-93.6	-42.0
Elgin South	1.01	0.41	0.85	0.69	0.17	0.28
	-51.7	-16.0	-33.6	-152.1	-75.8	-45.1
Farningham	1.90	0.64	0.42	0.25	0.43	0.14
	-72.2	-36.3	-60.4	-153.1	-92.0	-64.4
Felindre	7.15	2.24	0.67	0.47	1.15	0.22
	-40.8	2.2	-58.8	-172.8	-65.4	-66.2
Goosnargh	1.85	0.65	0.55	0.46	0.53	0.19
	-75.4	-29.3	-35.7	-149.5	-95.0	-45.0
Great Gonerby	2.98	0.93	0.36	0.30	0.61	0.13
	-50.0	-9.8	-44.6	-138.3	-74.7	-51.5
Gt Torrington	8.44	2.64	0.70	0.49	1.48	0.23
	-46.7	-3.6	-64.9	-178.7	-67.6	-72.5
Hampton Church	2.34	0.74	0.45	0.28	0.50	0.15
	-59.1	-21.9	-58.7	-157.6	-82.2	-64.0
Herstmonceux	1.02	0.46	0.50	0.30	0.25	0.17
	-127.0	-88.4	-59.6	-156.6	-124.2	-64.0
Herstmonceux Abs	1.02	0.46	0.50	0.30	0.25	0.17
	-125.4	-87.3	-59.7	-156.7	-123.2	-64.0
Histon	2.52	0.79	0.35	0.24	0.52	0.12
	-56.2	-17.2	-54.2	-141.3	-79.4	-58.6
Immingham	3.60	1.15	0.33	0.35	0.73	0.13
	-48.5	-4.7	-29.3	-123.9	-71.7	-39.3
Kelton	1.55	0.68	0.69	0.55	0.41	0.23
	-82.4	-31.1	-33.7	-152.3	-94.9	-43.4
Teddington KK Bld1	2.33	0.74	0.45	0.28	0.50	0.15
	-59.5	-22.3	-58.7	-157.3	-82.4	-63.9
Lairg	2.54	1.00	0.91	0.69	0.47	0.30
	-16.4	19.2	-38.8	-158.0	-29.6	-49.3
Lanivet	10.19	3.23	0.77	0.53	1.90	0.25
	-53.6	-11.7	-69.9	175.5	-72.0	-77.6
Lerwick	3.62	1.28	1.26	1.03	0.74	0.41
	94.4	131.4	-33.3	-153.3	81.6	-45.9
Malvern	3.82	1.20	0.52	0.37	0.74	0.17
	-49.2	-8.5	-54.3	-162.2	-75.2	-61.5

Table B.3. Ocean loading for BPGN sites, components M_2, S_2, K_1, O_1, N_2 and P_1. Upper value is amplitude (μgal), lower value is Greenwich phase lag (^{o}).

Site name	K_2	Q_1	L_2	μ_2	ν_2	$2N_2$
Dornie	0.51	0.24	0.13	0.11	0.16	0.07
	11.3	140.9	-8.5	-54.4	-36.9	-63.1
Easby	0.32	0.15	0.08	0.12	0.12	0.10
	-29.6	160.2	-44.2	-106.3	-85.6	-112.7
Edinburgh GI Abs	0.33	0.19	0.08	0.10	0.11	0.08
	-39.2	153.5	-55.5	-114.8	-94.1	-124.5
Elgin South	0.11	0.22	0.03	0.03	0.03	0.02
	-27.3	147.0	-34.5	-112.9	-75.1	-155.6
Farningham	0.19	0.10	0.05	0.08	0.08	0.07
	-46.9	151.4	-56.0	-105.7	-90.0	-119.7
Felindre	0.51	0.17	0.16	0.19	0.22	0.14
	-8.3	134.1	-25.1	-100.5	-65.3	-105.1
Goosnargh	0.24	0.16	0.05	0.12	0.09	0.10
	-38.1	155.3	-48.4	-106.5	-96.0	-120.6
Great Gonerby	0.26	0.11	0.07	0.11	0.11	0.09
	-18.3	160.2	-30.9	-98.6	-72.0	-101.5
Gt Torrington	0.67	0.18	0.20	0.23	0.28	0.18
	-11.3	128.1	-30.3	-99.5	-68.2	-102.0
Hampton Church	0.21	0.11	0.06	0.09	0.09	0.07
	-32.6	147.1	-42.3	-101.3	-80.0	-112.1
Herstmonceux	0.15	0.11	0.03	0.05	0.05	0.06
	-95.4	151.8	-116.8	-114.5	-125.8	-144.1
Herstmonceux Abs	0.15	0.11	0.02	0.05	0.05	0.06
	-94.5	151.8	-115.2	-114.2	-124.7	-143.5
Histon	0.22	0.09	0.06	0.10	0.10	0.07
	-26.6	158.5	-38.3	-100.1	-76.6	-105.8
Immingham	0.33	0.12	0.09	0.13	0.13	0.10
	-12.0	171.5	-28.4	-94.5	-68.9	-95.4
Kelton	0.23	0.20	0.04	0.09	0.07	0.08
	-38.9	153.3	-54.2	-103.3	-97.9	-123.6
Teddington KK Bld1	0.21	0.11	0.06	0.09	0.09	0.07
	-33.0	147.3	-42.6	-101.5	-80.3	-112.3
Lairg	0.27	0.23	0.07	0.07	0.09	0.04
	16.3	142.4	0.2	-52.9	-31.5	-53.3
Lanivet	0.86	0.19	0.25	0.30	0.36	0.23
	-16.9	123.2	-36.1	-102.4	-73.4	-103.4
Lerwick	0.36	0.31	0.09	0.11	0.14	0.11
	132.5	142.6	111.0	70.7	82.2	76.9
Malvern	0.32	0.13	0.09	0.13	0.14	0.10
	-19.6	141.8	-32.7	-101.9	-74.1	-107.9

Table B.4. Ocean loading for BPGN sites, components K_2, Q_1, L_2, μ_2, ν_2 and $2N_2$. Upper value is amplitude (μgal), lower value is Greenwich phase lag (^{o}).

Site name	M_2	S_2	K_1	O_1	N_2	P_1
Methven	2.63	1.01	0.71	0.57	0.50	0.24
	-62.1	-21.3	-34.6	-150.1	-79.6	-45.3
Moffat TH	2.40	0.92	0.63	0.51	0.52	0.21
	-69.4	-26.0	-33.9	-148.6	-87.7	-44.1
Montgomery	3.67	1.18	0.56	0.41	0.73	0.19
	-48.6	-8.5	-50.5	-161.8	-75.7	-58.4
Mounton	3.95	1.23	0.53	0.36	0.76	0.17
	-48.4	-7.3	-57.7	-165.0	-74.0	-64.6
New Luce	1.39	0.73	0.78	0.60	0.31	0.26
	-62.6	-16.5	-34.7	-156.5	-73.5	-43.9
Newlyn Absolute	16.37	5.25	0.99	0.72	3.07	0.32
	-58.9	-17.5	-75.3	168.0	-75.1	-83.3
North Petherton	6.12	1.90	0.63	0.43	1.05	0.20
	-41.6	2.3	-61.8	-173.2	-68.4	-69.0
North Pickenham	2.54	0.76	0.25	0.23	0.51	0.10
	-47.5	-6.7	-51.2	-120.1	-71.2	-53.2
Queenborough	2.07	0.79	0.37	0.16	0.43	0.12
	-107.3	-61.5	-69.0	-138.5	-118.2	-69.3
Rishworth	2.68	0.91	0.48	0.40	0.60	0.17
	-60.1	-18.4	-38.7	-146.1	-83.7	-47.6
Roybridge	3.33	1.29	0.81	0.60	0.60	0.27
	-37.8	0.7	-40.1	-157.9	-50.0	-49.7
Scourie	4.68	1.86	1.07	0.77	0.92	0.35
	-5.0	29.9	-42.2	-164.2	-16.4	-52.0
Shareshill	3.22	1.03	0.49	0.36	0.66	0.17
	-52.6	-12.5	-49.4	-155.7	-78.0	-56.9
Sproughton	2.07	0.68	0.29	0.18	0.43	0.10
	-71.1	-31.8	-63.2	-127.0	-90.3	-62.9
St John Commandery	2.30	0.87	0.40	0.17	0.41	0.13
	-143.6	-93.2	-67.2	-139.1	-150.5	-67.4
Strathpeffer	2.74	1.07	0.86	0.65	0.50	0.28
	-28.3	8.8	-39.3	-157.5	-41.5	-49.5
Talkin	2.53	0.94	0.58	0.49	0.56	0.20
	-71.1	-27.4	-32.4	-145.5	-90.4	-42.8
Talybont	4.39	1.40	0.66	0.49	0.80	0.22
	-36.3	4.2	-49.8	-165.4	-67.0	-57.9
Tannadice	2.47	0.95	0.72	0.61	0.48	0.24
	-77.8	-36.0	-30.0	-145.8	-97.7	-41.7
Taunton Absolute	6.15	1.92	0.63	0.43	1.08	0.21
	-43.6	0.1	-62.5	-173.9	-68.2	-69.7

Table B.5. Ocean loading for BPGN sites, components M_2, S_2, K_1, O_1, N_2 and P_1. Upper value is amplitude (μgal), lower value is Greenwich phase lag (^{o}).

Site name	K_2	Q_1	L_2	μ_2	ν_2	$2N_2$
Methven	0.29	0.19	0.07	0.08	0.09	0.06
	-27.8	149.7	-43.2	-104.1	-80.4	-116.1
Moffat TH	0.28	0.18	0.06	0.10	0.10	0.08
	-33.3	153.2	-47.7	-106.3	-88.6	-118.5
Montgomery	0.32	0.15	0.09	0.14	0.13	0.11
	-18.9	142.9	-30.1	-104.4	-74.9	-112.5
Mounton	0.32	0.13	0.09	0.13	0.14	0.10
	-18.6	139.6	-32.8	-100.0	-72.8	-105.7
New Luce	0.23	0.22	0.04	0.06	0.06	0.06
	-25.9	151.4	-39.2	-84.7	-77.4	-119.6
Newlyn Absolute	1.41	0.26	0.41	0.47	0.58	0.36
	-21.2	119.8	-41.1	-105.3	-77.4	-105.5
North Petherton	0.46	0.15	0.14	0.17	0.20	0.13
	-11.2	133.6	-28.8	-96.9	-68.0	-100.6
North Pickenham	0.21	0.08	0.06	0.09	0.09	0.07
	-16.1	175.0	-29.0	-93.7	-67.5	-95.3
Queenborough	0.24	0.07	0.05	0.07	0.08	0.07
	-69.1	161.8	-91.0	-120.2	-117.0	-138.9
Rishworth	0.27	0.14	0.07	0.12	0.11	0.09
	-27.2	155.3	-38.9	-104.1	-82.7	-112.3
Roybridge	0.35	0.21	0.09	0.08	0.11	0.06
	-3.7	143.8	-21.3	-74.4	-52.5	-84.5
Scourie	0.51	0.28	0.12	0.14	0.17	0.10
	29.9	138.2	12.6	-35.8	-19.4	-31.4
Shareshill	0.29	0.13	0.08	0.12	0.12	0.10
	-22.4	147.0	-34.3	-102.8	-76.7	-109.6
Sproughton	0.20	0.07	0.05	0.08	0.08	0.06
	-41.6	170.1	-54.1	-105.0	-87.4	-114.3
St John Commandery	0.27	0.08	0.06	0.05	0.08	0.07
	-97.5	166.2	-127.8	-142.0	-149.4	-159.4
Strathpeffer	0.29	0.22	0.07	0.07	0.10	0.04
	4.9	143.0	-11.6	-65.7	-43.6	-73.4
Talkin	0.29	0.17	0.06	0.11	0.10	0.09
	-34.7	155.6	-49.0	-108.2	-90.7	-118.6
Talybont	0.36	0.18	0.11	0.16	0.15	0.12
	-5.9	141.6	-17.2	-105.1	-65.8	-116.5
Tannadice	0.27	0.20	0.07	0.08	0.09	0.07
	-42.8	152.6	-57.7	-121.0	-97.6	-132.2
Taunton Absolute	0.48	0.16	0.14	0.18	0.20	0.13
	-11.0	132.8	-29.1	-96.7	-67.9	-100.2

Table B.6. Ocean loading for BPGN sites, components K_2, Q_1, L_2, μ_2, ν_2 and $2N_2$. Upper value is amplitude (μgal), lower value is Greenwich phase lag (^{o}).

Site name	M_2	S_2	K_1	O_1	N_2	P_1
Towcester	3.00	0.94	0.43	0.30	0.61	0.15
	-53.5	-13.9	-53.8	-154.0	-77.9	-60.0
Ullapool Mus	4.74	1.91	1.02	0.73	0.91	0.33
	-12.0	24.0	-41.9	-163.8	-21.7	-51.7
Wick Absolute	1.02	0.30	1.03	0.85	0.20	0.33
	71.4	106.6	-32.6	-154.6	70.0	-44.6
Wick church of S	0.79	0.25	0.98	0.80	0.14	0.32
	54.2	84.1	-33.3	-154.2	53.7	-45.2
Wimborne	4.42	1.37	0.62	0.41	0.84	0.20
	-42.0	3.0	-62.1	-170.8	-64.0	-68.8
Wooler	3.50	1.27	0.60	0.56	0.72	0.21
	-80.1	-36.8	-23.8	-137.3	-99.5	-36.4
Wylam	3.36	1.19	0.53	0.50	0.70	0.19
	-71.9	-28.5	-26.1	-136.9	-92.0	-37.9

Table B.7. Ocean loading for BPGN sites, components M_2, S_2, K_1, O_1, N_2 and P_1. Upper value is amplitude (μgal), lower value is Greenwich phase lag (^{o}).

Site name	K_2	Q_1	L_2	μ_2	ν_2	$2N_2$
Towcester	0.26	0.11	0.07	0.11	0.11	0.09
	-23.7	148.2	-36.0	-101.0	-75.9	-107.0
Ullapool Mus	0.51	0.27	0.12	0.14	0.17	0.09
	24.0	138.7	5.2	-39.9	-24.9	-39.4
Wick Absolute	0.08	0.27	0.02	0.03	0.04	0.04
	115.7	145.2	87.5	64.3	68.1	92.7
Wick church of S	0.06	0.25	0.02	0.02	0.03	0.03
	93.3	145.3	66.9	47.3	51.8	94.6
Wimborne	0.36	0.15	0.11	0.14	0.16	0.10
	-5.1	136.7	-24.5	-89.3	-63.0	-96.7
Wooler	0.38	0.18	0.09	0.13	0.13	0.10
	-42.8	160.4	-59.4	-119.0	-98.9	-124.8
Wylam	0.35	0.17	0.09	0.13	0.13	0.10
	-35.0	161.2	-51.0	-111.4	-91.1	-117.2

Table B.8. Ocean loading for BPGN sites, components K_2, Q_1, L_2, μ_2, ν_2 and $2N_2$. Upper value is amplitude (μgal), lower value is Greenwich phase lag (^{o}).

Appendix C

FG5-103 Results

This appendix contains details of data sets and results of FG5-103 used in this research. Those for Bidston using REPLAY were provided by Proudman Oceanographic Laboratory and include the errors as described in Section 5.6. The results are presented in the following tables:

Table	Site	Processing software
C.1	Aberdeen	DDT
C.2	Bidston (part 1)	DDT
C.3	Bidston (part 2)	DDT
C.4	Bidston (part 1)	REPLAY
C.5	Bidston (part 2)	REPLAY
C.6	Bidston (part 3)	REPLAY
C.7	Bidston (part 4)	REPLAY
C.8	Edinburgh	DDT
C.9	Herstmonceux	DDT
C.10	Lerwick	DDT
C.11	Newlyn	DDT
C.12	Taunton	DDT
C.13	Wick	DDT

Data set / year	Number of sets	Processed as whole Mean	Std Dev	Processed as sets Mean	Std Dev
1995					
MAC1505A	18	360.5	27.1	360.3	1.7
MAC1605A	24	364.9	32.5	364.4	2.5
MAC1805A	23	367.6	27.4	367.7	2.5
MAC0711A	24	371.8	24.5	371.6	2.2
MAC0811A	24	369.2	25.5	369.9	2.7
MAC0911B	24	370.8	27.0	371.1	4.0
1996					
MAC2309A	22	375.8	23.3	376.1	2.8
MAC2409A	24	367.1	25.7	366.9	3.8
MAC2509A	24	362.4	28.1	362.0	2.6
MAC2609A	24	361.0	39.5	361.2	5.6
1997					
MAC0707A	17	373.9	24.9	374.2	2.7
MAC0807A	20	368.1	23.7	368.1	1.4
MAC0907A	24	368.3	23.6	368.8	1.7
MAC1007A	24	368.3	22.6	368.4	1.3
1998					
MAC2007A	17	367.4	24.3	367.4	2.3
MAC2107A	24	366.9	19.9	366.4	1.5
MAC2207A	24	366.2	22.0	366.0	1.6
MAC2307A	24	366.0	21.6	365.9	1.1

Table C.1. DDT results for FG5-103 at Aberdeen. Gravity values are g - 981 688 000 μgal. Errors are in μgal.

Data set / year	Number of sets	Processed as whole Mean	Processed as whole Std Dev	Processed as sets Mean	Processed as sets Std Dev
1994					
POL1306A	18	356.3	16.3	356.3	1.4
POL1808A	24	355.2	22.7	355.0	3.8
POL3009A	24	357.5	21.1	357.5	2.6
1995					
POL1201A	24	376.3	21.6	376.4	2.3
POL0405A	24	364.3	21.4	364.1	13.7
POL2605A	44	362.0	17.5	361.4	2.9
POL1808A	24	357.9	11.4	357.8	1.3
POL1909A	24	361.9	13.8	361.8	1.9
POL3010A	24	362.4	18.2	362.3	1.9
POL1711A	24	363.7	20.6	363.7	3.3
1996					
POL0603A	24	361.1	16.3	361.1	1.9
POL3004A	24	353.4	13.2	353.5	2.2
POL0205A	24	361.3	16.5	361.4	2.7
POL0306A	24	360.6	23.5	360.6	4.3
POL1806A	24	359.6	18.0	359.2	1.7
POL0209A	24	356.6	13.4	357.1	2.4
POL2210A	24	359.8	29.4	359.8	1.9
POL1212A	24	364.1	27.9	364.4	4.0
1997					
POL0301A	24	363.9	18.3	364.0	2.3
POL1202A	24	370.3	50.5	370.6	6.6
POL1402A	24	368.9	41.9	368.8	4.2
POL1605A	24	359.8	24.8	360.3	5.1
POL2905A	24	359.3	10.1	359.3	1.1
POL0207A	24	359.5	9.8	359.4	1.5
POL1607A	24	358.0	10.6	357.8	1.5
POL2608A	24	353.9	14.6	353.7	1.3
POL1709A	24	353.3	17.4	353.3	1.5
POL1710A	24	359.1	22.0	359.1	2.5
POL2910A	24	358.5	27.3	358.6	4.5

Table C.2. DDT results for FG5-103 at POL1, Bidston. Gravity values are g - 981 367 000 μgal. Errors are in μgal.

Data set / year	Number of sets	Processed as whole Mean	Std Dev	Processed as sets Mean	Std Dev
1998					
POL0406A	24	361.7	18.0	361.1	4.1
POL1206A	24	364.1	15.7	363.9	3.0
POL1606A	24	364.1	11.6	364.1	3.2
POL1706A	24	364.1	9.9	364.2	1.3
POL1906A	24	361.5	17.1	361.4	1.8
POL0707A	24	362.3	27.4	362.6	4.8
POLl007A	24	361.7	20.8	361.4	3.4
POL0508A	24	361.4	11.8	361.4	1.0
POL0608A	24	361.2	10.8	361.2	0.9
POL0610A	24	358.8	14.7	358.5	2.4
POL1910A	24	359.9	25.9	359.5	3.6

Table C.3. DDT results for FG5-103 at POL1, Bidston continued. Gravity values are g - 981 367 000 μgal. Errors are in μgal.

Data set / year	Number of sets	Gravity Mean	Set Std Dev	Mean Std Dev
1994				
POL0606A	19	366.0	1.6	19.4
POL0706B	21	366.9	3.0	18.6
POL1306A	18	364.7	1.3	12.8
POL1506A	24	362.7	2.3	14.7
POL2206A	21	364.9	3.2	18.4
POL2906A	22	363.3	1.2	12.7
POL1107A	21	362.7	2.3	12.7
POL1207B	20	365.4	1.9	15.0
POL2607A	24	362.9	2.3	14.2
POL1808A	23	363.0	3.5	19.2
POL3008A	22	362.7	1.2	13.4
POL1209A	24	365.9	2.4	16.8
POL1409A	24	366.2	2.6	17.4
POL2909A	23	366.4	2.7	18.6
POL3009A	24	366.9	2.4	18.8
POL1110A	22	366.3	2.2	16.8
POL1810A	22	366.4	3.0	34.7
POL2410A	24	368.5	1.9	19.1
1995				
POL1101A	24	364.2	3.9	33.8
POL1201A	24	364.5	2.3	20.4
POL2401A	24	364.2	4.2	28.1
POL2302A	22	366.9	2.6	24.5
POL2402A	24	365.6	2.5	18.4
POL0303A	24	367.0	3.8	35.8
POL2303A	23	364.5	2.0	16.8
POL3103A	24	363.7	2.6	28.8
POL0704A	43	365.2	1.7	16.7
POL1004A	24	365.6	1.3	17.0
POL2104A	24	366.4	1.7	13.5
POL2404A	24	365.6	2.0	14.4
POL0405A	22	366.2	1.4	14.4
POL2305A	24	362.1	2.5	21.0
POL2605A	44	363.1	2.9	15.2

Table C.4. REPLAY results for FG5-103 at POL1, Bidston. Gravity values are g - 981 367 000 μgal. Errors are in μgal.

Data set / year	Number of sets	Gravity Mean	Set Std Dev	Mean Std Dev
1995				
POL0308A	24	357.7	1.7	11.0
POL0408A	47	358.3	1.7	9.5
POL1408A	24	357.8	2.4	11.4
POL1608A	24	357.8	1.2	20.7
POL1808A	24	358.6	1.0	9.5
POL2908A	24	361.6	1.5	11.6
POL0509A	24	360.5	3.6	17.7
POL0709A	23	362.6	4.2	19.4
POL1109A	23	363.3	1.8	12.5
POL1909A	24	361.9	2.0	12.1
POL0210A	22	361.3	4.6	31.9
POL2610A	24	364.7	3.7	27.0
POL3010A	24	364.0	1.7	16.6
POL1611A	22	365.6	3.0	19.5
POL1711A	24	363.8	3.6	18.7
POL2011A	23	365.2	2.4	22.0
POL2711A	23	364.0	2.0	18.6
POL3011A	23	363.3	2.4	18.1
POL0812A	24	364.7	3.1	28.2
POL1112A	22	363.4	1.7	24.9
1996				
POL2302A	24	361.9	2.7	47.7
POL2602A	24	363.3	1.7	14.8
POL2702A	22	362.6	1.6	15.9
POL2902A	23	361.3	2.7	17.9
POL0103A	24	361.2	1.7	18.0
POL0403A	23	361.9	1.7	12.3
POL0503A	22	361.6	1.6	13.0
POL0603A	24	361.3	1.4	12.7
POL2603A	24	358.9	3.4	19.6
POL2703A	20	361.6	4.5	21.2
POL0304A	23	361.0	1.7	13.1
POL1204A	24	356.6	3.7	19.5
POL1604A	24	359.7	3.5	19.2

Table C.5. REPLAY results for FG5-103 at POL1, Bidston continued. Gravity values are g - 981 367 000 μgal. Errors are in μgal.

Data set / year	Number of sets	Gravity Mean	Set Std Dev	Mean Std Dev
1996				
POL1804A	23	361.9	3.0	19.2
POL0105A	24	355.7	2.4	16.4
POL0205A	23	360.0	2.6	15.3
POL0306A	23	359.0	3.5	21.8
POL1306A	21	357.8	0.8	11.2
POL1406A	20	358.3	1.3	11.0
POL1706A	22	359.2	2.4	16.6
POL1806A	24	359.7	1.6	16.3
POL2307A	24	357.7	4.3	15.9
POL2607A	24	358.2	1.5	11.5
POL0608A	24	358.8	2.3	14.0
POL1308A	22	357.5	2.2	10.9
POL1608A	24	356.7	1.4	10.3
POL2208A	23	359.3	1.9	14.9
POL2708A	24	358.7	3.9	15.8
POL0209A	24	357.6	2.6	12.4
POL0509A	22	357.9	2.6	16.1
POL1009A	24	357.7	3.4	14.2
POL1209A	24	357.0	4.5	23.6
POL1610A	23	361.4	2.9	23.0
POL1810A	23	362.8	3.3	22.5
POL2210A	24	360.1	2.0	29.2
POL0111A	24	362.1	4.6	47.4
POL0711A	24	361.5	2.0	27.6
POL0811A	24	362.8	3.8	26.4
POL1212A	24	364.5	4.1	26.9
POL1712A	24	365.5	3.4	41.6
POL2012A	24	364.5	2.9	21.0
POL2312A	24	364.6	2.3	17.2
1997				
POL0201A	24	363.4	2.6	19.0
POL0301A	24	363.7	2.2	17.4
POL0601A	24	363.7	1.4	13.1
POL2101A	24	364.9	2.4	29.3
POL1402A	24	367.1	3.9	41.6

Table C.6. REPLAY results for FG5-103 at POL1, Bidston continued. Gravity values are g - 981 367 000 μgal. Errors are in μgal.

Data set / year	Number of sets	Gravity Mean	Set Std Dev	Mean Std Dev
1997				
POL1905A	24	363.9	1.0	14.8
POL2305A	24	362.8	1.1	10.7
POL2905A	24	363.8	0.9	9.0
POL0606A	23	362.8	2.7	18.8
POL1806A	24	363.4	3.3	19.6
POL3006A	23	363.8	3.0	20.7
POL0207A	24	363.9	1.5	9.9
POL1607A	24	362.6	1.5	10.6
POL2407A	24	362.4	1.3	15.3
POL2108A	24	362.0	2.0	15.0
POL2608A	24	358.3	1.4	14.6
POL1009B	24	357.3	1.0	13.1
POL1709A	24	356.9	1.6	17.5
POL1710A	24	363.5	3.1	21.9
POL2210A	24	363.6	1.8	15.4
POL0412A	24	366.3	1.1	11.6
1998				
POL1706A	24	368.8	1.5	10.1
POL1906A	24	368.9	1.6	17.2
POL1007A	24	364.1	4.1	20.6
POL0508A	24	368.7	1.6	11.9
POL0608A	24	368.3	1.3	11.3
POL0610A	24	366.1	2.0	15.6
POL1910A	24	367.4	3.7	25.7
POL1611A	18	367.4	3.5	23.7

Table C.7. REPLAY results for FG5-103 at POL1, Bidston continued. Gravity values are g - 981 367 000 μgal. Errors are in μgal.

Data set / year	Number of sets	Processed as whole Mean	Std Dev	Processed as sets Mean	Std Dev
1994					
EDI1807A	13	172.8	15.4	172.8	1.0
EDI1907A	24	180.4	15.8	180.3	1.1
EDI2007A	24	180.5	15.7	180.4	1.1
1995					
EDI1005A	14	196.1	16.1	196.1	2.1
EDI1105A	24	195.3	18.0	195.4	2.3
EDI1205A	24	195.0	18.7	194.9	1.9
EDI1305A	24	194.2	14.9	194.2	1.6
EDI1905A	21	192.7	19.5	192.7	3.2
EDI2005A	24	195.3	17.2	195.3	2.0
EDI0211B	24	193.9	15.8	193.9	1.9
EDI0311A	24	192.4	17.9	192.5	1.6
EDI0411A	24	193.7	18.0	193.9	1.2
EDI1211A	24	195.1	27.2	195.3	2.5
EDI1311A	24	196.3	15.5	196.2	1.4
EDI1411A	23	196.2	17.9	196.0	1.6

Table C.8. DDT results for FG5-103 at Edinburgh. Gravity values are g - 981 579 000 μgal. Errors are in μgal.

Data set / year	Number of sets	Processed as whole Mean	Std Dev	Processed as sets Mean	Std Dev
1996					
HER0905A*	21	984.5	35.3	984.9	8.3
HER1005A*	24	980.4	34.3	979.8	16.8
HER1105A	24	987.5	17.2	987.6	1.9
HER1205A	24	987.6	18.6	987.3	2.9

Table C.9. DDT results for FG5-103 at Herstmonceux. Gravity values are g - 981 123 000 μgal. Errors are in μgal. Data sets marked * were not used due to laser problems.

Data set / year	Number of sets	Processed as whole Mean	Std Dev	Processed as sets Mean	Std Dev
1996					
LER2909B	24	009.4	38.1	009.1	3.7
LER3009A	24	005.1	27.5	005.6	3.0
LER0110A	24	002.8	18.4	002.6	2.5
LER0210A	13	002.5	23.0	002.0	3.8
LER0310A	4	010.0	26.1	009.4	5.9
1998					
LER2707A	17	004.0	11.7	004.6	2.1
LER2807A	24	004.8	9.3	004.2	1.8
LER2907A	24	004.0	9.8	004.0	1.5

Table C.10. DDT results for FG5-103 at Lerwick. Gravity values are g - 981 944 000 μgal. Errors are in μgal.

Data set / year	Number of sets	Processed as whole Mean	Std Dev	Processed as sets Mean	Std Dev
1995					
NEW0910A	12	523.6	17.0	523.6	1.5
NEW1010A	24	525.3	14.1	525.2	1.8
NEW1110A	6	527.6	15.1	527.6	1.4
NEW1210A	24	527.4	17.9	527.6	2.0
NEW1310A	19	527.2	14.8	527.2	1.2
1997					
NEW2306A	15	523.5	9.9	523.4	2.0
NEW2406A	24	523.1	24.8	523.7	3.3
NEW2506A	24	525.0	22.3	525.7	4.1
NEW2606A	24	525.6	25.1	524.9	4.9
1998					
NEW2906A	18	528.5	44.5	528.1	7.6
NEW3006A	24	518.4	9.8	518.4	1.6
NEW0107A	24	521.1	10.2	521.3	1.8

Table C.11. DDT results for FG5-103 at Newlyn. Gravity values are g - 981 046 000 μgal. Errors are in μgal.

Data set / year	Number of sets	Processed as whole Mean	Processed as whole Std Dev	Processed as sets Mean	Processed as sets Std Dev
1994					
TAU0507B	24	828.2	18.9	828.3	1.4
TAU0607A	24	830.4	18.3	830.3	1.7
1995					
TAU0510A	24	842.7	20.4	842.6	2.9
TAU0610A	24	842.3	21.7	842.2	3.3
TAU0710A	24	845.2	21.8	844.8	7.3
TAU0810A	20	842.3	23.0	842.2	5.2
TAU1410A	15	841.1	19.1	841.0	1.9
TAU1510A	24	839.3	17.4	839.1	1.8
TAU1610A	24	839.9	19.4	839.8	1.7
TAU1710A	24	839.3	19.6	839.1	1.9

Table C.12. DDT results for FG5-103 at Taunton. Gravity values are g - 981 168 000 μgal. Errors are in μgal.

Data set / year	Number of sets	Processed as whole Mean	Processed as whole Std Dev	Processed as sets Mean	Processed as sets Std Dev
1996					
WIC0710B	24	407.2	41.0	406.5	3.4
WIC0810A	24	408.5	55.2	408.4	3.2
WIC0910A	24	406.6	47.6	406.3	2.4

Table C.13. Results for FG5-103 at Wick. Gravity values are g - 981 807 000 μgal. Errors are in μgal.

Appendix D

BPGN Site Gravity Values

The following tables contain BPGN site gravity values for the adjustment with constraint at all absolute sites and free linear scale factors. Details of this adjustment can be found in Table 6.3. The Edinburgh Absolute site has been used as the datum reference point.

Site	Code	Gravity	Standard Error	Weight	Number of obs^{ns}
Aberdeen Absolute	AA	688 721.6	2.4	40.24	44
Aberdeen St Machar's	Ab	688 816.0	2.6	49.04	54
Achnasheen FBM	Ac	688 344.7	3.2	21.48	37
Alvie	Av	598 841.7	3.1	22.08	53
Ambleston	Am	233 763.7	3.4	22.80	26
Annbank	An	551 544.2	3.6	21.80	33
Ashburton	As	97 720.0	2.5	47.64	49
Barry Buddon VLBI	BB	634 889.8	3.5	10.81	20
Beedon	Be	149 845.8	2.7	29.34	50
Bettyhill FBM	By	813 935.9	3.5	22.90	43
Bettyhill Museum	BM	825 271.4	3.6	8.63	22
Betws	Bt	362 656.7	3.2	19.03	29
Bidston POL1 Abs	Pl	367 635.3	2.5	21.58	13
Bidston South Porch	Po	366 353.7	2.7	31.40	24
Bishopton	Bi	583 340.4	2.7	43.14	59
Boxgrove	Bx	112 744.1	2.9	17.27	25
Broadway	Br	146 943.2	2.2	131.27	151
Carlton Colville	CC	285 451.0	3.1	29.41	16
Chapel Haddlesey	CH	387 546.5	3.3	56.62	73

Table D.1. BPGN site gravity values. Gravity is g - 981 000 000 μgal. Errors are in μgal.

Site	Code	Gravity	Standard Error	Weight	Number of obs^{ns}
Crianlarich FBM	Ci	564 580.2	3.1	24.59	41
Crooklands	Cr	442 034.2	3.2	17.27	30
Daresbury	Da	354 482.4	2.6	48.40	55
Dornie	Do	684 915.7	3.6	18.05	29
Easby	Ea	432 973.6	3.7	16.27	22
Edinburgh Absolute	GI	579 544.3	2.3	95.73	116
Elgin South	El	697 369.9	2.9	31.02	45
Farningham	Fa	161 790.4	2.6	59.22	67
Felindre	Fe	204 545.9	3.2	12.45	22
Goosnargh	Go	403 629.6	3.4	11.08	14
Great Gonerby	GG	309 248.1	3.0	55.88	60
Gt Torrington	GT	161 733.9	2.6	39.41	53
Hampton Church	Ha	180 088.8	3.1	33.10	34
Herstmonceux Abs	HA	124 284.3	2.4	95.62	75
Herstmonceux Church	Hx	122 343.1	2.5	64.46	85
Histon	Hi	260 188.5	2.8	41.34	50
Immingham	Im	360 672.0	3.4	27.20	38
Kelton	Ke	499 077.5	3.4	19.82	27
Teddington KK Bld1	KK	181 677.4	3.7	18.50	19
Lairg	Lg	725 583.5	2.7	79.83	90
Lanivet	La	76 354.8	2.5	75.77	101
Malvern	Ml	208 390.0	2.7	18.69	25
Methven	Me	612 131.4	2.7	21.76	43
Moffat TH	Mf	511 194.2	2.5	57.99	83
Montgomery	Mt	268 751.3	3.7	7.42	15
Mounton	Mu	201 297.2	2.3	79.19	87
New Luce	NL	516 636.3	3.9	18.59	25
Newlyn Absolute	PA	46 857.9	2.5	52.01	48
Newlyn ex-centre	Pa	46 785.0	2.6	72.39	88
North Petherton	NP	166 521.1	2.5	31.37	39
North Pickenham	Pi	289 200.1	2.9	77.67	65
Queenborough	Qb	179 411.8	3.1	25.42	16
Rishworth	Ri	352 776.6	3.2	14.80	21
Roybridge	Ry	637 970.0	3.3	22.11	41
Scourie	Sc	810 044.8	4.4	17.37	29
Shareshill	Sh	289 777.7	2.5	37.47	54
Sproughton	Sp	247 766.9	2.8	35.45	31

Table D.2. BPGN site gravity values continued. Gravity is g - 981 000 000 μgal. Errors are in μgal.

Site	Code	Gravity	Standard Error	Weight	Number of obs^{ns}
St John Commandery	SJ	127 441.3	3.2	28.72	38
Strathpeffer	Sf	710 637.1	2.8	46.53	71
Talkin	Tk	473 154.3	2.7	33.04	40
Talybont	Ta	303 826.6	3.1	26.73	34
Tannadice	Tn	636 557.4	3.0	28.19	43
Taunton Absolute	Tu	169 197.7	2.2	30.48	23
Taunton Loading Bay	LB	169 421.5	2.2	76.78	78
Towcester	To	232 294.6	2.7	29.46	35
Ullapool Mus	Ul	755 365.7	3.1	24.71	42
Wick Absolute	WA	807 688.7	2.6	79.44	63
Wick High School	WS	807 200.7	2.7	66.42	78
Wick Church	Wk	809 229.2	3.6	23.47	34
Wimborne	Wi	114 805.6	2.8	39.58	47
Wooler	Wo	529 133.0	3.1	28.59	33
Wylam	Wy	496 785.9	3.4	8.81	26

Table D.3. BPGN site gravity values continued. Gravity is g - 981 000 000 μgal. Errors are in μgal.

Bibliography

Anderson, O. B. (1995). Global ocean tides from ERS-1 and TOPEX/POSEIDON altimetry. *J. Geophys. Res.*, **100**(C12), 25,249 – 25,259.

Anderson, O. B., Woodworth, P. L., and Flather, R. A. (1995). Intercomparison of recent ocean tide models. *J. Geophys. Res.*, **100**(C12), 25,261–25,282.

Baker, T. F. (1980). Tidal gravity in Britain: tidal loading and the spatial distribution of the marine tide. *Geophys. J. R. Astr. Soc.*, **62**, 249–267.

Baker, T. F. (1984). Tidal deformation of the Earth. *Sci. Prog., Oxford*, **69**, 197 – 233.

Baker, T. F. (1985). Methods of tidal loading computation. *Bull. D'Inform. Marées Terrestres*, **94**, 6365 – 6373.

Baker, T. F. (1993). Absolute sea level measurements, climate change and vertical crustal movements. *Global and Planetary Change*, **8**, 149 – 159.

Baker, T. F., Edge, R. J., and Jeffries, G. (1991). Tidal gravity and ocean loading in Europe. *Geophys. J. Int.*, **107**, 1–11.

Baker, T. F., Woodworth, P. L., Blewitt, G., Boucher, C., and Wöppelmann, G. (1997). A European network for sea level and coastal land level monitoring. *J. Marine Systems*, **13**, 163 – 171.

Bastien, R. and Goodacre, A. K. (1990). The effect of humidity variations on long-term tidal gravity recordings. *Bull. D'Inform. Marées Terrestres*, **106**, 7506–7510.

Becker, M., Balestri, L., Bartell, R., Berrino, G., Bonvalot, S., Csapó, G., Diament, M., D'Errico, M., Gerstenecker, C., Gagnon, C., Jousset, P., Kopaev, A., Liard, J., Marson, I., Meurers, B., Nowak, I., Nakai, S., Rehren, F., Richter, B., Schnüll, M., Somerhausen, A., Spita, W., Szatmári, G., Ruymbeke, M. V., Wenzel, H. G., Wilmes, H., Zucchi, M., and Zürn, W. (1995). Microgravimetric measurements at the 1994 International Comparison of Absolute Gravimeters. *Metrologia*, **32**, 145 – 152.

Blundell, D. J. and Parkes, R. (1969). A study of the crustal structure beneath the Irish Sea. *Geophys. J. R. Astr. Soc.*, **17**, 45–62.

Carter, W. E., Aubrey, D. G., Baker, T. F., Boucher, C., LeProvost, C., Pugh, D., Peltier, W. R., Zumberge, M., Rapp, R. H., Schutz, R. E., Emery, K. O., and Enfield, D. B. (1989). Geodetic fixing of tide gauge bench marks. Technical report, Woods Hole Oceanographic Institution.

Charles, K. (1995). *High Precision Relative and Absolute Gravity*. Ph.D. thesis, University of Edinburgh.

Charles, K. and Hipkin, R. (1993). British precise gravity net 1993. Technical report, Department of Geology and Geophysics, University of Edinburgh, West Mains Road, Edinburgh, EH9 3JW.

Crossley, D. J., Jensen, O. G., and Hinderer, J. (1995). Effective barometric admittance and gravity residuals. *Phys. Earth Planet. Int.*, **90**, 221–241.

Curtis, D. (1996). *Ocean tide loading for geodetic applications*. Ph.D. thesis, Univ. of Nottingham.

Dehant, V. (1987). Tidal parameters for an inelastic Earth. *Phys. Earth Planet. Int.*, **49**, 97–116.

Delcourt-Honorez, M. (1991). Total effect of groundwater and internal fluid pressure variations on gravity. *Cahiers du Centre Européen de Géodynamique et de Séismologie*, **3**, 207–233.

Dittfeld, H. J. (1989). Tidal results of the gravimetric observatory Potsdam. *Proc. Int. Earth Tides*, pages 623–636.

Douglas, B. C. (1991). Global sea level rise. *J. Geophys. Res.*, **96**(C4), 6981 – 6992.

Dziewonski, A. M. and Anderson, D. L. (1981). Preliminary reference Earth model. *Phys. Earth Planet. Int.*, **25**, 297 – 356.

Egbert, G. D., Bennett, A. F., and Foreman, M. G. G. (1994). TOPEX/POSEIDON tides estimated using a global inverse model. *J. Geophys. Res.*, **99(C12)**, 24,821 – 24,852.

Ekman, M. and Mäkinen, J. (1994). Postglacial uplift, gravity change and mass flow in Fennoscandia 1966 - 1993. Nordic Geodetic Commission, 12th General Meeting.

Elstner, C., Jentzsch, G., Kroner, C., Weise, A., and Wenzel, H. G. (1997). Spatial coherence of air pressure results on gravity. *Proc. Int. Earth Tides*, pages 207–221.

Farrell, W. E. (1972). Deformation of the Earth by surface loads. *Rev. Geophys. Space Phys.*, **10**(3), 761–797.

Farrell, W. E. (1973). Earth tides, ocean tides and tidal loading. *Phil. Trans. R. Soc. Lond.*, **A274**, 253–259.

Hipkin, R. (1993). Software investigation (notes on FG5 processing software). Technical report, Department of Geology and Geophysics, University of Edinburgh, West Mains Road, Edinburgh, EH9 3JW.

Hipkin, R. G., Lagios, E., Lyness, D., and Jones, P. (1988). Reference gravity stations on the IGSN71 standard in Britain and Greece. *Geophys. J.*, **92**, 143 – 148.

Hosker, D. (1996). Industrial placement report: Klopping program investigation. Internal Report, Proudman Oceanographic Laboratory, Bidston Observatory, Birkenhead, L43 7RA.

Jentzsch, G. and Melzer, J. (1989). Calibration and stability of the gravimeter LCR ET18. *Bull. D'Inform. Marées Terrestres*, **104**, 7283–7291.

Klopping, F. J., Peter, G., Robertson, D. S., Berstis, K. A., Moose, R. E., and Carter, W. E. (1991). Improvements in absolute gravity observations. *J. Geophys. Res.*, **96**(B5), 8295 – 8303.

Kroner, C. and Jentzsch, G. (1997). Comparison of air pressure reducing methods and discussion of other influences on gravity. *Proc. Int. Earth Tides*, pages 423–430.

LaCoste & Romberg Gravity Meters Inc. (1989). *Instruction Manual: Model G & D gravity meter*. LaCoste & Romberg Gravity Meters Inc., 4807 Spicewood Springs Road, Bldg. 2, Austin, Texas, 78759 USA.

Lambeck, K. (1993). Glacial rebound of the British Isles - II. A high - precision model. *Geophys. J. Int.*, **115**, 960 – 990.

Lambeck, K., Johnston, P., Purcell, A., Kondilis, C., and Nakada, M. (1990). Geodynamics: Introduction. In *Research School of Earth Sciences Annual Report 1990*, pages 115 – 116. The Australian National University.

LeProvost, C., Genco, M. L., Lyard, F., Vincent, P., and Canceil, P. (1994). Spectroscopy of the world ocean tides from a finite element hydrodynamic model. *J. Geophys. Res.*, **99**(C12), 24,777 – 24,797.

Longman, I. M. (1963). A Green's function for determining the deformation of the Earth under surface mass loads, 2: Computations and numerical results. *J. Geophys. Res.*, **68**(485).

Mäkinen, J. and Tattari, S. (1989). The influence of variation in subsurface water storage on observed gravity. *XI Int. Symp. on Earth Tides, Helsinki.*

Marson, I., Faller, J. E., Cerutti, G., De Maria, P., Chartier, J. M., Robertsson, L., Vitushkin, L., Friederich, J., Krauterbluth, K., Stizza, D., Liard, J., Gagnon, C., Lothhammer, A., Wilmes, H., Mäkinen, J., Murakami, M., Rehren, F., Schnull, M., Ruess, D., and Sasagawa, G. S. (1995). Fourth international comparison of absolute gravimeters. *Metrologia*, **32**, 137 – 144.

Masson Smith, D., Howell, P. M., Abernethey-Clark, A. B. D. E., and Proctor, D. W. (1974). The national gravity reference net 1973. *Ord. Surv. prof. Pap., New Serv.*, **26**.

Merriam, J. B. (1992). Atmospheric pressure and gravity. *Geophys. J. Int.*, **109**, 488–500.

Merriam, J. B. (1993). The atmospheric pressure correction in gravity at Cantley, Quebec. *Proc. Int. Earth Tides*, pages 161–168.

Morelli, C., Gantar, C., Honkasalo, T., McConnell, R. K., Tanner, J. G., Szalo, B., Uotila, U., and Whalen, C. T. (1974). *International Gravity Standard Network 1971*. International Association of Geodesy, 19, rue Auber, 75009 Paris.

Neumeyer, J. (1995). Frequency dependent atmospheric pressure correction on gravity variations by means of cross spectral analysis. *Bull. D'Inform. Marées Terrestres*, **122**, 9212–9220.

Niebauer, T. M. (1988). Correcting gravity for the effects of local air pressure. *J. Geophys. Res.*, **93**(B7), 7989–7991.

Niebauer, T. M. (1989). The effective measurement height of freefall absolute gravimeters. *Metrologia*, **26**, 115–118.

Niebauer, T. M., Sasagawa, G. S., Faller, J. E., Hilt, R., and Klopping, F. (1995). A new generation of absolute gravimeters. *Metrologia*, **32**(3), 159–180.

Peltier, W. R. (1990). Glacial isostatic adjustment and relative sea - level change. In N. R. Council, editor, *Sea - Level Change*, chapter 4, pages 73 – 87. National Academy Press, 2101 Constitution Ave., Washington DC, 20418, USA. ISBN 0-309-04039-6.

Pertsev, B. P. (1970). The effect of ocean tides upon Earth tide observations. *Proc. 6th Int. Symp. on Earth Tides, Communications Observatoire Royal de Belgique*, **A9**(96), 113–115.

Peter, G., Klopping, F. J., and Berstis, K. A. (1995). Observing and modelling gravity changes by soil moisture and groundwater table variations with superconducting gravimeters in Richmond, Florida, USA. *Proc. Cahiers du Centre Européen de Géodynamique et de Séismologie*, **11**, 147–159.

Press, W. H., Teukolsky, S. A., Vetterling, W. T., and Flannery, B. P. (1992). *Numerical Recipes in Fortran*. Cambridge University Press, The Pitt Building, Trumpington Street, Cambridge, CB2 1RP.

Ray, R. D. (1993). Global ocean tide models on the eve of TOPEX/POSEIDON. *IEEE Transactions on Geoscience and Remote Sensing*, **31**(2), 355–364.

Schwiderski, E. W. (1980). Ocean tides, Part I: global ocean tidal equations; Part II: a hydrodynamical interpolation model. *Mar. Geod*, **3**, 161 – 255.

Shennan, I. (1989). Holocene crustal movements and sea - level changes in Great Britain. *J. Quat. Sci.*, **4**(1), 77 – 89.

Sun, H.-P., Ducarme, B., and Dehant, V. (1993). Correction of the atmospheric pressure on gravity measurements recorded by a superconducting gravimeter at Brussels. *Proc. Int. Earth Tides*, pages 317–330.

Telford, W. M., Geldart, L. P., and Sheriff, R. E. (1990). Applied geophysics. *Cambridge Uni. Press.*

UK Nirex Ltd. (1993). Geology and hydrogeology of the Sellafield area. *The Hydrogeology*, **3**(524).

Vauterin, P. (1997). The correction of the pressure effects for the superconducting gravimeter in Membach (Belgium). *Proc. Int. Earth Tides*, pages 447–454.

Wenzel, H. G. (1993). Tidal data processing on a P.C. *Proc. 12th Int. Symp. Earth Tides, Beijing.*

Wenzel, H. G. (1994). Earth tide analysis package - Eterna 3.20. *Bull. Inf. Marées Terrestres*, **120**, 9019–9022.

Wenzel, H. G. (1997). Analysis of Earth tide observations. In *Lecture notes in Earth sciences: Tidal phenomena*, pages 59–75. Springer - Verlag.

Wessel, P. and Smith, W. H. F. (1996). A global self-consistent, hierarchical, high-resoution shoreline database. *J. Geophys. Res.*, **101**(B4), 8741–8743.

Woodworth, P. L., Shaw, S. M., and Blackman, D. L. (1991). Secular trends in mean tidal range around the British Isles and along the adjacent European coastline. *Geophys. J. Int.*, **104**, 593 – 609.